Analysis of DNA mismatch repair system from *Neisseria Meningitidis*

Liang Xue

Division of Molecular Biosciences
Department of Life Sciences
Imperial College London

November 2016

A thesis submitted for the degree of Doctor of Philosophy and

The Diploma of Imperial College London

AUTHOR DECLARATION

I hereby declare that this thesis represents my own work. Information derived from other people's published and unpublished work in this thesis, has been fully acknowledged in the text and references are provided.

Liang Xue
November 2016

COPYRIGHT DECLARATION

The copyright of this thesis rests with the author and is made available under a Creative Commons Attribution Non-Commercial No Derivatives licence. Researchers are free to copy, distribute or transmit the thesis on the condition that they attribute it, that they do not use it for commercial purposes and that they do not alter, transform or build upon it. For any reuse or redistribution, researchers must make clear to others the licence terms of this work.

ABSTRACT

Neisseria meningitidis (*N. meningitidis*) mismatch repair (MMR) proteins MutS (*Nm*MutS) and MutL (*Nm*MutL) are reported to be involved in phase variation, which helps this bacterial pathogen survive in the human host. The MMR system is responsible for the correction of mismatch errors that occur during DNA replication. Unlike the extensively studied *E. coli* system, MMR from *N. meningitidis* lacks MutH endonuclease and is poorly understood in terms of its coordination and mechanism of strand discrimination. This project aims to investigate the function of MMR enzymes of *N. meningitis* via *in vitro* assays. As an irreplaceable polymerase in MMR, DNA Polymerase III holoenzyme (DNA Pol III HE) was reconstituted from individual components in good yield *in vitro*. Furthermore, in gel shift assays, *Nm*MutS exhibited weak mismatch binding, while *E. coli* MutS bound a mismatched DNA with high affinity. *Nm*MutL non-specifically bound to DNA duplexes without mismatch discrimination. The *Nm*MutS and *Nm*MutL combination also bound to non-specific DNA that pointed towards a downstream activity of *Nm*MutL, rather than mismatch recognition. *Nm*MutL carried out Mn^{2+}-dependent nuclease activity with low mismatch specificity in *in vitro* assays, and exhibited different degrees of digestion on two strands of the mismatched DNA in the presence of Mg^{2+}. The nuclease assay also suggest that *Nm*MutS may enhance the mismatch specific nuclease activity of *Nm*MutL. The addition of ATP inhibited the nuclease activity of *Nm*MutL under different mental ion conditions. This study assessed roles and interactions of *Nm*MutS and *Nm*MutL in the initiation of *N. meningitidis* MMR system which coordinated with ATP and metal ions *in vitro*.

Key words: DNA, DNA Pol III HE, Mismatch repair, *Nm*MutS, *Nm*MutL, *Neisseria meningitidis*

ACKNOWLEDGEMENTS

First and foremost, I sincerely appreciate my supervisor, Dr. Geoff Baldwin, for not only his continued guidance and support during my four year's laboratory work, but also for his useful feedback on my writing. I am also indebted to Dr. Jan Silhan for starting an excellent project in the Baldwin lab and sharing unpublished genetic data, which this research relied on. Thanks also go to Dr. Lucy Rayner, a great mentor inside the lab, for her assistance in lab techniques training and valuable advice in method development stage.

I would like to thank all the members of the Baldwin group: Qiyuan Zhao; Marko Storch; James Field; Ben Mackrow; Matthew Haines; Rebekah Byford; Haris Mallick and Ari Dwijayanti who have provided me with their input and moral support when needed.

Finally, I want to dedicate this thesis to my wonderful wife Yan Peng. My work cannot be completed with her encouragement, support and unfailing love. To my parents Liming Xue and Yuqin Shang, I'm grateful for their sincere care and generous financial support. My gratitude to all of you for believing in me! I feel I am so lucky to have you as my family!

CONTENTS

COPY DECLARATION **2**

ABSTRACT **3**

AUTHOR DECLARATION **4**

ACKNOWLEDGEMENTS **5**

TABLE OF CONTENTS **6**

LIST OF FIGURES **12**

LIST OF TABLES **16**

LIST OF ABBREVIATIONS **17**

CHAPTER ONE

Introduction 20

1.1 DNA 21

1.2 DNA replication 26

1.2.1 The chemical basis of DNA replication 26

1.2.2 General DNA replication mechanism 28

1.2.3 DNA replication in *E. coli* 31

1.3 DNA damage repair mechanisms 38

1.4 DNA mismatch repair 43

1.4.1 DNA mismatch repair in *E. coli* 43

1.4.2 The initiation of MMR in *E. coli* 47

1.4.3 MMR beyond *E. coli* 53

1.4.4 Protein-protein interactions in MMR 55

1.5 *Neisseria Meningitidis* 58

1.6 Hypothesis 61

CHAPTER TWO

Preparation of DNA Pol III HE from *N. meningitidis* 63

2.1 Background and objectives 64

2.2 Results 68

2.2.1 Expression and purification of DNA Pol III subunit δ' in vector pPROEX-HTb from *N. meningitides* 68

2.2.2 Solubility tests with detergents 73

2.2.3 Cloning, expression and purification of DNA Pol III subunit δ' from *N. meningitides* 75

2.2.4 Expression and purification of TEV protease 81

2.2.5 Expression and purification of DNA Pol III subunits 82

2.2.6 Reconstitution of *N. meningitides* DNA Pol III complex 85

2.2.7 Extension assay of DNA Pol III Holoenzyme 89

2.3 Discussion 92

2.3.1 MBP-Tag provides solubility factors for DNA Pol III subunits purification 92

2.3.2 Reconstitution of DNA Pol III complex was carried out using MonoQ anionic exchange column 94

2.3.3 Assembled DNA Pol III complex performed replication of various primed ssDNA 95

CHAPTER THREE

Detection of mismatch Recognition in *N. meningitidis* 97

3.1 Background and objectives 98

3.2 Results 100

3.2.1 Expression and purification of *Nm*MutS and *Nm*MutL 100

3.2.2 Gel shift assays of MutS and MutL with short DNA duplexes 103

3.2.3 Cloning, expression and purification of *Ec*MutS 112

3.2.4 Gel shift assays with mini-circular DNAs 115
3.2.4.1 Preparation of mini-circular DNAs 115
3.2.4.2 Gel shift assays of MutS proteins with mini-circular DNAs 120
3.2.5 Gel shift assays with 60-bp DNA duplexes 122
3.2.5.1 Preparation of blocked-end DNA duplexes 122
3.2.5.2 Gel shift assays of *Ec*MutS with 60-bp DNA duplexes 124
3.2.5.3 Gel shift assays of *Nm*MutS with blocked-end 60-bp DNA duplexes 127
3.2.5.4 Gel shift assays of *Nm*MutL with blocked-end 60-bp DNA duplexes 130
3.2.5.5 Gel shift assays of the combination of *Nm*MutS and *Nm*MutL with blocked-end 60-bp DNA duplexes 132
3.3 Discussion 134
3.3.1 Optimisation of gel shift assays 134
3.3.2 *Ec*MutS specifically bound to mismatched DNA 136
3.3.3 *Nm*MutS performed mismatch recognition with deficiency 137
3.3.4 *Nm*MutL non-specifically bound to the homoduplex DNA 139
3.3.5 The interaction of *Nm*MutS-*Nm*MutL and DNA 140

CHAPTER FOUR

Detection of *Nm*MutL nuclease activity 142
4.1 Background and objectives 143
4.2 Results 148
4.2.1 Nuclease assays of *Nm*MutL on blocked-end linear DNAs 148
4.2.2 Nuclease assays of *Nm*MutL with *Nm*MutS on blocked-end linear DNAs 155

4.2.3 Nuclease assays of *Nm*MutL on open-end linear DNAs with different metal ions 162
4.3 Discussion 168
4.3.1 MutL performed a Mn^{2+}-dependent nuclease activity 168
4.3.2 Strand-discriminated nuclease activity of *Nm*MutL in the presence of Mg^{2+} 170
4.3.3 *Nm*MutL nuclease activity was inhibited by ATP 173
4.3.4 The effect of *Nm*MutS on *Nm*MutL activity 176

CHAPTER FIVE

Conclusion & future work 180
5.1 Conclusion 181
5.2 Future work 182

CHAPTER SIX

Materials & methods 185
6.1 General materials 186
6.1.1 Chemicals and enzymes 186
6.1.2 Media 186
6.1.3 Antibiotics 187
6.1.4 Kits 187
6.1.5 Bacterial strains 187
6.1.5.1 Preparation of $CaCl_2$ chemically competent cells 188
6.1.6 Plasmids 188
6.2 Molecular and cellular methods 189
6.2.1 Plasmid DNA isolation 189
6.2.2 Polymerase chain reaction (PCR) 189
6.2.3 Agarose gel electrophoresis 191
6.2.4 Gel extraction of PCR products 191

6.2.5 Restriction enzyme digestion of DNA 192
6.2.6 Ligation of DNA 192
6.2.7 Transformation of competent cells 193
6.2.8 Storage of cell strains 193
6.2.9 Detection of target genes 194
6.2.10 Specific gene cloning strategies 194
6.2.10.1 Cloning for MBP-δ' fusion protein 194
6.2.10.2 Cloning for MBP-δ·δ' fusion protein 195
6.2.10.3 Cloning of MutS from *E. coli* 196
6.3 Biochemical methods of protein preparation 197
6.3.1 Expression and purification of DNA Pol III subunit δ and δ' with the MBP-tag 197
6.3.2 Expression and purification of MMR enzymes with the His-tag 199
6.3.3 Size-exclusion chromatography 200
6.3.4 SDS-polyacrylamide electrophoresis 201
6.3.5 Bradford protein assay 202
6.3.6 Quantification of protein 202
6.3.6.1 Folin Lowry protein assay 202
6.3.6.2 Qubit protein assay 203
6.3.7 Reconstitution of DNA Pol III complex 203
6.4 Enzyme assays *in vitro* 205
6.4.1 Polymerase extension assay 205
6.4.1.1 Preparation of M13KE ssDNA 205
6.4.1.2 Preparation of M13KE RF dsDNA 206
6.4.1.3 Preparation of primed ssDNA templates 207
6.4.1.4 DNA Pol III holoenzyme extension assay 207
6.4.2 Gel shift assay 208
6.4.2.1 Preparation of DNA substrates for gel shift assay 208

6.4.2.1.1 Preparation of 30-bp linear DNA 208
6.4.2.1.2 Preparation of mini-circular DNA 209
6.4.2.1.3 Preparation of 60-bp blocked-end DNA 211
6.4.2.2 Non-denaturing PAGE 212
6.4.2.3 Gel shift assay of mismatch repair proteins 212
6.4.3 Nuclease assay 214
6.4.3.1 Preparation of DNA substrates for nuclease assay 214
6.4.3.2 Urea denaturing PAGE 216
6.4.3.3 Nuclease activity assay 216

CHAPTER SEVEN

References 217

CHAPTER EIGHT

Appendices 239

Permissions of Copyrights 240

LIST OF FIGURES

Figure 1-1	Formation of Deoxynucleotides (dNTPs)	22
Figure 1-2	Tautomeric shifts of bases	23
Figure 1-3	The structure of DNA double helix	24
Figure 1-4	Schematic of DNA replication with relevant proteins	29
Figure 1-5	Historical schematic of DNA Pol III HE in *E. coli*	33
Figure 1-6	Schematic of composition of DNA Pol III HE in *E. coli*	34
Figure 1-7	General scheme of biological DNA repair	39
Figure 1-8	Schematic of the introduction of a mutation during DNA replication	44
Figure 1-9	Schematic of mismatch repair system in *E. coli*	46
Figure 1-10	Structure of the *Ec*MutS–DNA complex	48
Figure 1-11	Schematic of the mismatch-binding activity of *Ec*MutS	50
Figure 2-1	Graphic map of pPROEX-HTb vector	66
Figure 2-2	Expression and purification of DNA Pol III subunit δ' in pPROEX-HTb	69
Figure 2-3	Comparison of concentration of the soluble subunit δ' protein before and after precipitation	70
Figure 2-4	Chromatogram of subunit δ' protein from FPLC gel filtration	72
Figure 2-5	The stability test of DNA Pol III subunit δ' protein with detergents at 4°C	74
Figure 2-6	Graphic maps of petM43-delta_prime and petM43-delta.delta_prime	76
Figure 2-7	Cloning, expression and purification of DNA Pol III subunit δ' in pETM43 vector	78
Figure 2-8	Cloning, expression and purification of DNA Pol III subunit δ·δ' in pETM43 vector	80
Figure 2-9	Expression and purification of TEV protease	82
Figure 2-10	Expression and purification of DNA Pol III subunit α	83

Figure 2-11	Expression and purification of DNA Pol III subunit ε	84
Figure 2-12	Expression and purification of DNA Pol III subunit γ.τ	84
Figure 2-13	Analysis of FPLC purified fractions containing assembled core complex of DNA Pol III	86
Figure 2-14	Analysis of FPLC purified fractions containing assembled DNA Pol III complex	88
Figure 2-15	Schematic of three primed M13KE ssDNA templates for polymerase extension assays	90
Figure 2-16	Analysis of primed ssDNA extensions by DNA Pol III HE (*N. meningitis*)	91
Figure 2-17	Assembly strategy of DNA Pol III complex	94
Figure 3-1	Expression and purification of *Nm*MutS	101
Figure 3-2	Expression and purification of *Nm*MutL	102
Figure 3-3	Schematic of 30-bp linear DNA Duplexes ($OL30^{C/G}$ and $OL30^{T/G}$)	103
Figure 3-4	Gel shift assays *Nm*MutS with OL30 DNAs	105
Figure 3-5	Gel shift assays of *Nm*MutL with OL30 DNAs	107
Figure 3-6	Gel shift assays of *Nm*MutS and *Nm*MutL with OL30 DNAs	109
Figure 3-7	Gel shift assays of *NmMutS* and *NmMutL* with ATP and ADP	111
Figure 3-8	Cloning and expression of MutS *E. coli* in pPROEX-HTb vector	113
Figure 3-9	Expression and purification of *Ec*MutS	114
Figure 3-10	Schematic of mini-circular DNA	115
Figure 3-11	Schematic of oligonucleotide components for mini-circular DNAs	116
Figure 3-12	Procedure of Mini-circular DNA purification	117
Figure 3-13	Detection of Mini-circular DNAs preparation	118

Figure 3-14	Detection of various digestions by restriction enzymes with MC120$^{C/G}$ and MC120$^{T/G}$	119
Figure 3-15	Gel shift assays of *Ec*MutS or *Nm*MutS with mini-circular DNAs	121
Figure 3-16	Schematic of blocked-end DNA duplexes	122
Figure 3-17	Streptavidin-biotin binding assay	123
Figure 3-18	Gel shift assays of *Ec*MutS with BL60 DNAs	126
Figure 3-19	Gel shift assays of *Nm*MutS with BL60 DNAs	129
Figure 3-20	Gel shift assays of *Nm*MutL with BL60 DNAs	131
Figure 3-21	Gel shift assays of *Nm*MutS with *Nm*MutL with BL60 DNAs	133
Figure 4-1	Sequence alignments of part of C-terminal domain of MutL proteins	144
Figure 4-2	Structure of 60-bp blocked-end linear DNAs with fluorescent labels (BL60$^{C/G}$ or BL60$^{T/G}$)	147
Figure 4-3	The nuclease assay of *Nm*MutL with BL60$^{C/G}$ DNA without metal ions	151
Figure 4-4	The nuclease assay of *Nm*MutL with BL60$^{C/G}$ DNA with 5mM $MgCl_2$	152
Figure 4-5	The nuclease assay of *Nm*MutL with BL60$^{C/G}$ DNA with 5mM $MnCl_2$	153
Figure 4-6	The nuclease assay of *Nm*MutL with BL60$^{T/G}$ DNA without metal ions	155
Figure 4-7	The nuclease assay of *Nm*MutL with BL60$^{T/G}$ DNA with 5mM $MgCl_2$	156
Figure 4-8	The nuclease assay of *Nm*MutL with BL60$^{T/G}$ DNA with 5mM $MnCl_2$	157
Figure 4-9	The nuclease assay of *Nm*MutL with *Nm*MutS on BL60$^{C/G}$ DNA without metal ions	159

Figure 4-10 The nuclease assay of *Nm*MutL with *Nm*MutS on $BL60^{C/G}$ DNA with 5mM $MgCl_2$ 160
Figure 4-11 The nuclease assay of *Nm*MutL with *Nm*MutS on $BL60^{C/G}$ DNA with 5mM $MnCl_2$ 161
Figure 4-12 The nuclease assay of *Nm*MutL with *Nm*MutS on $BL60^{T/G}$ DNA without metal ions 164
Figure 4-13 The nuclease assay of *Nm*MutL with *Nm*MutS on $BL60^{T/G}$ DNA with 5mM $MgCl_2$ 165
Figure 4-14 The nuclease assay of *Nm*MutL with *Nm*MutS on $BL60^{T/G}$ DNA with 5mM $MnCl_2$ 166
Figure 4-15 The nuclease assay of *Nm*MutL on $OL60^{T/G}$ DNA without metal ions 168
Figure 4-16 The nuclease assay of *Nm*MutL on $OL60^{T/G}$ DNA with 5mM $MgCl_2$ 169
Figure 4-17 The nuclease assay of *Nm*MutL on $OL60^{T/G}$ DNA with 5mM $MnCl_2$ 170
Figure 4-18 The nuclease assay of *Nm*MutL with *Nm*MutS on $OL60^{T/G}$ DNA without metal ions 173
Figure 4-19 The nuclease assay of *Nm*MutL with *Nm*MutS on $OL60^{T/G}$ DNA with 5mM $MgCl_2$ 174
Figure 4-20 The nuclease assay of *Nm*MutL with *Nm*MutS on $OL60^{T/G}$ DNA with 5mM $MnCl_2$ 175
Figure 4-21 MutL nuclease activity on 60-bp linear DNA (- ATP) 178
Figure 4-22 *Nm*MutL nuclease activity on OL60T/G DNA (-ATP) 179
Figure 4-23 Sequence alignments of part of N-terminal domain of MutL homologues 182
Figure 4-24 Nuclease activity of *Nm*MutL and *Nm*MutS on $BL60^{C/G}$ and $BL60^{T/G}$ 184
Figure 4-25 Nuclease activity of *Nm*MutL and *Nm*MutS on $OL60^{T/G}$ 186

LIST OF TABLES

Table 1-1	DNA Polymerase III holoenzyme subunits in *E. coli*	32
Table 1-2	*E. coli* MMR proteins and their function	45
Table 2-1	DNA Pol III HE subunits in *N. meningitidis* strain MC58 serogroup B	65
Table 6-1	Compositions of media	186
Table 6-2	Antibiotics' stock and working concentrations	187
Table 6-3	Summary of commercial kits	187
Table 6-4	Summary of DNA plasmids used in this study	188
Table 6-5	PCR Reaction system	190
Table 6-6	PCR conditions	190
Table 6-7	Double digestion of DNA by restriction enzymes	192
Table 6-8	Ligation system	192
Table 6-9	PCR primers for the cloning of MBP-δ' (*N. meningitidis*)	195
Table 6-10	PCR primers for the cloning of MBP-δ•δ' (*N. meningitidis*)	196
Table 6-11	PCR primers for the cloning of MutS (*E. coli*)	197
Table 6-12	Components of SDS-PAGE electrophoresis gel	201
Table 6-13	Components of SDS-PAGE electrophoresis buffers and dyes	201
Table 6-14	Summary of primers used in extension assays	207
Table 6-15	Oligonucleotides for 30-bp linear DNA used in gel shift assays	209
Table 6-16	Oligonucleotides for mini-circular DNA used in gel shift assays	210
Table 6-17	Oligonucleotides for 60-bp blocked-ended DNA in gel shift assays	211
Table 6-18	Components of non-denaturing PAGE gels	212
Table 6-19	Oligonucleotides used in all nuclease assays	214
Table 6-20	Components of urea denaturing PAGE gels	216

LIST OF ABBREVIATIONS

A	Adenine
aa	Amino acid
AAA+	ATPase Associated Activities
A. aeolicus	*Aquifex aeolicus*
*Aa*MutL	MutL from *Aquifex aeolicus*
*Aa*MutS	MutS from *Aquifex aeolicus*
ADP	Adenosine diphosphate
Alt-NHEJ	Alternative nonhomologous end-joining
APS	Ammonium persulfate
ATP	Adenosine 5'-triphosphate
BER	Base excision repair
$BL60^{C/G}$	60-bp Blocked-end linear DNA without mismatch
$BL60^{T/G}$	60-bp Blocked-end linear DNA with a T/G mismatch
BME	β-mercaptoethanol
bp	Base pair
BSA	Bovine serum albumin
B. subtilis	*Bacillus subtilis*
*Bs*MutL	MutL *from Bacillus subtilis*
C	Cytosine
C-terminal	Carboxyl-terminal
dATP	Deoxyadenosine triphosphate
dCTP	Deoxycytidine triphosphate
dGTP	Deoxyguanosine triphosphate
Da	Dalton
Dam	Deoxyadenosine methylase
DSBs	Double strand breaks
DNA	Deoxyribose nucleic acid
DNA-PKcs	DNA-dependent protein kinase catalytic subunit
DNA Pol III HE	DNA Polymerase III Holoenzyme
dNTP	Deoxynucleotide
DTT	Dithiothreitol
dTTP	Deoxythymidine triphosphate
E. coli	*Escherichia coli*
*Ec*MutL	MutL from *Escherichia coli*
*Ec*MutS	MutS from *Escherichia coli*
EDTA	Ethylene diamine tetra-acetic acid
ExoI	Exonuclease I
ExoVII	Exonuclease VII
ExoX	Exonuclease X
FPLC	Fast protein liquid chromatography
G	Guanine
Hex	6-carboxy-2',4,4',5',7,7',-hexachlorofluorescein

His-tag	Polyhistidine-tag
HR	Homologous recombination
hMutLα	MutLα from human
HPLC	High performance liquid chromatography
H. sapiens	*Homo sapiens*
IPTG	Isopropyl-β-D-thiogalatopyranoside
kbp	Kilo base pair
kDa	Kilo dalton
LB	Lauria Bertani
M	mol L^{-1}
MBP	Maltose binding protein
$MC120^{T/G}$	120-bp mini-circular DNA with a T/G mismatch
min	Minute
MMR	Mismatch repair
MutH	Mutator H
MutL	Mutator L
MutS	Mutator S
NER	Nucleotide excision repair
NHEJ	Non-homologous end-joining
N-terminal	Amino-terminal
N. meningitidis	*Neisseria meningitidis*
*Nm*MutL	MutL from *Neisseria meningitidis*
*Nm*MutS	MutS from *Neisseria meningitidis*
N. gonorrhoeae	*Neisseria gonorrhoeae*
*Ng*MutL	MutL from *Neisseria gonorrhoeae*
nt	nucleotide
^{o}C	Degrees Celsius
OD280	Optical density at 280nm
OD600	Optical density at 600nm
OH	Hydroxyl
$OL30^{C/G}$	30-bp open-end linear DNA without mismatch
$OL30^{T/G}$	30-bp open-end linear DNA with a T/G mismatch
$OL60^{C/G}$	30-bp open-end linear DNA without mismatch
$OL60^{T/G}$	30-bp open-end linear DNA with a T/G mismatch
P. aeruginosa	*Pseudomonas aeruginosa*
PAGE	Polyacrylamide gel electrophoresis
*Pa*MutL	MutL from *Pseudomonas aeruginosa*
PCNA	Proliferating cell nuclear antigen
PCR	Polymerase chain reaction
PEG	Polyethylene Glycol
Pol	Polymerase

PSAD	Plasmid-Safe ATP-Dependent DNase
RFC	Replication factor C
RNA	Ribose nucleic acid
rpm	Revolutions per minute
RT	Room temperature
s	Second
S. cerevisiae	*Saccharomyces cerevisiae*
SDS	Sodium dodecyl sulfate
SSB	Single strand binding protein
T	Thymine
Taq	*Thermus aquaticus*
TBE	Tris/Borate/EDTA
TEMED	N, N, N', N'-etramethylethylenediamine
TEV protease	*Tobacco Etch Virus nuclear-inclusion-a endopeptidase*
TLS	Translesion synthesis
T. thermophiles	*Thermus thermophiles*
*Tt*MutL	MutL from *Thermus thermophiles*
*Tt*MutS	MutS from *Thermus thermophiles*
UV	Ultraviolet
yMutLα	MutLα from *Saccharomyces cerevisiae*

Chapter 1

Introduction

1.1 DNA

Deoxyribonucleic acid, abbreviated as DNA, stores genetic information and is constituted of genetic codes to instruct the operation of living functions and the evolutionary development of all eukaryotes and most prokaryotes. DNA was firstly spotted from the nuclei of human white blood cells by Swiss physiological chemist Friedrich Miescher in 1869. However, it wasn't until 1944 that DNA was confirmed as the active hereditary substance by the crucial experiment from Oswald Avery and his colleagues (Avery, Macleod & McCarty, 1944). In 1951, Maurice Wilkins and Rosalind Franklin obtained high-quality X-ray diffraction photographs of DNA. It suggested that DNA had the latent helical structure and might consist of more than one polynucleotide chain (Franklin & Gosling, 1953).

In 1953, based on the previous studies, James Watson and Francis Crick discovered the complementary double helical structure of DNA which was a significant revolution and laid the foundation of modern molecular biology and genetics studies. In Watson and Crick's model, the two polynucleotide chains of DNA are intertwined with each other to form a regular double helix, which are linked by hydrogen bonding between base pairs (Watson & Crick, 1953).

In 1930, Phoebus Levene firstly elucidated the chemical structures of DNA (Levene & Bass, 1931). DNA is built by "fundamental bricks" nucleotides, is composed of a phosphate group joined to a pentose, which a nitrogen base attached. Between two nucleotides, one nucleotide's 3'-hydroxyl of 2'-deoxyribose joins the phosphate on the 5'-carbon of another nucleotide's 2'-deoxyribose to form a phosphodiester linkage. As a consequence, nucleotides compose the polynucleotide chain, and phosphodiester linkages contribute as the surgar-phosphate backbone of it. Generally, a free 5'-phosphate at one end in DNA is called 5'-end, and a free 3'-hydroxyl at the other end is called 3'-end. Therefore, DNA chains have the inherent 5'-to-3' polarity because of the joined

pattern of nucleotides by phosphodiester linkages. Nitrogen bases which composed DNA are divided into two categories, purine including Adenine (A) and Guanine (G), and pyrimidine, Thymine (T) and Cytosine (C). Hence, four types of fundamental nucleotides in DNA are deoxyribonucleotides, including deoxyadenosine-5'-phosphate, deoxyguanosine-5'-phosphate, deoxycytidine -5'-phosphate and deoxythymidine-5'-phosphate (Fig. 1-1).

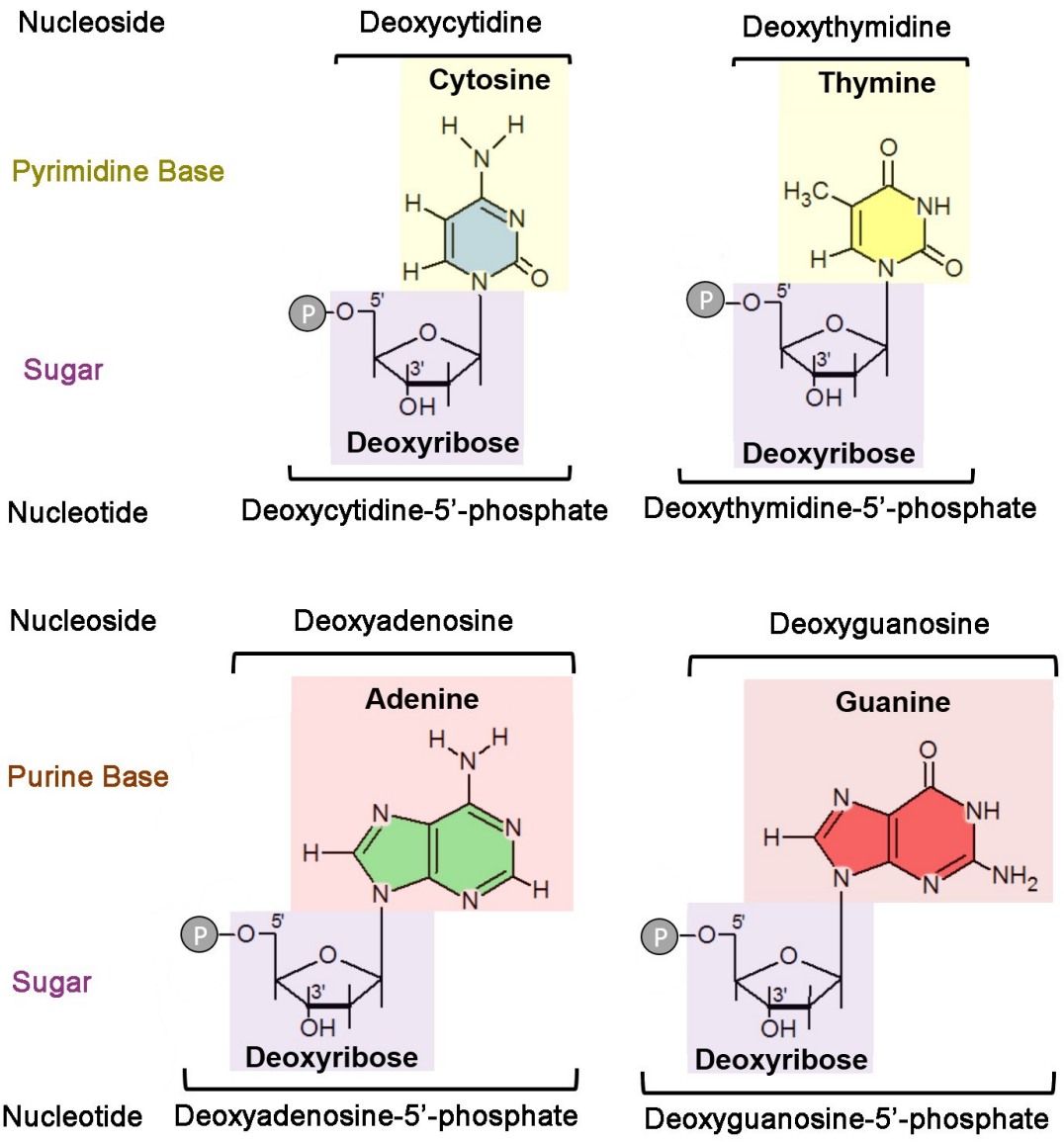


Figure 1-1. Formation of Deoxynucleotides (dNTPs)

By the 1950s, Erwin Chargaff concluded that, in almost all DNA, the amount of thymine was nearly equal to the amount of adenine, and the amount of cytosine usually approximated the amount of guanine (Chargaff, 1951). Due to the shape of bases and the complementary of the hydrogen bonds, the pair of adenine and thymine containing two hydrogen bonds, and guanine binds cytosine with three hydrogen bonds (Fig. 1-3B). Importantly, each base has two possible tautomeric states, a predominant form and a rare form. On most of the adenine and the cytosine, the attached nitrogen atoms are the amino forms; only few perform as the imino forms. Likewise, the attached oxygen atoms on the thymine and the guanine are commonly the keto forms, and have the enol conformation rarely (Fig. 1-2). The presence of tautomers is the main basis of mismatches during DNA replication (Watson *et al.*, 2004).

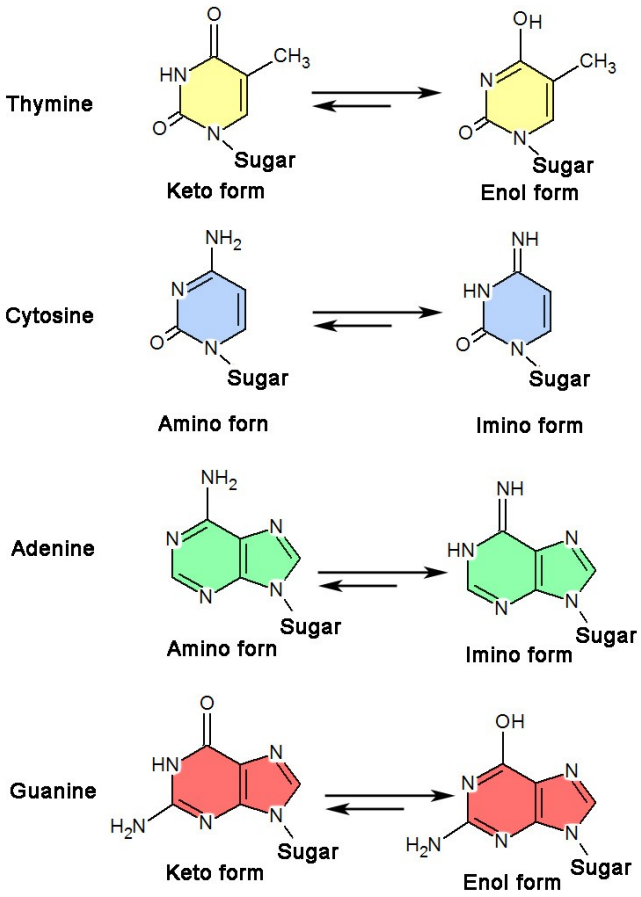


Figure 1-2. Tautomeric shifts of bases

Rosalind Franklin and Maurice Wilkins revealed the helical structure of DNA strands via DNA fiber photographs by X-ray diffraction in 1951. The diameter of DNA helix is 20Å. The pitch between two adjacent bases, which are nearly perpendicular to the axis of the helix, is 3.4Å. Each turn of the helix performs 34Å so that 10 based exist in a complete turn of the helix (Fig. 1-3A). In the Watson-Crick model, two helical polynucleotide chains are connected via hydrogen bonds between complementary base pairs with the antiparallel orientation. Commonly, the structure of DNA is considered to adopt the right-handed helical conformation, which is called B-form. With the stacking of base pairs, the sugar-phosphate backbones exhibit a minor groove with the narrow angle and a major groove with the large angel on the edge of the base pairs (Fig. 1-3A).

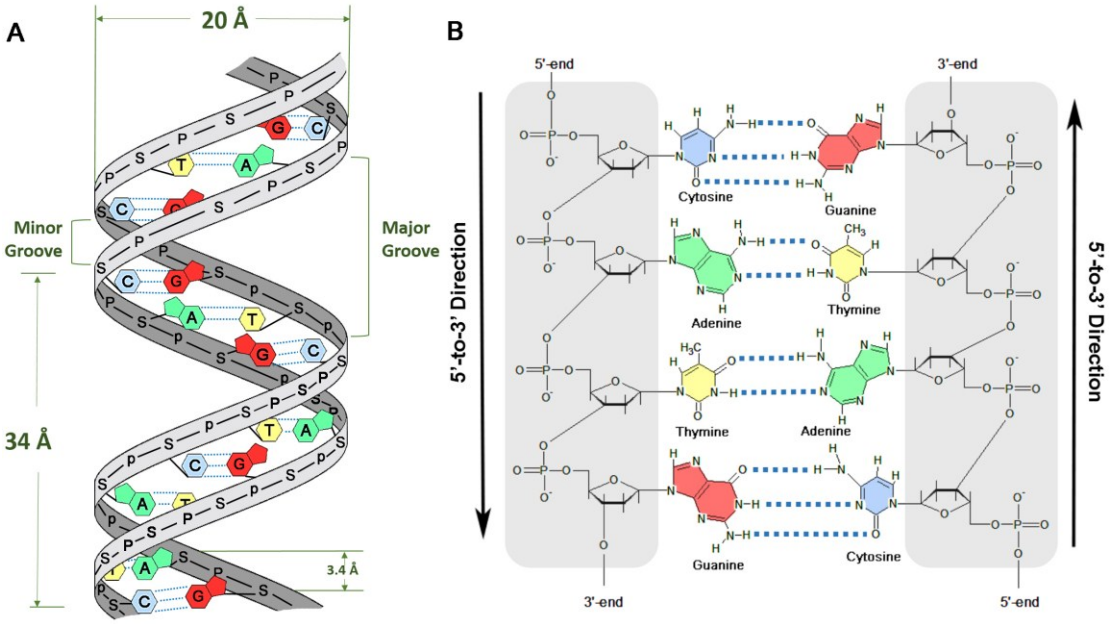


Figure 1-3. The structure of DNA double helix

(A) The right-handed double helical DNA with a diameter of ~2nm (20Å) and contains 10 base pairs, which are perpendicular to the helical axis, in one helical turn. (B) Two 5'-to-3' antiparallel DNA strands are linked by hydrogen bonds between complementary "A-T" and "G-C" base pairs.

Although the B-form structure is the major conformation of DNA in cells, multiple DNA conformations have also been discovered. The right-handed A-form structure is observed that has 11 base pairs in one complete helical turn via X-ray diffraction studies. Compared to the B-form, the major groove of DNA with the A-form structure is deeper and narrower, and the minor groove is shallower and broader. The active Z-form DNA is also observed in cells which present the left-handed double helical conformation. Unlike the B-form and A-form DNA structure, the Z-form DNA has little difference in width of its major and minor grooves.

In eukaryotes, including animals, plants and fungi, nuclear chromosomes contain a long and linear double helical DNA molecule, which coiled with the surface of histone proteins. However, the chromosomes of some organisms are circular. In prokaryotes, such as *E. coli*, its chromosome is a circular double helix DNA, stored in the nucleoid. Furthermore, some DNA molecules can be interchanged between circular and linear forms. For example, lambda phage has the double-strand linear DNA genome in its head. When lambda phage infects its host, *E. coli*, the lambda DNA is inserted into the *E. coli* chromosome and is circularized at the sticky ends, called the *cos* site (Neidhardt & Curtiss, 1996).

In 1956, Francis Crick theorized the approach the “central dogma”, which described genetic information was transferred following “DNA to RNA to protein”. According to the “central dogma”, DNA is the template of self-replication, and it is transcribed by a complementary RNA intermediate, called messenger RNA (mRNA). mRNA is then translated into protein via RNA adaptors, called transfer RNAs (tRNAs). RNA, the abbreviation of ribonucleic acid, is constituted of a phosphate, a ribose sugar and a nitrogen base. The base is at the 1'-position of the ribose, including adenine, cytosine, guanine or uracil (U), instead of

thymine. The genetic code flows from four base units of DNA to corresponded mRNA's four base units, and the triplet codon is translated by tRNA to the protein. Each triplet codon in a gene can encode an amino acid. In all 64 (4x4x4) different codons, 61 of them encode the 20 amino acids of the protein and 3 of them are used to terminate the encoding signal. Following the elaboration of the central dogma, reverse transcription was found in retroviruses, such as Rous sarcoma virus (RSV), which transcribed RNA to synthesize cDNA by catalyzing from the reverse transcriptase (Temin & Mizutani, 1970). This affirms the presence of the transcription from RNA to DNA.

Nearly half a century ago, the study of DNA complementary double helical structure by James Watson and Francis Crick profoundly influenced the research of molecular biology. Based on the base pairing, DNA self-replicated mechanism is greeted to explain how the genetic material is copied with the high fidelity (Watson & Crick, 1953).

1.2 DNA replication

Genetic information of living organisms is encoded on DNA molecules with specific nucleotide sequences. Through DNA replication, genetic information is passed from cells to cells, thereby preserving the genome integrity in species.

1.2.1 The chemical basis of DNA Replication

In the Watson–Crick model, they predicted that DNA was copied via the semiconservative replication. During DNA replication, the breakage of hydrogen bonds between base pairings results unwound DNA double helix and separates the DNA into two single chains. Exposed bases on each single strand are only able to pair with complementary bases, C with G and A with T. Therefore, each unwound single strand serves as the template to synthesize its complementary strand. Subsequently, the newly synthesized

complementary strand and the corresponding template strand constitute the progeny DNA molecule. Due to the progeny DNA molecule retains a single strand of the parental DNA molecule, this replication pattern was called as semiconservative replication. In 1958, Matthew Meselson and Franklin Stahl verified the hypothesis of the Watson–Crick model of DNA replication using the isotope labeling of the nitrogen bases and the cesium chloride gradient centrifugation.

Through years of research, we learned that the synthesis of DNA required the chemical basis. There are two crucial substrates must be present to proceed the synthesis of DNA, a primer-template junction and dNTPs (Brautigam & Steitz, 1998). The primer-template junction is the template element of DNA replication. The template is the parental single strand DNA, which provides the guidance for the addition of complementary deoxynucleotides. The primer is a short fragment of deoxynucleotides which is complementary to the template. The primer has an exposed 3'-OH adjacent to the single stranded region of the template so that it can be extended when the new nucleotides are added. dNTPs perform as the raw materials of DNA replication. The nucleophilic attack on the dNTP substrate at the α-phosphate triggers the synthesis of DNA and leads to the extension of a nucleotide from the 3'-end of the primer. Meanwhile, a pyrophosphate, formed by the β-phosphate and γ-phosphate of the dNTP substrate, is released and hydrolyzed into two phosphate molecules by the pyrophosphatase. The hydrolysis of pyrophosphates results in the breakdown of energetic phosphate bonds, which provides the impetus for DNA synthesis (Jäger & Pata, 1999).

The process of DNA synthesis is catalysed by DNA polymerases using its right hand-like structure, including finger, thumb and palm domains (Doublié & Ellenberger, 1998). The palm domain contains the essential catalyze site which

consists of a β sheet. Moreover, the palm domain of DNA polymerases proofreads the incoming C: G or A: T base-pairings to remove the majority mismatches from incorrect nucleotides (Steitz, 1998). In the finger domain, some residues can associate with dNTPs and then force the triphosphates to contact with the catalytic metal ions fully (Doublié *et al.*, 1998). In addition, when the finger domain binds to the template, the phosphodiester bond is folded behind the active site so that the first base on the template is exposed at the catalytic site (Doublié *et al.*, 1998). On the other hand, the thumb domain does not closely link to the catalyzing function of DNA synthesis. It keeps the position of the catalyze site and the primer and also maintains the close contact between the polymerase and the substrates (Doublié *et al.*, 1998).

1.2.2 General DNA replication mechanism

In the bacterial chromosome, DNA replication starts at one single origin and proceeds bidirectionally. Differently, in *Eukaryotes*, the replication of chromosomal DNA is initiated bidirectionally at many origins only in the S-phase. The replication origin was called the replicator in the Jacob-Brener-Cuzin model which was firstly presented in 1963. The replication origin contains particular sequences which bind to initiator proteins to trigger DNA replication (Berg *et al.*, 2002). Initiator protein is DnaA in *E. coli*; it is the origin recognition complex in Eukaryotes (Weigel *et al.*, 1997). The replication origin varies by diffierent sequences in the genome from various species (Baker & Wickner, 1992; Nasheuer *et al.*, 2002; Kelman & Kelman, 2004). However, the replication origin generally contains rich adenine-thymine base pairs, which have two hydrogen bonds rather than the three bonds in the guanine-cytosine base pairs and contribute to the separation of strands (Lodish *et al.*, 2000; Yakovchuk, Protozanova & Frank-Kamenetskii, 2006).

Once the initiator protein binds to the replication origin, it distorts and unzips the DNA area nearby its binding site and then recruits other relevant proteins to form the pre-replication complex. It is responsible for assembling and activating DNA helicases onto the unwind strands to begin DNA replication. Overall, the initiation of DNA replication is carried out by the interaction between the initiator protein and replication origin sequences and protein-protein interaction in the pre-replication complex.

In living cells, when DNA replication is initiated, the double helix is unwound by DNA helicase from the replication origin in 5'-to-3' direction, and is formed by two template strands as a Y structure called as Replication Fork (Fig. 1-4).

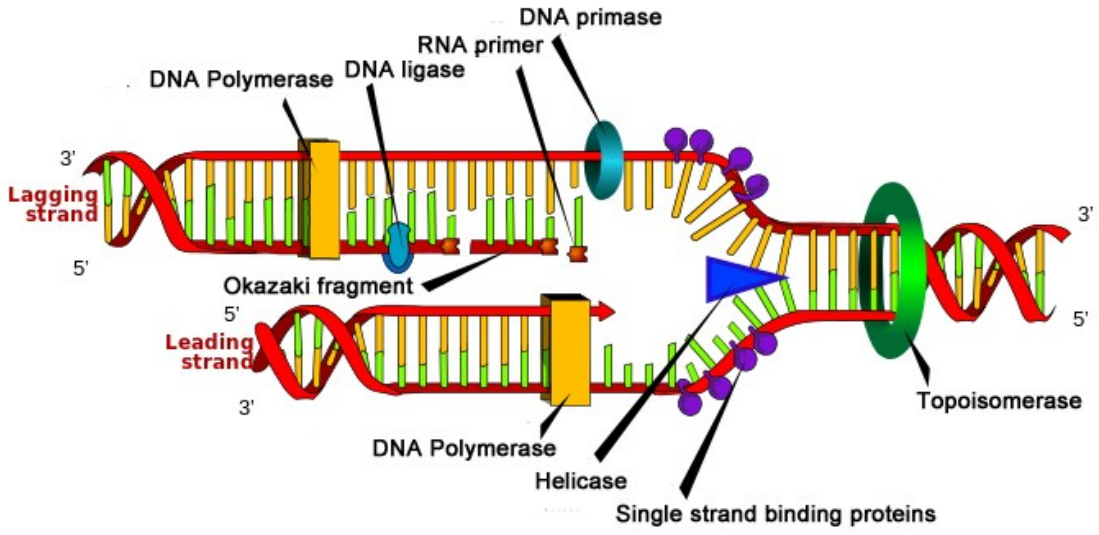


Figure 1-4. Schematic of DNA replication with relevant proteins (Adapted from Ruiz, 2007)

At the replication origin, two replication forks constitute a replication bubble moving opposite directions. Replication fork moves forward following DNA helicase and continuously leave the template strands, which direct the synthesis of daughter DNA. To stabilize the unwound strands, single strand binding proteins (SSB) cooperatively binds to the single-stranded templates followed by the activity of DNA helicase (Mapelli, Panjikar & Tucker, 2005).

Meanwhile, with the separation between the bases of double-stranded by DNA helicase, the double helix before replication fork would become overwound to raise the pressure of the replication system. Topoisomerase catalyzes the instantaneous cleavage of DNA single strand or double strands to regulate the overwinding of DNA (Champoux, 2001).

DNA replication performs on both template strands of the replication fork at the same time. As discussed above, the primer with an exposed 3'-OH is essential for DNA replication. DNA primase is recruited DNA helicase and products the short RNA primers on the template strands so that DNA polymerases are provided the start sites to extent the newly synthesized strands. However, DNA polymerases are only able to synthesize DNA from the 5'-end to the 3'-end. Due to the anti-parallel structure of double-stranded DNA, DNA synthesis is only carried out continuously on one template strand, which is called the leading strand. On the other strand, the synthesis of DNA has to wait the exposure of a sufficient length of template DNA by the movement of replication fork. Consequently, DNA replication is performed discontinuously on this strand, which is called the lagging strand. The newly synthesized DNA fragments on the lagging strand are Okazaki fragments. Since an Okazaki fragment requires a RNA primer to start the synthesis of DNA, thousands of RNA primers are required for DNA replication on the lagging strand. On the contrary, the leading strand only needs one RNA primer to prime the continuous DNA synthesis (Fig. 1-4).

After DNA synthesis by DNA Polymerases, initial RNA primers must be replaced by DNA. RNA fragments are specifically removed by Ribonuclease H (RNase H) via the cleavage of the 3'-O-P bonds between two ribonucleotides (Moore & Sharp, 1985). The last ribonucleotide was degraded by specific 5'-3' exonucleases, including DNA Polymerase I in prokaryotes and DNA

polymerase in eukaryotes. The gaps which are caused by the removal of RNA primers are filled by newly synthesized deoxyribonucleotides from DNA polymerases. DNA ligase then produces the phosphodiester bonds between 5'-Phosphate and 3'-OH to seal the breaks. When the nicks of deoxyribonucleotides had been joined together, the process of DNA replication is completed (Watson *et al.*, 2004).

In most prokaryotes, when the circular chromosome is replicated, two daughter DNAs maintain a hinge-like connection. If two ring chromosomes cannot be separated, it will lead to cell death. To separate the knot of two DNA molecules, type II topoisomerases catalyze the cleavage on one circular DNA and allow the second DNA to pass through the break (Wang, 2002). The cut DNA is then ligated again. Consequently, two daughter circular chromosomes are disentangled by type II topoisomerases and then distributed to progeny cells.

1.2.3 DNA replication in *E. coli*

In *E. coli,* there are five known DNA polymerases, including DNA polymerase I, II, III, IV and V (DNA Pol I, II, III, IV and V), which have different compositions of subunits and various enzymatic properties (Sutton & Walker, 2001). DNA Pol I and DNA Pol III are directly involved in the DNA replication process with high accuracy, and both have the 3'-to-5' proofreading exonuclease activity (Camps & Loeb, 2004). In addition, DNA Pol I also performs exonuclease activity from the 5'-end to the 3'-end so that it carries out the removal of RNA primer at the upstream DNA synthesis site. However, DNA Pol I has a lower processivity which limits the amount of the newly synthesized DNA (Camps & Loeb, 2004). Hence, DNA Pol I is compatible to synthesis the short deoxyribonucleotide fragment to fill the occupied area from RNA primers during DNA replication.

DNA Pol III is an essential enzyme which carries out prokaryotic DNA replication with a high processivity via its holoenzyme (DNA Pol III HE) (Kelman & O'Donnell, 1995). DNA Pol III HE and other replicative proteins are called DNA replisome, which is the complex machine carries out DNA replication (Pomerantz & O'Donnell, 2007). In *E. coli*, DNA Pol III HE is constituted of three major components, the core polymerase, the clamp loader and the sliding β-clamp, containing 10 different subunits (Table 1-1). The previous study revealed that DNA PolIII HE could be reconstituted *in vitro* from the subunits that had been expressed and purified in *E. coli* (Fay *et al.*, 1982).

Subunit	Gene	Function
α	*dnaE*	Plymerase activity
ε	*dnaQ, mutD*	3'-to-5' proofreading exonuclease acitivity
θ	*holE*	Stimulating ε exonuclease
τ	*dnaX*	Coordination of the core on DNA strands; Binding DNA Helicase; ATPase, the role of γ
γ	*dnaX*	ATPase, the motor of clamp loader
δ	*holA*	Interaction with the β-clamp
δ'	*holB*	Cofactor for γ; Stimulating δ for loading β clamp
χ	*holC*	Interaction with SSB
ψ	*holD*	Intermediate protein between χ and γ
β	*dnaN*	Prioviding processivity by sliding alone the DNA strand

Table 1-1. DNA Polymerase III holoenzyme subunits in *E. coli* (Kelman & O'Donnell, 1995)

In the previous long-term studies, the structure and composition of DNA Pol III HE from *E. coli* has been most extensively characterized *in vitro.* The holoenzyme was considered to have two copies of the core polymerase complex (comprising α, ε and θ subunits), two τ subunits, one copy of the clamp loader complex (comprising 2γ, 1δ, 1δ', 1χ, 1ψ subunits) and the β clamp (Fig. 1-5) (Kelman & O'Donnell, 1995).

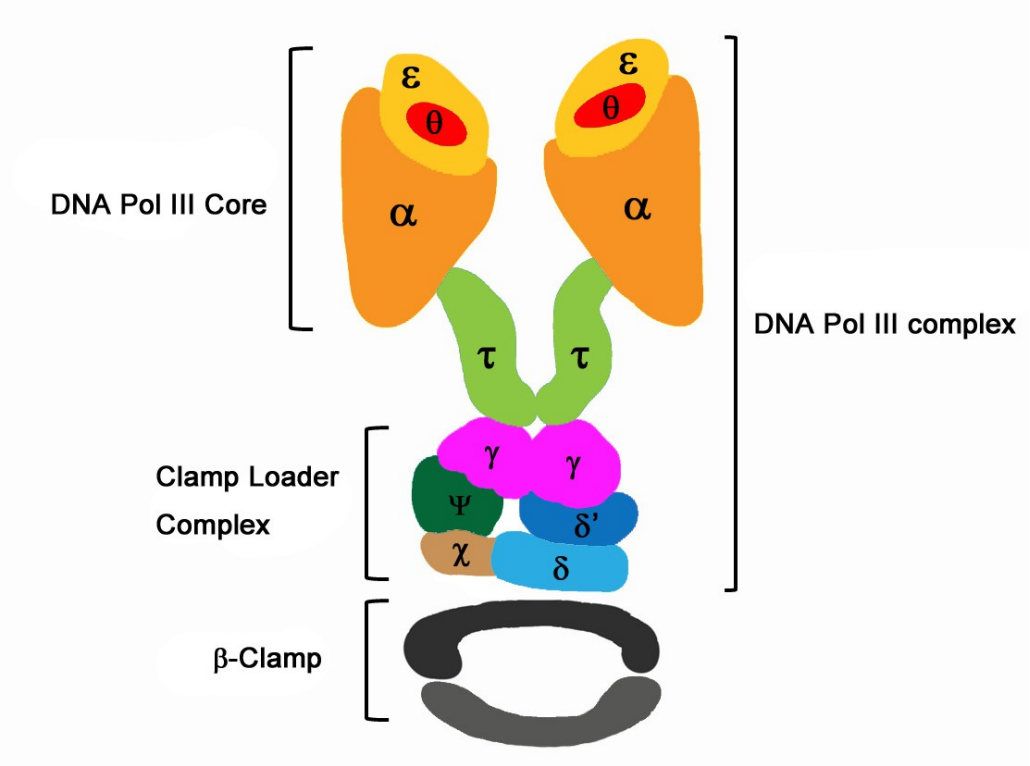


Figure 1-5. Historical schematic of DNA Pol III HE in *E. coli* (Referred to Maki, Maki & Kornberg, 1988)

However, the study of DNA Pol III HE in *E. coli* was further developed with new research achievements. Through millisecond single molecule fluorescence microscopy, Reyes-Lamothe, Sherratt & Leake (2010) examined the stoichiometry and architecture of *E. coli* DNA Pol III HE *in vivo*. The results demonstrated that during DNA replication, three molecules of core polymerase complex interacted with three τ subunits and one clamp loader complex contained three copies of subunit γ , one subunit δ, one subunit δ', one subunit χ and one subunit ψ in one molecules of replisone in *E. coli* (Reyes-Lamothe, Sherratt & Leake, 2010) (Fig. 1-6). Furthermore, three more copies of subunit $\chi\cdot\psi$ was found that interacted with SSB proteins (Reyes-Lamothe, Sherratt & Leake, 2010). Two of the three DNA Pol III core are considered to conduct DNA synthesis on the lagging strand, the other one core polymerase synthesizes the leading strand with the high processivity (Watson *et al.*, 2013).

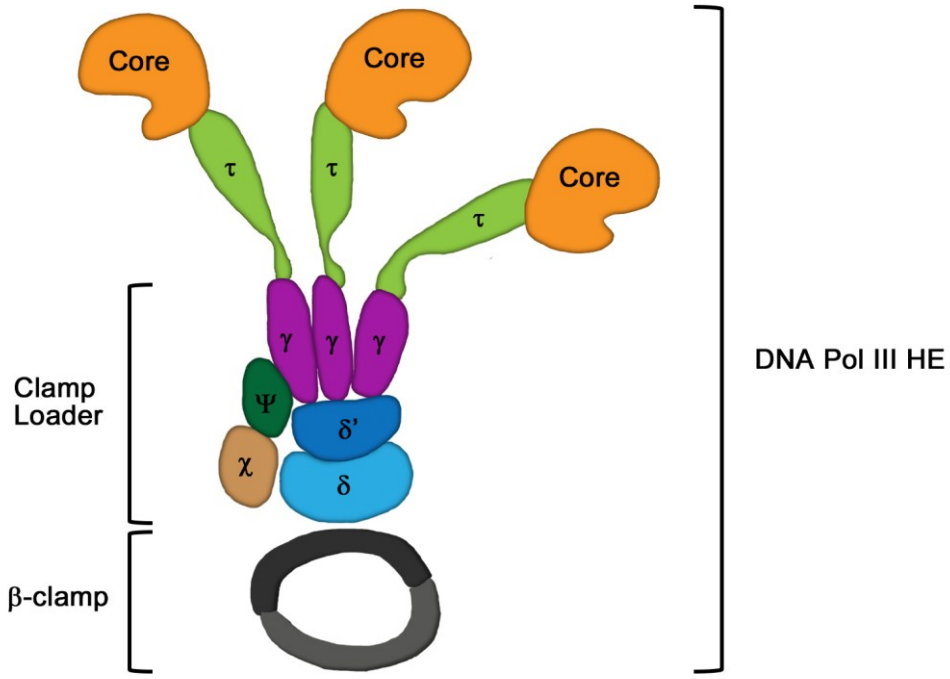


Figure 1-6. Schematic of composition of DNA Pol III HE in *E. coli* (Referred to Watson *et al.*, 2013; Reyes-Lamothe, Sherratt & Leake, 2010)

DNA Pol III core formed by subunits α, ε and θ, is responsible for the synthesis of DNA (Kelman & O'Donnell, 1995). Subunit α performs DNA polymerase activity, and subunit ε is a 3'-to-5' proofreading exonuclease (Stukenberg, Studwell-Vaughan & O'Donnell, 1991). Subunit θ interacts with subunit ε but doesn't with subunit α (Studwell-Vaughan & O'Donnell, 1993). The θ-ε interaction is reported that improves the binding between subunit α and subunit ε and stimulates the proofreading exonuclease activity of subunit ε (Studwell-Vaughan & O'Donnell, 1993; Taft-Benz & Schaaper, 2004). Conte *et al.* (2012) also suggests that subunit θ could stabilize subunit ε and impact the amounts of in cells.

The polymerase activity of DNA Pol III core is stimulated by the β-clamp (LaDuca *et al.*, 1986). The β-clamp is constituted by two β subunits as a dimeric ring-shaped complex (Oakley *et al.*, 2003). It binds the free 3'-OH of an RNA primer at a primer-template junction, and interacts with DNA Pol III core at the

seven C-terminal residues of subunit α (Stukenberg, Studwell-Vaughan & O'Donnell 1991; Burnouf *et al.*, 2004). DNA Pol III core is linked by the β-clamp and synthesizes DNA in the 5'-to -3' direction with the high processivity (LaDuca *et al.*, 1986).

According to the discontinuous DNA synthesis on the lagging strand, when the "first" core polymerase arrives the terminal of the Okazaki fragment, it leaves the β-clamp, and then the β-clamp is loaded off by the clamp loader from DNA (Watson *et al.*, 2013). Meanwhile, when another β-clamp targets the newly primed lagging strand, the unengaged "second" DNA Pol III core recognizes the next primer-β complex on the lagging strand and starts to synthesize the new Okazaki fragment. The "first" DNA Pol III core becomes the unoccupied state and waits to recognize the next replicative start point on the lagging strand. On the other band, the "third" DNA Pol III core synthesizes DNA on the leading strand continuously from the initiation of DNA replication and has no rotation (Watson *et al.*, 2013). Importantly, both the loading and the unloading of the β-clamp on DNA template require the function of the clamp loader complex (Leu *et al.*, 2000; Yao *et al.*, 2000). In general, this model envisages a mechanism that two core polymerases alternately synthesize new Okazaki fragments along the lagging strand in *E. coli*.

The clamp loader complex of *E. coli* is formed by five subunits, γ, δ, δ′, χ and Ψ (Kelman & O'Donnell, 1995). The core and the clamp loader are bridged by subunits τ (Kelman & O'Donnell, 1995). Interestingly, subunits τ and γ are all encoded in the *dnaX* gene (Blinkowa & Walker, 1990). Subunit τ is expressed with the full length (~71 kDa), γ protein is smaller (~47 kDa) (see Table 1-1). Due to a ribosomal frameshift, subunit γ is truncated by a stop codon, and subunit τ contains the additional sequence at its C-terminal (Tsuchihashi & Kornberg, 1990). The extra C-terminal sequence provides the capacity for

subunit τ to bind to the core complex of DNA Pol III and DNA helicase DnaB (Stukenberg, Studwell-Vaughan & O'Donnell 1991; Kim *et al.*, 1996a; Yuzhakov, Turner & O'Donnell, 1996). Two independent domains had been reported to be performed the τ-α interaction and the τ-DnaB interaction respectively at the C-terminal of subunit τ (Gao & McHenry, 2001a; Gao & McHenry, 2001b). Each subunit τ binds a subunit α and dimerizes DNA Pol III core complex to synthesize DNA on both two template strands (Studwell-Vaughan & O'Donnell, 1991; Kim *et al.*, 1996a). Furthermore, subunit τ interacts with DNA Pol III core at the β binding site of subunit α with high affinity on dsDNA and low affinity primed ssDNA (de Saro, Georgescu & O'Donnell, 2003). When DNA synthesis is completed, subunit τ blocks the association between the core and the β-clamp and leads DNA Pol III core to leave beta clamp (Kim *et al.*,1996b).

In addition, subunit τ interacts with DnaB helicase at its fourth domain (Gao & McHenry, 2001a). Previous studies revealed that at least two subunits of τ protein interact with DnaB together during DNA replication (Gao & McHenry, 2001a; Dallmann *et al.*, 2000). This τ-DnaB interaction is pivotal for DNA Pol III HE to perform prossitive DNA synthesis forward the replication fork (Kim *et al.*,1996a; Dallmann, Thimmig & McHenry, 1995). Without the τ-DnaB interaction, the process of DNA synthesis by DNA Pol III HE was rapidly slowed down from one thousand nucleotides to thirty-five per second (Kim *et al.*, 1996a). According to the lacking of C-terminal domains of subunits τ, subunit γ cannot interact with neither DNA Pol III core nor DnaB helicase (Yuzhakov, Turner & O'Donnell, 1996). In both subunits τ and subunit γ, the shared domain directs their oligomerization and also contains the binding sites for clamp loader components (Glover, Pritchard & McHenry, 2001). As a consequence, subunits τ and γ perform the clamp loading function, which is interconvertible during DNA replication (Gao & McHenry, 2001a).

Subunits τ and γ are AAA+ family ATPases, and each protein can interact with one molecule of ATP (Tsuchihashi & Kornberg, 1989; O'Donnell *et al.*, 1993). Structural study of γ crystal shows subunit γ has a conformational change at the N-terminal induced by ATP-binding (Podobnik *et al.*, 2003). Therefore, subunit τ.γ is considered as the motor of the clamp loader (O'Donnell, Jeruzalmi & Kuriyan, 2001). The conformational change of the τ.γ motor affects the interaction between subunit δ′ and δ in ATP-bound state (O'Donnell, Jeruzalmi & Kuriyan, 2001). Subunit δ interacts with one subunit of the β dimer and opens the ring clamp up from the interface between two β subunits (Stewart *et al.*, 2001). Subunit δ' is responsible for stabilizing the binding of δ with β-clamp (Oyama *et al.*, 2001). As a consequence, the opened β-clamp is loaded onto the newly primed strands. The clamp loader then leaves the β-clamp after the ATP hydrolysis (O'Donnell, Jeruzalmi & Kuriyan, 2001). The β-clamp binds to the primer-template junction and directs DNA Pol III core to synthesize DNA on parental strands as described above. On the lagging strand, when an Okazaki fragment is completed, the interaction of the β-clamp and DNA Pol III core is blocked by τ protein (de Saro, Georgescu & O'Donnell, 2003). After the core polymerase leaves the β-clamp, subunit δ binds to the β-clamp, the activity of the ring opening allows the β-clamp to be released from DNA (Turner *et al.*, 1999).

On the other hand, the clamp loader interacts with the ssDNA covered with SSB protein rather than the naked ssDNA (Fradkin & Kornberg, 1992). The interaction between the clamper loader and SSB protein is bridged through the role of subunits χ and Ψ (Tondnevis *et al.*, 2015). Subunits χ and Ψ constitute a tight heterodimer with a molar ratio of 1:1 (O'Donnell & Studwell, 1990; Xiao, Dong & O'Donnell, 1993). Meantime, Subunit ψ associates with γ protein at its C-terminal domain, and stabilises the conformational change of the clamp loader induced by γ-ATP binding (Glover & McHenry, 1998; Gao & McHenry,

2001a). Subunits χ directly binds to SSB protein at SSB's C-terminal domain, and the binding is significantly enhanced when SSB proteins coat on the DNA template (Kelman *et al.*, 1998; Witte, Urbanke & Curth, 2003).

Multiple proteins involved in DNA replication is a pivotal and complicated mechanism, which performs with high accuracy and integrity in various living organisms. As an important modern organism, the process of *E. coli* DNA replication has been most extensively studied. Simultaneously, with the improvement of research technologies *in vitro* and *in vivo*, its mechanism is constantly extended and developed as a more fascinating system. Notably, DNA Pol III HE is not only the crucial replication machinery but also have an irreplaceable role in *E. coli* mismatch repair system (Modrich & Lahue, 1996).

1.3 DNA damage repair mechanisms

For living cells, many metabolic activities and environmental factors may lead to DNA damaging lesions. These lesions are able to induce structural damages or create potentially harmful mutants which affect gene coding and the integrity of genome and cell survival (Lodish *et al.*, 2004). To defend the genomic stability, intrinsic multiple DNA repair mechanisms are activated to response these lesions that resisting DNA damage and restoring the original inherent DNA sequence and structure (Fig. 1-7).

Two types of response pathways are carried out by DNA repair systems. One is to directly reverse DNA damage. Only few damaging lesions can be repaired by the mediation of relevant proteins in direct reversal. For sample, O^6-Alkyl-guanine dimer is caused by alkylating agents, and is repaired by alkyl transferase-mediated reversal.

On the other hand, most damaging lesions are repaired via the pathway of DNA excision, which is carried out by stepwise catalytic processes from relevant enzymes. Based on different biochemical and mechanical properties, the repair pathway of DNA excision can be divided into three systems, base excision repair, mismatch repair and nucleotide excision repair (Watson *et al.*, 2004).

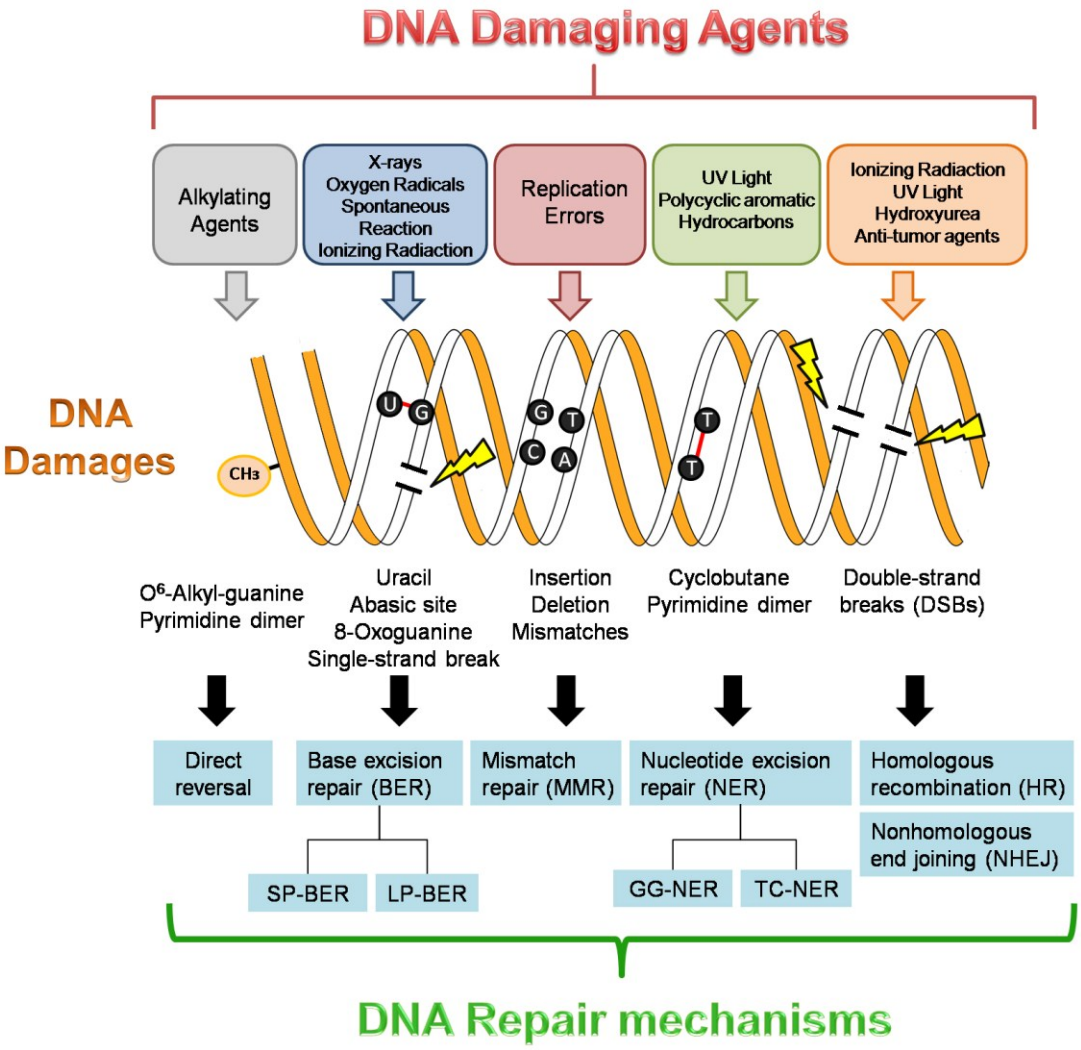


Figure 1-7. General scheme of biological DNA repair

Base excision repair (BER) particularly recognises and corrects small and non-distorting base damaging lesions, including oxidation, alkylation, deamination and even the absence of bases. Moreover, BER is also able to repair single strand breaks of DNA (Bjelland & Seeberg, 2003). In BER system, DNA with

damaged based is restored through multiple coordinated activities from relevant enzymes, including removing the damaged base, cleaving the phosphodiester backbone and resulting an apurinic/apyrimidinic site, digesting the termini from the flank, re-synthesizing nucleotides and sealing the remaining nick (Liu *et al.*, 2007). Based on the amount of nucleotides to be synthesized, the BER system is divided by short-patch BER (SP-BER) (synthesizing one nucleotide) and long-patch BER (LP-BER) (synthesizing 2-20 nucleotides) (Liu *et al.*, 2007).

Nucleotide excision repair (NER) is a widespread repair mechanism which is able to repair UV-induced DNA damage. In comparison with the BER mechanism, which can only respond to and correct damaged bases by initiation of the specific glycosylase class, enzymes of NER recognize bulkier distortion lesions in the shape of the DNA double helix, such as pyrimidine dimers (Fuss & Cooper，2006). More than 20 proteins are coordinated in the process of NER, inclucing recognising the damage, unwinding the double helix nearby the damage lesion, cleavage of damaged strand on both side of the lesion, re-synthesising DNA with the correct sequence and sealing the nick by ligase (Nakano *et al.*, 2007). The NER system proceeds via two different modes, transcription-coupled repair (TCR-NER) and global genome repair (GGR-NER). TCR-NER specifically repairs lesions that block transcription whereas GGR-NER removes DNA damage from any place in the genome (Fuss & Cooper，2006).

Mismatch repair (MMR) performs the correction of mispaired nucleotides that arise during DNA replication, including base mispairings and short insertion-deletion loops, thereby avoiding mutations from being permanently retained after cell divisions (Modrich & Lahue, 1996; Kolodner & Marsischky, 1999). Since MMR is responsible for repairing replication-related mismatches, genetic

defects in MMR cause the increased rate of spontaneous mutations and seriously affect genomic stability (Harfe & Jinks-Robertson, 2000). As the focus of this study, MMR is elaborated in following sections of this chapter.

Furthermore, not only errors of nucleotides can arise, but the direct damage of the sugar-phosphate backbone is also inevitable in the living process of a normal cell. DNA double-strand breaks (DSBs) occur in living cells via the induction by reactive oxygen species in metabolic activities and other harmful factors in the environment, including chemical agents, irradiation and even UV light. Two key mechanisms for repairing DSBs have been reported, including non-homologous end-joining (NHEJ) and homologous recombination (HR) (Lieber, 2010).

In NHEJ, the Ku protein recognises the break and binds to both sides of the break by its ring structure. By the Initiation of Ku, DNA-dependent protein kinase catalytic subunit (DNA-PKcs) is recruit to bridge DNA ends and activate end-modifying proteins, polymerases and ligase IV to restore the damaged DNA. A special type of NHEJ, alternative nonhomologous end-joining (Alt-NHEJ), is found to proceed via a Ku-DNA-PKcs independent mechanism, which always leads to the deletion of sequences (McVey & Lee, 2008). Due to the lack of homologous sequence, the method of NHEJ, including Alt-NHEJ, is error-prone when broken DNA pieces are directly rejoined (Boulton & Jackson, 1996). In higher eukaryotes, NHEJ pathway occurs in all phases in the cell cycle (Pardo, Gómez-González, & Aguilera, 2009).

Unlike NHEJ, HR pathway requires a sister chromatid as a template to align the genetic information, thereby repairing the damaged chromosome accurately (Wyman, Ristic & Kanaar, 2004). Therefore, in the cell cycle, HR is only available to repair DSB in late S phase or G2 phase in eukaryotes, during which

mitosis occurs (Pardo, Gómez-González, & Aguilera, 2009). The process of HR is sequentially coordinated by activities of relvant enzymes. In *E. coli,* firstly, the single strand 3' overhangs are generated on both sides of the DNA break by the RecBCD complex (Dillingham & Kowalczykowski, 2008). The strand of one 3' overhang then invades the homologuos template by the RecA protein (De Vlaminck *et al.*, 2012). Following the strand invasion, DNA polyermerase extends the invading strand at the 3' end based on the undamaged DNA strand. Meanwhile, the non-invading strand of the damaged DNA is also extended on the homologuos complementary strand during strand invasion. Subsequently, branch migration is carried out by RuvA and RuvB, and double Holliday junctions are nicked by the RuvC resolvase (West, 2003). Finally, DNA ligase seals the nick of DNA strands. Although more protein complexes are involved in the eukaryotic HR mechanism, they implement a similar general pathway of prokaryotic HR (Wyman, Ristic & Kanaar, 2004).

In the mechanisms discussed above, DNA repair mainly undergos the process of damage recognition, erros removal and the re-signthesis of correct DNA. However, sometimes DNA polymerases may encounter an DNA contianing unrepaired errors during DNA replication. Therefore, translesion synthesis (TLS) is stimulated to lead the relication machinery to bypassing the error and proceeding the replication (Waters *et al*., 2009). Specific DNA polymerases carried out TLS in both prokaryotes (DNA Pol II, Pol IV and Pol V) and eukaryotes (DNA Pol η, Pol κ, Pol ι and Rev1). In *E. coli*, DNA polymerases of TLS do not occur in normal DNA replication. Therefore, the genes of TLS polymerases are expression as a pathway of SOS response (Patel *et al*., 2010). Although this mechanism is erro-prone and induces mutations without the removal of damage, it avoids the worse results which may cause incompletely replicated chromosomes in cells (Waters *et al*., 2009).

The biological DNA damage response system may be stimulated at the checkpoints of the cell cycle, which modulates the network of signalling pathways that provides extra time to repair damaged DNA in cells. There are three major checkpoints which occur before entering the S phase of the cell cycle, before entering mitosis and in the process of replication (Löbrich & Jeggo, 2007). The checkpoints verify that the integrity of cell processes at each phase of the cell cycle as their names suggests that have been finished before progression into the next phase (Löbrich & Jeggo, 2007).

In cells, global responses to DNA damage is responsible for various DNA repair systems, the control cell cycles checkpoints, transcriptional regulations, or apoptosis (Friedberg *et al*., 2005). When a cell experiences DNA damage, it would face two consequences, undergoing apoptosis (multicellular organisms only) and death, or surviving with the repaired genome.

1.4 DNA mismatch repair

1.4.1 DNA mismatch repair in *E. coli*

In both prokaryotes and eukaryotes, maintenance of genome integrity is the key to organism survival. Due to the presence of base tautomers, DNA code errors can be introduced by DNA replication (Fig. 1-8). DNA polymerases have proofreading 3'-5' exonuclease activity to degrade incorrect nucleotides from the 3 'end of the new chain of DNA. In general, DNA polymerases reduce the appearance of a mismatch to one in each 10^7 synthesized nucleotides (Watson *et al.*, 2004). However, this mismatch rate is still approximately a thousand times of the actual appearance of mutation in a typical living cell (Watson *et al.*, 2004). Therefore, the correction of mismatched DNA which escaped polymerase proofreading requires specific DNA repair systems in organisms.

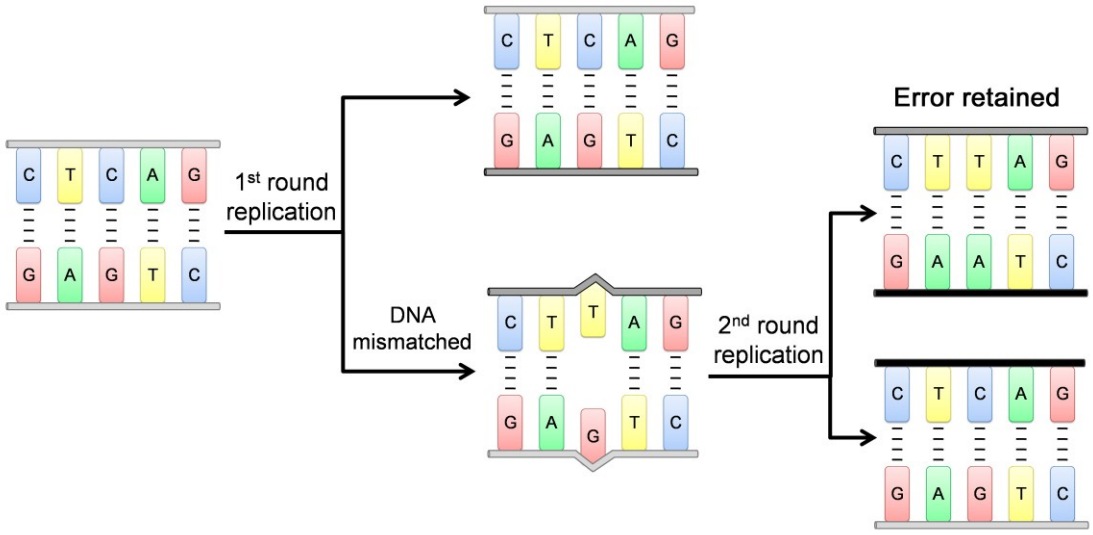


Figure 1-8. Schematic of the introduction of a mutation during DNA replication (Referred to Watson *et al.*, 2004)

In the first round of DNA replication, a "T" base may be mismatched with the "G" base. This mutation could be permanently retained in the second round of DNA replication

One of several DNA repair systems is the DNA mismatch repair (MMR) system, which recognises and corrects base mispairings and short insertion-deletion loops that occur during DNA replication (Belland, 1991; Schofield & Hsieh, 2003). Deficiencies in MMR systems lead to frameshifts and alterations in gene transcription and translation, potentially leading to loss of gene function (Belland, 1991). For most organisms, MMR and the proteins required to perform it fully are integral parts of cellular function and survival.

The study of MMR systems has been developed in both prokaryotes and eukaryotes, including *Thermus Aquaticus*, *Escherichia coli*, *Saccharomyces cerevisiae* and even humans. Out of these organisms, studies in *E. coli*'s MMR system have been most extensively and distinctly reported. MMR from *E. coli* is carried out by four major steps, mismatch recognition, strand discrimination, mismatch removal and DNA re-synthesis. The mismatch recognition was carried out by MMR protein MutS. Through the coordination with other two

MMR proteins MutL and MutH, strand discrimination is achieved. Subsequently, DNA helicase UvrD and an exonuclease, including RecJ, ExoI, ExoVII and ExoX, remove the mismatched DNA. The correct DNA is then resynthesized by DNA Pol III HE and and is sealed by DNA ligase (Table 1-2) (Fig. 1-9) (Schofield & Hsieh, 2003; Spampinato *et al.*, 2009). Compared to other model organisms, the machinery of MMR system from *E. coli* has been determinded via varied studies *in vitro* and *in vivo* (Lahue, Au & Modrich, 1989; Cooper, Lahue & Modrich, 1993; Burdett *et al.*, 2001).

Protein	Function
$(MutS)_2$	Mismatch recognition and binding
$(MutL)_2$	Intermediate protein for strand discrimination; Mismatch excision termination
MutH	Endonuclease; Strand discrimination based on Dam methylation
UvrD	DNA helicase
ExoI, ExoVII, ExoX, RecJ	Exonuclease; Mismatch and DNA excision
DNA Pol III HE	Re-synthesis of excised DNA
SSB	Binding and protection of ssDNA
DNA Ligase	Ligation of DNA nick

Table 1-2. *E. coli* MMR proteins and their function (Spampinato *et al.*, 2009)

This MMR system is initiated by the action of MutS, the mismatch recognition protein (Su *et al.*, 1988). MutS recognizes and binds 7 types of base pair mismatches (except the “C-C” mismatch) and short nucleotide insertion-deletion (Su & Modrich,1986; Parker & Marinus, 1992; Jiricny, 1998; Obmolova *et al.*, 2000). In addition, the ATPase activity of MutS is required for actuating the process of MMR (Bjornson *et al.*, 2003). Once MutS arrests the mismatched DNA, MutL is recruited to MutS (Larrea, Lujan & Kunkel, 2010). MutL is a homodimic protein and also possess the ATPase activity. MutL’s ATP-hydrolysis activity is essential to activate strand discriminate, which is carried out by endonuclease MutH and is coordinated by the MutS-MutL complex (Larrea,

Lujan & Kunkel, 2010). MutH is stimulated by MutL and specifically distinguishes the newly syntheiszed strand which containing the mismatch, from the template strand at dGATC sites via the different Dam methylation status (Au, Welsh & Modrich, 1992; Schofield & Hsieh, 2003).

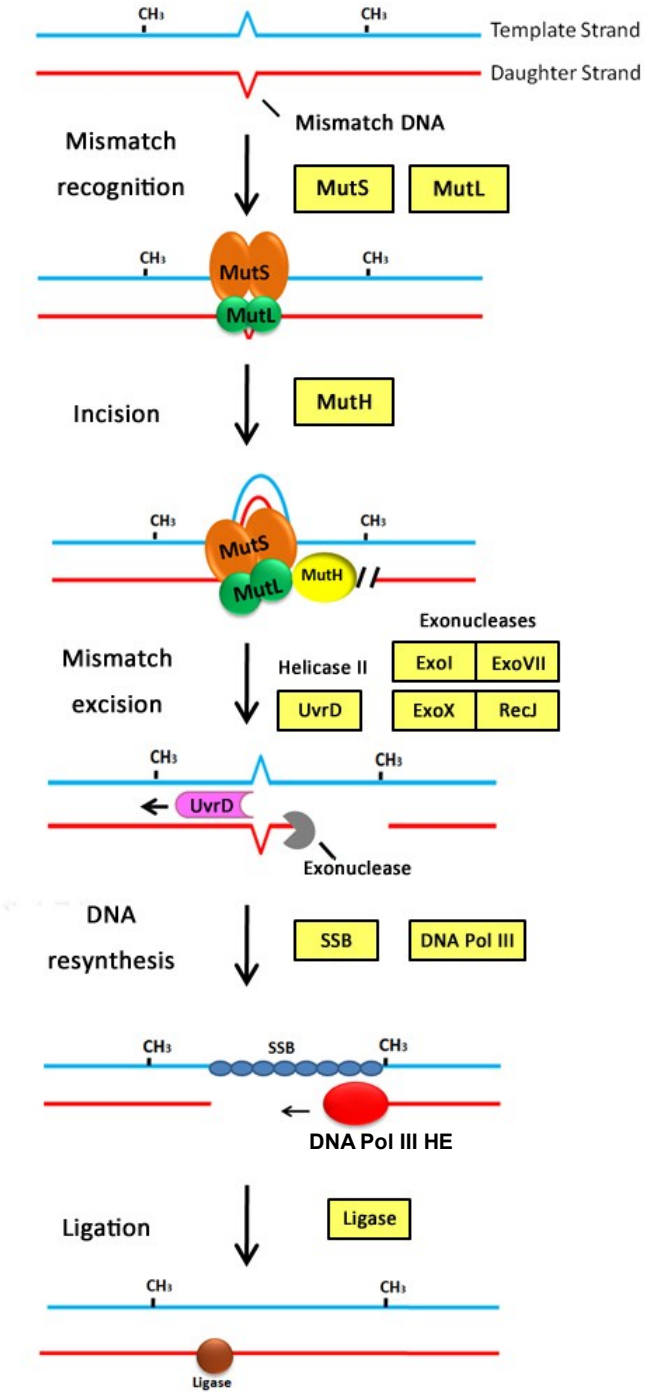


Figure 1-9. Schematic of mismatch repair system from *E. coli.*

MutH nicks the daughter strand at the unmethylated dGATC site (Lee *et al.*, 2005). As a result of the nick, DNA helicase UvrD and SSB protein are loaded onto the strand which leads to digestion of ssDNA by either 3' or 5' exonucleases from the nick to the site of mismatch (Lee *et al.*, 2005). Exonuclease I or X as a 3' exonuclease degrades the single strand from the 3'-end to the 5'-end. If the nick is located on the 5' terminal of the site of mismatch, RecJ or Exonuclease VII will digest ssDNA from 5' to 3' direction (Lee *et al.*, 2005). The DNA fragment containing the error is replaced by resynthesis by DNA Pol III HE. Finally, DNA ligase binds the remaining nick to complete the MMR process (Fig. 1-9) (Spampinato *et al.*, 2009).

1.4.2 The initiation of MMR in *E. coli*

E. coli MutS protein (*Ec*MutS) is a homodimer and shaped like the praying hands in the co-crystal with a mismatched DNA (Fig. 1-10A) (Lamers *et al.*, 2000). *Ec*MutS is a modular protein, is constituted by several domains, including the clamp domain, the core domain, the connector domain, the mismatch-recognition, the ATPase domain and the Helix-turn-helix domain (Fig. 1-10A) (Lamers *et al.*, 2000; Obmolova *et al.*, 2000).

The clamp domain is the "fingertip", which is constructed by a four-stranded antiparallel β-sheet and performs the switching function of the clamp-like structure (Acharya, 2008; Lamers *et al.*, 2000). The "fingers" are composed of two α-helices of the core domain, which join with each other to compose a helical bundle, called the "levers" (Lamers *et al.*, 2000). The connector domain is linked to the core domain, and has a similar fold to the Holliday junction resolvase ruvC (Ariyoshi *et al.*, 1994; Lamers *et al.*, 2000). The core and connector domains constitute the palm part of the praying hands together, and enfold around, but does not contact with DNA (Lamers *et al.*, 2000). The mismatch-recognition domain is located at the "thumbs", and specifically

identifies and binds to mismatches in DNA (Lamers *et al.*, 2000; Jiricny, 2006). The ATPase domain is connected with the core domain and contains the Walker A motif [GX4GK(T/S)], as known as the P-loop, which is associated with the binding of ATP (Walker *et al.*, 1982; Lamers *et al.*, 2000). In addition, the "wrists" of hands are composed and associated by the ATPase domains and the Helix-turn-helix domains of two *Ec*MutS subunits, thereby contributing to the dimerization (Lamers *et al.*, 2000; Jiricny, 2006).

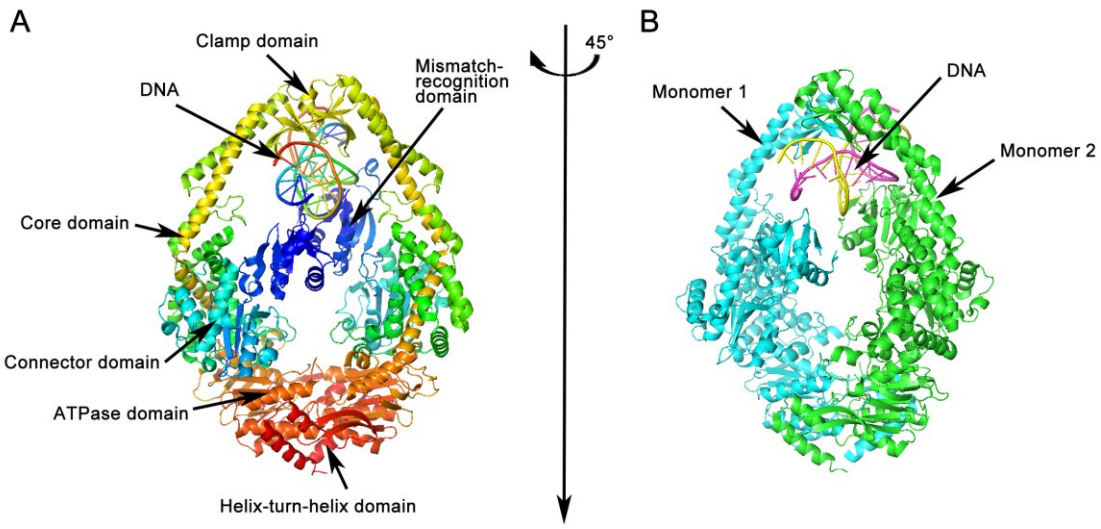


Figure 1-10. Structure of the *Ec*MutS–DNA complex

A crystal structure of *Ec*MutS binding to DNA contained a G-G mismatch (PDB: 1OH7), was analysed using the PyMOL software. A) The front view of *Ec*MutS mismatch binding. Domains of *Ec*MutS were exhibited with different colours. B) The side view of *Ec*MutS mismatch binding, rotated 45° from the A structure. The first monomer was in cyan-blue and was free of DNA. The second monomer was in green and bound to DNA in the mismatch-recognition domain.

At the other side of *Ec*MutS, in the absence of DNA, two clamp domains of *Ec*MutS monomers maintain a limited interaction and form a loose clamp-like structure (Lamers *et al.*, 2000). When *Ec*MutS contacts with DNA, the dimer is opened and weakly associates with DNA in a mismatch-independent manner at the clamp domain. This loose and non-mismatch discriminated interaction is considered to be directed from the formation of salt bridges between the phosphate group on DNA backbone and positively changed surfaces of the

clamp domain (Lamers *et al.*, 2000; Obmolova *et al.*, 2000). A mismatch on the DNA is recognised and bound by the mismatch-recognition domain whereas DNA without mismatch dissociates from *Ec*MutS (Obmolova *et al.*, 2000; Jiricny, 2006). It is worth noting that only one subunit of *Ec*MutS dimer specifically bind the mismatch site at the mismatch-recognition domain, while the other subunit maintains weak contacts with DNA (Lamers *et al.*, 2000; Kunkel & Erie, 2005). As a consequence, *Ec*MutS dimer displays as an asymmetry at the structural level due to different conformations of the two subunits on mismatch recognition (Fig. 1-10B) (Mendillo, Putnam & Kolodner, 2007). This observation suggests that there is asymmetry in the homodimer-DNA complex and the protein might be considered heterodimer-like, as MutS in eurkaryotes (Acharya, 2008).

In the mismatch-bound subunit, the mismatch site is specifically anchored by wedging the phenylalanine residue (Phe36) of the Phe-X-Glu motif in the mismatch-recognition domain (Lamers *et al.*, 2000; Jiricny, 2006). The previous mutational study was reported when the Phe36 residue of *Ec*MutS was substituted by an alanine, the F36A protein failed to recognise and bind to base pairing and insertion-deletion mismatches neither *in vitro* nor *in vivo* (Yamamoto *et al.*, 2000). The Phe36 insertion of DNA is performed from the side of the minor groove and stacks the mismatched bases towards the major groove, thereby resulting in the kink and a widened minor groove (Lamers *et al.*, 2000; Obmolova *et al.*, 2000). Consequently, this kink destabilises surrounding base pairs and bends the DNA chain around the mismatch site with an angle of approximately 60° degrees (Isaacs, Rayens & Spielmann, 2002; Natrajan *et al.*, 2003). Meanwhile, the glutamate residue (Glu38) of the Phe-X-Glu motif constructs a hydrogen bond to two mismatched bases (Lamers *et al.*, 2000; Jun, Kim & Ban, 2006).

In addition to these mismatch-specific interactions from Phe36 and Glu38, other protein side chains of the mismatch-recognition domain non-specifically interact with the DNA backbone via van der Waals contacts and hydrogen bonds (Lamers *et al.*, 2000; Jun, Kim & Ban, 2006). When *Ec*MutS binds to the mismatched bases, the joint action of the mismatch-recognition and clamp domains constantly bends the DNA backbone (Lamers *et al.*, 2000). The flexibility of DNA backbone where mismatch arising may determine the stability and formation of mismatch recognition and binding by *Ec*MutS (Yang, 2006).

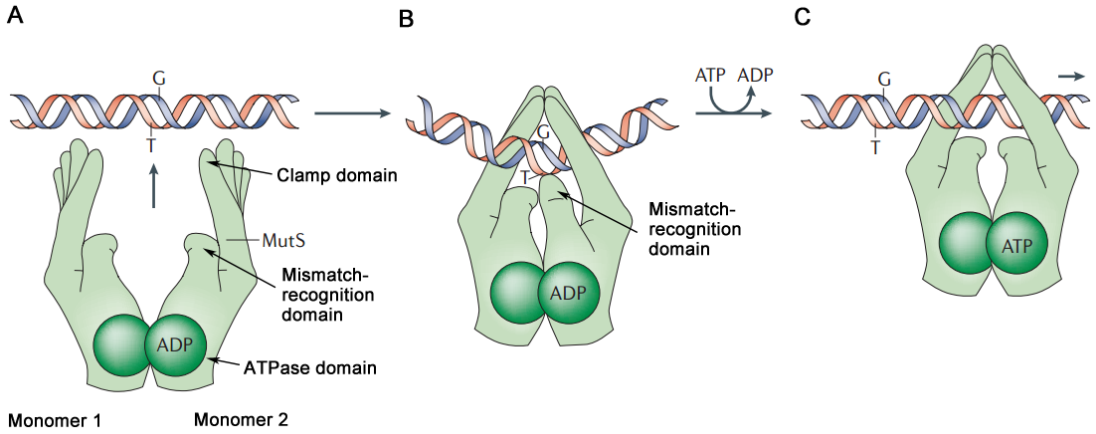


Figure 1-11. Schematic of the mismatch-binding activity of *Ec*MutS [Adapted from Jiricny, 2006. Copyrights with permission (see Chapter 8 Appendix)]

(A) *Ec*MutS dimer binds to DNA with a T/G mismatch in the ADP-bound state. When *Ec*MutS contacts DNA, the clamp domains are open, and the homodimer is dimerised in the ATPase sites. (B) The mismatch-recognition domain specifically binds to the mismatch site. Phe36 residue of one subunit inserts into the mismatches bases from the minor goove side and wedges the DNA backbone, and Glu38 from the same subunit interact with the mismatched bases via hydrogen bonds. The DNA backbone is bent by the joint activity of the mismatch-recognition and clamp domains. (C) Due to the exchange of ADP-ATP, the conformation of *Ec*MutS is changed so that the mismatch site is released, and the clamp domains are closed tightly around DNA. This sliding clamp structure could allow *Ec*MutS to translocate along DNA.

Many studies reveal that the communication between ATPase and mismatch-recognition domain of *Ec*MutS occurs during MMR (Alani *et al.*, 2003). The mismatch binding is inclined to be performed when *Ec*MutS is in the ADP-bound state (Blackwell *et al.*, 2001; Acharya *et al.*, 2003; Acharya, 2008). Co-crystal of *Ec*MutS and the mismatched DNA indicates that the mismatch-bound subunit

of *Ec*MutS is bound to ADP in its ATPase domain whereas the ATPase domain of the other *Ec*MutS subunit is unoccupied (Lamers *et al.*, 2000). With the binding of ATP, a larger surface of *Ec*MutS is observed to contact the mismatched DNA and the ATPase domain becomes more compact (Lamers *et al.*, 2000; Alani *et al.*, 2003; Jiricny, 2006). Previous studies suggest that the ATP binding and downstream hydrolysis can modulate the changes of the C-terminal conformation, and impact the mismatch-recognition domain of *Ec*MutS by transmitting through domains (Kunkel & Erie, 2005). The conformational change leads the inserted Phe36 to be pulled out from DNA, and two clamp domains are closed tightly (Lamers *et al.*, 2004; Acharya, 2008). Therefore, the ATP-binding is considered to promote *Ec*MutS to form the conformation as a sliding clamp, which is able to translocate along DNA (Fig. 1-11) (Biswas & Vijayvargia, 2000; Jiricny, 2006).

In addition, the other functional study demonstrates that mismatched DNA is dissociated from *Ec*MutS with the addition of ATP, and this releasing activity is abolished in the presence of the *E. coli* MutL (*Ec*MutL) (Galio, Bouquet & Brooks, 1999). It implies *Ec*MutL may stabilize the mismatch binding of *Ec*MutS.

In *E. coli*, the ATP-bound *Ec*MutS is known to interact with an *Ec*MutL homodimer to direct downstream strand discrimination (Jiricny, 2006). However, since the strand discriminational dGATC site can be far from the mismatch site (~1000 base pairs away), the mechanism that links the signal for mismatch recognition and downstream strand discrimination are hotly debated. There are three avaible models to amply to explain the binding of *Ec*MutS-*Ec*MutL.

The first model is established on electron microcopy studies, which observed that *Ec*MutS converted the mismatched DNA as a α-like loop structure, which contained the mismatch site, and was dependent on ATP-hydrolysis (Allen *et*

al., 1997). Therefore, a model of the MMR initiation was proposed that *Ec*MutS translocates DNA after mismatch recognition, and is powered by ATP hydrolysis bi-directionally. The flanking DNA is pulled toward *Ec*MutS and formes a DNA loop nearby the mismatch site. This loop leads the location of mismatch and Dam methylation to being closer. Subsequently, *Ec*MutL and *E. coli* MutH (*Ec*MutH) are recruited sequentially to *Ec*MutS and then *Ec*MutH performs the nicking activity at the unmethylated GATC site (Allen *et al.*, 1997).

The second model was based on the sliding clamp structure of *Ec*MutS bound ATP. When *Ec*MutS dissociates with the mismatch site in the ATP-bound state, the sliding clamp interacts with *Ec*MutL, and *Ec*MutS- *Ec*MutL complex tracks along the DNA in search of the signal for strand discrimination. In combination with *Ec*MutH, the dGATC site is recognised (Acharya *et al.*, 2003). ATP-hydrolysis does not occur with the binding of *Ec*MutS–*Ec*MutL complex until MutH is found. The mainly difference between first two models is focused on how *Ec*MutS approaches the strand discrimination signal. However, both models suggest that *Ec*MutS has to move away from the mismatch site before activating the repair process.

In the other model, the complex of *Ec*MutS–*Ec*MutL with ATP remains bound at the mismatch site during the process of MMR. The activity of hunting the signal for strand discrimination is carried out by the interaction between *Ec*MutS–*Ec*MutL and *Ec*MutH bound separately at the mismatch and dGATC sites respectively. Communication occurs via looping the DNA between the mismatch site and the hemi-methylated site, rather than translocating along the DNA by *Ec*MutS–*Ec*MutL (Junop *et al.*, 2001; Schofield *et al.*, 2001).

Furthermore, Bjornson *et al.*'s study (2003) reveals that *Ec*MutS can exist as a mixture of dimers and tetramers, which increases the binding of the mismatched DNA. This study also suggests a possible model that one *Ec*MutS dimer of the tetramer remains bound at the mismatch site, while the other dimer perfroms tracking for strand discrimination signals along the DNA (Bjornson *et al*., 2003).

To sum up, in *E. coli*, the major role of the *Ec*MutS-*Ec*MutL interaction is to bind mismatch and recruit *Ec*MutH to perform stand discrimination at the hemi-methylated dGATC site and directs the excision of mismatch. However, for other organisms, prokaryotes and eukaryotes alike, the key question of stand discrimination remains. To advance this, the MMR mechanism from a wider number of organisms is considered.

1.4.3 MMR beyond *E. coli*

As a classic model organism, *E. coli* is always a starting point for studies of biological mechanisms which extends to other prokaryotes and eukaryotes. *E. coli* MMR system is the thus far most understood system and widely reported, however, it condusts a unique paradigm which can not completely apply to most prokaryotes and all eukaryotes. Some reasons could explain for the specific system of *E. coli* MMR. Firstly, MutH is a critical strand discrimination endonuclease in *E. coli*, but there is no MutH homologue in no *E. coli* relative organisms. Secondly, DNA methylation gene *dam* is not conserved in all organisms, and not all organism methylates their DNA to media with MMR proteins. Consequently, the role of MutH endonuclease must be taken by other proteins or a larger complex for a variant pattern in MutH-lacking organisms.

As MutS from *E. coli* (*Ec*MutS), many MutS homologues from MutH-lacking organisms also recognise mismatches and directly bind to mismatched DNA

and subsequently recruit MutL into the MMR system (Fukui *et al.*, 2011). Bacterial MutS homologues contain the ATPase domain, and the ATPase activities are indicated to be critical for the MMR function. The P-loop (GXXXGKS/T) is a glycine-rich motif, has a role in the interaction with ATP. In *Salmonella typhimurium*, the mutant lysine residue in the P-loop of MutS decreased either DNA binding or ATPase activities (Haber & Walker, 1991). In addition, MutS activity is found to modulated according to ATP hydrolysis situations in both *E. coli* and human. Once ATP binds to MutS, the MutS-mismatch interaction is destabilised, and the conformation of MutS is reorganised as a sliding clamp (Allen *et al.*, 1997; Gradia, *et al.*, 1999; Biswas & Vijayvargia, 2000; Joshi *et al.*, 2000).

When the mismatch recognition and the MutS-MutL complex are achieved, *E. coli* MMR carry on the strand discrimination via the coordination between the MutS-MutL complex and MutH. However, due to the loss of MutH homologues, the MutS-MutL complex from other organisms should proceed a different pathway. It's important to realise that *Ec*MutL from *E. coli* has no endonuclease activity, but some MutL homologues from MutH-lacking organisms are demonstrated their endonuclease activities *in vitro* assays (Duppatla *et al.,* 2009; Pillon *et al.,* 2010; Iino *et al.,* 2011). Therefore, to achieve strand discrimination, MutL from MutH-lacking species should involve in tracing an alternative replication singal which is different from Dam methylation and then nick on the newly synthesized strand.

Futhermore, Shimada *et al.,* indicated that the ATPase activity of MutL also impacts its endonuclease activity. In *Thermus thermophilus*, the endonuclease activity of *Tt*MutL was significantly inhibited by the addition of ATP in physiological concentrations, but it was activated by the addition of MutS in the presence of a mismatch (Shimada *et al.*, 2013). This implies that the ATP

hydrolysis of MutL may contribute to its endonuclease activation. However, it is still not able to explain if the ATP hydrolysis directly stimulates the nicking or promotes the combination of MutS and MutL and DNA to further support the complex to seek the signal of the strand discrimination along the DNA.

In *P. aeruginosa*, a MutH-lacking bacterium, the ATPase domain of MutL has been reported that reveals different structural and oligomerisation coditions from *Ec*MutL according to ATP hydrolysis situations via *in silico* structure prediction (Miguel *et al.*, 2013). The most obvious difference between *E. coli* MMR paradigm and others' is that ATP hydrolysis of *Ec*MutL is required for an intermediate function to proceed MMR, while it is still not confirmed if that is necessary for other MutH-lacking species (Baitinger, Burdett & Modrich; Shimada *et al.*, 2013). So far, to develop the MMR paradigm beyond the known system from *E. coli*, the strand discrimination mechanism is the major issue to be elaborated. How does MutL regulate and nicke the newly synthesized strand containing mismatches or the insertion-deletion loop? How does MutS coordinate with MutL to carry out the strand discrimination? Several protein-protein interactions related to either MutS or MutL may provide opinions towards the potential mechanism.

1.4.4 Protein-protein interactions in MMR

In MMR systems, MutS not only recruits and interacts with MutL, but also has been found to bind to the β-clamp. As mentioned above, the β-clamps including the eukaryotic homologue PCNA are shaped as the ring structure that direct DNA Polymerase III to slide along the DNA strands with the high processivity during DNA replication. Two binding sites for the β-clamp have been identified within MutS from bacteria, including *E. coli*, *B. subtilis* and *P. aeruginosa* (de Saro *et al.*, 2006).

In *E. coli*, the first β–clamp binding site (^{15}QQYL^{18}) of *Ec*MutS is located at the N-terminal domain that involves in the mismatch binding (de Saro *et al.*, 2006). Moreover, at the C-terminal domain, the second motif for β-clamp interaction (^{812}QMSLL^{816}) have been also exposed in *Ec*MutS. However, this motif has been found that is not required for *E. coli* MMR system (de Saro *et al.*, 2006). Unlike *E. coli*, the C-teriminal β-clamp binding motif has a major role in MMR system from *B. subtilis. In vivo* studies showed that the MMR activity was completely eliminated after the truncation of the last 8 residues at the C-terminal of *Bs*MutS, and the rates of mutation were grown (de Saro *et al.*, 2006). Furthermore, removal of the last 58 residues at the C-teriminal of *Bs*MutS, the β-clamp interaction from *Bs*MutS was abolished (de Saro *et al.*, 2006). These results imply that the mismatch binding from MutS may be stabilised via the MutS-β interaction (de Saro *et al.*, 2006). Nevertheless, in the MutH-lacking MMR system, MutH's role could be performed by MutL that nicks on the newly synthesized strand. Therefore, the MutL-β interactions may reveal an alternative MMR pattern in MutH-lacking organisms.

Under normal conditions, the levels of *Ec*MutS and *Ec*MutL are equivalent in the wild-type cell strains in *E. coli*, but the cellular amount of *Ec*MutL becomes limiting the MMR activity when several mismatches are induced (Feng, Tsui & Winkler, 1996; Negishi, Loakes & Schaaper, 2002). Further *in vivo* studies demonstrated that more *Ec*MutL foci were observated than *Ec*MutS when *mutH* is absent in strains that *Ec*MutS and *Ec*MutL are fused to YFP co-localise with the red fluorescent at mismatches, which in an *Ec*MutS dependent condition (Elez *et al.*, 2010; Elez, Radman & Matic, 2012). In addition to be recruited by MutS and form the MutS-MutL complex, MutL is also reported to associate with DNA Pol III HE components, including the β–clamp and the clamp loader from MutH-lacking organisms (Li *et al.*, 2008; Pillon, Miller & Guarné, 2011).

The MutL-β interaction is reported to build up at the β-clamp binding site "QLXLF" in MutL homologues (Fukui *et al*., 2011). *In vivo* study shows that all the MMR activity is almost abolished by the I490D mutation of MutL from *B. subtilis* (Pillon *et al.*, 2010). It implies the importance of the MutL-β interactions to perform the successful MMR activity. In *E. coli*, this β-clamp binding motif of MutL is also reported in *Ec*MutL, and the mutation of this motif did not eliminate the *Ec*MutL-β interaction between clamp interaction (de Saro *et al.*, 2006). It suggests that further unknown residues may mediate the interaction between *Ec*MutL and the β-clamp. Another important motif is the metal binding site, D(M/Q)HAX_2EX_4E, in MutL from many MutH-lacking organisms, but it is not observed in *Ec*MutL (Kadyrov *et al.*, 2006; Kadyrov *et al.*, 2007; Fukui *et al.*, 2008; Duppatla *et al.*, 2009; Pillon *et al.*, 2010; Correa *et al.*, 2011; Iino *et al.*, 2011). In *N. gonorrhoeae*, the metal-dependent endonuclease activity is presented at *Ng*MutL C-terminal domain (residues 460-658) (Duppatla *et al.*, 2009). Moreover, D491N and E497Q mutations led to the subdued endonuclease activity of MutL (Duppatla *et al.*, 2009). These key residues have been indicated that essential for the MMR activity from *B. subtilis in vivo* (Pillon *et al.*, 2010). A second metal binding motif, CPRGHP, has been reported that the cysteine residue is responsible for zinc ions binding, and modulates the endonuclease activity of *Aquifex aeolicus* MutL (*Aa*MutL) as well (Iino *et al.*, 2011).

Studies in *Bs*MutS indicated its C-terminal was essential for foci formation in MutS-GFP fusion cells *in vivo* when mismatches were induced (Pillon *et al.*, 2011). Despite C-terminal truncated *Bs*MutS carried out the viable mismatch binding, by *in vitro assays,* this mutant has been reduced to bind to the β-clamp (Pillon *et al.*, 2011). Complete truncation of the final 58 amino acids at the C-terminal abolished the *Bs*MutS - β-clamp interaction (Pillon *et al.*, 2011). Consequently, these studies implied that the β-clamp might involve in stabilising

the activity of MutS in the MMR system (Simmons *et al.*, 2008). In addition, the increased muatation rates were presented in the strain contained mutations in the β-clamp (Dupes *et al.*, 2010). Mutation of G73R and S181G created that mutation rates that was similar to those found when the β-clamp binding motif of MutS is mutated (Dupes *et al.*, 2010).

In contrast to *Bs*MutS, mutant MutS from *Pseudomonas aeruginosa (Pa*MutS*)* which is fail to bind to the β-clamp has been found not to adversely impact the MMR activity of the mutagenic strain compared to the wild-type strain (Monti *et al.*, 2012). Furthermore, the mutation rates are not affected by the MutS mutation, relative to the strain under natural conditions (Monti *et al.*, 2012). It is worth to notice that MMR from both *B. sutilis* and *P. aeruginosa* are MutH-independent, and this indicates that there should be variations in repair systems between MutH-lacking organisms.

1.5 *Nesseria Meningitidis*

Neisseria meningitidis (*N. meningitidis*)*,* as known as meningococcus, is a human pathogenic bacterium which mainly causes meningitis and other meningococcal infections (Stephens, Greenwood & Brandtzaeg, 2007). *N. meningitidis* is known to have six pathogenic serogroups. According to the report of the genomic sequence, serogroup B of *N. meningitidis* MC58 strain contains approximately 2.2 million bases which is able to encode more than 2000 genes (Tettelin *et al.*, 2000).

The motivation of studying on the mismatch repair system from *N. meningitidis* involves in two inspects. In the first place, MMR proteins are demonstrated that are highly related to phase variation which facilitates pathogen strains to escape and survive from a changing environment and host immune system (Martin *et al.*, 2004). In the next place, as a MutH-lacking organism, the MMR

system from *N. meningitidis* could represent an alternative paradigm compared to extensively studied *E. coli* MMR system.

Phase variation performs an escaping mechanism of infectious microorganisms that elude the host immune system, which is regulated by switching on/off of antigenic genes expression (Deitsch, Lukehart & Stringer, 2009). In *Neisserial* species, genes involving phase variation mainly direct the expression of surface structures and capsule (Richardson & Stojiljkovic, 2001; Stephens, Greenwood & Brandtzaeg, 2007). The phase variation genes within *N. meningitidis* and *N. gonorrhoeae,* two important *Neisserial* pathogens, carry out slipped strand mispairing to enhance their virulence (Martin *et al.*, 2004; Stephens, Greenwood & Brandtzaeg, 2007; Deitsch, Lukehart & Stringer, 2009).

The effect of phase variation in Neisserial species is reflected in reversible mismatches and frameshifts by homopolymeric sequences within or around the promoter region or in gene coding areas (Moxon *et al.*, 1994; Richardson & Stojiljkovic, 2001). Notably, the mismatches and frameshifts caused by short repeat sequences mostly occur in the period of DNA polymerase activity during DNA replication or some processes of DNA repair (Hallet, 2001). In many bacterial organisms, MMR proteins are demonstrated that involve in regulating phase variation activities (Bayliss, van de Ven & Moxon, 2002). In *Haemophilus influenza,* when MutS is inactived, repeat dinucleotide tracts were destabilised, relative to the native conditions (Bayliss, van de Ven & Moxon, 2002).

Through functional inactivation of *N. meningitidis* MutS and MutL (*Nm*MutS and *Nm*MutL), phase variation levels of the strain with slow mutation is increased equivalent to a strain with fast mutation (Richardson & Stojiljkovic, 2001; Richardson *et al.*, 2002). Meanwhile, the level of missense mutations is also moderately enhanced (Richardson & Stojiljkovic, 2001; Richardson *et al.*, 2002).

However, manipulations of Dam methylase, including completely removal and complementation by plasmid, does not impact mutation rates in both aspects of phase variation and missense mutations (Richardson & Stojiljkovic, 2001). It suggests that the regulation of *Neisserial* mutation rates may be determinded by *Nm*MutS and *Nm*MutL (Richardson & Stojiljkovic, 2001). In some fast mutator strains, when *Nm*MutS and *Nm*MutL are functionally inactivated, plasmid complementation performs a functional equivalent to reduce the rates of mutation. However, in the cases of many strains with fast mutation, no defective *Nm*MutS or *Nm*MutL occurs (Richardson & Stojiljkovic, 2001). Spontaneous rifampicin resistance had been increased by approximately 20 times when *Nm*MutS was knock-out (serogroup B strain MC58) in slow, medium and fast mutator strains (Richardson & Stojiljkovic, 2001; Martin *et al.*, 2004). Moreover, five genes involving in the expression and maintenance of capsules, *siaD*, *porA*, *nadA*, *spr* and *lgtG*, contain repeat nucleotide tracts either in the promoter region or in coding areas and perform phase variation in *Nm*MutS deficient strains (Martin *et al.*, 2004).

In *N. meningitidis*, approximately 30 genes have been recognised that involve in phase variation, and over 100 genes are putative as well (Parkhill *et al.*, 2000; Tettelin *et al.*, 2000; Davidsen & Tønjum, 2006). The significant features of governed by phase variation are repeat nucleotide tracts within or around the promoter sites or in coding areas (Richardson & Stojiljkovic, 2001). These single nucleotide repeats perform as slipped or mis-repaired during DNA replication, and lead to transcriptional changes around or in the promoter region and ribosomal frameshifts within the coding region (Moxon *et al.*, 1994). Despite the regulation mechanism which capacitates phase variation is yet to interpreted, *Nm*MutS and *Nm*MutL are considered that have critical roles in governing *Neisserial* phase variation (Richardson & Stojiljkovic, 2001). Inhibition of either *Nm*MutS or *Nm*MutL gives rise to enhanced phase variation

in slow mutator strains, and *Nm*MutL deficiencies have been recognised in the strains containing the most mutants (Richardson & Stojiljkovic, 2001).

Defective strains of MMR proteins, including MutS, MutL and UvrD, have been indicated that phase variation levels are increased (Richardson & Stojiljkovic, 2001; Richardson *et al.*, 2002; Alexander, Rasmussen & Stojiljkovic, 2004; Alexander, Richardson & Stojiljkovic, 2004; Martin *et al.*, 2004). Additionally, the *Neisserial* MMR system has been found that is critical for *N. meningitidis* to escape and survive from human immune system because of the involvement of MMR genes during phase variation. These results encourage the motivation to study *Neisserial* MMR components further to develop the detailed functional mechanism that this pathogen can repair base mis-pairings and the insertion-deletion loops. On the other hand, it's able to further explain the *Neisserial* MMR system which allows those specific mismatches to escape severe repair processes and perform phase variation activities to achieve the survival of organisms.

1.6 Hypothesis

Compared to widely reported E. coli, there are fewer components of Neisserial MMR system (Davidsen & Tønjum, 2006). Additionally, none of MutH homologue has been exposed in all *Neisseria* species, and this fact is the same with a wide variety of most bacterial and all eukaryotic organisms (Fukui, 2010). Without the MutH homologue, MMR system from *N. meningitidis* may abide by the basic mechanism that carries out in other MMR pathways. Firstly, the mismatch repair system would recognise a mismatch. The newly synthesized strand is then discriminated by relevant proteins and demarcated by nicking. Subsequently, the mismatched region on the newly synthesized strand would be removed by the exonuclease activity. Finally, DNA polyemerase should re-synthesized the removed DNA, and the nick on the strand is sealed.

Up to now, studies on *Neisserial* mismatch repair system have been limited in both *in vitro* and *in vivo* aspects. Therefore, this project aims to investigate the initial procedures of the MMR system in the pathogen *N. meningitidis*. This study aims to reconstitute the active DNA Pol III holoenzyme and detect the roles of *N. meningitidis* MMR proteins MutS and MutL (*Nm*MutS and *Nm*MutL) using *in vitro* assays. Furthermore, the possible mechanism of strand discrimination without the MutH homologue is investigated by testing the endonuclease activity of *Nm*MutL *in vitro*.

Therefore, from the desire to explore the unknown *Neisserial* MMR system, the work presented here attempts to explain following pendent questions:

1. Can we actively re-constitute DNA Pol III HE for *N. meningitidis* in DNA replication?
2. What is the capability of *Nm*MutS binding to mismatched DNA compared to *Ec*MutS?
3. How does *Nm*MutL affect mismatch recognition?
4. Is *N. meningitidis* MutL an endonuclease?
5. How do different metal ions and ATP impact on *Nm*MutL?
6. How does *Nm*MutS impact on *Nm*MutL's activity?

Chapter 2

Preparation of DNA Pol III HE from *N. meningitidis*

2.1 Background and objectives

DNA Pol III HE is not only an essential enzyme complex involved in prokaryotic DNA replication but also implements the resynthesis of cleaved DNA in the MMR system. In *E. coli* MMR system, previous studies indicate that DNA Pol III HE cannot be substituted by other polymerases, including T4 DNA polymerase, T7 DNA polymerase, DNA Pol I and AMV reverse transcriptase (Lahue, Au, & Modrich,1989; Modrich & Lahue, 1996). Although the necessity of DNA Pol III HE is still unkown, this replication machinery may possess some inherent special association with the MMR system, which is required to be verifid. Consequently, the purification of active DNA Pol III HE is basical and significiant procedure to carry out the relevant enzymological study.

Fay *et al.*'s research (1982) revealed that *E. coli* DNA PolIII HE was reconstituted by ten individual subunits via expression and purification *in vitro*. *In vitro* prepration, DNA Pol III complex from *E. coli* is formd by DNA Pol III core units (α, ε and θ subunits), two τ subunits and one clamp loader complex (comprising 2γ, 1δ, 1δ', 1χ and 1ψ subunits) (Fay *et al.*, 1982). The β clamp associates DNA Pol III complex at the core and the clamp loader to processivity during DNA replication (O'Donnell, 1987).

Compared to *E. coli,* current knowledge of DNA repair pathways in *N. meningitides* are limited (Davidsen & Tønjum, 2006; Carpenter *et al.*, 2007). In the DNA Pol III HE of *N. meningitidis*, subunit genes, including the clamp loader subunit τ, γ, δ and δ', subunit α and ε of the core complex and the β-clamp have been identified. However, the genes of subunit θ, χ and ψ are not reported in the genome of *N. meningitidis* (Tettelin *et al.*, 2000). The structure of *N. meningitidis* DNA Pol III is currently unknown and relative functional differences with DNA Pol III in *E. coli* are to be determined.

This part of study aims to elucidate the active DNA Pol III HE in *N. meningitides in vitro*. In the previous study of this project, *N. meningitidis* strain MC58 (serogroup B) has been used as the template organism. Dr. Jan Silhan successfully amplified and cloned individual DNA Pol III subunits γ, τ, ε, α, δ, δ' and β-clamp (Table 2-1) into a N-terminal His-tag containing vector pPROEX-HTb (Fig. 2-1). A TEV cleavage site was designed between the His-tag and target genes, which was used to remove His-tags after purification by TEV protease.

Protein	Gene	Molecular Weight (KDa)	Vector	Assembly		
Alpha Subunit	*dnaE*	127.1	pPROEX–HTb	Core DNA Pol III	DNA Pol III complex	DNA Pol III Holo-enzyme
Epsilon Subunit	*dnaQ*	27.1	pPROEX–HTb			
Tau Subunit	*dnaX*	76.3	pPROEX–HTb	Clamp Loader complex		
Gamma Subunit	*dnaX*	47.1	pPROEX–HTb			
Delta Subunit	*holA*	36.3	pPROEX–HTb			
Delta Prime Subunit	*holB*	37.0	pPROEX–HTb			
Beta Clamp	*dnaN*	40.9	pPROEX-HTb			

Table 2-1. DNA Pol III HE subunits in *N. meningitidis* strain MC58 serogroup B

In earlier studies of this project, purification results showed β-clamp was expressed and purified in good yield (Dr. Jan Silhan, unpublished data). Subunit δ' was not cleavable via the inserted TEV sequence between tag and target protein after purification. Initial insolubility occurred in another clamp loader subunit δ during and after purification. Purification issues of the clamp loader subunits needed to be overcome by careful selection of purification conditions. Therefore, purification strategies of subunit δ and δ' needs to be optimized to obtain the active proteins. Moreover, DNA Pol III subunits γ, τ, ε and α are required to be prepared with sufficient yields. TEV protease is also necessary to be prepared for the cleavage to remove His-tags after the purification of each protein.

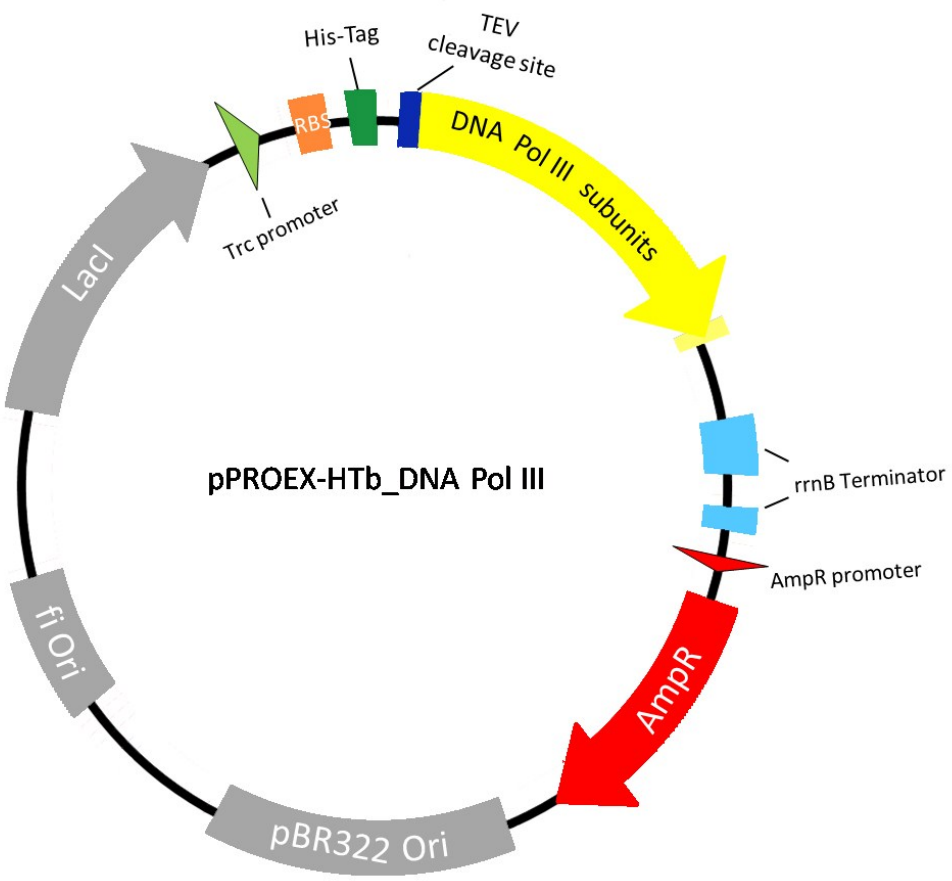


Figure 2-1. Graphic map of pPROEX-HTb vector (supplied by Dr. Jan Silhan)
The *trc* promoter in pPROEX-HTb vector is inhibited by the product of the upstream $lacI^q$ gene. The repressor is released with the addition of IPTG, and the expression of target genes is then induced by the *trc* promoter.

In the downstream case of DNA Pol III complex reconstitution, studies in other organisms has shown that several subunit stoichiometries are possible *in vitro*, and that some individual subunits may be completely omitted without apparent detrimental effects on DNA Pol III complex extension activity (Studwell & O'Donnell, 1990). In order to isolate only DNA Pol III complex and remove unbound subunits, the reconstituted Pol III core ($\alpha\cdot\varepsilon$) and DNA Pol III complex would be purified using ion exchange chromatography. The clamp loader ($\delta\cdot\delta'\cdot\gamma\cdot\tau$) would be reconstituted from parts and then incubation of the clamp loader and core to yield DNA Pol III complex. DNA Pol III complex needs to be purified from unbound subunits using ion exchange chromatography.

The conditions and protocol would be developed based on the purification of DNA Pol III complex from *E. coli* (O'Donnell & Studwell, 1990; Studwell & O'Donnell,1990; McInerney & O'Donnell, 2004) but buffer constituents should be altered to enhance subunit solubility from initial purification to DNA Pol III complex isolation. Primed ssDNA extension assays also would be performed to provide the activities of reassembled DNA Pol III complex.

2.2 Results

2.2.1 Expression and purification of DNA Pol III subunit δ' in vector pPROEX-HTb from *N. meningitides*

As mentioned above, DNA polymerase III subunit δ' gene was previously cloned in the pPROEX-HTb vector (Fig. 2-1) with a polyhistidine-tag (His-tag) at the N-terminus (Dr. Jan Silhan). A cleavage site (ENLYFQG/S) exists at the linker between the His-tag and the subunit δ' which is recognized by TEV protease to remove the His-tag from the subunit δ' after purification. In the last study, however, subunit δ' protein was reported that cannot be digested by TEV protease after His-tag purification. The fresh protein sample was needed urgently to perform any assay. Therefore, the purification of DNA polymerase III subunit δ' is the first task.

The δ' over-expressing construct was transformed into $CaCl_2$ competent *E. coli* K12 strain DH5α cells. The plasmid DNA was extracted and confirmed by sequencing. Subsequently, the plasmid DNA was transformed into the expressing strain BL21 (DE3) cells, which are suited for high gene expression and show limited proteolysis due to a low background of protease enzymes. Transformed cells were selectively grown on LB plates and individual colonies were picked to inoculate starter cultures, which were incubated overnight.

In the pPROEX-HTb_δ' vector, the *trc* promoter for the expression of subunit δ' is inhibited by the product of *lacI* gene. The addition of IPTG causes release of the repressor and switches on protein expression. 1mM IPTG was added to starter cultures at an OD600 of 0.4 and culture aliquots taken after 4 hours and analysed by SDS-PAGE. The over-expression of subunit δ' produced a protein with a molecular weight of 40.5kDa (Fig. 2-2A).

Colony 4 was chosen for full scale expression and purification (Materials and Methods). The over-expression levels were analysed by SDS-PAGE (Fig. 2-2B)

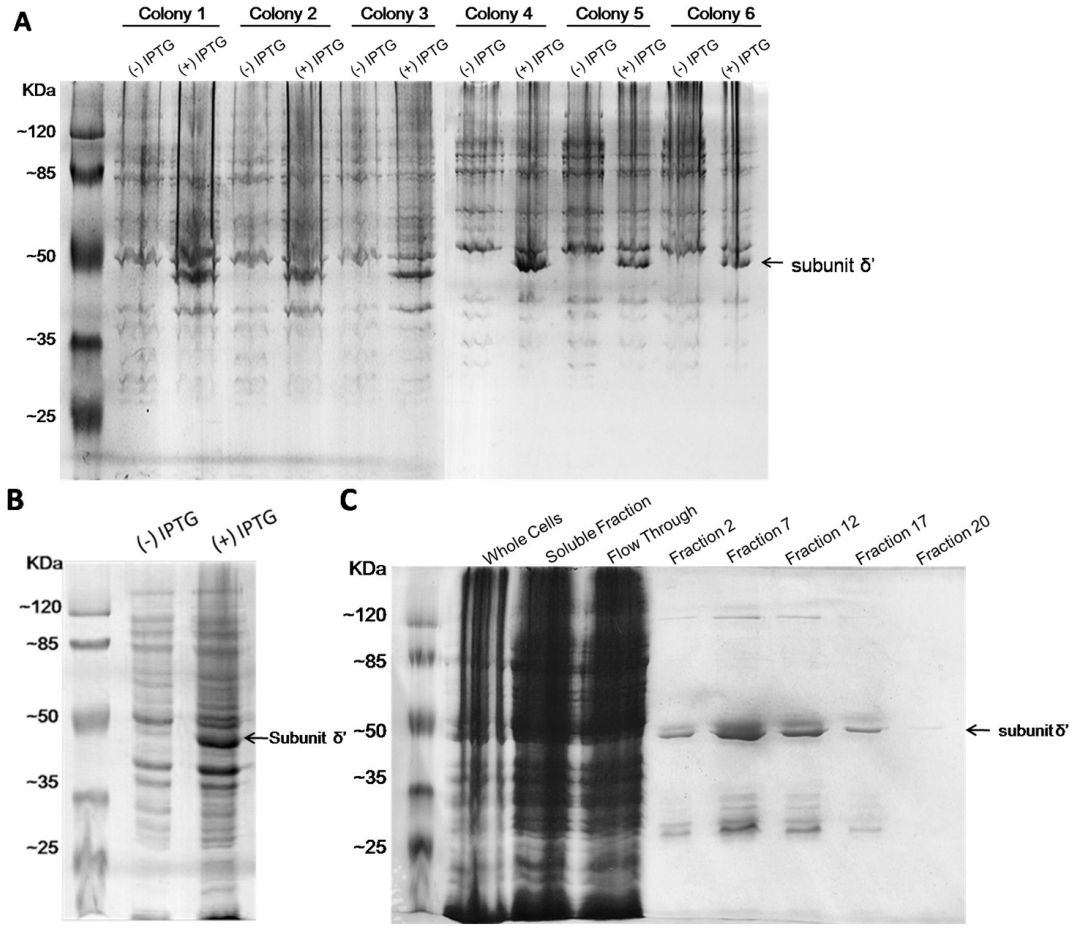


Figure 2-2. Expression and purification of DNA Pol III subunit δ' in pPROEX-HTb
12% SDS-PAGE analysis of subunit δ' expression level of 1mM IPTG-induced *E. coli* BL21(DE3) cell colonies at OD_{600} of 0.4 in 4 hrs at 25°C. (A) 12% SDS-PAGE analysis of TEV expression level of 1mM IPTG-induced *E. coli* BL21 (DE3) cell culture at OD_{600} of 0.4 in 5hrs at 25°C. (B) 12% SDS-PAGE analysis of TEV protein fractions collected from the Ni-column.

Cell debris free supernatants were loaded onto Ni^{2+} chelating column after sonication and ultracentrifugation and equilibrated in HT Buffer A. His-tag was trapped and specific bound with Ni^{2+} chelating beads when all the cell particulates flew through the column. His-tag bound beads were washed by HT Buffer A in three column volumes to dislodge non-specific proteins. His-tagged DNA Pol III subunit δ' was then eluted from the Ni-column with 500mM imidazole. Eluted fractions are analysed via SDS-PAGE (Fig. 2-2C). After

combining the fractions containing subunit δ' protein, the concentration of protein was monitored at the OD_{280} and calculated via the Beer-Lambert law based on its extinction coefficient. The purified subunit δ' protein was added with 10% (v/v) glycerol and then stored at -20°C.

However, during thawing on ice and storage at 4°C, the δ' protein samples were all precipitated. After centrifugation, the rest supernatant of the precipitated protein was quantified and compared to the concentration of freshly purified protein (Fig. 2-3). Apparently, the only 7.8% of purified protein remained the solubility, the most of subunit δ' protein was lost after protein precipitation.

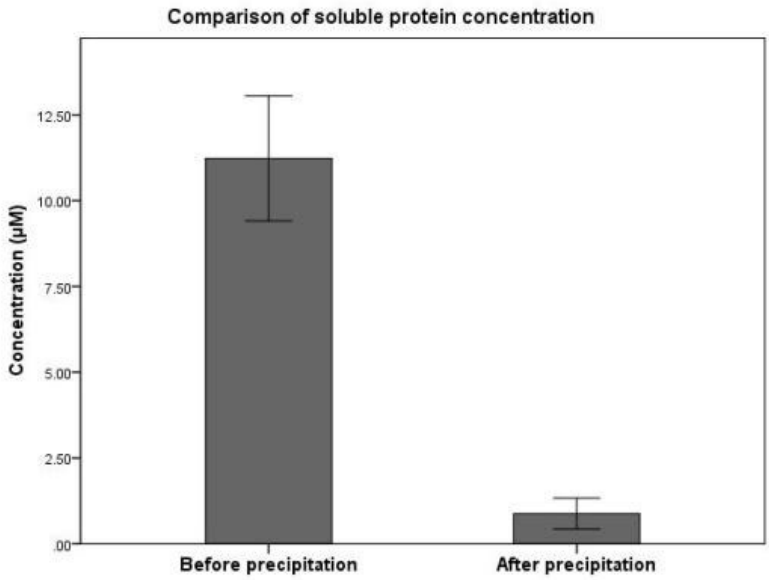


Figure 2-3. Comparison of concentration of the soluble subunit δ' protein before and after precipitation

The absorbance of proteins was monitored at the OD_{280} and calculated based on the Beer–Lambert law. This figure clearly shows that most soluble protein was lost after protein precipitation.

To improve the yield, another purification of subunit δ' was performed from 2L of LB culture using the same conditions. After assessment by SDS-PAGE gel (not shown), purified subunit δ' protein was concentrated by a centrifugal ultrafiltration at 4°C. After washing the inner wall and membrane of the centrifugal ultrafilter repeatedly, some white precipitation was revealed. It showed that a large amount of protein was precipitated and attached to the centrifugal ultrafilter when the volume of protein was changed. The results of two repeated purifications of δ' protein reveal that the current conditions of δ' purification is not suitable for promoting the solubility of protein.

The precipitation of δ' protein could be attributed to a couple of factors. Firstly, after the initially purification by Ni^{2+}chelating beads column, subunit δ' protein was concentrated from a large volume (~20ml) to a small volume (~1.5ml) in the centrifugal ultrafilter. Therefore, the protein reached the point at which was an aggregate during concentrating. Secondly, the centrifugal ultrafilter provided a surface on which the protein was more likely to precipitate. Additionally, it was probably a result caused by these two reasons. Reality provided an important enlightenment that unnecessary protein concentration and the use of centrifugal ultrafilter should be avoided during handling δ' protein.

Another purification of subunit δ' protein was performed using low concentration of imidazole (250mM) using the air pressure concentrator which was a gentler method to concentrate subunit δ' protein after purification. Further purification of subunit δ' protein was carried out by a gel filtration column in Fast Protein Liquid Chromatography (FPLC) system (see Materials and Methods). However, the graph of gel filtration chromatograph peaks indicated the yield of subunit δ' protein was extremely low (Fig. 2-4). The pressure of the gel filtration was significantly increased which illustrated that there may occur protein precipitation during gel filtration so that blocked the flow rate and brought a high pressure in the FPLC purifier.

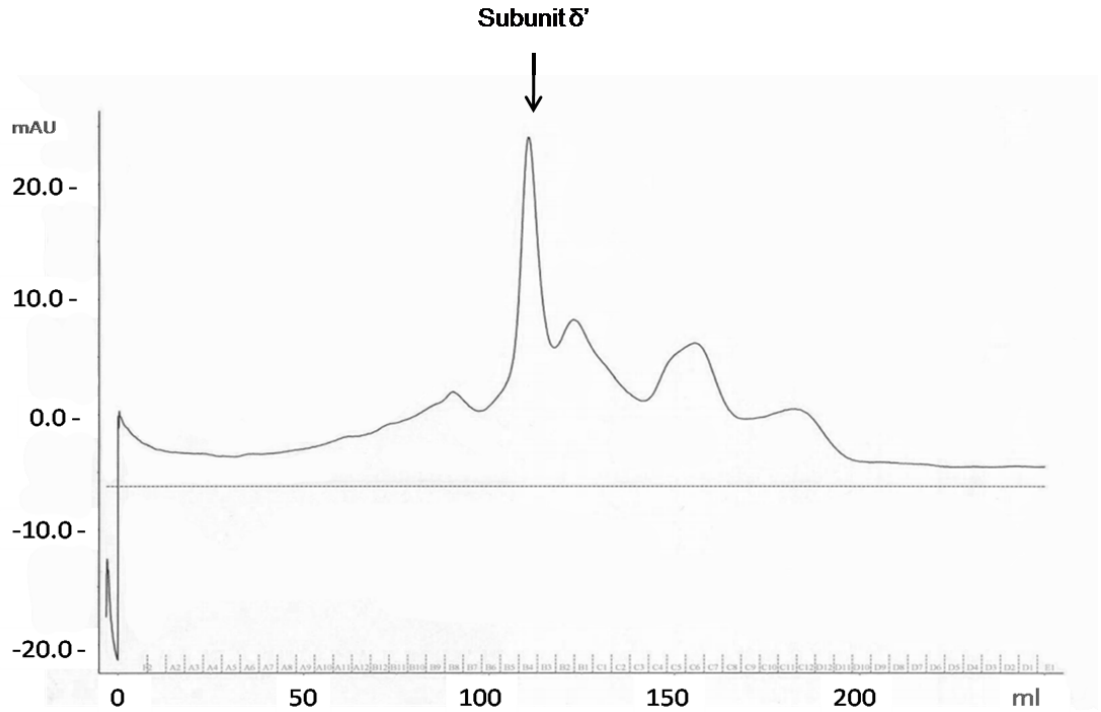


Figure 2-4. Chromatogram of subunit δ' protein from FPLC gel filtration

X-axis value is the volume of the flow through from SuperDex-75 column during the gel filtration chromatography. Y-axis values is UV level of the flow through. The yield of subunit δ' protein from FPLC was extremely low.

According to the results of precipitation, protein insolubility issue bothered the preparation of subunit δ' protein. A series of methods were carried out to attempt to improve the solubility of subunit δ' protein and then proceed to the downstream DNA Pol III complex assembly.

2.2.2 Solubility test with detergents

Triton X-100 and Tween-20 are frequently used nonionic detergents which consist of an uncharged hydrophilic headgroup and a hydrophobic tail (Garavito & Ferguson-Miller, 2001). They are considered as mild surfactants which are effective in protein solubilization (Luche, Santoni & Rabilloud, 2003). Sarkosyl is a gentle anionic detergent with alkyl groups which is able to increase solubility (Frangioni & Neel, 1993). In many cases, the denaturation effect of protein is very slight in the low concentration condition of Sarkosyl (Frangioni & Neel, 1993). For cheaper alternatives, these three detergents are good options to perform the solubility test for DNA Pol III subunit δ'. However, because of the presence of a phenyl ring, many detergents interfere with ultra-violet (UV) so that the concentration of protein with detergent at 280nm is inaccurate (Lever, 1977). Therefore, the detergent compatible kit was used based on the Folin Lowry method at 750nm absorbance in this work.

The concentration of newly purified DNA Pol III subunit δ' was measured calculated. Since the subunit δ' has to undergo several further purification stages to yield the pure DNA Pol III, this solubility test was performed at 4°C. 1ml one detergent free sample and three 0.5% (v/v) detergent addition (Triton X-100, Tween-20 and Sarkosyl NL-30) samples was spun down at 4 different time points (1, 2, 3 and 7 days). The result was assessed by the quantitation of remained soluble protein. The percentage of protein stability was equal to protein concentrations at different time points divided by the original concentration of protein (31.73μM) (Fig. 2-5).

The percentage changes of soluble subunit δ' protein in detergent free buffer and detergent containing buffers within a week (Fig. 2-5). The ratio of soluble protein in detergent free buffer continued to decrease over 1 week. After 1 day incubation at 4°C, approximately 25% of soluble protein was lost in detergent

free buffer and 0.5% Sarkoysl NL-30 buffer. In comparison, both 0.5% Trition X-100 and 0.5%Tween-20 buffer prevented the loss of soluble protein and kept the soluble ratio at about 85%. Over time, the detergent effect of solubilising protein was approaching the same effects after three days.

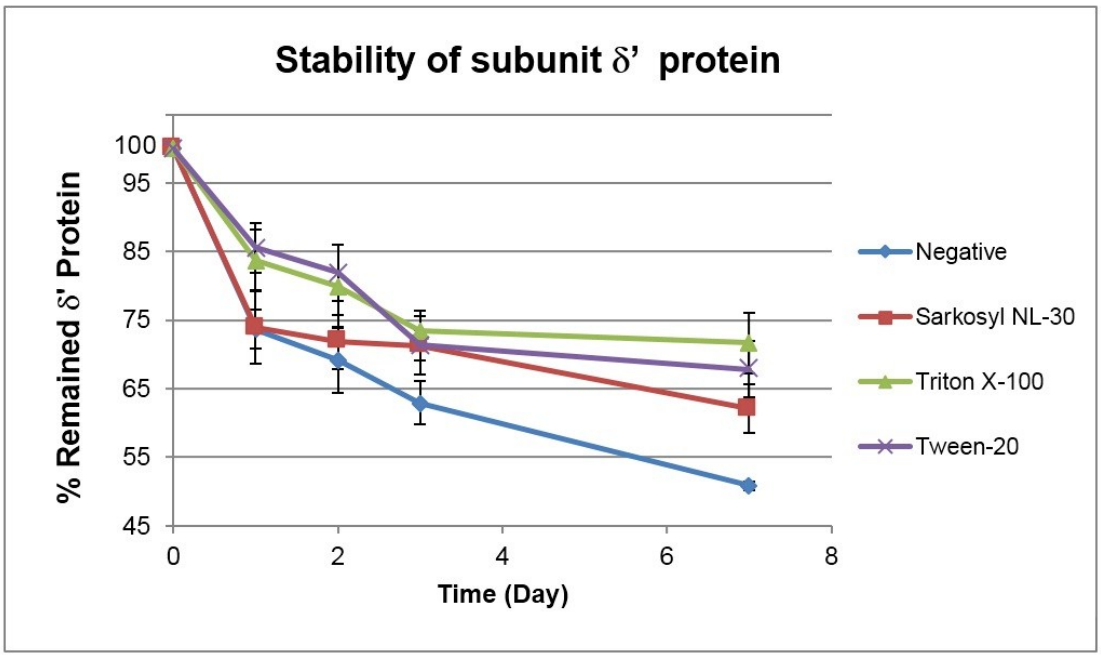


Figure 2-5. The stability test of DNA Pol III subunit δ' protein with detergents at 4°C

The absorbance of proteins was monitored at the 750nmand quantified by the microplate protocol of Folin Lowry method via Bio-Rad DC Protein Assay Kit. All point data of protein concentration were the averages of triplicates. Error bars were labelled using standard deviation.

Meanwhile, a small amount of precipitation appeared in the detergent negative sample after centrifuging at day three. However, there was no visibly clear precipitation in any sample containing detergents. At the 7th day time point, nearly 68% of soluble protein was lost in the buffer without detergents and a high amount of precipitation was seen in this sample. Slight white precipitations also appeared in the 0.5% Sarkosyl NL-30 sample, and approximately 64% soluble δ' was remain after seven days. There was no clear precipitation in the 0.5% Tween-20 and TritonX-100 contained samples. In general, the stability of δ' was rescued in these detergents contained samples after seven days' 4°C

incubation. In addition, the highest ratio of soluble subunit δ' protein was in the 0.5% Triton X-100 buffer. There was approximately 72% soluble protein remaining after seven days incubation at 4°C.

Despite the addition of all three detergents saved the solubility of purified subunit δ' protein in various degrees, further issues had been raised. TEV protease cleavage still cannot be performed because it does not bind the Ni^{2+} chelating column with detergents in the buffer. Furthermore, the purification of DNA Pol III subunits is the initial preparation for the downstream assembly of DNA Pol III HE complex. The usage of detergents implies that we would need to determine the impact of detergents on the activity of individual DNA Pol III components. Therefore, in order to obtain tag-free proteins for downstream work efficiently, other strategies to improve solubility of subunit δ' protein was considered.

2.2.3 Cloning, expression and purification of DNA Pol III subunit δ' from *N. meningitides*

As mentioned above, the insoluble status of DNA Pol III subunit δ' appeared during the low temperature storage after the purification from the vector pPROEX-HTb which includes a His-tag at the N-terminal. In order to enhance the solubility, the subunit δ' was cloned into a new vector petM43 which includes a maltose binding protein tag (MBP-tag), the solubility promoter, at the N-terminal and a His-tag at the C-terminal, and is resistant to kanamycin. Furthermore, in previous work, the other clamp loader component, subunit δ also seem to precipitated after purification (Dr. Jan Silhan, unpublished data). Therefore, two cloning strategies were implemented to acquire the optimum solution. One is to clone the subunit δ' singly into the vector petM43 and express the MBP-δ' fusion protein. The other is to clone the subunit δ and δ' together into the vector petM43 and co-express these two subunits (Fig. 2-6).

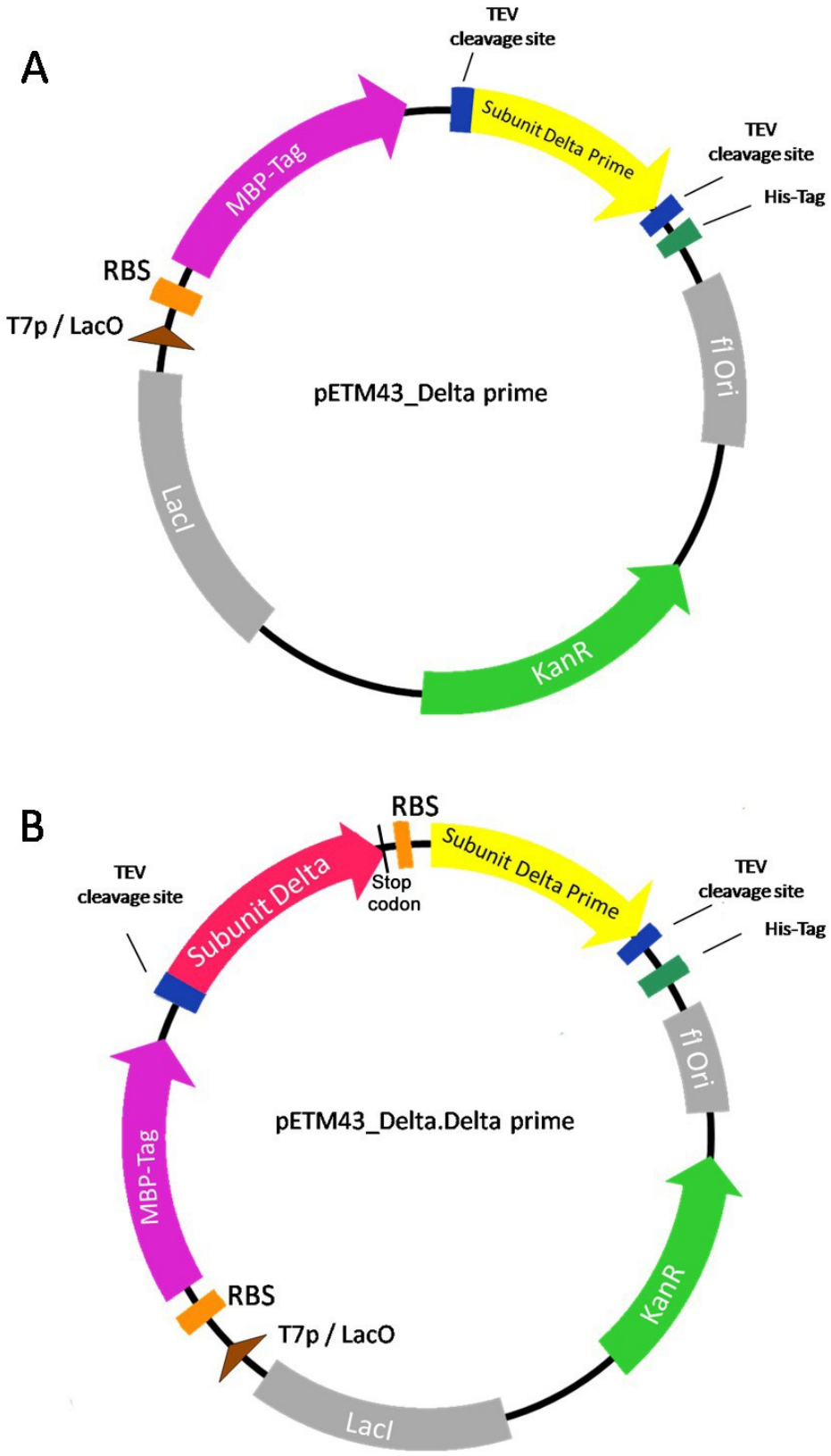


Figure 2-6. Graphic maps of petM43-delta_prime and petM43-delta.delta_prime

In the first cloning strategy, *N. meningitidis* DNA Polymerase III subunit δ' gene *holB* of approximately 1.1kbp was amplified from *N. meningitidis* MC58 genomic DNA via PCR (Fig. 2-7A) and cloned into an expression vector pETM43 (supplied by Dr. Marko Storch, lab data) using NcoI and XhoI sites, which adds a MBP-tag with cleavage site for TEV protease at the N-terminal of the final protein. The constructed DNA Pol III subunit δ' over-expressing plasmid was designated as pETM43_delta_prime and transformed into competent DH5α cells. Individual colonies were picked to inoculate cultures.

The pETM43_delta_prime plasmids were purified and verified for the presence of the insert *holB* gene by sequencing prior to being transformed into BL21(DE3) cells. The petM43 vector is resistant to kanamycin and contains the T7 promoter to control the expression of downstream genes. Before the addition of IPTG, the product of *lacI* gene represses the T7 promoter. When IPTG is added, the repressor is released and allows the T7 promoter to perform the downstream expression of target genes. In this study, 1mM IPTG was added to 50ml starter cultures within 3 single colonies at OD_{600} of 0.4 and culture aliquots taken under 25°C for 5hrs and analysed via SDS-PAGE. The over-expression of MBP and subunit δ' fused protein (MBP-δ') produced a protein with a molecular weight of 79.5KDa (Fig. 2-7B).

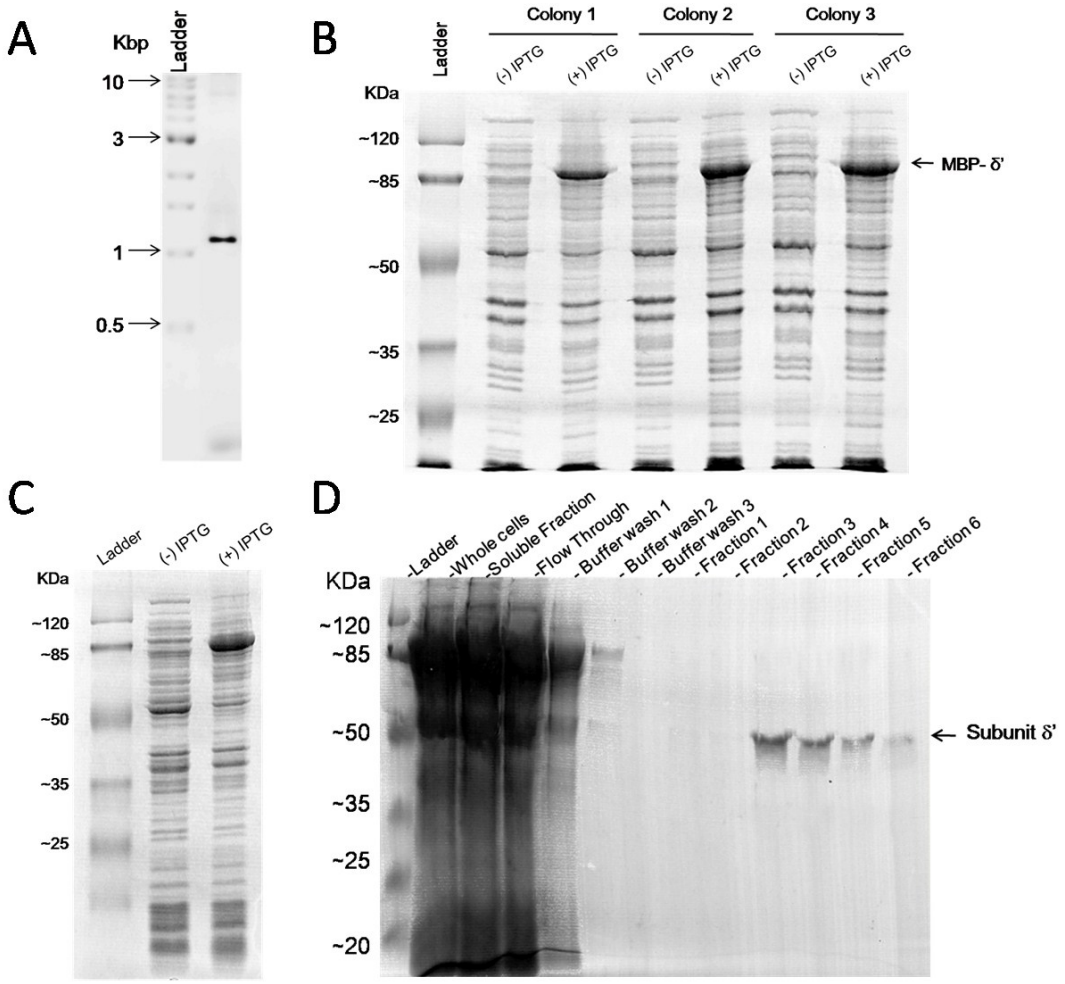


Figure 2-7. Cloning, expression and purification of DNA Pol III subunit δ' in pETM43 vector

(A) ~1.0kbp *N. meningitidis* DNA Pol III subunit δ' gene *holB* was produced via PCR-amplification of *N. meningitidis* MC58 genomic DNA and analysed by 1% agarose gel electrophoresis. (B) 12% SDS-PAGE analysis of subunit δ' expression level of 1mM IPTG-induced *E. coli* BL21(DE3) cell colonies at OD_{600} of 0.4 in 5hrs at 25°C. (C) 12% SDS-PAGE analysis of DNA Pol III subunit δ' expression level of 1mM IPTG-induced *E. coli* BL21 (DE3) cell culture at OD_{600} of 0.4 in 5hrs at 25°C. (D) 12% SDS-PAGE analysis of DNA Pol III subunit δ' protein fractions collected from the amylose resin column after TEV protease cleavage.

Colony 3 was utilized for the full-scale purification. Cultures for MBP and subunit δ' fused protein over-expression were grown in LB media to an OD_{600} of 0.4 at 37°C, and were then induced by IPTG, and growth continued at 25°C for further 5 hours (Fig. 2-7C). The cell debris free supernatant after sonication and ultracentrifugation (labelled as "Soluble Fraction" in Fig. 2-7D) was loaded onto amylose resin column, equilibrated in MBP Buffer. The MBP-tag was

trapped and bound with amylose resin which all the cell particulates flew through the column. The MBP bound resin was washed by MBP Buffer in three column volumes to dislodge non-specific proteins. After washing, there were no non-specific bindings (Fig. 2-7D). To avoid wasting time and effort on elution and the maltose-free dialysis, MBP bound resin was cleaved directly by TEV protease in the dialysis tubing against MBP Buffer. After TEV cleavage, 1ml tag-free fractions were flown through the column and were analysed on SDS-PAGE (Fig. 2-7D). Despite the low efficiency of TEV cleavage with the affinity resin, soluble subunit δ' was gained successfully. Tag-free proteins were then passed through the Ni^{2+} chelating column to remove TEV protease which has a N-terminal His-tag, and were dialysed against MonoQ Buffer MonoQ Buffer, the specific buffer for subsequent reconstitution with other subunits of DNA Pol III, and was quantified. The final concentration of subunit δ' was 32.4μM in 3.5ml.

In the second cloning strategy, *N. meningitidis* DNA Polymerase III subunit δ gene *holA* and subunit δ' gene *holB* of approximately ~1.0kbp were amplified from *N. meningitidis* MC58 genomic DNA via PCR (Fig. 2-8A). Gene *holB* was cloned into the expression vector pETM43 using HindIII and XhoI sites, which adds a ribosomal binding site (RBS) at N-terminal and a cleavage site for TEV protease at the C-terminal. Subsequently, gene *holA* was cloned into the expression vector pETM43 included gene *holB* using KpnI and SpenI site, which adds an N-terminal MBP-tag with TEV protease cleavage site for the final protein (Fig. 2-6). The constructed DNA Pol III MBP-δ·δ' co-expressing plasmid was designated as "pETM43_delta.delta_prime" and transformed into $CaCl_2$ competent *E. coli* DH5α cells. This cloning strategy was collaborated with Ms. Sarah Woolley and Dr. Lucy Rayner.

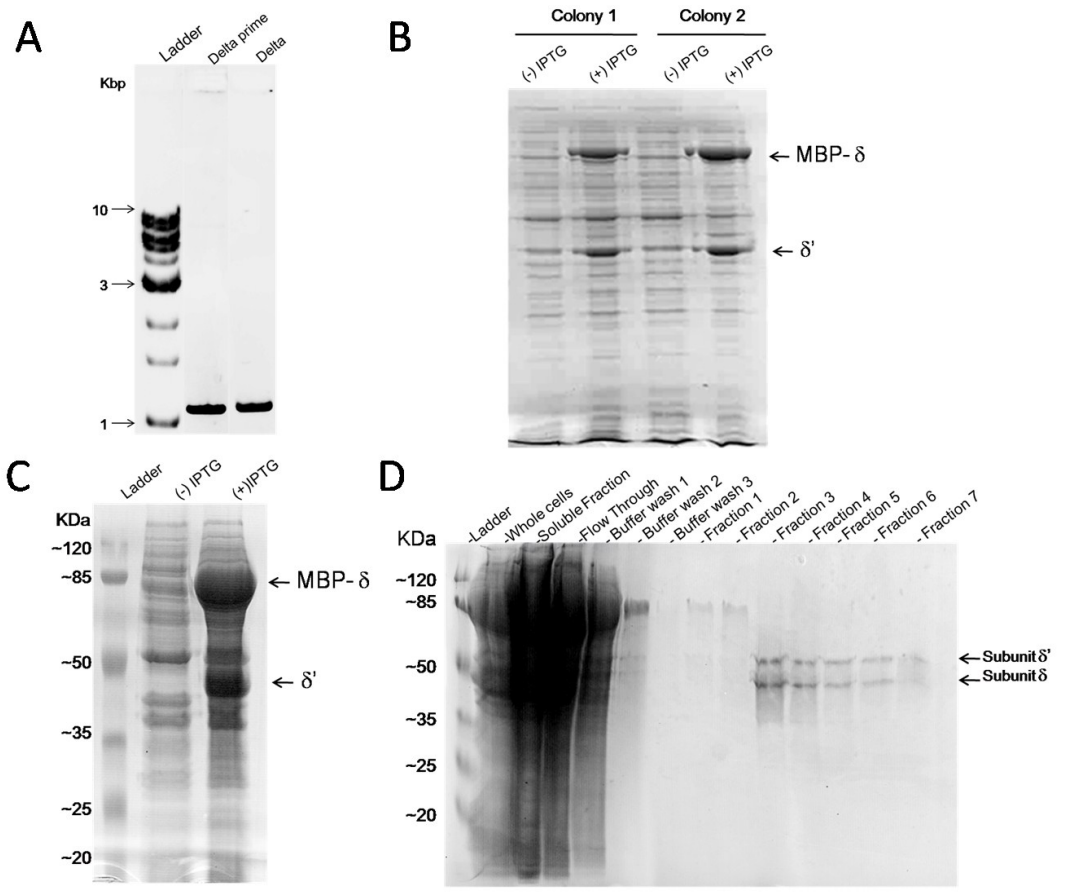


Figure 2-8. Cloning, expression and purification of DNA Pol III subunit δ.δ' in pETM43 vector

(A) ~1.0kbp *N. meningitidis* DNA Pol III subunit δ gene *holA* gene and subunit δ' gene *holB* was produced via PCR-amplification of *N. meningitidis* MC58 genomic DNA and analysed by 1% agarose gel electrophoresis. (B) 12% SDS-PAGE analysis of subunit δ.δ' co-expression level of 1mM IPTG-induced *E. coli* BL21(DE3) cell colonies at OD_{600} of 0.4 in 4hrs at 25°C. (C) 12% SDS-PAGE analysis of DNA Pol III subunit δ·δ' co-expression level of 1mM IPTG-induced *E. coli* BL21 (DE3) cell culture at OD_{600} of 0.4 in 4hrs at 25°C. (D) 12% SDS-PAGE analysis of DNA Pol III subunit δ' protein fractions collected from the amylose resin column after TEV protease cleavage.

Successfully transformed cells were selectively grown on LB plates and individual colonies were picked to inoculate starter cultures, which were incubated overnight. pETM43_delta.delta_prime plasmids were purified and then transformed into the expression strain cells as before. IPTG-induced over-expression from two colonies was performed (Fig. 2-8B). Colony 2 was used for full scale expression and examined via SDS-PAGE (Fig. 2-8C).

MBP-δ•δ' protein was purified via the same methods as mentioned in the first strategy by amylose resin columns and buffers. TEV protease was added with protein bound resin during overnight 4°C dialysis against MonoQ Buffer. Tag-free proteins were then flown through the Ni^{2+} chelating column to remove TEV protease. Tag-free fractions were analysed by SDS-PAGE (Fig. 2-8D). Taq-free δ·δ' was quantified and was then added 20% glycerol and stored in -20 °C. The final concentration of subunit δ·δ' was 22.6μM in 3.6ml.

2.2.4 Expression and purification of TEV protease

TEV protease is a widely used sequence-based protease to remove the fusion tag during the purification of proteins, which has stricter specificity than other proteases, such as factor Xa (Phan *et al.*, 2002). In this study, TEV protease cleavage sites were designed at the N-terminal between His-tag and target genes in all over-expression constructions to remove His-tag after protein purifications.

In the previous study, TEV protease gene was amplified from *tobacco etch virus* genomic DNA and cloned into the expression vector pPROEX-HTb (Lab Data, Dr. Jan Silhan). TEV protease was over-expressed in BL21(DE3) cells and analysed via SDS-PAGE. (Fig. 2-9A). His-tag purification of TEV protease via Ni^{2+} chelating column was same as mentioned above. His-tagged TEV protease was eluted from the Ni-column with imidazole. Eluted fractions are analysed via SDS-PAGE (Fig. 2-9B). Fractions containing subunit proteins were pooled, desalted and concentrated. The concentration of TEV protease was quantified and was then added glycerol to 20% (v/v) and stored at -80°C.

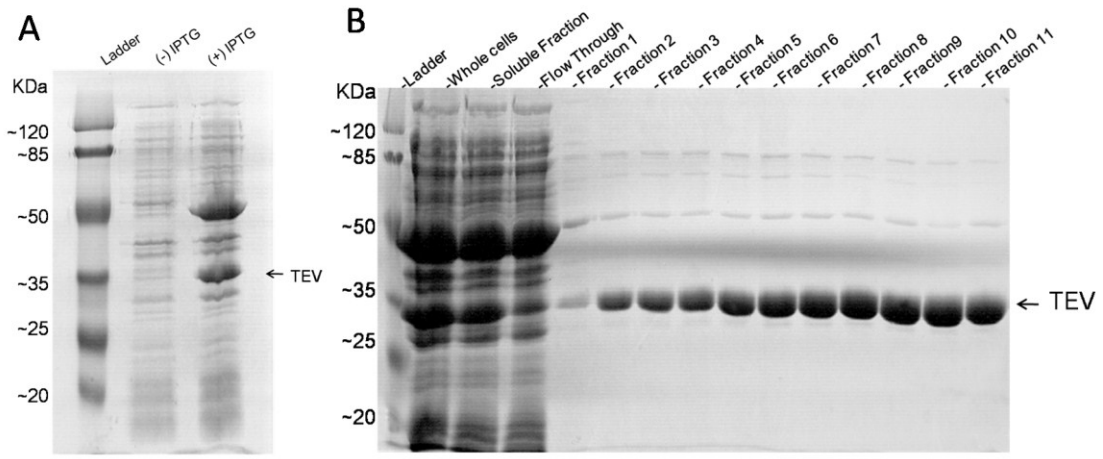


Figure 2-9. Expression and purification of TEV protease

(A) 12% SDS-PAGE analysis of TEV expression level of 1mM IPTG-induced *E. coli* BL21 (DE3) cell culture at OD_{600} of 0.4 in 5hrs at 25°C. (B) 12% SDS-PAGE analysis of TEV protein fractions collected from the Ni-column.

2.2.5 Expression and purification of DNA Pol III subunits

In the previous study, *N. meningitidis* DNA Polymerase III subunit α gene *dnaE*, subunit ε gene *dnaQ* and subunit $\gamma.\tau$ gene *dnaX* were amplified from *N. meningitidis* MC58 genomic DNA and cloned into the expression vector pPROEX-HTb respectively (achieved by Dr. Jan Silhan). The constructed DNA Pol III subunits were over-expressed in BL21(DE3) cells with IPTG induction and analysed via SDS-PAGE. (Fig. 2-10A, 2-11A, 2-12A). His-tag purification of TEV protease via Ni^{2+} chelating column was same as mentioned above. His-tagged DNA Pol III subunits were then eluted from the Ni-column with imidazole and analysed via SDS-PAGE (Fig. 2-10A, 2-11A, 2-12B). Fractions containing subunit proteins were pooled, desalted and concentrated prior to being incubated with TEV protease to cut off the His-tag from DNA Pol III subunits. Further purifications were carried out via a gel filtration column by FPLC system (Fig. 2-10B, 2-11B, 2-12C).

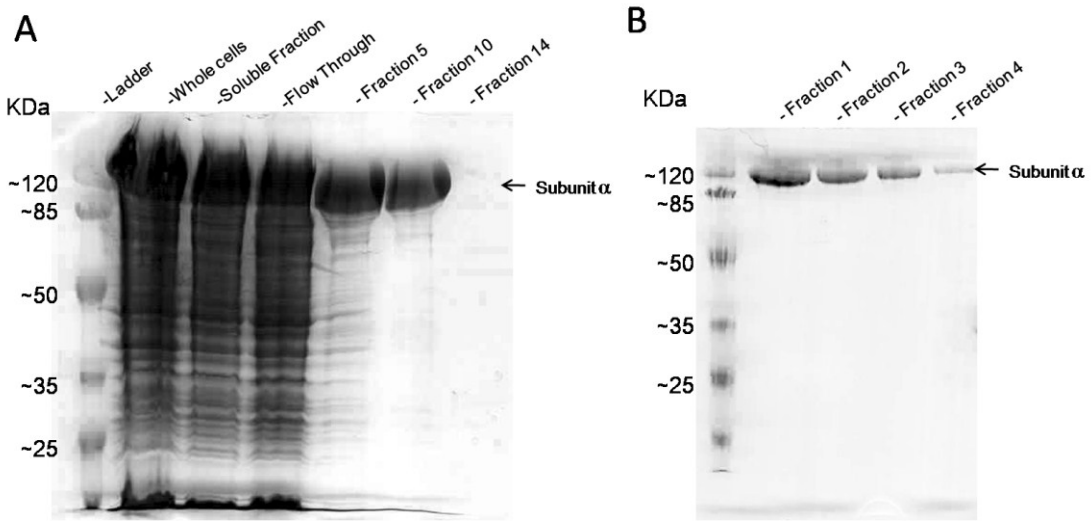


Figure 2-10. Expression and purification of DNA Pol III subunit α

(A) 12% SDS-PAGE analysis of DNA Pol III subunit α protein fractions collected from the Ni-column. (B) 12% SDS-PAGE analysis of DNA Pol III subunit α protein fractions collected from the size exclusion gel filtration after TEV protease cleavage.

Highly purified DNA Pol III subunit proteins were analysed via SDS-PAGE (Fig. 2-10B, 2-11B, 2-12C). DNA Polymerase III subunit α, subunit ε and subunit γ·τ were then pooled and concentrated respectively. 4ml of 6.8μg/ml subunit α, 2ml of 9.8μg/ml subunit ε and 8ml of 14.8μg/ml subunit γ·τ stock solution were obtained after adding glycerol to 20% (v/v) and stored at -80°C.

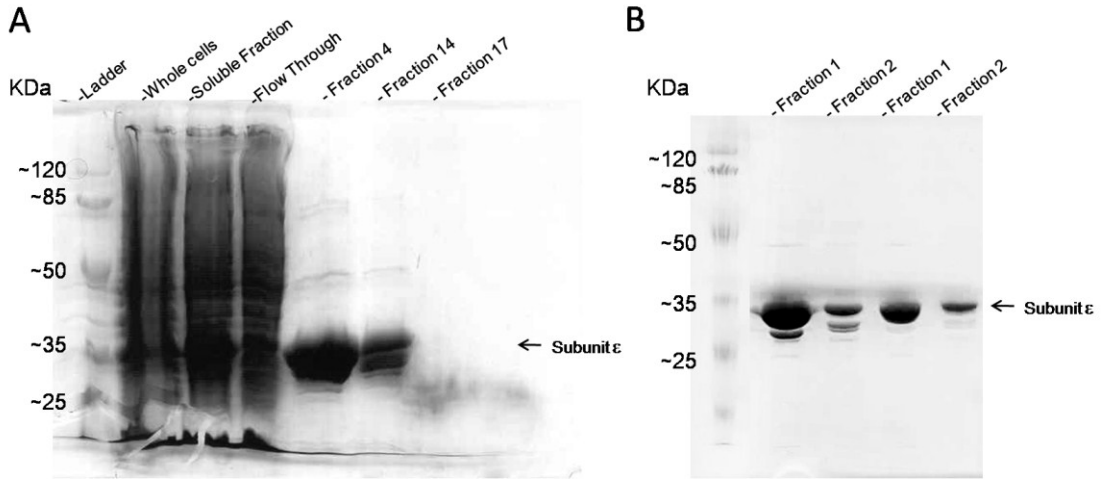


Figure 2-11. Expression and purification of DNA Pol III subunit ε

(A) 12% SDS-PAGE analysis of DNA Pol III subunit ε protein fractions collected from the Ni-column. (B) 12% SDS-PAGE analysis of DNA Pol III subunit ε protein fractions collected from the size exclusion gel filtration after TEV protease cleavage.

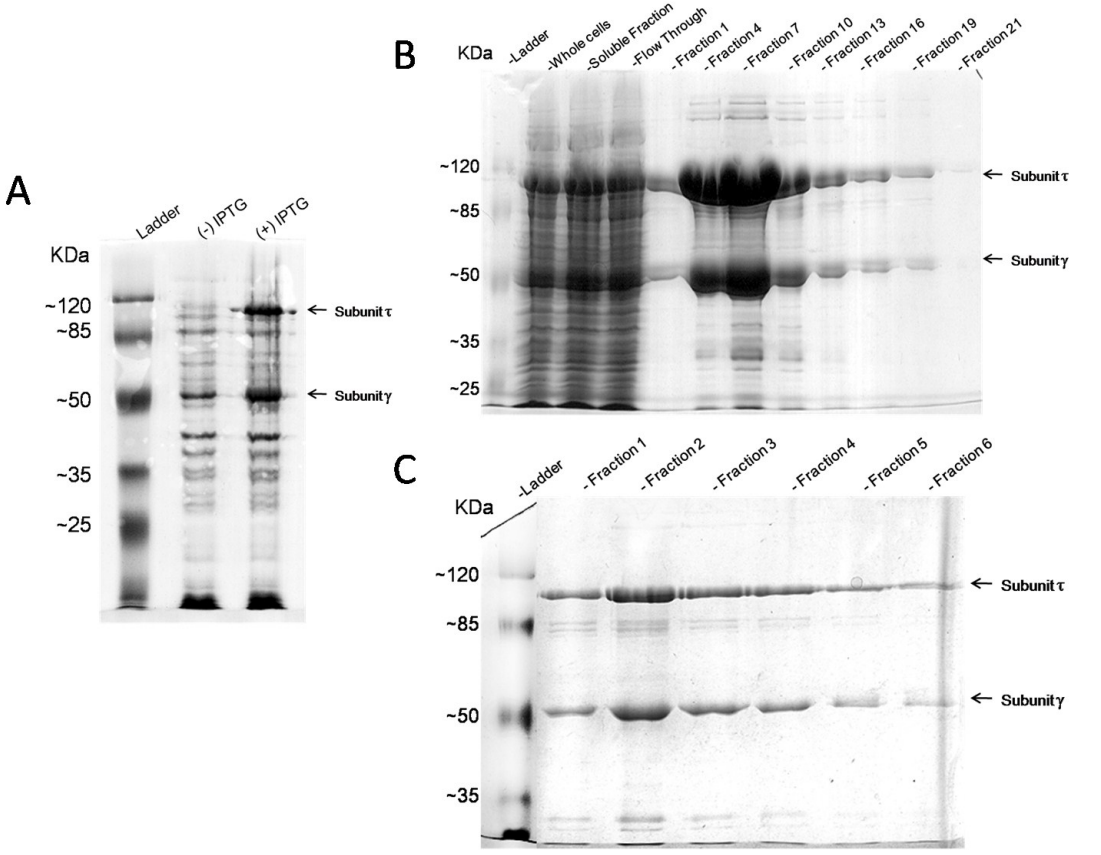


Figure 2-12. Expression and purification of DNA Pol III subunit γ.τ

(A) 12% SDS-PAGE analysis of DNA Pol III subunit γ.τ expression level of 1mM IPTG-induced *E. coli* BL21 (DE3) cell culture at OD_{600} of 0.4 in 5hrs at 25°C. (B) 12% SDS-PAGE analysis of DNA Pol III subunit γ.τ protein fractions collected from the Ni-column. (C) 12% SDS-PAGE analysis of DNA Pol III subunit γ.τ protein fractions collected from the size exclusion gel filtration after TEV protease cleavage.

2.2.6 Reconstitution of *N. meningitides* DNA Pol III complex

Component subunits (α, ε, τ, γ, δ, δ′, β) of the DNA Polymerase III HE from *N. meningitides* have been prepared in the purification process above. Subunits α, ε, τ, γ, β were stored in the Imidazole-free buffer at -80°C. All these subunits were dialysed against MonoQ Buffer which is applied in the subsequent reconstitution at 4°C overnight.

The core complex of DNA Pol III was formed by subunits α and ε in *N. meningitidis*. Purified subunit α and ε were incubated together with a molar ratio of 1:1.5 on ice for 30min. Separating from remaining free α and ε by FPLC chromatography on a MonoQ column. The elution profile of FPLC shows two small peaks were eluted before the α·ε complex (Fig. 2-13A). Elution was collected by a 500μl aliquot in each fraction. The peak fractions of FPLC chromatography were analysed on SDS-PAGE gel (Fig. 2-13B, C). The unpurified α-ε complex was also loaded onto the SDS-PAGE gel for reference. The first eluted peak before the α·ε complex presents fractions of free ε (Fraction 72 - Fraction 75). The second small peak was the unspecific protein that remained after the purification of subunit ε. The molar ratio of α:ε is assumed to be 1:1 in subsequent constitution. Fractions of pure α·ε complex (Fraction 81 - Fraction 86) were pooled together and then quantified.

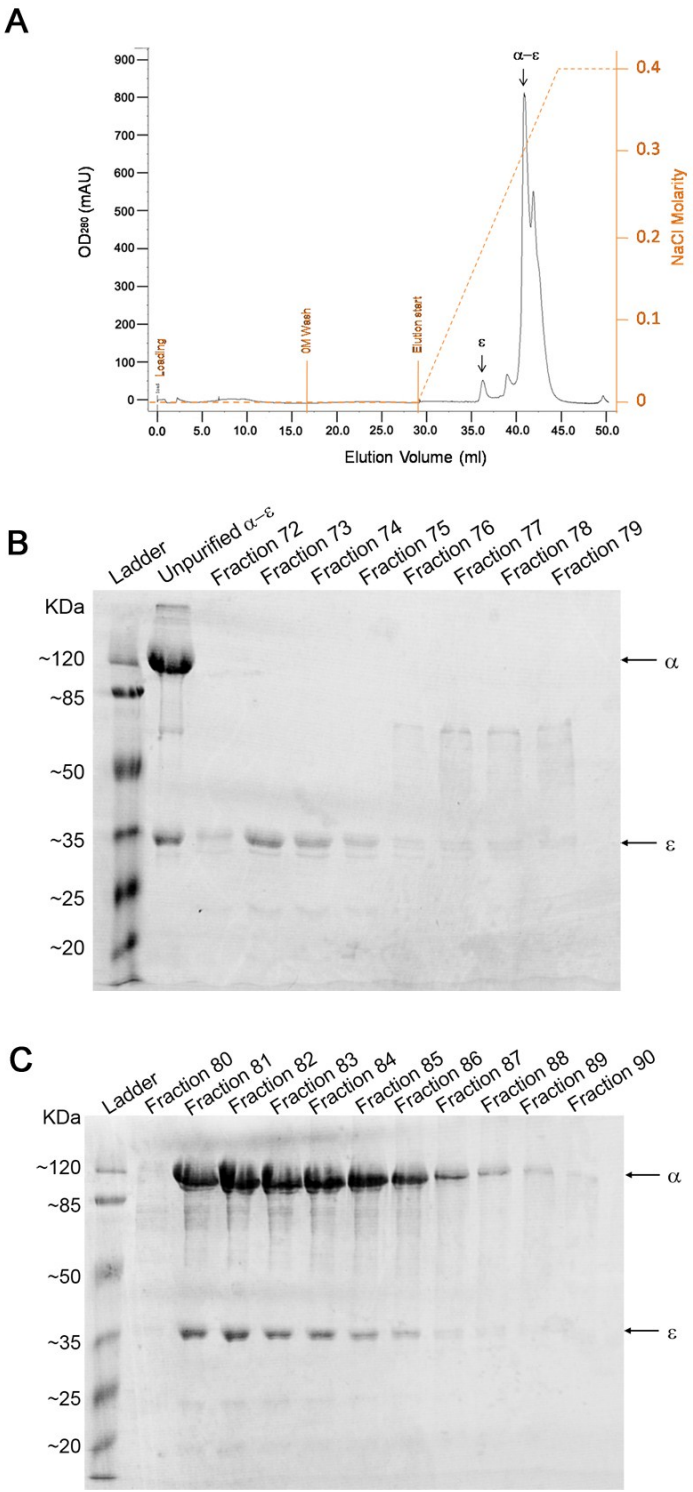


Figure 2-13. Analysis of FPLC purified fractions containing assembled core complex of DNA Pol III

(A) Chromatogram at OD_{280} from assembly of the core complex of DNA Pol III using the Mono-Q 5/50 GL column (GE). (B) Fractions of two small peaks form the FPLC chromatograph by 12% SDS-PAGE. (C) Fractions containing assembled core complex of DNA Pol III by 12% SDS-PAGE.

Subunit γ and τ were expressed in the same gene and purified together. The formation of the clamp loader complex requires that $\gamma\cdot\tau$ complex and $\delta\cdot\delta$' complex should associate with each other. Because of the amounts of each subunit in the active clamp loader complex was unclear, a 2:1 molar ratio of $\gamma\cdot\tau$ to $\delta\cdot\delta$' was used for formation. To assemble DNA Pol III complex, the core polymerase and the clamp loader complex were mixed in a 1:1 molar ratio for 4ºC incubation, and were purified by the same method on the MonoQ column. The single peak with the high absorbance appeared on the FPLC chromatography at approximately 0.3M NaCl (Fig. 2-14A). Elution was collected by a 1ml aliquot in each fraction. The fractions of the peak were analysed by SDS-PAGE (Fig. 2-14B). Following the elution of $\delta\cdot\delta$' complex from Fraction 72 to Fraction 76, DNA Pol III holoenzyme was eluted with a good yield from Fraction 81 to Fraction 84 at 0.4M of NaCl. The fractions of the holoenzyme were pooled together and quantified for downstream extension assay.

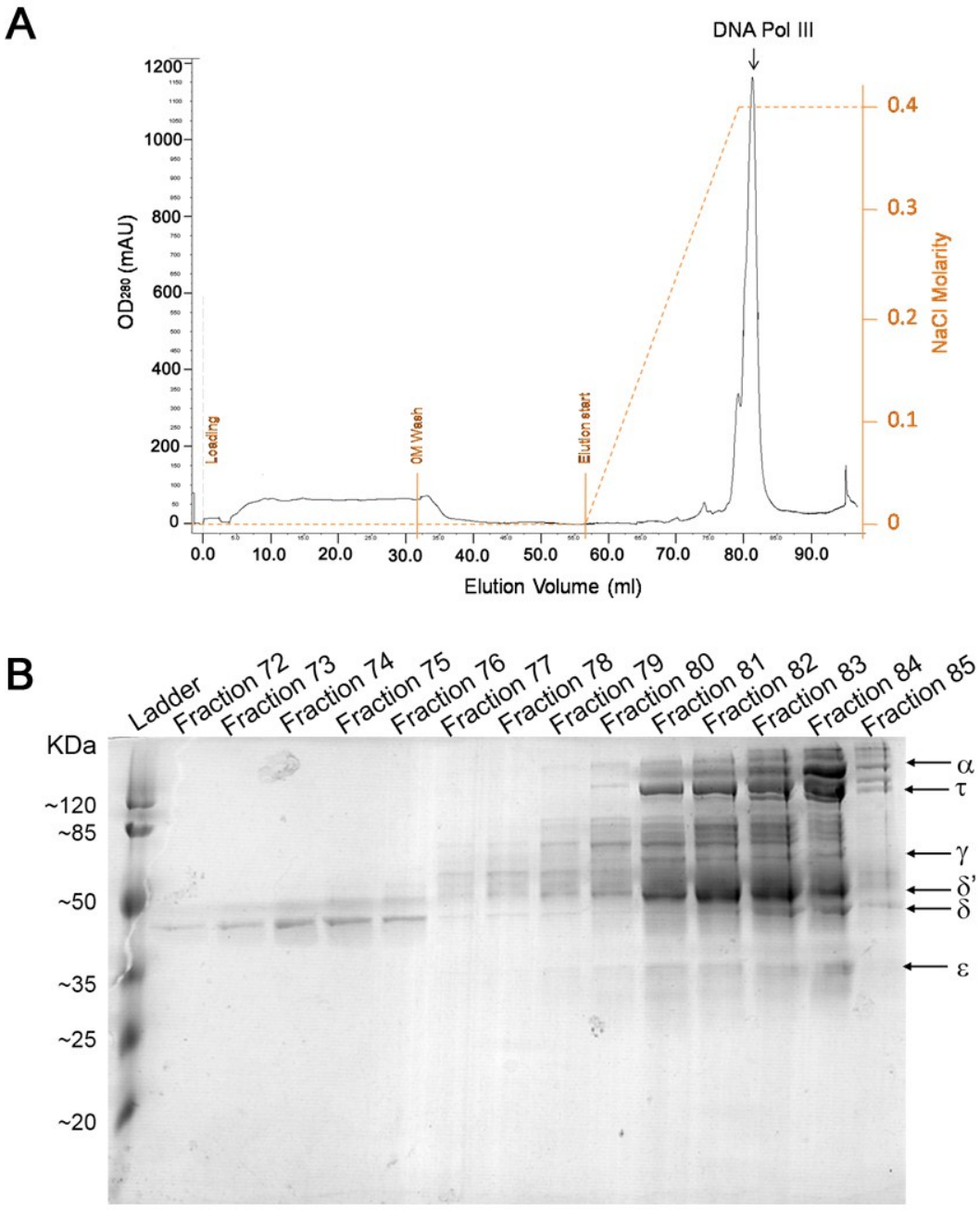


Figure 2-14. Analysis of FPLC purified fractions containing assembled DNA Pol III complex

(A) Chromatogram from assembly of DNA Pol III complex at OD_{280} using the Mono-Q 5/50 GL column (GE). (B) Analysis of fractions containing assembled DNA Pol III complex via 12% SDS-PAGE.

2.2.7 Extension assay of DNA Pol III Holoenzyme

A polymerase extension assay was performed in *in vitro* to explore the activity of the new assembled DNA Pol III complex to verify the effectiveness of the reconstitution of component DNA Pol III subunits. In this assay, the synthetic primed circular M13KE ssDNA was used as the template. M13KE ssDNA was isolated from M13KE phage and infected in *E. coli*, purified by PEG and further extracted by DNA extraction method from the agarose gel (Materials and Methods). In addition, M13KE replicative form (RF) double-strand DNA (dsDNA) was prepared simultaneously by alkaline lysis method (Materials and Methods). Two forms of M13KE DNA were examined via sequencing and analysed on a 0.8% agarose gel (Fig. 2-16A). The band of M13KE dsDNA presented a slower migration than the ssDNA band due to the difference of molecular size.

Three strategies of primed ssDNA template for polymerase extension assay were prepared via annealing (Fig 2-15). “Primer_1”, a 26-base oligonucleotide, was primed on M13KE ssDNA for “Template 1”. Two primer primed templates, “Template 2” and “Template 3” were constructed via annealing to simulate DNA replication fork. A 201 bases gap was designed between “Primer_1” and “Primer_2” in the “Template 2”. “Primer_3” was located opposite to “Primer_1” in the “Template 3”. There was a 3537 bp gap between two annealed primers. Three templates were quantified via Qubit ssDNA assay (Materials and Methods).

In the polymerase extension assay, primed ssDNA templates were incubated with resembled *N. meningitiids* DNA Pol III complex and β-clamp at 25°C for 1 hour in the precence of dNTPs and inactivated by heating, and were then analysed by 0.8% agarose gels (Fig. 2-16). Pure M13KE ssDNA was also analysed in the same gel as the negative controls.

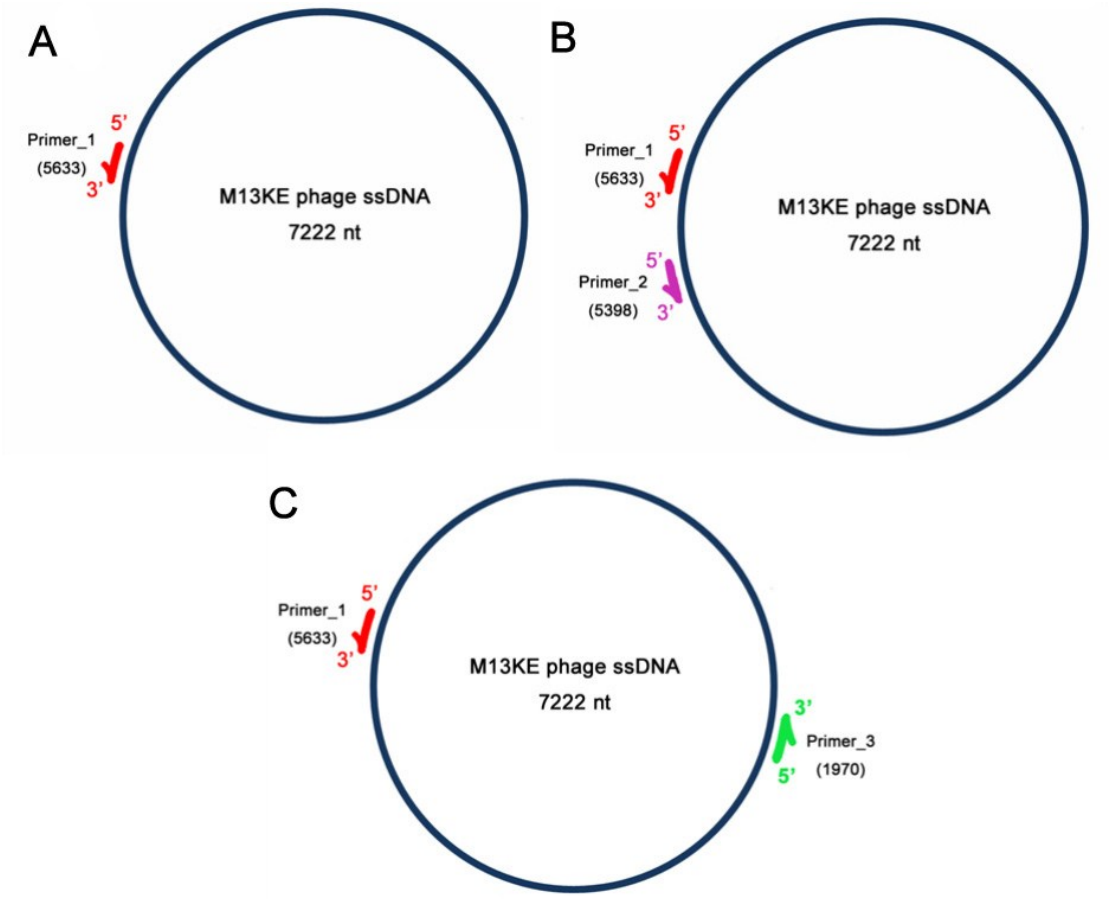


Figure 2-15. Schematic of three primed M13KE ssDNA templates for polymerase extension assays

A) In the Template 1, Primer1 was annealed with M13KE ssDNA B) Primer_1 and Primer_2 were annealed with M13KE ssDNA. A 201-base gap is designed between two primers. C) Primer_1 and Primer_3 were annealed with M13KE ssDNA. A 3637 bases gap is designed between two primers.

In the presence of both DNA Pol III complex and β-clamp, the template-2 and the template-3 were detectablly extended with slower migration compared to enzyme-free ssDNA (Fig. 2-16B). It indicates that the reconstituted DNA Pol III HE is active and can synthesize from primed ssDNA to dsDNA. On other hand, the extension of the ssDNA template-1 was less visible in the gel (Fig. 2-16B). It shows that DNA Pol III HE may prefer to synthesize DNA with multiple primers. During DNA replication, DNA systhesis is performed simultaneously on the leading and the lagging strands (Watson *et al*., 2004). Therefore, a single primer is unusual to be occurred alone in the replication fork.

When the β-clamp was absent in the assay, the extension of all three-primed ssDNA was weakened and less obvious (Fig. 2-16C). It suggests that the β-clamp is crucial for DNA Pol III HE during DNA synthesis, which requiring the processivity provided by the β-clamp.

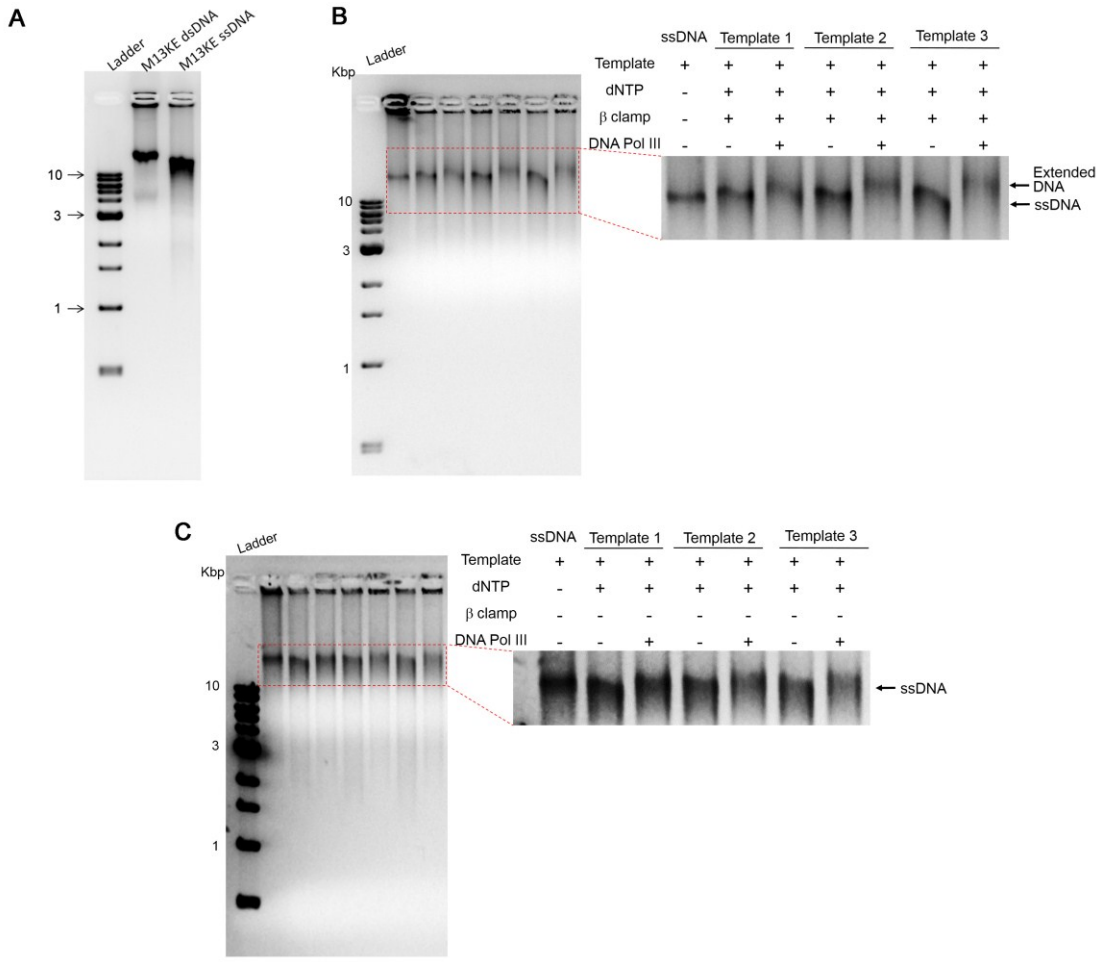


Figure 2-16. Analysis of primed ssDNA extensions by DNA Pol III HE (*N. meningitis*)

DNA products were analysed by 0.8% agarose gels and strained by 0.5 μg/ml of EtBr against 1kb DNA ladder (NEB). (A) 10nM of M13KE ssDNA and dsDNA (B) The incubation products of three primed ssDNA with DNA Pol III HE, including DNA Pol III complex and β-clamp. (C) The incubation products of three primed ssDNA with DNA Pol III complex only, without β-clamp.

2.3 Discussion

2.3.1 MBP-Tag provides solubility factors for DNA Pol III subunits purification

As presented above, protein insolubility significantly hampered effects to purify subunit δ and δ' proteins. The solubility of protein is influenced by many other factors, such as the ingredients of the storage buffer, pH of buffer, temperature and cellular proteases. Because the purification was performed at low temperature and the addition of protease inhibitor tablets, temperature and proteases were dismissed. Because downstream purifications of DNA Pol III subunits would require defined salt and pH conditions for MonoQ ionic exchange column, there was limited opportunity to enhance solubility with different buffer and salt conditions. Therefore, two methods were utilized to increase solubility of proteins in this project.

Firstly, the addition of detergents was performed to attempt to improve the solubility of subunit δ'. Detergents were widely used as solubilisers during isolation and purification of proteins, especially integral membrane proteins (Luche, Santoni & Rabilloud, 2003). In fact, the results proved that all three detergents Triton X-100, Tween-20 and Sarkosyl did recued the solubility of DNA Pol III subunit δ' to different extents. However, the disruption of TEV protease cleavage from detergents was incapable for further purification. Meanwhile, the addition of detergents brought potential risks to affect the downstream activities of DNA Pol III complex. Consequently, the other method which constructed a soluble chaperone to the target gene was carried out.

MBP is a widely employed tag protein which is able to raise the solubility of recombined fusion protein expressed in *E. coli* (Kapust & Waugh, 1999). Although the mechanism of MBP cannot be concluded firmly due to various

reasons for the insolubility of partner proteins, the function of MBP was investigated to boost general molecular chaperone to prevent aggregation of folding intermediates (Kapust & Waugh, 1999). In addition, studies have shown that soluble fusion proteins are achieved when MBP was fused at the N-terminal of the partner protein (Sachdev & Chirgwin, 1998). Notably, the His-tag was uncleavable by TEV protease at the N-terminal of δ' in the pPROEX-Htb construct, which discussed in the beginning of this study. In addition, Dr. Jan Silhan reported that subunit δ had the insoluble issue during and after his-tag purification in the previous study (lab data, unpublished).

In order to overcome these issues, the new expression construct was developed with a MBP-tag included vector pETM43. Two alternative strategies were performed to maintain the experimental efficiency of this project. One construct was designed to contain the subunit δ' fused to MBP directly. The other construct was created the subunit δ fused to MBP tag, followed by a δ' sequence so that subunits δ and δ' could be co-expressed and co-purified in this strategy. In the studies of *E. coli*, subunits δ and δ' were reported to have close functional interaction to direct the loading of β-clamp during DNA replication (Stewart *et al.*, 2001; Oyama *et al.*, 2001). Therefore, the co-expression construct was necessary to improve the stability of subunits δ and δ' and also reduce the loss of protein in the purification process. TEV cleavage sites were created between MBP tag and target proteins. Both constructs were over-expressed in good yield. However, MBP binds maltose with a Kd in the low μM range during the elution of fusion proteins. To remove the remaining full-length fusion proteins and cleaved MBP-tag, several dialysis steps are needed to go from a high mM concentration of maltose to low nM. In order to avoid the tedious dialysis of maltose in the elution, tag-free proteins were cleaved with amylose resin by TEV protease. Both subunit δ' protein and δ.δ' co-expressed protein was gained in good yield at soluble conditions during and after

purifications. Meanwhile, DNA Pol III subunit α, ε, γ·τ and β-clamp were prepared from the initial His-tag vector pPROEX-HTb in good yield.

2.3.2 Reconstitution of DNA Pol III complex was carried out using MonoQ anionic exchange column

The reconstitution of DNA Pol III complex from *N. meningitidis* was performed via the formation of two intermediate complexes, the core complex (α·ε) and the clamp loader complex (δ·δ'·γ·τ). The conditions and protocol was based on the purification of DNA Pol III complex from *E. coli* (O'Donnell & Studwell, 1990; Studwell & O'Donnell,1990; McInerney & O'Donnell, 2004).

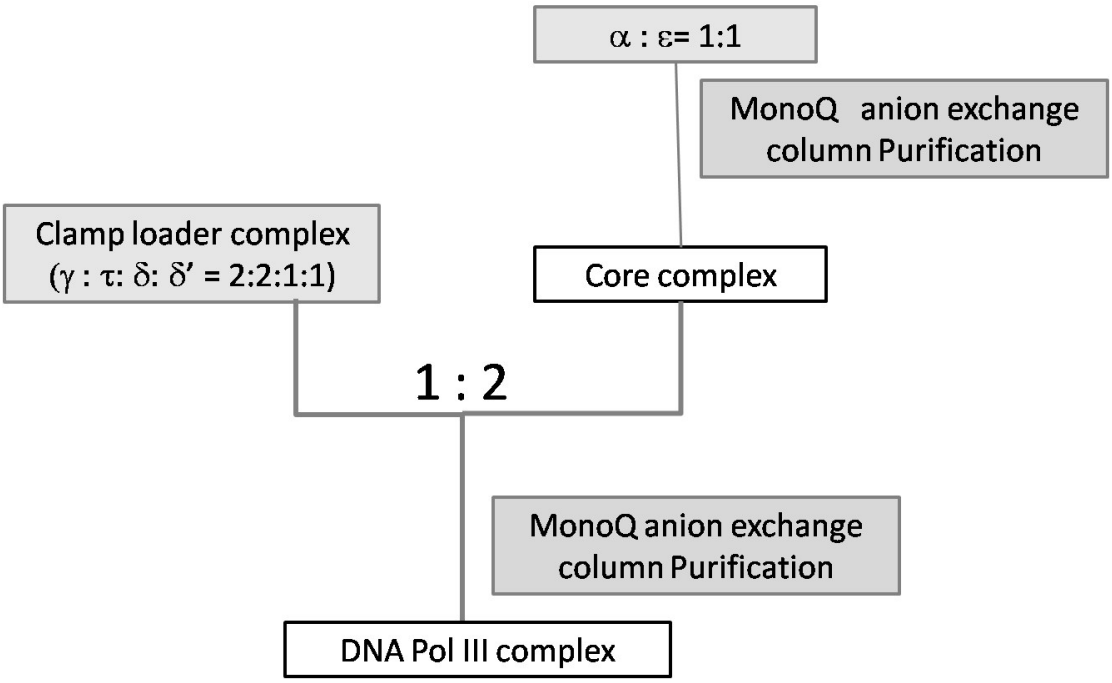


Figure 2-17. Assembly strategy of DNA Pol III complex

Owing to the lacking of structural study data of DNA Pol III complex, the actual ratio of each component in the complete complex is still not clear. According to the structure of DNA Pol III complex from *E. coli,* the study of reconstitution of DNA Pol III complex from *N. meningitidis* assumed the ratio of subunit

$\alpha \cdot \varepsilon \cdot \delta \cdot \delta' \cdot \gamma \cdot \tau$ is 2:2:1:1:2:2 which is idencial with the stoichiometry of *E. coli* DNA Pol III HE in *in vitro studies.* Meanwhile, in *E. coli*, the core complex is purified by MonoQ chromatography while the clamp loader is purified by MonoS chromatography. In *N. meningitidis*, the assembly and purification of core complex was achieved in good yield. However, the clamp loader complex was unable to be purified by the MonoS protocol (reported by Dr. Lucy Rayner, lab data). During the purification in the MonoS column, the majority of the proteins were unable to bind the MonoS column. Consequently, MonoS purification of the clamp loader was omitted. The clamp loader complex was formed on ice without purification and then formed with the core complex. The purification of DNA Pol III complex was performed from unbound subunits in the MonoQ column (Fig. 2-17). Through the analysis on MonoQ chromatograph and SDS-PAGE, the reconstitution of DNA Pol III complex was performed in good yield using this modified protocol.

2.3.3 Assembled DNA Pol III complex performed extension of various primed ssDNA

In order to examine whether the purified *N. meningitidis* DNA Pol III and β-clamp were able to extend primed ssDNA, extension assays were performed with primed M13KE ssDNA. During DNA replication, DNA Pol III HE synthesizes DNA continuously on the leading strand, and extend short, separated segments on the lagging strand (Banach-Orlowska *et al.*, 2005).

In this study, the extension assay was carried out to evaluate the resembly *Neisserial* DNA Pol III HE. The result shows that the reconstituted DNA Pol III HE is able to extend ssDNA templates which primed by multiple primers from ssDNA to dsDNA in the precence of dNTPs. Moreover, the β-clamp cannot be removed during DNA resynthesis, which could be effected the processivity of DNA Pol III. Certainly, the results of the polymerase extension assay are not

very strong evidences that can fully determine the activity of *Neisserial* DNA Pol III HE. However, this assay initially detected the feasibility of the preparation strategy of DNA Pol III HE from *N. meningitids in vitro*. Further studies are required to be carry out to assess the role of DNA Pol III HE in MMR with specific DNA substrates.

Furthermore, in *E. coli*, subunit χ and ψ were involved in the interaction with single-strand binding proteins during DNA replication (Tondnevis *et al.*, 2015). In *N. meningitidis*, however, due to lacking the gene fragments which encode subunit χ and ψ, the pattern that how DNA Pol III HE associates with single-strand binding proteins is still unknown. At least, this study indicated that DNA Pol III HE could carry out DNA synthesis without the addition of single-strand binding proteins in *N. meningitidis.* The next stage in this project was to detect the role of *N. meningitidis* MMR system, including *Nm*MutS and *Nm*MutL proteins, using *in vitro* assays.

Chapter 3

Detection of mismatch recognition in *N. meningitidis*

3.1 Background and objectives

The MMR system recognises and corrects mismatches that arise during DNA replication to prevent the accumulation of gene mutations and maintain genome integrity (Friedberg *et al.*, 2005). In the best understood *E. coli* MMR system, MutS recognises the mismatch and then specifically binds to DNA at the mismatched site (Su & Modrich, 1986). MutS initiates the MMR system of *E. coli* and then recruits MutL by the ATP-binding (Su & Modrich, 1986). MutL further recruits MutH endonuclease to perform strand discrimination by nicking at the "GATC" site on the strand without Dam methylation (Modrich & Lahue, 1996). Strand discrimination is essential of the MMR system which directs the downstream removal of the mismatch and DNA re-synthesis (Su & Modrich, 1986).

However, the unique paradigm of strand discrimination in the MMR system of *E. coli* is not applicable for all eukaryotes and other bacteria due to the lack of a homolog of MutH and Dam methylase. Therefore, strand discrimination must proceed with an alternative mechanism. Unlike MutH, MutS and MutL homologues maintain the high conservation and widely exist in MutH-lacking organisms (Fukui *et al.*, 2011). Genetic defect in MutS and MutL leads to the accumulation of mismatches during DNA replication (Harfe & Jinks-Robertson, 2000). In human, lacking homologues of MutS and MutL may lead patients to have the microsatellite instability and relates to hereditary nonpolyposis colon cancer (Fishel *et al.*, 1993; Fishel & Wilson, 1997).

The genes of MMR proteins were identified in *N. meningitidis*, including *mutS* and *mutL*, but MutH homologue was not found (Richardson & Stojiljkovic, 2001). In this study, using *N. meningitidis* as a new model organism, MMR enzymes *N. meningitidis* MutS (*Nm*MutS) and MutL (*Nm*MutL) would be over-expressed

and purified based on previous lab cloning data (Dr. Jan Silhan, lab data). To investigate the interaction of MMR proteins and mismatched DNA, the electrophoretic gel shift assay was the major method that was performed in this chapter. The gel shift assay is a widely-used affinity electrophoresis method to investigate interactions between protein and nucleic acid (Hendrickson, 1985). During the assay, the migration of DNA is shifted by the interaction with protein via non-denaturing polyacrylamide gel electrophoresis (PAGE). The complex of protein and DNA with various stoichiometric ratios is provided a matrix to enhance its stabilisation by the native PAGE gel (Fried & Crothers, 1981). As a consequence, the migration of protein-DNA complex is slower than the free DNA (Revzin, 1989). In this study, to detect the activity of *Nm*MutS and *Nm*MutL in the initial of MMR, gel shift assays were carried out with DNA substrates containing a T/G mismatch *in vitro*. Meanwhile, the values of dissociation constant were measured based on the observation of gel results.

3.2 Results

3.2.1 Expression and purification of *Nm*MutS and *Nm*MutL

*Nm*MutS and *Nm*MutL were respectively cloned in the vector pPROEX-HTb which described above included a His-tag at the N-terminus and were resistant to ampicillin (Dr. Jan Silhan, lab data). Both plasmids containing *Nm*MutS and *Nm*MutL were extracted and confirmed by sequencing. The molecular weight of *Nm*MutS is 95240 g/mol, and *Nm*MutL protein is 71647 g/mol.

After transformation of the plasmid DNA into BL21(DE3) cells, both *Nm*MutS and *Nm*MutL were sufficiently over-expressed due to the induction by IPTG and was detected by SDS-PAGE gel (Fig. 3-1A, 3-2A). His-tag purification of *Nm*MutS and *Nm*MutL was identical with DNA Pol III subunits with N-terminus His-tags via Ni^{2+} chelating beads (described in Chapter 2), and was analysed by SDS-PAGE gel (Fig. 3-1B, 3-2B). His-tagged *Nm*MutS and *Nm*MutL was eluted from Ni-column separately with imidazole. Eluted fractions were analysed by SDS-PAGE gel (Fig. 3-1C, 3-2C). Fractions containing proteins with the His-tag were combined, desalted and concentrated prior to being incubated with TEV protease to cut off the His-tag. Purified His-tag free *Nm*MutS and *Nm*MutL was respectively gained after flew through a fresh Ni-column and was analysed by SDS-PAGE gel (Fig. 3-1D, 3-2D). Further purification was carried out via HPLC size exclusion chromatography. Both *Nm*MutS and *Nm*MutL were collected and concentrated. Purified proteins were quantified and then stored in the storage buffer at -20°C.

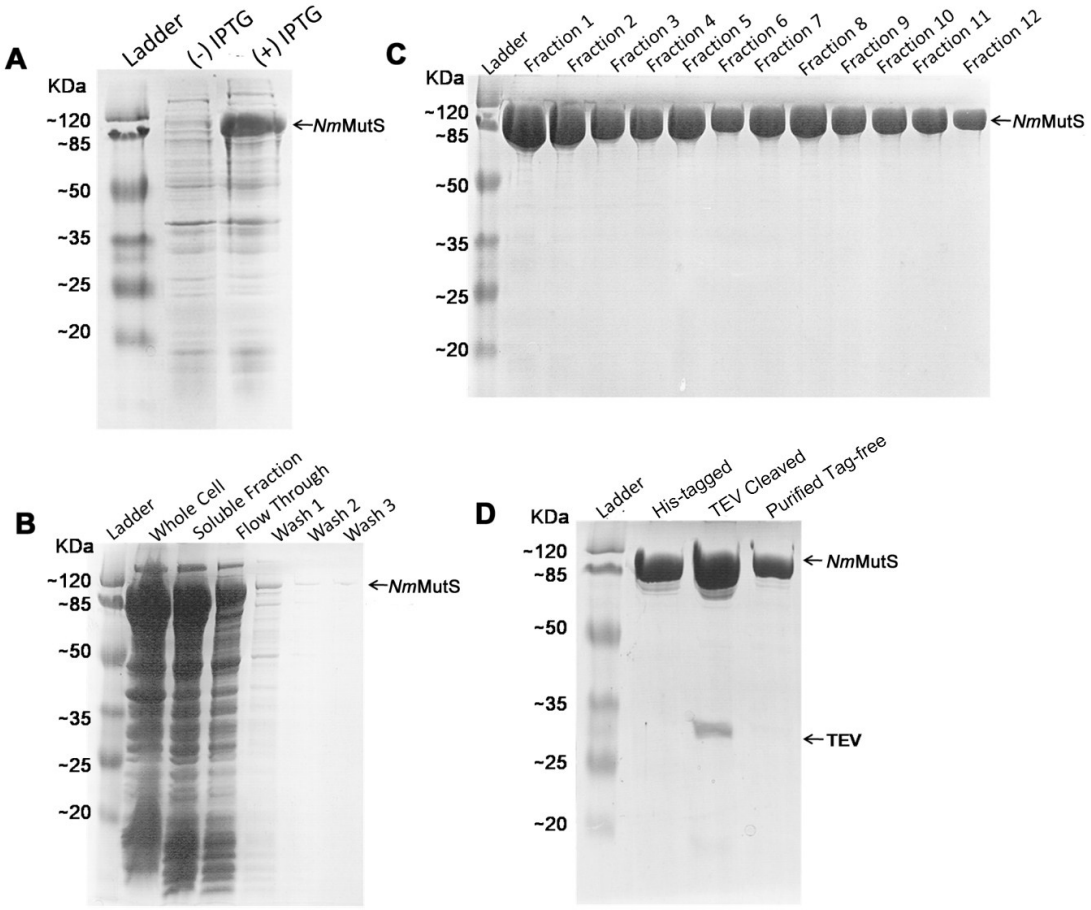


Figure 3-1. Expression and purification of *Nm*MutS

(A)12% SDS-PAGE analysis of *Nm*MutS expression level of 1mM IPTG-induced *E. coli*BL21(DE3) cell colonies atOD_{600} of 0.4 in 4hrs at 25°C. (B)(C) 12% SDS-PAGE analysis of *Nm*MutS protein fractions collected from the Ni-column. (D) 12% SDS-PAGE analysis of *Nm*MutS after TEV protease cleavage and flow through the fresh Ni-column.

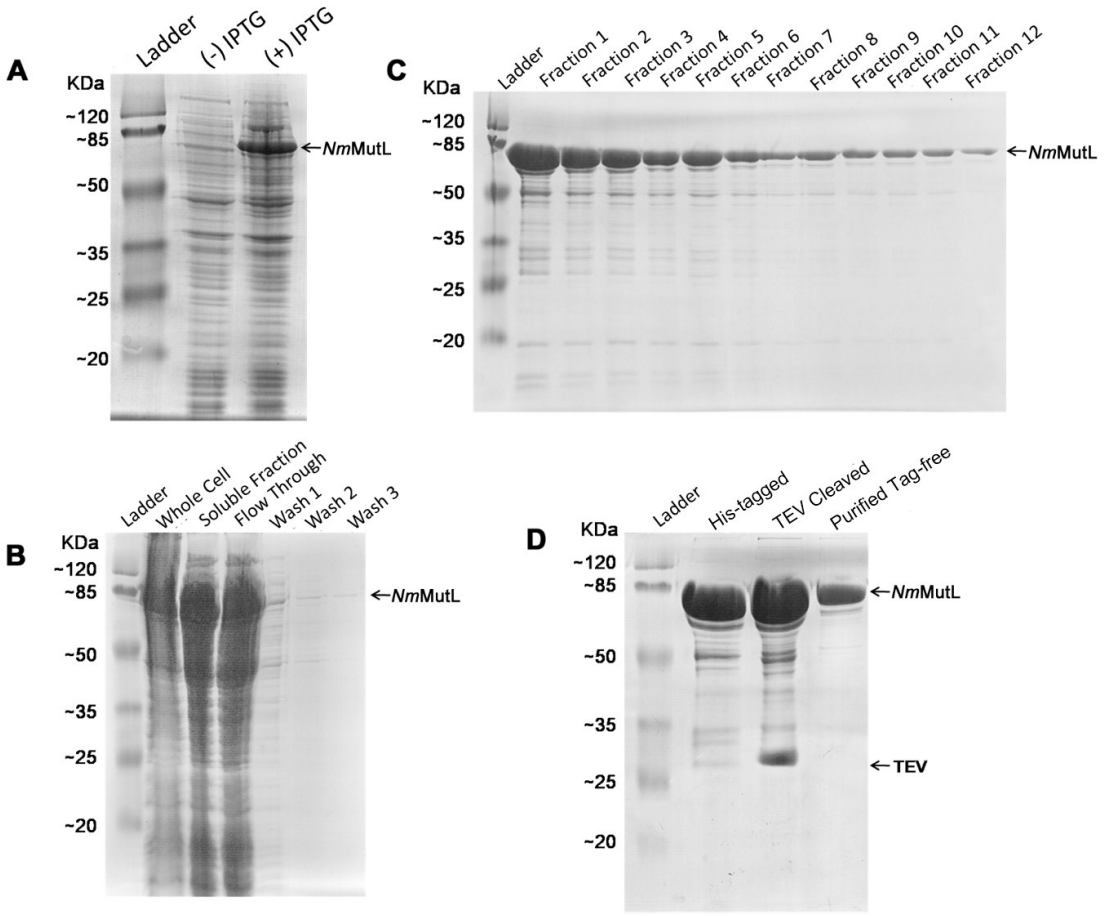


Figure 3-2. Expression and purification of *Nm*MutL

(A) 12% SDS-PAGE analysis of *Nm*MutL expression level of 1mM IPTG-induced *E. coli* BL21(DE3) cell colonies atOD_{600} of 0.4 in 5hrs at 25°C. (B)(C) 12% SDS-PAGE analysis of *Nm*MutL protein fractions collected from the Ni-column. (D) 12% SDS-PAGE analysis of *Nm*MutL after TEV protease cleavage and flow through the fresh Ni-column.

3.2.2 Gel shift assays of MutS and MutL with short DNA duplexes

To detect interactions between individual MMR components with mismatched DNA at the initial stage of MMR system, the gel shift assay was carried out using purified *Nm*MutS and *Nm*MutL with 30-bp open-end linear DNA duplexes (OL30) *in vitro* (Fig. 3-3). The complement duplex was performed as the native control without mismatch ($OL30^{C/G}$). A T/G mismatched base pair was located at the midpoint of the heteroduplex ($OL30^{T/G}$). DNA duplexes were prepared via annealing and were purified via native PAGE (see Materials and Methods). A 6-carboxyfluorescein (FAM) was labelled at the 5-terminus on the down oligonucleotide strand of both DNA duplexes (Fig. 3-3). FAM is a commonly used fluorescent dye for labelling oligonucleotides as hybridization probes for various studies *in vivo* and *in vitro* (Livak, *et al.*, 1995). When conjugated to DNA, the FAM fluorophore exhibited fluorescence signal to present the mobility status of DNA-protein complexes.

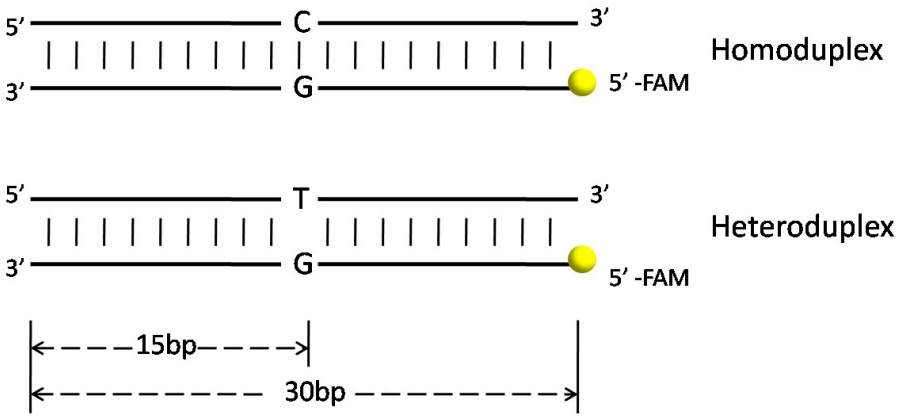


Figure 3-3. Schematic of 30-bp linear DNA Duplexes ($OL30^{C/G}$ and $OL30^{T/G}$)

Gel shift assays were performed by 40nM $OL30^{C/G}$ and $OL30^{T/G}$ with various concentrations of *Nm*MutS, *Nm*MutL and the mixture of *Nm*MutS and MutL (see Materials and Methods). Moreover, the addition of 2mM ATP was used to exam the role of ATP in mismatch recognition. To facilitate the quantitation of data, DNA bands were quantified to determine the percentage of bound DNA by

proteins and were further analysed by the charts of non-linear curves fitting the Hill equation (see Materials and Methods).

In the assay carried out by *Nm*MutS alone, *Nm*MutS did not bind to the homoduplex DNA with all concentrations of *Nm*MutS (Fig. 3-4A, C). With DNA containing a T/G mismatch, a weak shifted band was observed above the free DNA duplex (Fig. 3-4B, D). When increasing concentrations of *Nm*MutS, the shifted band was enhanced. This result revealed that *Nm*MutS bound specifically to mismatched DNA. However, there was still a large amount of unbound DNA remaining, and only about 36% $OL30^{T/G}$ DNA was interacted with 2μM of *Nm*MutS. It demonstrated that the *Nm*MutS-mismatch binding was very weak. The addition of ATP did not evidently affect the assays with either $OL30^{C/G}$ or $OL30^{T/G}$ DNA.

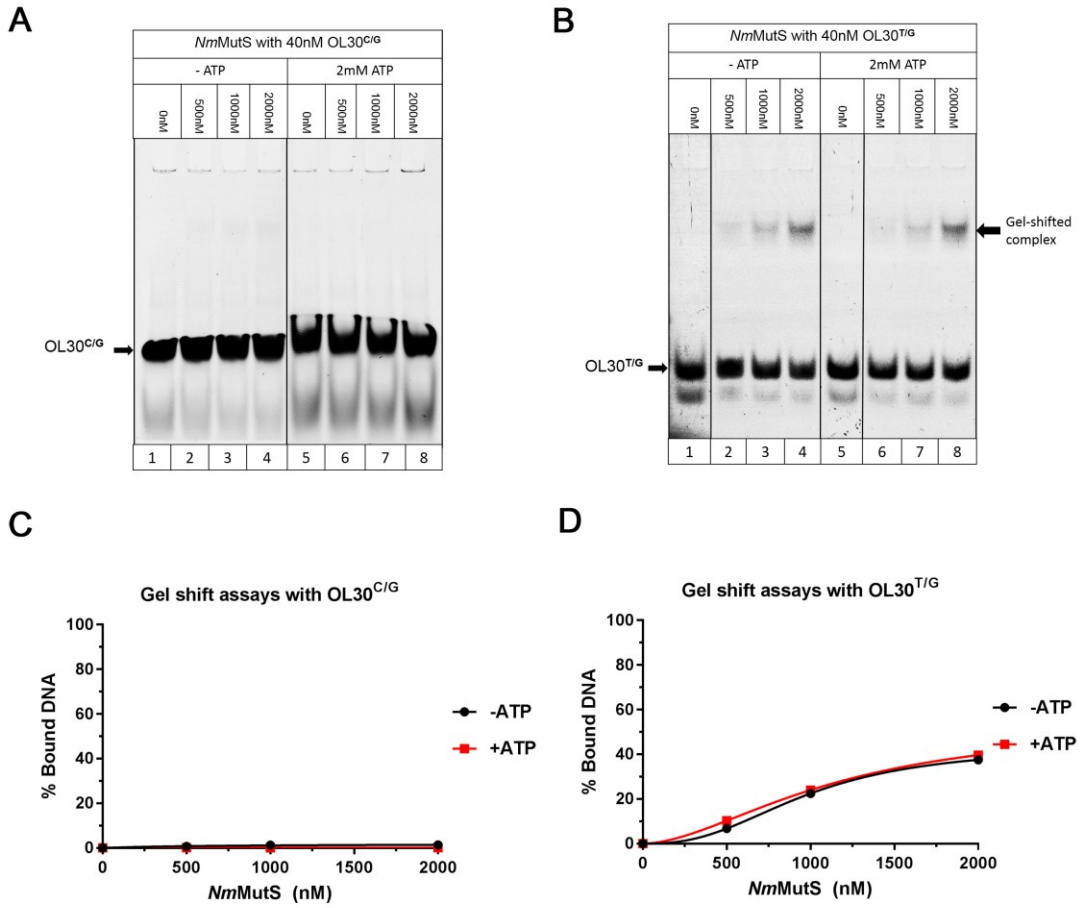


Figure 3-4. Gel shift assays *Nm*MutS with OL30 DNAs

Gel shift assays were performed under (-/+) ATP conditions in the gel shift buffer at 25°C for 20 minutes and were resolved by 10% native PAGE (see Materials and Methods). **(A)** Increasing concentrations of *Nm*MutS were incubated with 40nM FAM labelled $OL30^{C/G}$. Lane1-4 and Lane 5-8 were run in the two independent physical gels. For clarity, the two separate gels are indicated by the vertical line between lanes 4 and 5. **(B)** Increasing concentrations of *Nm*MutS were incubated with 40nM FAM labelled $OL30^{T/G}$. Lane1, lanes 2-4 and lanes 5-8 were run in three independent physical gels the same condition. Lane 5 and Lane 6-8 was run in the same physical gel discontinuously. This is indicated by the vertical lines between Lanes 1 and 2, 4 and 5 and 5 and 6. The control lanes 1 and 5 are also used in Fig. 3-5B and Fig. 3-6B. **(C)(D)** Gels(A)(B) were quantitated to determine the percentage bound DNA using ImageJ software and the data was analysed via GraphPad Prism 7. Data of reactions in the absence of ATP was shown with black lines and markers whereas data in the presence of ATP was exhibited by red lines and markers. The data is representative of two independent experiments.

In *E. coli*, *Ec*MutL is an intermediate protein, which is activated by *Ec*MutS mismatch recognition and then simulates the activity of strand discrimination from MutH (Su & Modrich, 1986). To investigate the role of *Nm*MutL, we also perform the gel shift assay with *Nm*MutL *in vitro*.

Firstly, the assay of *Nm*MutL was carried out with both $OL30^{C/G}$ and $OL30^{T/G}$ DNA. *Nm*MutL bound to the homoduplex DNA at the highest concentration of protein (2μM) (Fig. 3-5A). There was a weak shifted band closed to the gel well. The amount of unbound DNA was reduced with the binding complex. With DNA containing a T/G mismatch, the interaction of *Nm*MutL and $OL30^{T/G}$ DNA was also very weak. A faint shifted band was observed in the assay of 2μM *Nm*MutL (Fig. 3-5B). It revealed that *Nm*MutL might non-specifically bind to both the homoduplex DNA and DNA with a T/G mismatch. Meanwhile, although free DNA duplex was reduced by the *Nm*MutL-DNA interaction, the rest of unbound DNA was markedly detectable. No more than 22% of $OL30^{C/G}$ or $OL30^{T/G}$ DNA was bound to *Nm*MutL at high concentrations of *Nm*MutL (Fig. 3-5C, D). It demonstrated that the binding of *Nm*MutL and DNA duplexes was very weak. Additionally, it showed that the addition of ATP slightly promoted the binding of *Nm*MutL with either $OL30^{C/G}$ or $OL30^{T/G}$ DNA (Fig. 3-5C, D), although their bindings still kept still in low degrees (Fig. 3-5C, D).

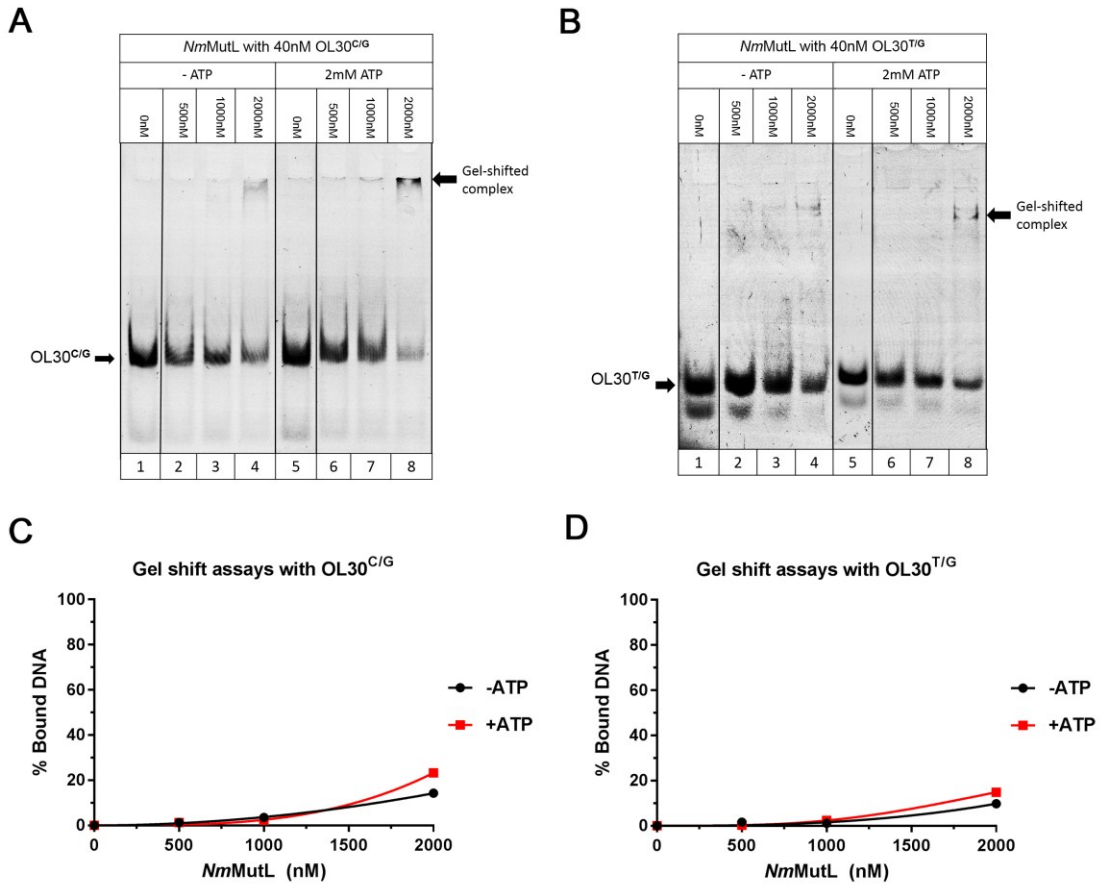


Figure 3-5. Gel shift assays of *Nm*MutL with OL30 DNAs

Gel shift assays were performed under (-/+) ATP conditions in the gel shift buffer at 25°C for 20 minutes and were resolved by 10% native PAGE (see Materials and Methods). **(A)** Increasing concentrations of *Nm*MutL were incubated with 40nM FAM labelled $OL30^{C/G}$. Lanes 1-8 were run in the same physical gel discontinuously. This is indicated by the vertical lines between Lanes 1 and 2, 4 and 5 and 5 and 6. **(B)** Increasing concentrations of *Nm*MutL were incubated with 40nM FAM labelled $OL30^{T/G.}$ Lane1, lanes 2-3, lane 5 and Lane 6-8 were run in three independent physical gels the same condition. This is indicated by the vertical lines between Lanes 1 and 2, 4 and 5 and 5 and 6. The control lanes 1 and 5 are also used in Fig. 3-4B and Fig. 3-6B. **(C)(D)** Gels(A)(B) were quantitated to determine the percentage bound DNA using ImageJ software and the data was analysed via GraphPad Prism 7. Data of reactions in the absence of ATP was shown with black lines and markers whereas data in the presence of ATP was exhibited by red lines and markers. The data is representative of two independent experiments.

To further investigate if *Nm*MutS and *Nm*MutL modulate the activity of mismatch recognition, we also perform the gel shift assay of *Nm*MutS and *Nm*MutL at the same concentration with $OL30^{C/G}$ and $OL30^{T/G}$ DNA.

With the homoduplex DNA, there was a weak and smearing binding complex only observed with 2uM of *Nm*MutS and *Nm*MutL (Fig. 3-6A, C). With the addition of ATP, the binding complex was slightly promoted that there was a faint smearing band with 1μM of *Nm*MutS and *Nm*MutL (Fig. 3-6A, C). Compared with the assay of *Nm*MutS alone, the non-specific binding with the homoduplex DNA was increased after adding *Nm*MutL into the assay.

In the assay of DNA with a T/G mismatch, a defined shifted band occurred and increased with rising concentrations of *Nm*MutS and *Nm*MutL. This shift had the similar size with the shifted band in the assay of *Nm*MutS alone. In addition, a slight shift of *Nm*MutL also appeared with the highest concentration of *Nm*MutL after adding 2mM ATP (Fig. 3-6B, D). The maximum binding occurred with 1μM of *Nm*MutS and *Nm*MutL in the presence of ATP, nearly 50% of mismatched DNA was bound (Fig. 3-6D). It was noteworthy that with MutS and MutL, the shifted bands were consistent with arising from binding of the indiviaual proteins, rather than the formation of super-shifted complex of *Nm*MutS-*Nm*MutL.

Over all, the specific binding of DNA with a T/G mismatch only occurred in assays in the presence of *Nm*MutS and was very weak (Fig. 3-4A, B). *Nm*MutL exhbited nonspecific binding with both the homoduplex DNA or the heteroduplex DNA with a T/G mismatch (Fig. 3-5A, B). The greatest binding was observed with the combination of *Nm*MutS and *Nm*MutL with T/G mismatched DNA after adding ATP (Fig. 3-6). There was no evidence to support that *Nm*MutL could contribute the recognition activty of mismatch from *Nm*MutS.

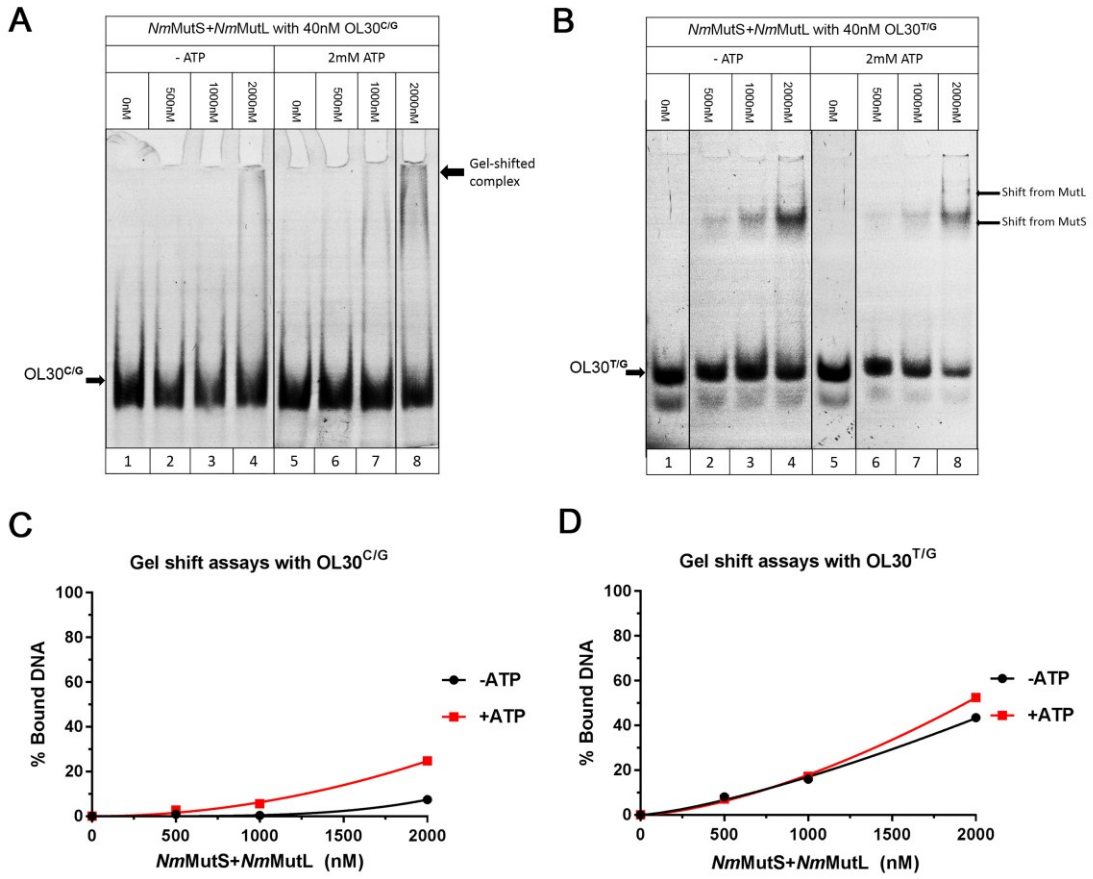


Figure 3-6. Gel shift assays of *Nm*MutS and *Nm*MutL with OL30 DNAs

Gel shift assays were performed under (-/+) ATP conditions in the gel shift buffer at 25°C for 20 minutes and were resolved by 10% native PAGE (see Materials and Methods). **(A)** Increasing concentrations of the mixture of *Nm*MutS and *Nm*MutL were incubated with 40nM FAM labelled $OL30^{C/G}$. Lanes 1-4 and lanes 5-8 were run in the two independent physical gels. Lanes 5-7 and lane 8 were run in the same physical gel discontinuously. This is indicated by the vertical lines between Lanes 4 and 5 and 7 and 8. **(B)** Increasing concentrations of the mixture of *Nm*MutS and *Nm*MutL were incubated with 40nM FAM labelled $OL30^{T/G}$. Lane1, lanes 2-4 and lanes 5-8 were run in three independent physical gels the same condition. Lane 5 and Lane 6-8 was run in the same physical gel discontinuously. This is indicated by the vertical lines between Lanes 1 and 2, 4 and 5 and 5 and 6. The control lanes 1 and 5 are also used in Fig. 3-4B and Fig. 3-5B. **(C)(D)** Gels(A)(B) were quantitated to determine the percentage bound DNA using ImageJ software and the data was analysed via GraphPad Prism 7. Data of reactions in the absence of ATP was shown with black lines and markers whereas data in the presence of ATP was exhibited by red lines and markers. The data is representative of two independent experiments.

Although the band shift was observed in the presence of *Nm*MutS or *Nm*MutL, the interactions were too weak to measure dissociation constants for binding by fitting a binding equation. In previous studies, *Ec*MutS has been reported to prefer to bind mismatched DNA in the ADP-bound state (Acharya *et al.*, 2003). Therefore, we suspected if the lacking of ADP resulted that neither *Nm*MutS nor *Nm*MutL cound suffiently bind to OL30 DNAs.

To examine the role of ADP in mismatch binding, we also carried out the gel shift assay of *Nm*MutS and *Nm*MutL with high concentration (1μM) and mismatch DNA ($OL30^{T/G}$) in the presence of ADP. The result revealed that there was no detectable change with the addition of ADP or ATP in the gel shift assay of *Nm*MutS or *Nm*MutL or a combination of both (Fig. 3-8). It suggested that the insuffient binding of DNA and proteins in the gel shift assays might not be cause by cofactors.

In *E. coli*, the binding of ATP could lead *Ec*MutS to form a sliding clamp to translocate along DNA strands (Lamers *et al.*, 2000). Moreover, human MutS homologue MutSα is shown the evident dissociation with eithor homoduplex or mismatch DNA in the presence of ATP and is considered due to the translocation of MutSα sliding clamp structure (Gradia, Acharya & Fishel, 1997; Blackwell *et al.*, 1998). However, when the linear DNA is blocked at both ends, the mismatch-binding of MutSα is rescued (Gradia, Acharya & Fishel, 1997; Blackwell *et al.*, 1998). Hence, the insuffient binding in this study might be caused by the open-end linear structure of DNA probes which did not trap proteins effiently. To enhance the tightness of DNA-protein bindings, two alternative design strategies of more closed DNA structure were carried out in following studies.

Furthermore, to determine if DNA substrates are feasible for the gel shift assay, a positive control is necessary to be introduced in this study. As an extensively studied mismatch recognition protein, *Ec*MutS was reported to significantly bind to the heteroduplex DNA containing a T/G mismatch in the gel shift assay (Acharya, 2008). In this study, therefore, *Ec*MutS was also prepared to determine the appropriate DNA substrate and conditions of the gel shift assay in the following section.

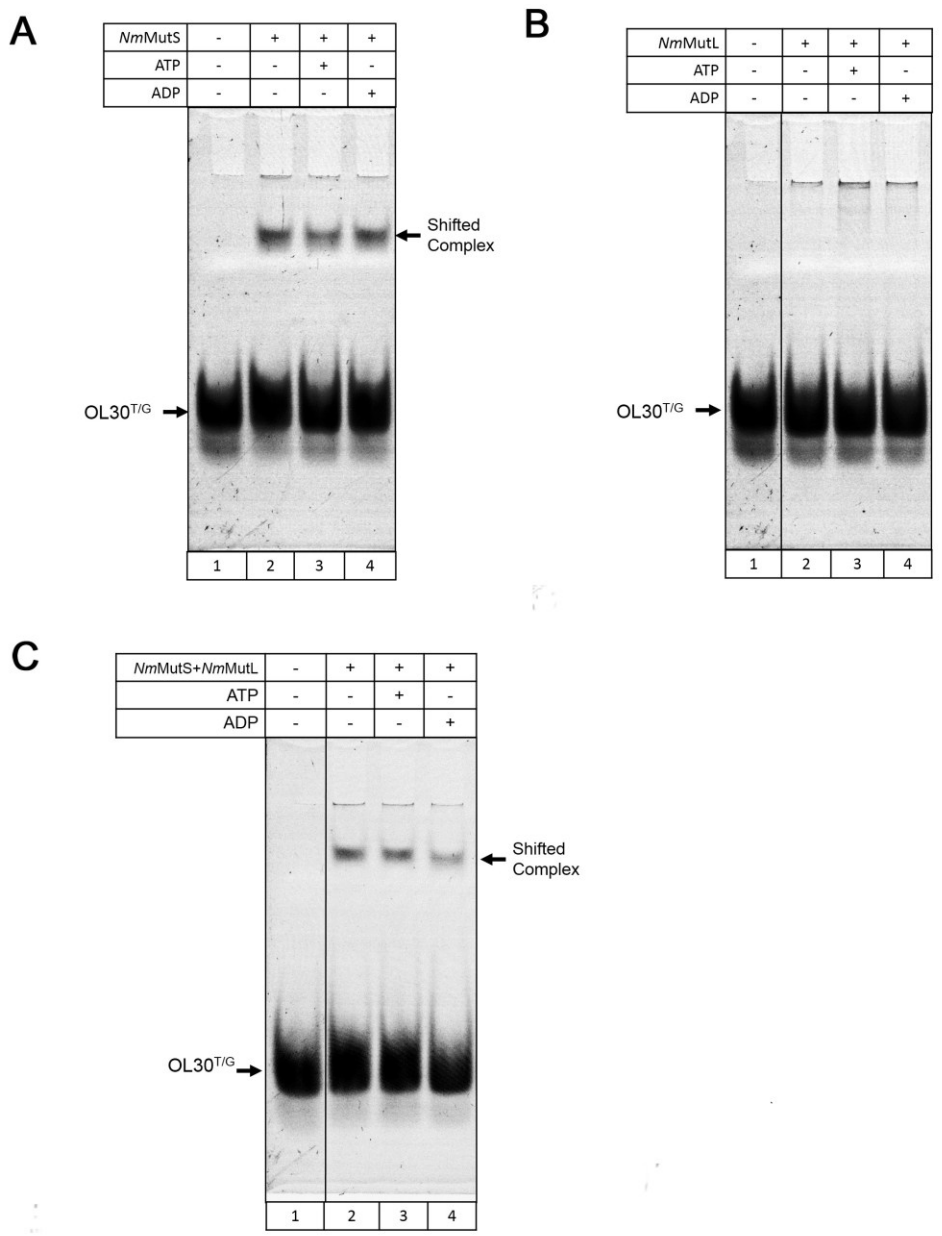


Figure 3-7. Gel shift assays of *Nm*MutS and *Nm*MutL with ATP and ADP

Gel shift assays were carried out by mismatched DNA ($OL30^{T/G}$) with *Nm*MutS and *Nm*MutL under 2mM of ATP, 2mM of ADP and negative conditions as shown. Incubation was performed in the gel shift buffer at 25°C for 20 minutes and were resolved by 10% native PAGE (see Materials and Methods). **(A)** 1μM of *Nm*MutS were incubated with 40nM $OL30^{T/G}$ DNA. Lanes 1-4 were run in the same physical gel contiguously. The control lane 1 are also used in Fig. 3-7B. **(B)** 1μM of *Nm*MutL were incubated with 40nM $OL30^{T/G}$ DNA. Lane 1 was run in the same physical gel with lanes 2-4 discontinuously. This is indicated by the vertical lines between Lanes 1 and 2. The control lane 1 are also used in Fig. 3-7A. **(C)** 1μM of a combination of *Nm*MutS and *Nm*MutL were incubated with 40nM $OL30^{T/G}$ DNA. Lane 1 was run in the same physical gel with lanes 2-4 discontinuously. This is indicated by the vertical lines between Lanes 1 and 2. This data is only conducted once.

3.2.3 Cloning, expression and purification of *Ec*MutS

*Ec*MutS gene *mutS* of approximately 2.6kbp was amplified from *E. coli K12* genomic DNA by PCR (Fig. 3-8A) and cloned into the expression vector pPROEX-HTb using BamHI and HindIII sites, which adds an N-terminal His-tag (His-tag) with cleavage site for TEV protease to the final construct. T4 ligation produce was transformed into DH5α cells, and plasmids containing were extracted and confirmed by sequencing. Subsequently, the constructed *Ec*MutS plasmid was transformed into BL21(DE3) cells.

Firstly, over-expression of *Ec*MutS was carried out by small scales to evaluate the best expression time point and isolate (Fig. 3-8B-E). The over-expression of His-tag and *Ec*MutS produced a protein with a molecular weight of 95.2KDa. Colony 4 was used to carry out the full-scale expression (Fig. 3-9A). His-tag free *Ec*MutS was purified via a method identical to that used for *Nm*MutS. The entire procedure of purification was analysed by SDS-PAGE gel (Fig. 3-9B-D). Further purification was carried out via HPLC size exclusion chromatography. Purified *Ec*MutS was quantified and then stored in the storage buffer at -20°C.

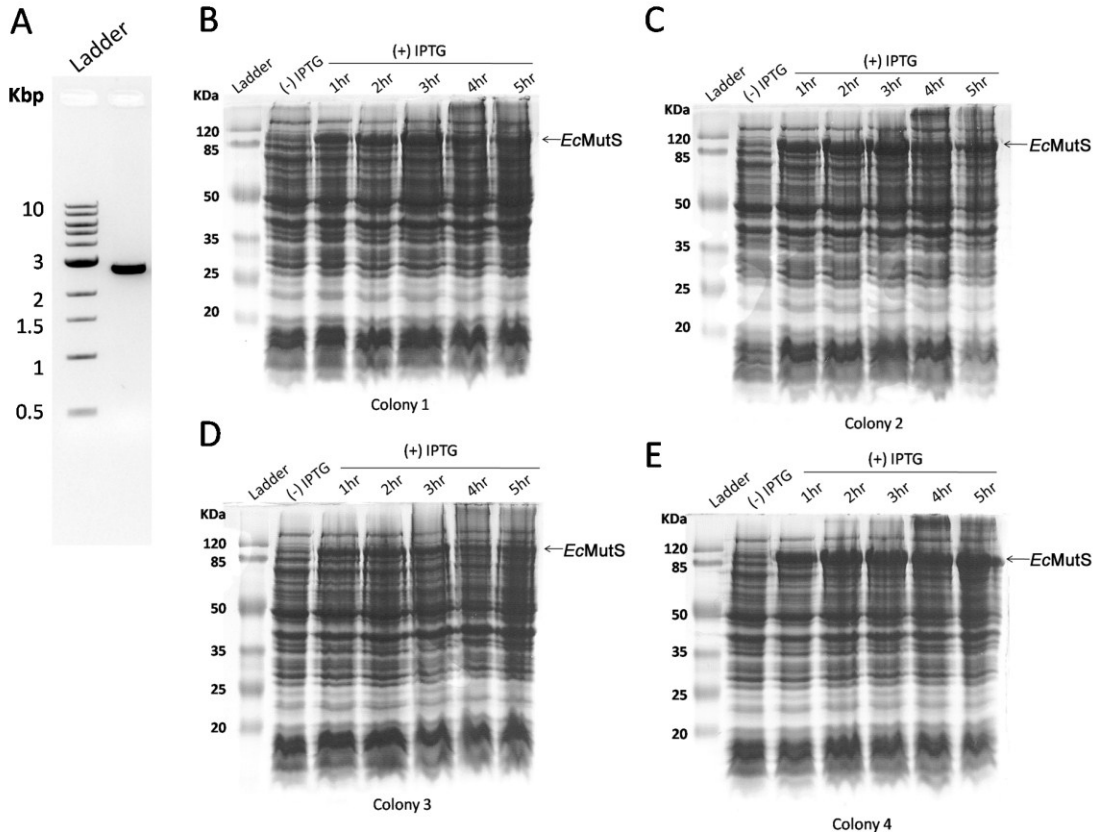


Figure 3-8. Cloning and expression of MutS *E. coli* in pPROEX-HTb vector

(A) ~2.6kbp *E. coli* MutS gene *mutS* was produced by PCR-amplification of *E. coli K12* genomic DNA and analysed by 1% agarose gel electrophoresis. (B)(C)(D)(E)12% SDS-PAGE analysis of subunit δ' expression level of 1mM IPTG-induced *E. coli* BL21(DE3) cell colonies atOD_{600} of 0.4 in 0-5hrs at 25°C.

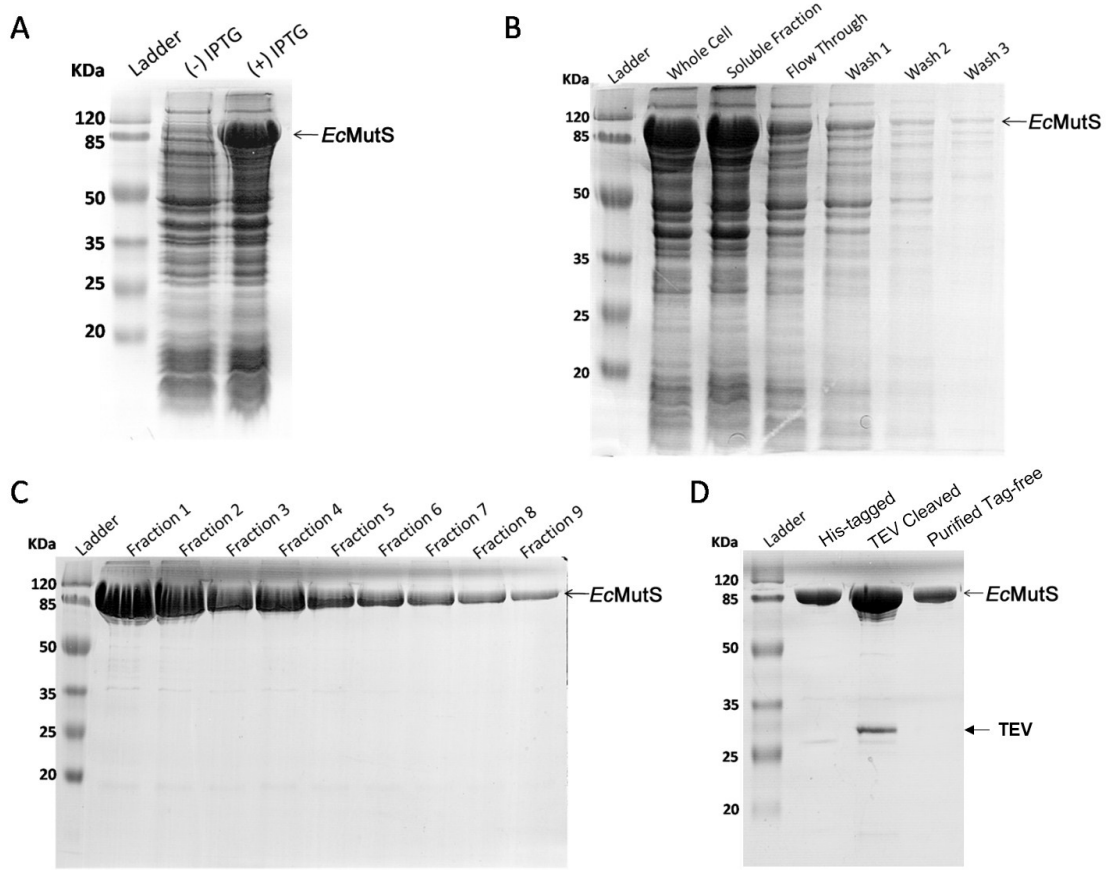


Figure 3-9. Expression and purification of *Ec*MutS

(A) 12% SDS-PAGE analysis of *Ec*MutS expression level of 1mM IPTG-induced *E. coli* BL21(DE3) cell colonies at OD_{600} of 0.4 in 3hrs at 25°C. (B)(C) 12% SDS-PAGE analysis of *Ec*MutS protein fractions collected from the Ni-column. (D) 12% SDS-PAGE analysis of *Ec*MutS after TEV protease cleavage and flow through the fresh Ni-column.

3.2.4 Gel shift assays with mini-circular DNAs

3.2.4.1 Preparation of mini-circular DNAs

To establish a stable assay system of protein-DNA interactions, the strategy of 120-bp mini-circle DNA (Fig. 3-10) was carried out to provide a closed dsDNA structure which was assumed to tightly integrate with MMR proteins. A molecular size of 120-bp circular DNA was considered to be applicable for native PAGE in the gel shift assay.

The circular DNA was composed of two dsDNAs (dsDNA_1 and dsDNA_2) (Fig. 3-11A, B) containing complementary overhangs at both ends. One overhang was 14-bp, and the other was shorter (2-bp). Moreover, there was a length difference between two dsDNAs to distinguish them during the gel analysis. On the DNAs with mismatch, a T/G mismatch was located at the middle point of "Oligo_MC3" (Fig. 3-11C). Four restriction enzyme sites were designed to detect the formation of circular DNAs (Fig. 3-10). Sites of EcoRI and BamHI were closed to two overhangs. The HindIII site was located at the middle point of "dsDNA_1". The PstI site contained the mismatch site.

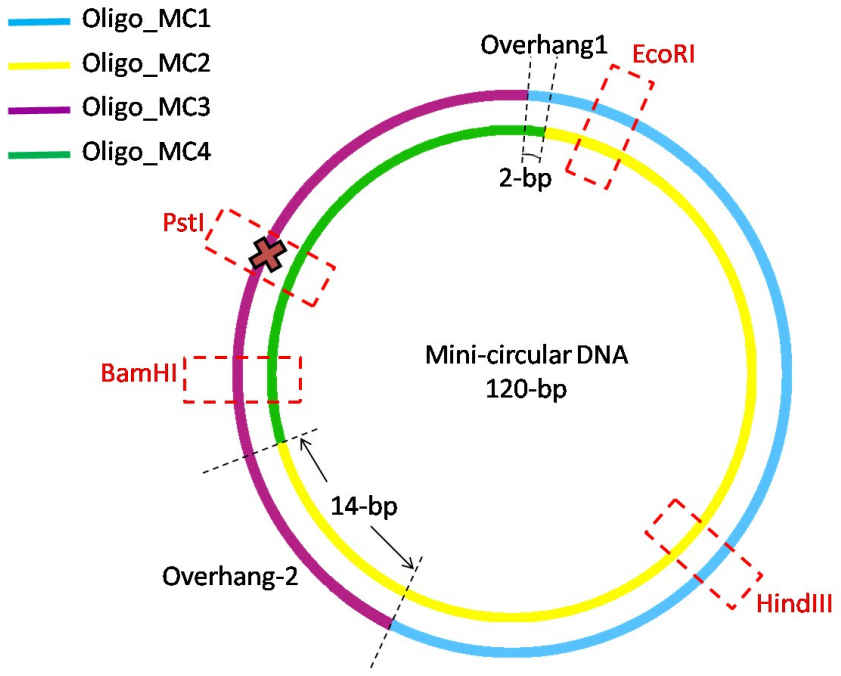


Figure 3-10. Schematic of mini-circular DNA

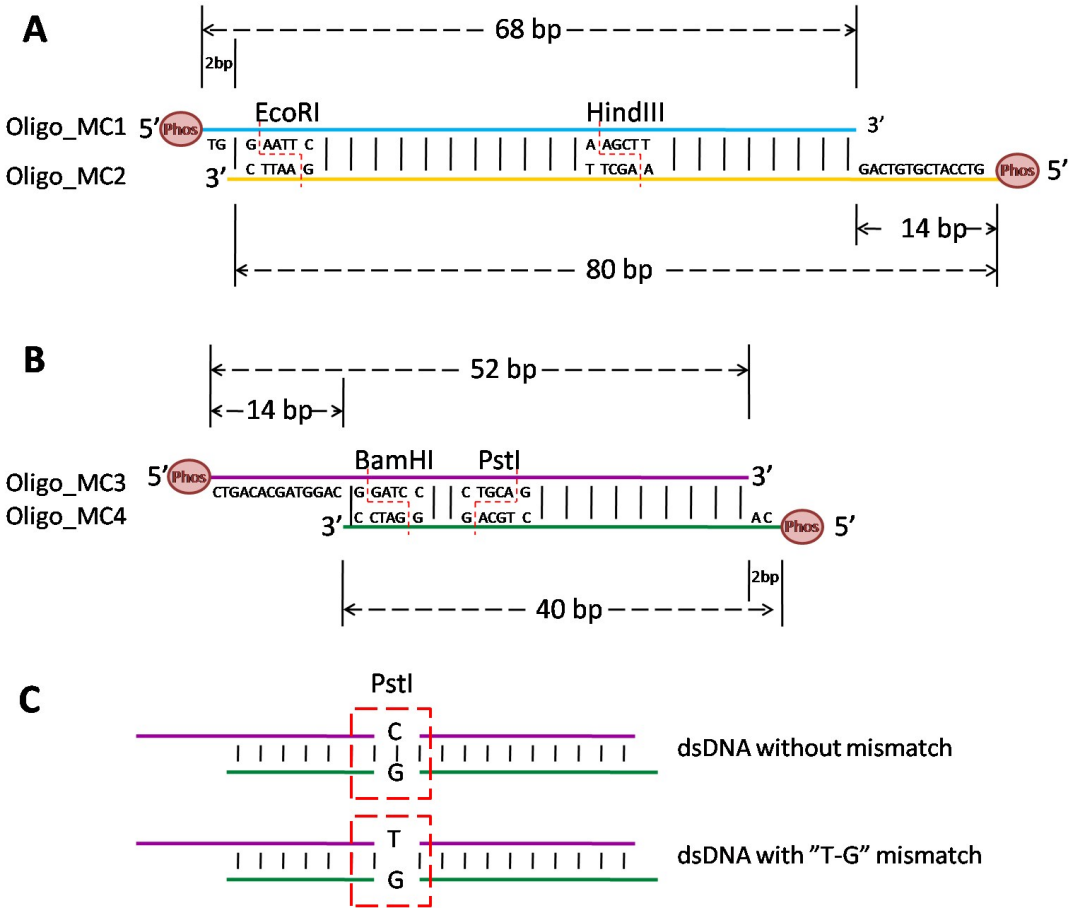


Figure 3-11. Schematic of oligonucleotide components for mini-circular DNAs

Preparation procedure of mini-circular DNAs was presented in the Figure 3-12. Each dsDNA was formed by two complemented oligonucleotides via annealing Two types of dsDNA were linked using a second annealing process at the longer complemented overhang. After annealing, the complemented overhang was sealed by Taq ligase, which was specifically utilised to ligate accurately hybridized and paired DNA strands. As a consequence, the 14-bp overhang was ligated, but the 2-bp overhang was not. Thus far, the entire DNA structure was formed as a linear dsDNA with 2-bp overhangs at both ends.

After gel purification of ligated 120-bp linear DNAs, the circular structure of DNA was assembled by T4 ligation. T4 DNA ligase could join both blunt end and cohesive end of duplex DNA and was widely used for DNA hybrids (Engler & Richardson, 1982). After T4 ligation, both series of linear DNAs and circular

DNAs may be produced. In order to confirm circular DNAs, Plasmid-Safe ATP-Dependent DNase (PSAD) was used to digests linear dsDNA from the ligated mixture. PSDA can selectively remove linear dsDNA from closed-circular dsDNA or supercoiled DNA (Ren & Nassal, 2001). The remaining circular DNA was further purified using agarose gels and was then concentrated and quantified.

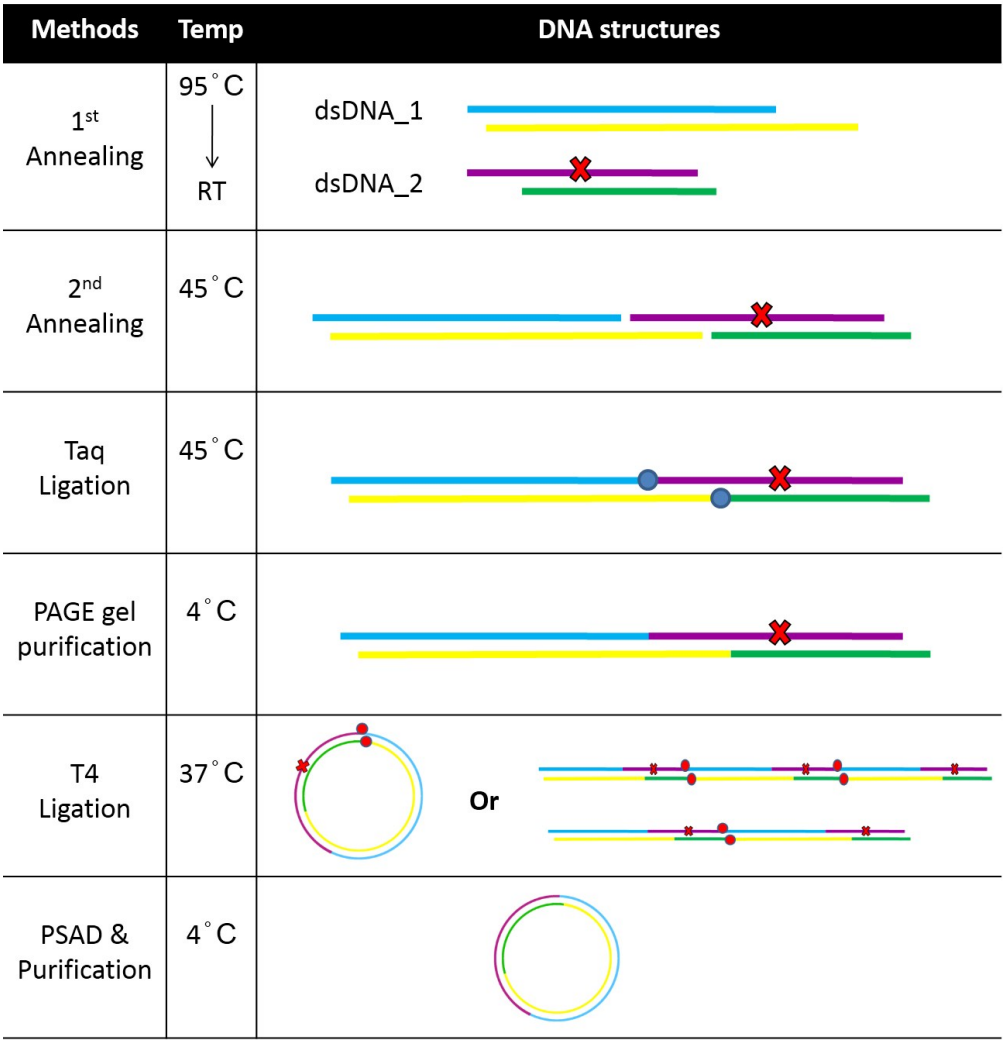


Figure 3-12. Procedure of Mini-circular DNA purification

Each step of the preparation of mini-circular DNA was detected via agarose gel. After the digestion from PSAD, the smallest circular DNA was approximately 300-bp in the agarose gel (Fig. 3-13). Compared to ligated concatemers, the production of circular DNA was very low.

Following large scale preparation, both mini-circular DNAs with and without T/G mismatch ($MC120^{C/G}$ and $MC120^{T/G}$) were examined whether mini-circular DNAs were as designed via restriction digestions. Digestions were performed by four restriction enzymes (EcoRI, BamHI, HindIII and PstI) respectively. PstI digested homoduplex DNA presented a molar weight as same as 120-bp linear DNA, whereas mismatched DNA was not digested by PstI (Fig. 3-14). Digestions from ther other three restriction endonucleases all resulted in a 120-bp linear DNA (Fig. 3-14). Consequently, these results suggested than the formation of prepared DNA was consistent with the original design.

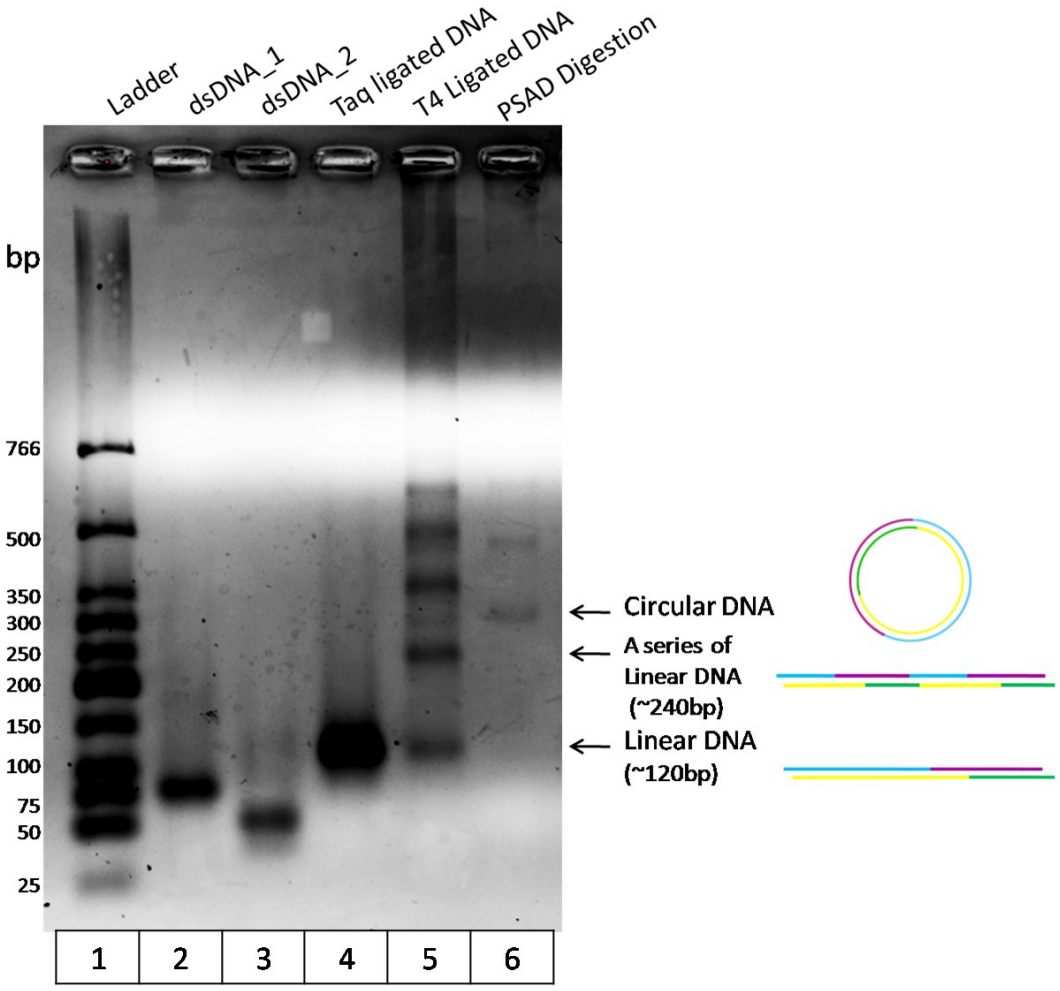


Figure 3-13. Detection of Mini-circular DNAs preparation

Ligated DNA products was resolved in 2% agarose gel electrophoresis. Lane 2 is "dsDNA_1" after 1st annealing. Lane 3 is "dsDNA_2" after 1st annealing. Lane 3 is the purified 120-bp line DNA after 2nd annealing and Taq ligation. Lane 5 is T4 ligated DNA complexes. Lane 6 is remaining DNA after PSAD digestion (see Materials and Methods).

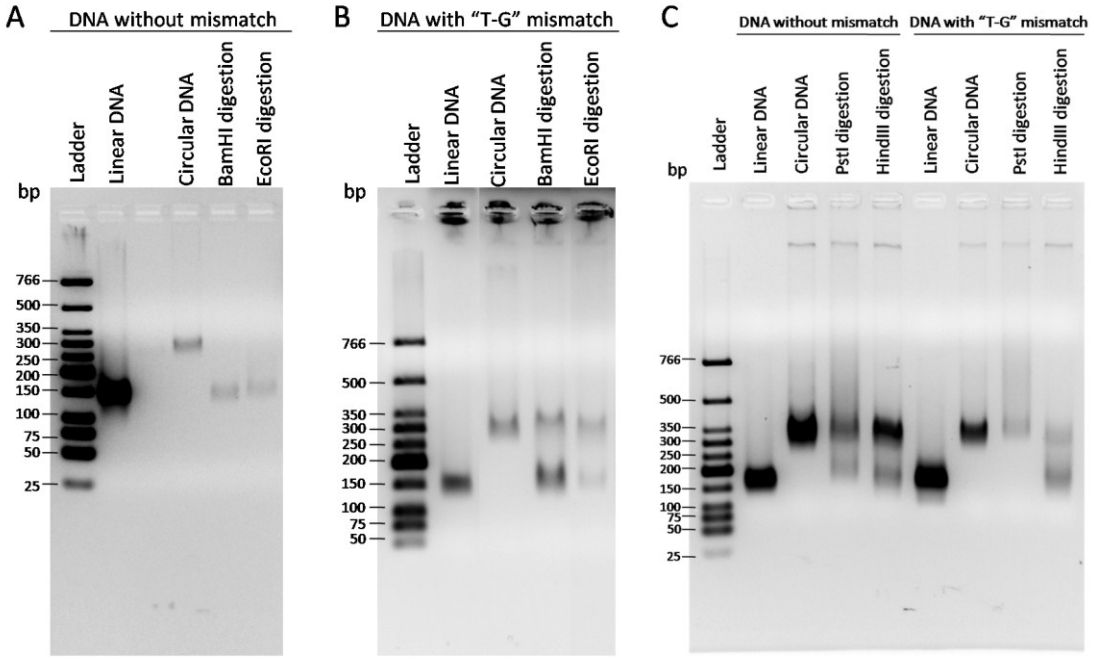


Figure 3-14. Detection of various digestions by restriction enzymes with MC120$^{C/G}$ and MC120$^{T/G}$

The digestion products were mixed with 1X SYBR green and resolved in 2% agarose gel electrophoresis (A) BamHI digestion and EcoRI digestion with MC120$^{C/G}$. (B) BamHI digestion and EcoRI digestion with MC120$^{T/G}$. (C) PstI digestion and HindIII digestion with MC120$^{C/G}$ and MC120$^{T/G}$.

3.2.4.2 Gel shift assays of MutS proteins with mini-circular DNAs

With the achievement of mini-circular DNA, gel shift assays of mini-circular DNAs were performed at varying concentrations of freshly purified *Ec*MutS and *Nm*MutS and mini-circular DNAs *in vitro* (see Materials and Methods).

In the assay of *Ec*MutS, it bound to both $MC120^{C/G}$ and $MC120^{T/G}$ DNA at high concentrations of proteins and displayed no role of mismatch discrimination with all concentrations of *Ec*MutS (Fig. 3-15A, B). Additionally, there were very weak signs of shifted binding complexes in the assays of both homoduplex DNA and DNA with a T/G mismatch. Meanwhile, some binding complexes was stacked in the gels which was nearly indistinguishable in the assays of between DNA $MC120^{C/G}$ and $MC120^{T/G}$. This result is in contrast with many studies on mismatch discrimination by *Ec*MutS activity using the gel shift assay (Acharya, 2008).

In the assays of *Nm*MutS, both $MC120^{C/G}$ and $MC120^{T/G}$ DNAs were bound at high concentrations of *Nm*MutS as well (Fig. 3-15C, D). Although some shifted bands occurred above the free duplexes, there was no detectable difference between the assays of $MC120^{C/G}$ and $MC120^{T/G}$. As with the assay of *Ec*MutS, there was binding complex in the gel wells with *Nm*MutS.

Apparently, both *Ec*MutS and *Nm*MutS did not perform any mismatch recognition activity in these assays with mini-circular DNA. Meanwhile, the amount of stacked DNA complexes in gel wells was raised with increasing concentrations of proteins. These complexes were seriously affected bands shifts.

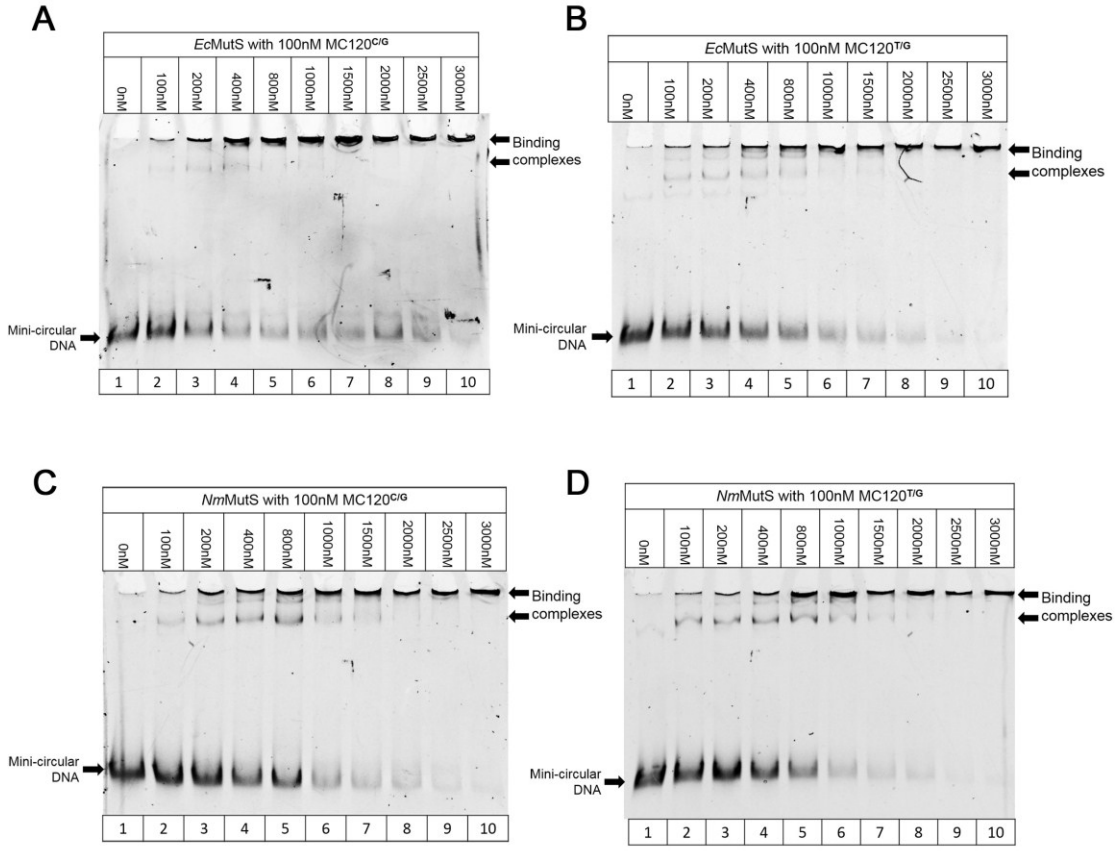


Figure 3-15. Gel shift assays of *Ec*MutS or *Nm*MutS with mini-circular DNAs

(A)(B)(C)(D) Increasing concentrations of *E*cMutS and *Nm*MutS were incubated with 100Nm 120-bp mini-circular DNA without mismatch(MC120$^{C/G}$) and with a T/G mismatch (MC120$^{T/G}$) in the gel shift buffer at 25^{o}C for 20 minutes.1M betaine glycine was added into binding mixtures and incubated for further five minutes before native PAGE. Reactions were resolved by 6% native PAGE (see Materials and Methods). The data is representative of three independent experiments.

It was notable that the preparation of mini-circular DNA could only be performed with very low yields due to the difficulty in limiting concatenation. In the repeated preparation of mini-circular DNA, frequently the T4 ligase ligated DNA mixture was completely degraded after PSDA digestion (Data not shown). These results implied that the mini-circular DNA was afficult to form as a closed and stable structure. It was therefore decided that it was inappropriate to be used as the DNA substrate to detect the recognition activity of MMR proteins at the current stage. To ensure the progress of this project, an alternative strategy of blocked-end linear DNA substrate was carried out for further gel shift assays.

3.2.5 Gel shifty assays with 60-bp DNA duplexes

3.2.5.1 Preparation of blocked-end DNA duplexes

To ensure robust recognition of MutS proteins, an alternative strategy of model substrates was prepared with a 60-bp linear dsDNA containing a T/G mismatch at the middle point or C/G homoduplex ($L60^{T/G}$ or $L60^{C/G}$) (Fig. 3-16A) (see Materials and Methods). Both $L60^{T/G}$ and $L60^{C/G}$ were labelled with biotin at the 5'-ends on each strand to achieve a blocked-end DNA duplex structure ($BL60^{T/G}$ or $BL60^{C/G}$) via the interaction of biotin and Streptavidin (Fig. 3-16B). Streptavidin is a protein derived from *Streptomyces avidinii*, which have the extraordinarily high affinity to bind up to four biotin molecules, as shown in the diagram below (Fig. 3-16C) (Weber, 1989). Previous studies in human MutSα shows that the Streptavidin-biotin ends could contribute to stabilising the mismatch binding with the potential slide clamp structure of MutSα (Blackwell *et al.*, 1998)

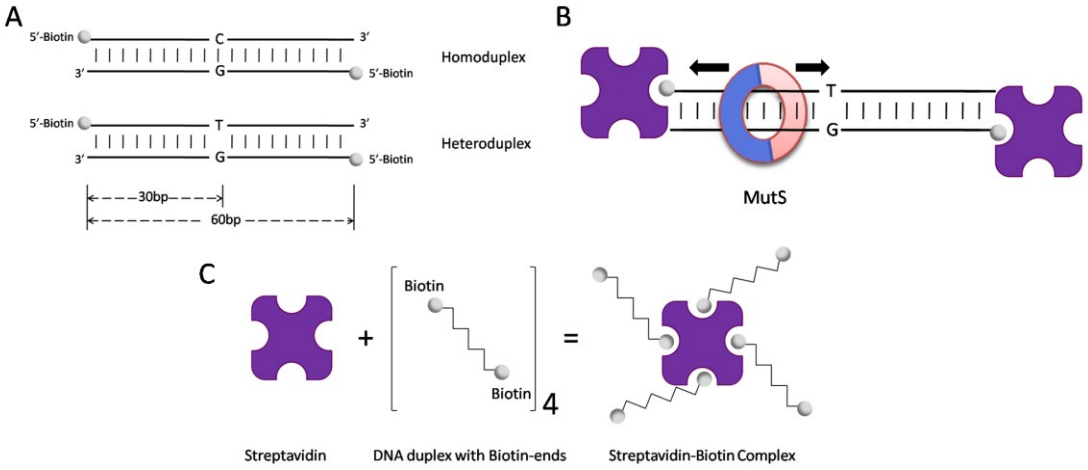


Figure 3-16. Schematic of blocked-end DNA duplexes

(A) Structures of 60-bp linear dsDNA ($OL60^{T/G}$ or $OL60^{C/G}$) (B) Schematic of MutS binds Blocked-end DNA. (C) Schematic of the Streptavidin-biotin interaction.

Open-end linear 60-bp DNA duplexes ($OL60^{T/G}$ or $OL60^{C/G}$) were gained after annealing and were purified via native PAGE (see Materials and Methods). Stoichiometry of biotin-labelled DNA and Streptavidin was designed as 1:2 to

form the blocked-end DNA duplex. However, the 1:1 binding of Streptavidin and biotin needs to be strengthened by excessive Streptavidin to reduce multiple binding to biotins by its homo-tetramers during reactions (Fig. 3-17A). To achieve the stable double blocked-end DNA duplex, the actual stoichiometry of Streptavidin-DNA binding was detected via native PAGE after the incubation of open-end DNA without mismatch ($OL60^{C/G}$) and Streptavidin with concentration variables (Fig. 3-17B).

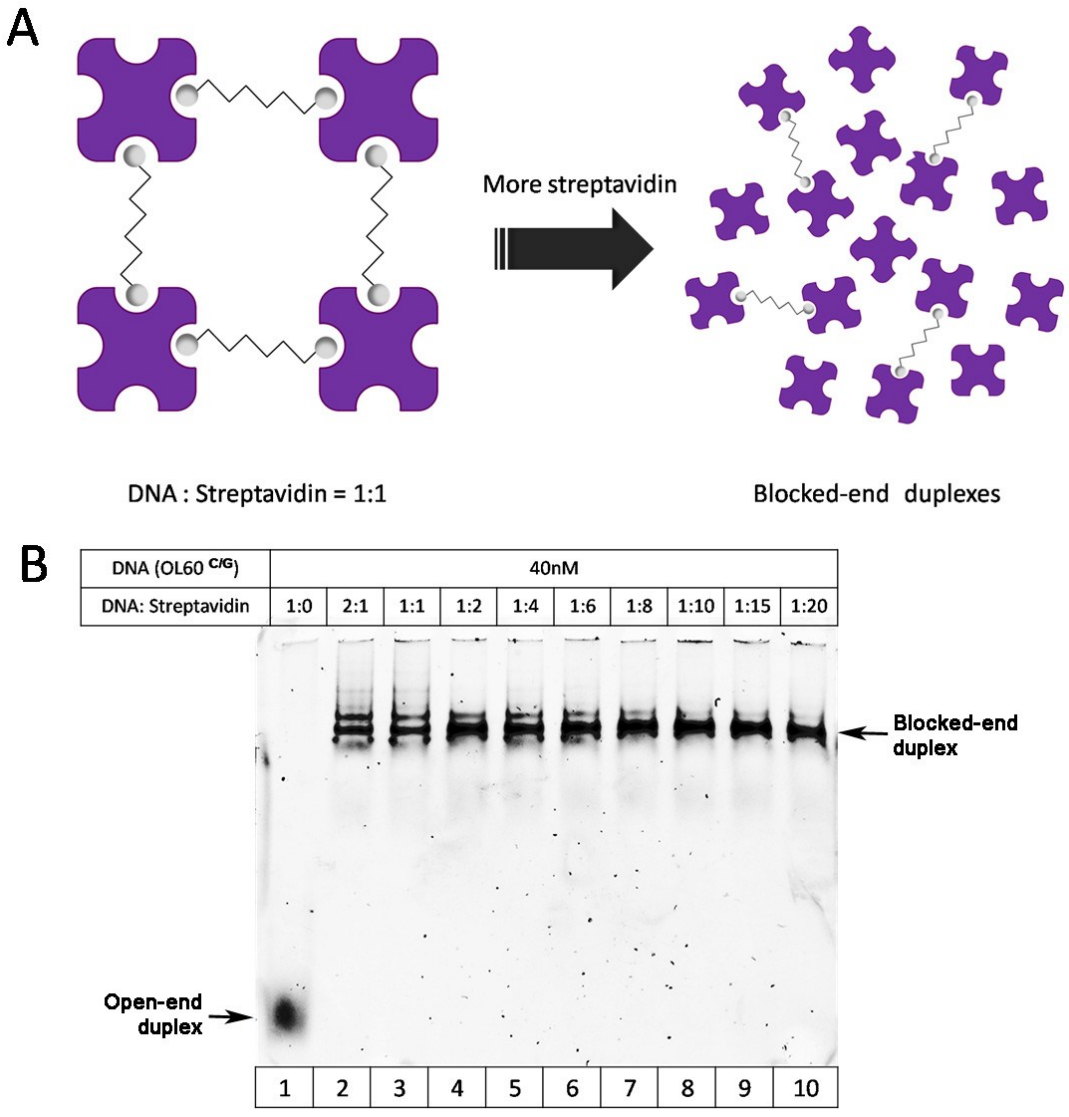


Figure 3-17. Streptavidin-biotin binding assay

(A) Schematic of the formation of blocked-end DNA duplexes by excessive Streptavidin.

(B) Streptavidin-biotin binding assay via 6% native PAGE (see Materials and Methods)

Streptavidin-biotin binding assay demonstrated that increasing the ratio of streptavidin in the reaction promotes the formation of double blocked-end DNA duplex as a clear single band (Fig. 3-17B). The least multiple biotin-binding of Streptavidin occurred when the molar ratio of DNA and Streptavidin reached 1:10. Significantly, 5% (v/v) glycerol was essential to stabilize Streptavidin-DNA binding as a neutral solute which could not be removed.

3.2.5.2 Gel shift assays of *Ec*MutS with 60-bp DNA duplexes

After the achievement of blocked-end linear DNA duplexes, the gel shift assay was initially performed with varying concentrations of *Ec*MutS. Since EcMutS performed well interactions with mismatch in the ADP-binding state, 25μM of ADP was contained in the assay buffer, refered to previous studies (Acharya *et al.*, 2003). Data of gel shift assays with *Ec*MutS were quantitated by the percentage of protein-DNA complex, were then analysed using non-linear curves, which fitted to the Hill equation.

In the gel shift assay with the homoduplex DNA, *Ec*MutS did not evidently bind to $BL60^{C/G}$ DNA at all concentrations of proteins (Fig. 3-18A). Approximately 30 % of DNA binding was observed with 1mM *Ec*MutS and merged in the gel wells (Fig. 3-18A, E). With DNA containing a T/G mismatch, to the contrary, *Ec*MutS significantly bound to $BL60^{T/G}$ DNA with K_d =163.1 ± 8.53nM and n=2.83 ± 0.32 (Fig. 3-18B, F). The significant shifted band of DNA-protein occurred when the concentration of *Ec*MutS reached 400nM with the T/G mismatched DNA, and nearly no free DNA duplex remained (Fig. 3-18B). Moreover, gels of assays with both $BL60^{C/G}$ and $BL60^{T/G}$ had some binding complexes blocking in the gel wells with the addition of high concentrations protein. Therefore, these blocked binding complex were considered as non-specific binding complexes.

With the addition of an escess of ATP (2mM), the assay of *Ec*MutS with the homoduplex DNA had no apparent change (Fig. 3-18C, E). In the assays of $BL60^{T/G}$ DNA in the presence of ATP, the binding of *Ec*MutS and mismatched DNA was slightly weaker than previous observed with lower affinity (K_d =278.8 ± 13.01nM) (Fig. 3-18D, F). It implies that the addition of ATP dissociated the binding of *Ec*MutS and the mismatch. The results also revealed that *Ec*MutS had a cooperative binding with $BL60^{T/G}$ DNA due to values of the Hill coeffient were greater than 1 in the presence and absence of ATP.

In this assay, *Ec*MutS specifically bound to DNA with a T/G mismatch and did not associate with the homoduplex DNA that was consistent with the previous study (Acharya, 2003). Therefore, it indicates that the blocked-end linear DNA duplexes could provide a stable structure to perform the interaction of mismatched DNA and the mismatch recognition protein.

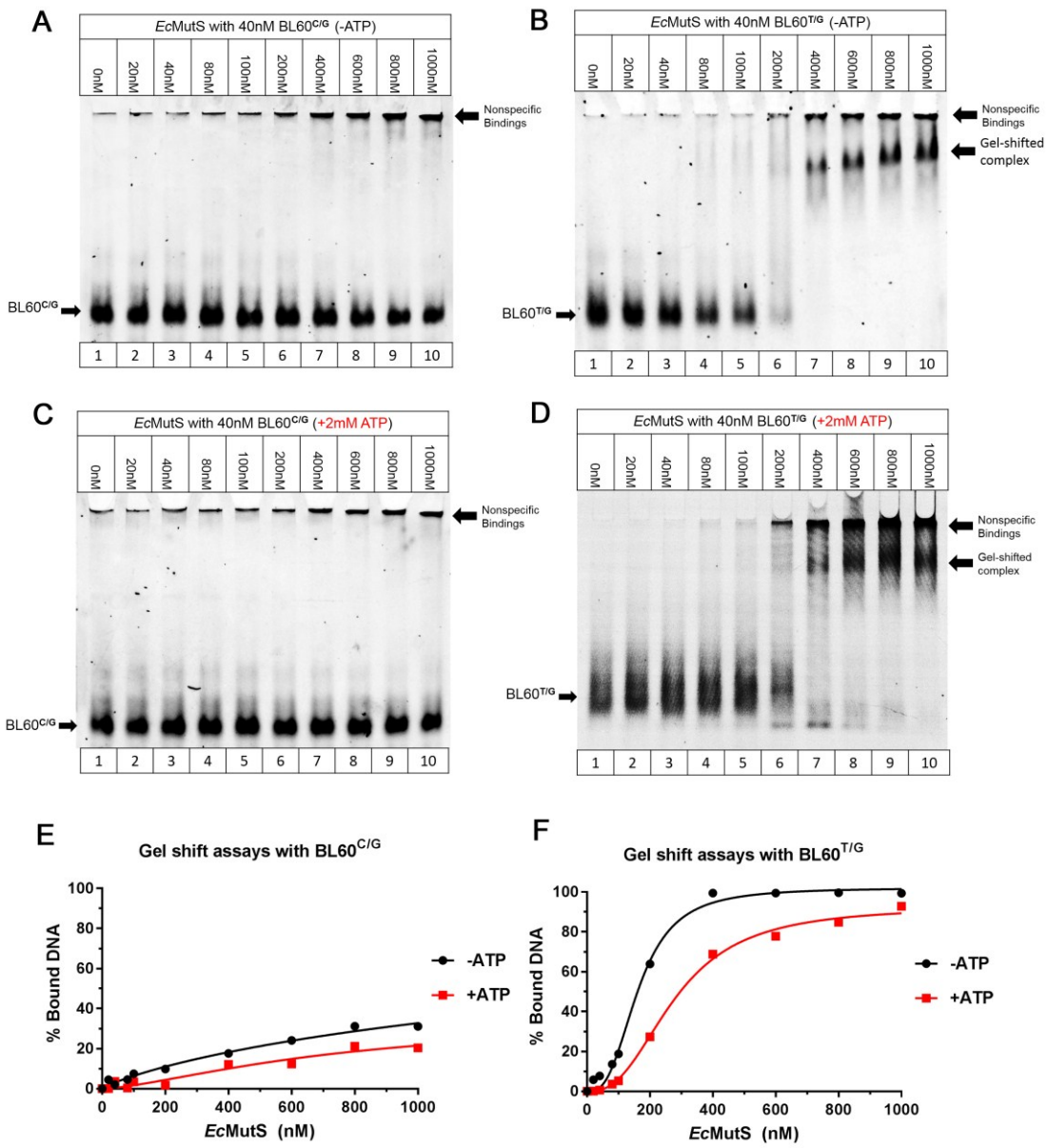


Figure 3-18. Gel shift assays of *Ec*MutS with BL60 DNAs

(A)(B)(C)(D) Increasing concentrations of *Ec*MutS were incubated with 40nM 60-bp blocked-end DNA without mismatch(BL60$^{C/G}$) or with T/G mismatch (BL60$^{T/G}$) with (-/+ 2mM) ATP in the gel shift buffer at 25^{o}C for 20 minutes, and reactions were analysed by 6% non-denaturing PAGE. (E)(F) Gels(A)(B)(C)(D) were quantified to determine the degree of DNA binding using ImageJ software and the data was analysed via GraphPad Prism 7. Data from (F) is presented with best fitting to the Hill equation: in the absence of ATP (black line), K_d= 163.1 ± 8.53nM, n=2.83 ± 0.32; in the presence of ATP (red line), K_d= 278.8 ± 13.01nM, n=2.56 ± 0.22. The data is representative of two independent experiments.

3.2.5.3 Gel shift assays of *Nm*MutS with blocked-end 60-bp DNA duplexes

Based on the significant mismatch binding of *Ec*MutS with the blocked-end DNAs, the gel shift assay was then performed with *Nm*MutS on $BL60^{C/G}$ and $BL60^{T/G}$ DNA under the identical conditions to the assay of *Ec*MutS.

With the homoduplex DNA, *Nm*MutS did not evidently bind to $BL60^{C/G}$ DNA (Fig. 3-19A). Some binding complexes were slightly blocked in the gel wells at high concentrations of *Nm*MutS (Fig. 3-19A, E). In the assay of DNA with a T/G mismatch, there was no detectable band shift from the *Nm*MutS-$BL60^{T/G}$ interaction, although approximately 40% of $BL60^{T/G}$ DNA was bound at 1μM of *Nm*MutS (Fig. 3-19B, F). Compared to the assay of $BL60^{C/G}$ DNA, there were more binding complexes merged as a blocking of the gel wells with a K_d=470.1 ± 102.3nM. However, it is difficult to determine if these complexes are specific binding from *Nm*MutS or non-specific.

With the addition of ATP, no clear effect occurred in the assay of the homoduplex DNA and *Nm*MutS (Fig. 3-19C, E). On other hand, in the assay of $BL60^{T/G}$ DNA, a faint band shift was observed at 1μM of *Nm*MutS in the presence of ATP (Fig. 3-19D). Additionally, the binding of $BL60^{T/G}$ DNA was slightly reduced at lower concentrations of *Nm*MutS with the addition of ATP and had lower affinity (K_d= 627.1 ± 67.09nM) (Fig. 3-19F). In general, the mismatch binding of *Nm*MutS was very weak regardless the addition of ATP or not. These results showed that a deficiency of mismatch discrimination by *Nm*MutS in comparison to *Ec*MutS.

As discussed earlier, mismatch recognition is the initial step of the MMR system. MutS homologues has been widely reported to perform the specific binding of a mismatch in many organisms, including *E. coli*, human and yeast (Fukui *et*

al., 2011). Therefore, as with other MutS homologues, *Nm*MutS should be involved in the identification of mismatched DNA in some way. The result in this study raises a new conjecture, whether *Nm*MutS needs assistance from other MMR proteins to achieve mismatch recognition? Because of the known interaction between *Ec*MutS and *Ec*MutL in *E. coli* MMR system, *Nm*MutL was examined in the contact of mismatch recognition.

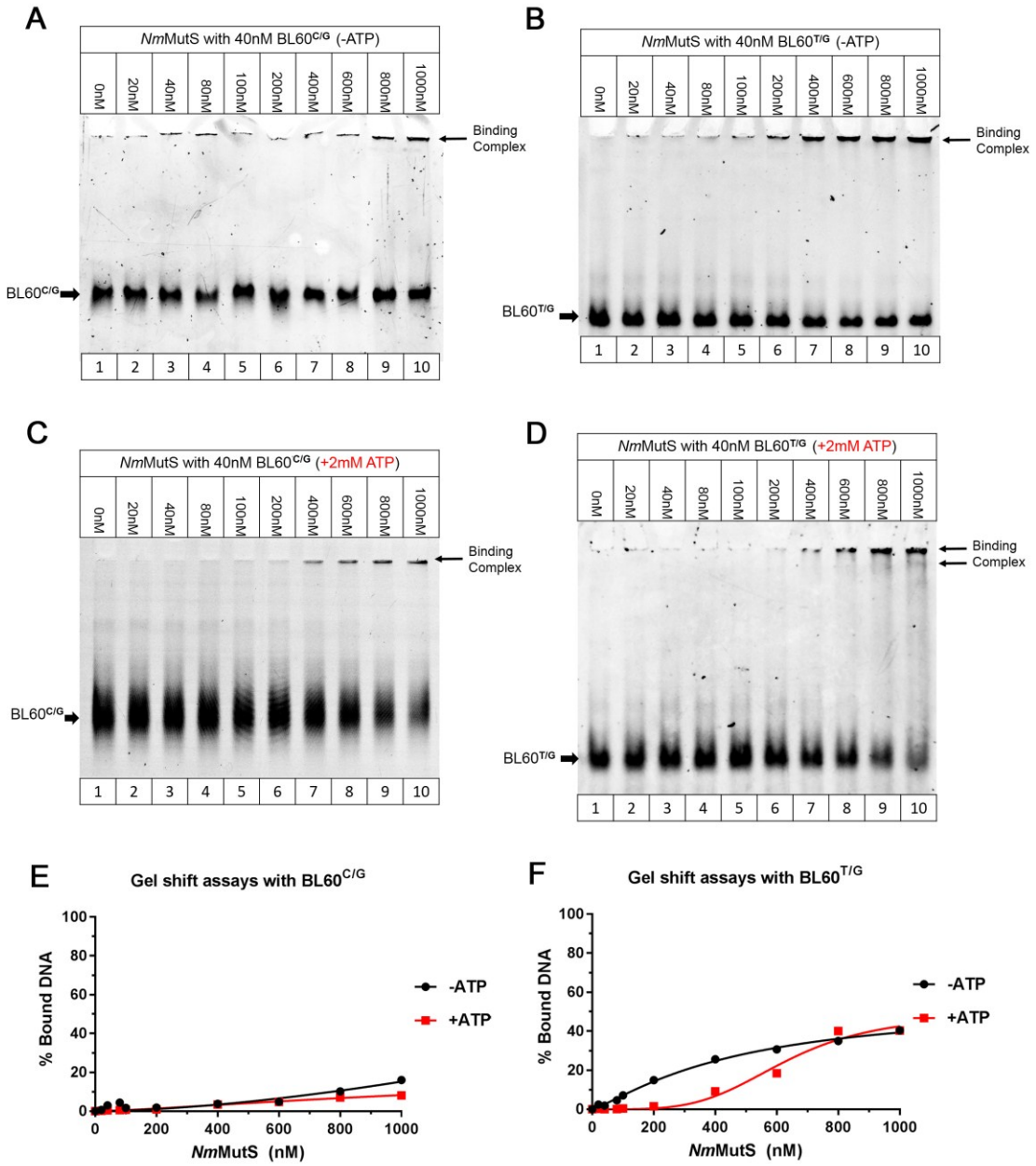


Figure 3-19. Gel shift assays of *Nm*MutS with BL60 DNAs

(A)(B)(C)(D) Increasing concentrations of *Nm*MutS were incubated with 40nM 60-bp blocked-end DNA without mismatch ($BL60^{C/G}$) and with T/G mismatch ($BL60^{T/G}$) with (-/+ 2mM) ATP in the gel shift buffer at 25°C for 20 minutes, and reactions were analysed by 6% non-denaturing PAGE. **(E)(F)** Gels(A)(B)(C)(D) were quantified to determine the degree of DNA binding using ImageJ software and the data was analysed via GraphPad Prism 7. Data from (F) is presented with best fitting to the Hill equation: in the absence of ATP (black line); in the presence of ATP (red line). The data is representative of three independent experiments.

3.2.5.4 Gel shift assays of *Nm*MutL with blocked-end 60-bp DNA duplexes

To explore the role of *Nm*MutL in the process of mismatch recognition, *Nm*MutL was also introduced into the gel shift assay. Firstly, the gel shift assay was performed by *Nm*MutL alone with $BL60^{C/G}$ and $BL60^{T/G}$ DNA under the same conditions with the assay of *Ec*MutS and *Nm*MutS.

In gel assays, *Nm*MutL significantly bound to both the homoduplex DNA and DNA with a T/G mismatch, and free DNA duplex of either $60^{C/G}$ or $BL60^{T/G}$ DNA was almost completely bound to *Nm*MutL when the concentration of *Nm*MutL reached 600nM (Fig. 3-20A, B, E, F). Furthermore, the binding of *Nm*MutL-$BL60^{T/G}$ and *Nm*MutL-$BL60^{C/G}$ had similar affinity ($K_{d\text{-}BL60}{}^{T/G}$=127.5 ± 8.49Nm; $K_{d\text{-}BL60}{}^{C/G}$ =110.6 ± 15.76nM) (Fig. 3-20E, F). This result displayed that the interaction of *Nm*MutL and DNA substrates had low mismatch specificity.

With the addition of ATP, the binding of *Nm*MutL with either both $60^{C/G}$ or $BL60^{T/G}$ DNA was slightly promoted. Compared to the assay in the absence of ATP, the free duplex of both $BL60^{C/G}$ and $BL60^{T/G}$ DNA was more effectively bound to 200nM of *Nm*MutL in the presence of ATP (Fig. 3-20C, D, E, F). The affinity of *Nm*MutL binding to either $BL60^{C/G}$ or $BL60^{T/G}$ was increased (K_d of $BL60^{C/G}$ =74.32 ± 3.62nM; K_d of $BL60^{T/G}$ =71.62 ± 2.27nM). This result suggests that ATP may contribute in the mismatch-independent interaction between *Nm*MutL and DNA.

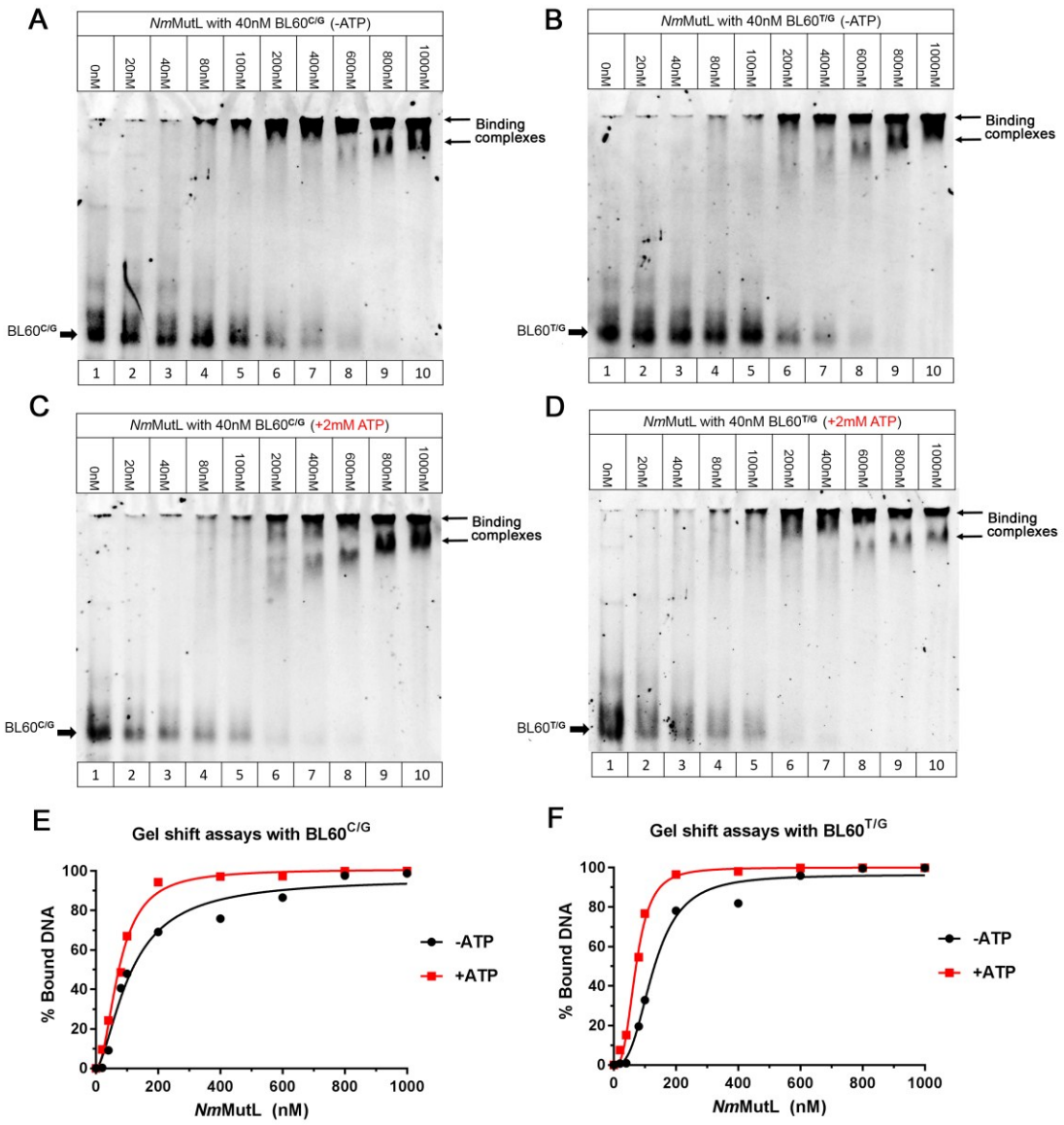


Figure 3-20. Gel shift assays of *Nm*MutL with BL60 DNAs

(A)(B)(C)(D) Increasing concentrations of *Nm*MutL were incubated with 40nM 60-bp blocked-end DNA without mismatch ($BL60^{C/G}$) or with a T/G mismatch ($BL60^{T/G}$) with (-/+ 2mM) ATP in the gel shift buffer at 25°C for 20 minutes, and reactions were analysed by 6% non-denaturing PAGE. **(E)(F)** Gels(A)(B)(C)(D) were quantified to determine the degree of DNA binding using ImageJ software and the data was analysed via GraphPad Prism 7. Data from (E)(F) are presented with best fitting to the Hill equation: (E) in the absence of ATP (black line), K_d= 110.6 ± 15.76nM, n=1.62 ± 0.34; in the presence of ATP (red line), K_d= 74.32 ± 3.62nM, n=2.04 ± 0.20. (F) in the absence of ATP (black line), K_d= 127.5 ± 8.49nM, n=2.81 ± 0.43; in the presence of ATP (red line), K_d= 71.62 ± 2.27nM, n=2.99 ± 0.28. This data is only conducted once.

3.2.5.5 Gel shift assays of the combination of *Nm*MutS and *Nm*MutL with blocked-end 60-bp DNA duplexes

To evaluate if *Nm*MutL affect the role of *Nm*MutS for mismatch recognition, we further carried out the gel shift assay by a combination of *Nm*MutS and *Nm*MutL with identical concentrations of proteins.

In the gel shift assay, both the homoduplex DNA and mismatched DNA were significantly bound to *Nm*MutS-*Nm*MutL from 400nM of *Nm*MutS and *Nm*MutL (Fig. 3-21A, B, E, F). It shows that *Nm*MutS and *Nm*MutL bind to more DNA with a T/G mismatch than the homoduplex DNA when the concentration of *Nm*MutS and *Nm*MutL reached 200nM (Fig. 3-21A, B, E, F). The shifted band was observed with a slower migration compared to the shift of *Nm*MutL, and most of shifted bands were merged in the gel wells (Fig. 3-21A, B). It might be caused by DNA binding of a larger *Nm*MutS-*Nm*MutL complex. The affinities of *Nm*MutS-*Nm*MutL with $BL60^{C/G}$ and $BL60^{T/G}$ DNA were similar (K_d of $BL60^{C/G}$ =240.5 ± 14nM; K_d of $BL60^{T/G}$ =231.1 ± 17.78nM), but were lower than that of *Nm*MutL bound to BL60 DNA alone. The result showed that *Nm*MutL seemed not to contribute in the *Nm*MutS activity of mismatch recognition. It was more likely that *Nm*MutS slightly dissociate non-specific DNA binding of *Nm*MutL.

In the presence of ATP, there were no distinct effect on the binding of $BL60^{C/G}$ DNA and *Nm*MutS-*Nm*MutL (Fig. 3-21C, E). The affinity of the *Nm*MutS-*Nm*MutL-$BL60^{C/G}$ interaction was not obviously change after adding ATP (K_d=224.9 ± 12.61nM). For DNA containing a T/G mismatch, the *Nm*MutS-*Nm*MutL-DNA binding was weakly enhanced at low concentrations of *Nm*MutS and *Nm*MutL with the addition of ATP (Fig. 3-21D, F). The affinity of of *Nm*MutS-*Nm*MutL-$BL60^{T/G}$ binding was increased in the presence of ATP (K_d=156.1 ± 8.76nM) in the presence of ATP.

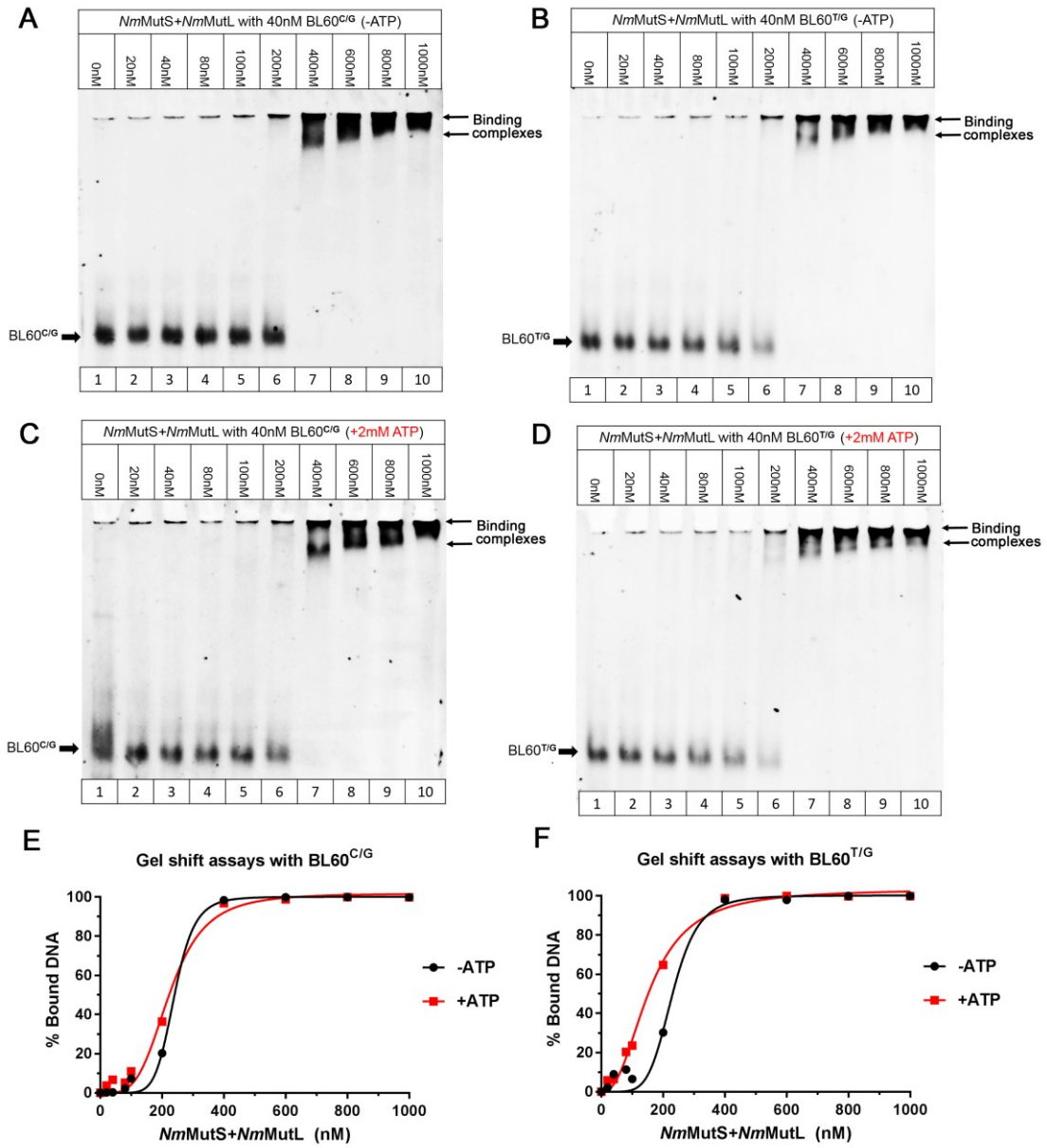


Figure 3-21. Gel shift assays of *Nm*MutS with *Nm*MutL with BL60 DNAs

(A)(B)(C)(D) Increasing concentrations of *Nm*MutS with *Nm*MutL were incubated with 40nM 60-bp blocked-end DNA without mismatch(BL60$^{C/G}$) or with T/G mismatch (BL60$^{T/G}$) with (-/+ 2mM) ATP in the gel shift buffer at 25^{o}C for 20 minutes, and reactions were analysed by 6% non-denaturing PAGE (see Materials and Methods). **(E)(F)** Gels(A)(B)(C)(D) were quantified to determine the degree of DNA binding using ImageJ software and the data was analysed via GraphPad Prism 7. Data from (E)(F) are presented with best fitting to the Hill equation: (E) in the absence of ATP (black line), K_d= 240.5 ± 14nM, n=7.40 ± 2.18; in the presence of ATP (red line), K_d= 224.9 ± 12.61nM, n=3.89 ± 0.81. (F) in the absence of ATP (black line), K_d= 231.1 ± 17.78nM, n=5.52 ± 2.29; in the presence of ATP (red line), K_d= 156.1 ± 8.76nM, n=2.40 ± 0.25. This data is only conducted once.

3.3 Discussion

In *E. coli*, MutS is the 'mismatch recognition protein' and binds to insertion-deletion loops and base pairing mismatches (Su & Modrich, 1986; Jiricny *et al.*, 1988; Schofield & Hsieh, 2003), which initiate the post replication mismatch repair (Modrich & Lahue, 1996). In organisms beyond *E. coli,* the activity of MutS and MutL with a DNA mismatch may point towards an unknown mechanism. As a MutH-lacking organism, *N. meningitidis* MMR enzymes *Nm*MutS and *Nm*MutL were prepared and introduced into a series of gel shift assays to detect the initiation of *Neisserial* MMR systems.

3.3.1 Optimization of gel shift assays

In this study, three types of DNA substrates were applied in the gel shift assay. The 30-bp open-end linear DNA duplex was used in the initial investigation of this study. *Nm*MutS weakly bound to DNA with a T/G mismatch. *Nm*MutL slightly bound to both DNA with or without mismatch. Shifted DNA bands also faintly occurred in the assays of the combination of *Nm*MutS and *Nm*MutL with both homoduplex and heteroduplex DNA. However, all bindings of protein-DNA were too weak to measure the affinity of these interactions. These results demonstrate that the 30-bp open-end linear DNA substrate may be not compatible to provide a stable structure to interaction with proteins.

To improve the performance of the gel shift assay, the DNA substrate was re-designed in two inspects. One is to increase the length of DNA duplex provide adequate space to interact with proteins. The other is to enhance the tightness of DNA to avoid the open-ends of DNA duplexes. If *Nm*MutS has a clamp-like structure as *Ec*MutS, it will allow *Nm*MutS sliding out of DNA with the open-ends. Meanwhile, the results inspired us to use a positive control protein was necessary to determine the availability of the DNA substrate. Therefore, *Ec*MutS was also prepared and used in following assays.

At first, circular DNA was considered to provide the closed structure to avoid the potential “sliding out” activity of MutS protein which may track from the mismatch base along DNA. However, plasmid DNAs were too large to be used for the gel shift assay in the non-denaturing PAGE gel. A mini-circular DNA with 120-bp was therefore designed to provide a closed DNA structure while maintaining the appropriate molecular size in the native PAGE gel. After two steps of annealing and two steps of ligations, the mini-circular DNA was achieved according to the digestion of restriction enzymes and the plasmid-safe DNase. However, the yield of the mini-circle DNA was limited due to the large amount of non-specific ligation from T4 ligase and the loss of DNA during gel purification.

In the gel shift assays of mini-circular DNAs, both *Ec*MutS and *Nm*MutS bound to the homoduplex DNA and DNA with a T/G mismatch, and the binding complex was merged in the gel wells. The binding of *Ec*MutS with the homoduplex DNA was inconsistent with results from previous studies (Acharya *et al.,* 2003). Because the band shift was rarely to be observed, it was difficult to determine the interaction of MutS proteins and DNA. Additionally, in the repetitive preparation process, the mini-circular DNA was found that it could not be formed as the closed circle every time, even if the condition and operation of experiments were strictly controlled. It suggests that the designed mini-circular DNA may be not stable enough that possibly introduces other interferences to affect the result of the gel shift assay. Considering the efficiency of experiments, we had to abandon this strategy of the mini-circular DNA and moved forward with alternative methods.

Finally, the DNA structure was applied as a 60-bp linear DNA duplex which had two blocked ends. The blocking of DNA ends is based on the high affinity of streptavidin and biotin ($K_d = 10^{-15}$). Biotin labels were added to the 5’-ends on

each strand of DNA so that streptavidin tetramer sealed each ends of DNA duplexes. With the addition of streptavidin (60KDa) to seal the ends of DNA, the complex of MMR proteins and DNA would have a much larger molecular size. Therefore, to avoid merging complexes to block wells of the native PAGE gel, the polyacrylamide solution was particularly chosen with a ratio of Acrylamide/Bis-acrylamide as 75:1. Less content of bis-acrylamide could reduce the cross-link in the gel matrix and provide an appropriate condition for gel shift assays with the large complex (Hellman & Fried, 2007).

3.3.2 *Ec*MutS specifically bound to mismatched DNA

In the gel shift of *Ec*MutS, DNA with a T/G mismatched ($BL60^{T/G}$) was significantly bound to *Ec*MutS with a clear band shift. On the other hand, *Ec*MutS did not interact with the homoduplex DNA. It indicates that *Ec*MutS specifically binds to mismatched DNA and performs mismatch recognition. This result was consistent with known studies of *E. coli* MMR system. Moreover, it also demonstrates that the 60-bp blocked-end linear DNA is able to be applied as the DNA substrate to investigate the interaction of *Neisserial* MMMR proteins and mismatched DNA.

In the assay with the addition of ATP, *Ec*MutS bound to mismatched DNA with lower affinity, but did not release from mismatched DNA. It implied that the addition of ATP might dissociate the binding of *Ec*MutS-mismatch, but did not completely force to *Ec*MutS leave mismatched DNA. This result is consistent with the model that the ATP-binding causes the conformation change of the mismatch-binding domain of *Ec*MutS and further affect the association with the mismatch (Lamers *et al.*, 2004). However, the gel shift assay is difficult to explain if *Ec*MutS translocates along DNA with the formation of a sliding clamp.

In addition, because the purpose of the gel assay of *Ec*MutS and mismatched DNA was mainly to explore the feasibility of the DNA substrate, further gel assays of *E. coli* MMR protein were not performed. Further discussion was referred to other known literatures of *E. coli* MMR system using *in vitro* assays.

3.3.3 *Nm*MutS performed mismatch recognition with deficiency

The gel shift assay of *Nm*MutS were carried out under the identical conditions with the assay of *Ec*MutS. In the assay of *Nm*MutS alone, *Nm*MutS did not significantly interact with the mismatch DNA to present a shifted complex as *Ec*MutS. Meanwhile, there were no obvious interaction of *Nm*MutS and the homoduplex DNA. It shows that *Nm*MutS alone does not bind to DNA containing a T/G mismatch efficiently. The gel shift assay reflected the binding state of *Nm*MutS and DNA in the natural conditions *in vitro*. Therefore, in this assay, the key question is to determine if *Nm*MutS cannot recognise the mismatch or *Nm*MutS do bind to the mismatch but the binding complex is very unstable. For the assay of OL30 DNA, a defined mismatch-specific band shift of *Nm*MutS-OL30$^{T/G}$ occurs in the absence or presence of ADP and ATP. Consequently, it implies that *Nm*MutS can recognise the mismatched DNA, but the binding complex is not tightly as EcMutS.

In addition, it was reported that *Ec*MutS preferred to perform mismatch recognition in the ADP-binding state (Acharya *et al.*, 2003). In this study, *Nm*MutS did not efficiently bind to mismatch as *Ec*MutS with the same concentration of ADP. We also carried out the gel shift assay of *Nm*MutS with BL60$^{T/G}$ in the presence of excess ADP (Data not shown). The results had no detectable difference with that with lower concentration of ADP. With the addition of ATP, the affinitiy of *Nm*MutS-mismatch interactions slightly reduced in assays of either OL30$^{T/G}$ or BL60$^{T/G}$ DNA. It implied that the binding of *Nm*MutS and mismatch might be dissociated in the ATP-bound state. Obviously,

it is too far to determine how the binding state of ADP or ATP modulates the interaction of *Nm*MutS and mismatch.

On the other hand, this result of the gel shift assay of *Nm*MutS is not consistent with the assay of *E. coli* MMR system. As other MutS homologs in MutH-lack bacteria, the mismatch-binding and the ATPase domain of *Nm*MutS are highly conserved with *E. coli* (Blattner *et al.*, 1997; Tettelin *et al.*, 2000; Acharya, 2008; Fukui *et al.*, 2011). However, there are various differences between *Nm*MutS and *Ec*MutS in other domains. It is possible that some key residues direct different mismatch response activities between *Nm*MutS and *Ec*MutS.

As a MutH-lacking bacterium, *B. subtillis* MutS (*Bs*MutS) interacts with β-clamp at the C-terminal binding motif instead of the N-terminal β-clamp binding motif in *E. coli* (Simmons *et al.*, 2008). *In vivo* study suggests may be involved in the stabilisation of the mismatch binding of *Bs*MutS (Simmons *et al.*, 2008). The truncation mutants of *Bs*MutS C-terminal domain defect the interaction between *Bs*MutS and β-clamp and affect mismatch recognition *in vivo*, even if does not interfere with the mismatch-binding *in vitro* study (Bjornson *et al.*,2003; Simmons *et al.*, 2008). In addition, the interaction between MutS and β-clamp homologues was also reported in studies of human and *S. cerevisiae*, which suggests that the interaction of MutS-β homologues may contribute the translocation of MutS forward to the site between two Okazaki fragments during DNA replication and then direct downstream strand discrimination (Zhang *et al.*, 2005; Lee & Alani, 2006; Shell, Putnam & Kolodner, 2007). *Nm*MutS contains the N-terminal β-clamp binding site (^{11}QQYL^{14}) whereas the C-terminal β-clamp binding site is still unknown. The deficiency of the mismatch-binding implies that *Nm*MutS might need the assist from other MMR proteins, such as β-clamp, to perform mismatch recognition suffiently.

Furthermore, since the structural study of *N. meningitidis* MMR system is limited at the current stage, it's also hardly to determine whether *Nm*MutS is composed as a clamp-like dimeric structure as *Ec*MutS to recognise mismatch. Further structural and mutational studies are required to more precisely elaborate the difference between *Nm*MutS and *Ec*MutS.

3.3.4 *Nm*MutL non-specifically bound to the homoduplex DNA

In the gel shift assay of *Nm*MutL, both the homoduplex DNA and the DNA duplex with a T/G mismatch were significantly bound to *Nm*MutL without marked differences. It evidences that *Nm*MutL interacts with DNA without mismatch discrimination. This result is consistent with the study of *Ec*MutL, which is proved to have non-specific binding with DNA (Bende & Grafström, 1991). This result suggests that *Nm*MutL may be not directly involved in the activity of mismatch recognition. Moreover, MutL homologues was also reported to non-specifically bound to the homoduplex DNA in other MutH-lacking organisms, including human, *Saccharomyces cerevisiae* and *Thermus thermophilus* (Guarné, Junop & Yang, 2001; Fukui *et al.*, 2008; Ranjha, Anand & Cejka, 2014).

Additionally, in eukaryotes and MutH-lacking bacteria, MutL homologues were found to possess an endonuclease activity, but *Ec*MutL did not (Kadyrov *et al.*, 2006; Kadyrov *et al.*, 2007; Duppatla *et al.*, 2009; Pillon, *et al.*, 2010; Iino *et al.*, 2011). The endonuclease activity of MutL homologues was proved to non-specifically digest supercoiled plasmid in some bacteria, including B. subtillis, P. aeruginosa, and A. aeolicus (Pillon, *et al.*, 2010; Iino *et al.*, 2011; Correa *et al.*, 2001). Therefore, the non-specific DNA binding activity of *Nm*MutL may be caused by the endonuclease activity of *Nm*MutL, if *Nm*MutL is an endonuclease.

On the other hand, In the gel shift assay of *Nm*MutL alone, the binding of either $BL60^{C/G}$ or $BL60^{T/G}$ DNA was weakly promoted with the addition of ATP. It implied that the ATP-binding may affect on the activity of *Nm*MutL. Eukaryotic and bacterial MutL homologues were reported to retain an inherent ATPase activity (Ban, Junop & Yang, 1999). The APase activity of *Ec*MutL is essential to recruit MutH protein by the ATP-hydrolysis and directs the downstream stand discrimination (Welsh *et al.*, 1987). The ATP-hydrolysis state of MutL is also associated with MutL homologues endonuclease activity (Shimada *et al.*, 2013). According to the lacking of key endonuclease MutH, the endonuclease activity of MutL may have a major role in the MMR system beyond *E. coli*, which must proceed an alternative mechanism to discriminate two strands without Dam methylation. Therefore, the study of *Nm*MutL activity may promote the understanding how the *Neisserial* MMR system tracks the strand discriminatory signal. Furthermore, through detecting whether *Nm*MutS modulates the activity of *Nm*MutL, the pattern of mismatch recognition in *N. meningitidis* may be further explained. Further studies on nuclease activities of *Nm*MutL were discussed in the next chapter.

3.3.5 The interaction of *Nm*MutS-*Nm*MutL and DNA

In the gel shift assay containing *Nm*MutS and *Nm*MutL, both the homoduplex DNA and mismatched DNA were bound to *Nm*MutS-*Nm*MutL. It reveals that the interaction of *Nm*MutS-*Nm*MutL is still difficult to achieve mismatch discrimination. The previous study suggests that *Ec*MutL may contribute to the stabilisation of the *Ec*MutS-mismatch binding in *E. coli* (Gradia *et al.*, 1999). However, it was not observed in the gel shift assay of *Nm*MutS-*Nm*MutL.

It is notable that the binding of *Nm*MutS-*Nm*MutL and DNA seems to perform a slower migration than the *Nm*MutL-DNA binding in the presence of ATP and lower concentration of ADP, which may be caused by the complex of *Nm*MutS-

*Nm*MutL. To further evaluate the interaction of *Nm*MutS-*Nm*MutL, the assay is required to carry out in a longer electrophoresis gel property.

Moreover, interactions of *Nm*MutS-*Nm*MutL and BL60 DNAs had lower affinity than *Nm*MutL-DNA in the presence of low concentration of ADP. With the addition of ATP, the affinity of *Nm*MutS-*Nm*MutL-mismatch was increased, but the affinity of *Nm*MutS-*Nm*MutL and non-mismatch DNA was not. These results imply the ADP-ATP exchange may be involved in *Nm*MutS-*Nm*MutL modulated activity with the mismatched DNA. Furthermore, the non-specific DNA binding of *Nm*MutS-*Nm*MutL is more likely to point forward the downstream activity of *Nm*MutL. Based on completing the reconstitution of DNA Pol III HE in this study, it is also worthwhile to carry out *in vitro* assays of *Nm*MutS with β-clamp and other components of DNA Pol III HE to investigate if DNA replication machinery contributes in the initiation of *Neisserial* MMR system.

Chapter 4

Detection of *Nm*MutL nuclease activity

4.1 Background and objectives

The primary function of mismatch repair is the correction of mispaired errors, which occur in DNA replication, to maintain the integrity of the genome (Iyer *et al.*, 2006). After the recognition of mismatched DNA, the crucial process is to discriminate the newly synthesized strand and remove the mismatched base (Su & Modrich, 1986). In the most extensively studied system from *E. coli*, DNA methylation is used to discriminated the strands. The parental strands have been methylated at the adenine of the "GATC" site by its unique Dam methylase whereas the newly synthesized daughter strands have not been methylated immediately after DNA replication (Modrich, 1989; Modrich & Lahue, 1996). MutH is recruited into the MMR system by MutS-MutL complex in the presence of ATP (Welsh *et al.*, 1987; Grilley *et al.*, 1989). MutH recognizes the "GATC" Dam sites when it encounters a Dam methylated strand, and then nicks on the unmethylated strand at the "GATC" site (Modrich, 1989; Modrich & Lahue, 1996). MutH endonuclease activity directs the subsequent unwinding by UvrD helicase (Cooper, Lahue & Modrich, 1993) and the degradation of DNA containing errors by ssDNA exonucleases (Matson, 1986; Viswanathan & Lovett, 1998) and further resynthesized by DNA Pol III HE and ligated by DNA ligase (Lahue, Au & Modrich, 1989).

However, MutH and d(GATC) methylase homologues are unique for *E. coli* and Gram-negative bacteria and are absent in most bacteria and higher organisms (Friedhoff, Thomas & Pingoud, 2003). For MutH-lacking organisms, therefore, the mismatch repair must carry out strand discrimination by some other process. Paul Modrich and his colleagues reported that human MutL homolog MutLα (hMutLα) (subunits MLH1-PMS2) and *Saccharomyces cerevisiae* MutLα (yMutLα) (subunits MLH1-PMS1) were endonucleases which nicked heteroduplex DNA with a mismatch (Kadyrov *et al.*, 2006; Kadyrov *et al.*, 2007). Additionally, current studies revealed that the strand cleavage was generated

via the endonuclease activity from some MutL homologues; *Thermus thermophiles* MutL (*Tt*MutL) (Fukui *et al.*, 2008), *Neisseria gonorrhoeae* MutL (*Ng*MutL) (Duppatla *et al.*, 2009), *Bacillus subtilis* MutL (*Bs*MutL) (Pillon *et al.*, 2010), *Aquifex aeolicus* MutL (*Aa*MutL) (Iino *et al.*, 2011) and *Pseudomonas aeruginosa* (*Pa*MutL) (Correa *et al.*, 2011).

MutL proteins was reported to perform the endonuclease activity dependent on the conserved D(Q/M)HAX$_2$EX$_4$E motif in the C-terminal domain (Kadyrov *et al.*, 2006; Kadyrov *et al.*, 2007; Fukui *et al.*, 2008; Duppatla *et al.*, 2009; Pillon *et al.*, 2010; Correa *et al.*, 2011; Iino *et al.*, 2011). In this motif, the first aspartate and two residues of histidine are considered to involve in the coordination with metal ions to stimulate the endonuclease activity (Kadyrova & Kadyrov, 2016). Fig. 4-1 presents amino acid sequence alignments of the metal binding motif residues of MutL homologues whose MMR system is commonly studied.

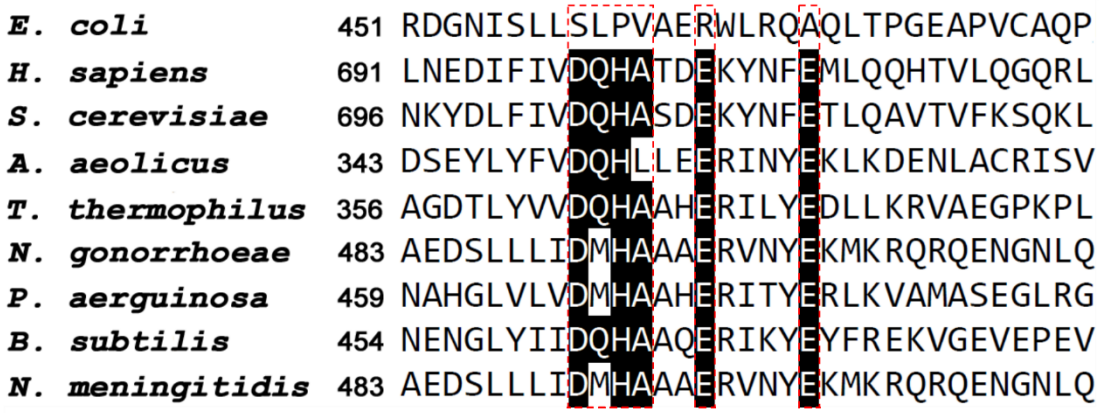


Figure 4-1. Sequence alignments of part of C-terminal domain of MutL proteins
Alignments of the D(Q/M)HAX$_2$EX$_4$E metal-binding motif residues was performed using ClustalW and was highlighted with red-dashed lines. The NCBI GI number are as follows: 4505913 (hMutLα), 46562124 (yMutLα), 499183481 (*Aa*MutL), 730578203 (*Nm*MutL), 998401886 (*Ng*MutL), 970333247 (*Pa*MutL), 16078768 (*Bs*MutL), 55981292 (*Tt*MutL), and 269852789 (*Ec*MutL)

The originally reported metal-binding motif is DQHAX$_2$EX$_4$E in hMutLα. This motif is identical with hMutLα's in *S. cerevisiae*, *B. subtilis* and *T. thermophiles*

(Fig. 4-1). *Aa*MutL's metal-binding motif has a conservative amino acid change, a replacement of the 354th alanine with leucine (Fig. 4-1). In *Ng*MutL and *Nm*MutL, the metal-binding motif has a non-conservative amino acid change, a replacement of the 492nd glutamine with methionine (Fig. 4-1). *Pa*MutL also has the same change of glutamine to methionine as *Neisserial* bacteria in the metal-binding motif (Fig. 4-1). However, the D(Q/M)HAX_2EX_4E metal-binding motif has not been found in *E. coli* MutL (*Ec*MutL).

In *E. coli*, *Ec*MutL was reported to have no endonuclease activity (Fukui *et al.*, 2011). However, human MutLα has endonuclease activity, which was activated with a mismatch, MutSα protein, other MMR proteins and a pre-existing nick in a concerted reaction with Mg^{2+} (Kadyrov *et al.*, 2006; Gueneau *et al.*, 2013). In addition, bacterial MutL from *T. thermophilis, A. aeolicus, B. subtillis, P. aeruginosa* and *N. gonorrhoeae* performed the endonuclease activity in the presence of Mn^{2+} (Fukui *et al.*, 2008; Duppatla *et al.*, 2009; Pillon *et al.*, 2010; Correa *et al.,* 2011; Iino *et al.*, 2011). In *N. gonorrhoeae* and *P. aeruginosa*, MutL protein is active in the presence of Mg^{2+} as well (Duppatla *et al.*, 2009; Correa *et al.,* 2011).

The endonuclease activity of MutL homologues was reported to be related to ATP hydrolysis (Shimada *et al.*, 2013). In hMutLα and yMutLα, MutL endonuclease activity was activated by the addition of ATP (Kadyrov *et al.*, 2006; Kadyrov *et al.*, 2007). However, the mechanism of MutL's activation is still not clear if it caused by ATP-binding or ATP-hydrolysis. Two presumptive strategies of ATP-hydrolysis were considered (Shimada *et al.*, 2013). One is that ATP-hydrolysis directly activates MutL's endonuclease activity. The other is that ATP hydrolysis contributes to the modelling of MutS-MutL complex to associate it with DNA. The MutS-MutL complex is thought to interact with DNA and search for the strand discriminatory signal.

Alternatively, in some MutH-lacking bacteria, MutL endonuclease activity is modulated by the addition of ATP with different effects (Fukui *et al.*, 2008; Duppatla *et al.*, 2009). Moreover, the endonuclease activity of *Ng*MutL, *Pa*MutL and *Tt*MutL was inhibited by ATP (Fukui *et al.*, 2008; Duppatla *et al.*, 2009; Correa *et al.*, 2011). In *B. subtilis*, the endonuclease activity of *Bs*MutL was activated by the low concentration of ATP. On the contrary, *Bs*MutL was suppressed by the high concentration of ATP (Pillon *et al.*, 2010). In addition, the role of ATP for *Aa*MutL might depend on the concentration of MutL protein (Iino *et al.*, 2011). The endonuclease activity of *Aa*MutL was activated by the addition of ATP at high concentrations of *Aa*MutL but was repressed by ATP at low concentrations of AaMutL (Iino *et al.*, 2011).

As discussed earlier, understanding the mechanism of strand discrimination is crucial for the MMR system in organisms beyond *E. coli.* Precious studies of MutL homologues from different organism has been carried out in both structural and functional aspects. However, the pattern of MutL activity still requires be further investigation to elucidate the mechanism of strand discrimination in the MMR system. In addition, the interactions of MutS and MutL with mismatched DNA may thus point towards possible mechanisms. Therefore, this study focused on evaluating how this occurs in *N. meningitidis*.

In this chapter, we sought to establish an oligo based assay to examine if *Nm*MutL has endonuclease activity *in vitro. Nm*MutL protein was freshly prepared as described in Chapter 3. For the purpose of investigation from mismatch recognition, the strands were either homoduplex or heteroduplex with a single T/G mismatch (Fig. 4-2). DNA templates have the same 60-bp sequence as used in gel shift assays in Chapter 3. To form a stable complex, DNA templates contained Biotin labels at each 5'-end to bind Streptavidin to

form a blocked-end DNA structure (Fig. 4-2). To specifically evaluate strand discrimination in *Nm*MutL activity, each DNA strand was labelled with different fluorescent dyes, 5-(and-6)-Carboxyfluorescein (FAM) or 5-Carboxytetramethylrhodamine (TAMRA), at each 3'-end respectively (Fig. 4-2). Because *Nm*MutL contains the metal binding site at its C-terminal, to elucidate the role of metal ions on any possible activity of *Nm*MutL, assays were carried out in the presence of Mn^{2+} or Mg^{2+} or in the absence of metal ions. The addition of 2mM ATP was used to determine the effect of ATP in *Nm*MutL activity. Moreover, to inspect the coordination of *Nm*MutS on *Nm*MutL activity, fresh purified *Nm*MutS (prepared in Chapter 3) were introduced with the same concentration of *Nm*MutL in assays. Furthermore, when products of the nuclease assays were resolved in denaturing PAGE, purified 60-nt oligonucleotides with the fluorescent label were used as the control to instruct the size of DNAs.

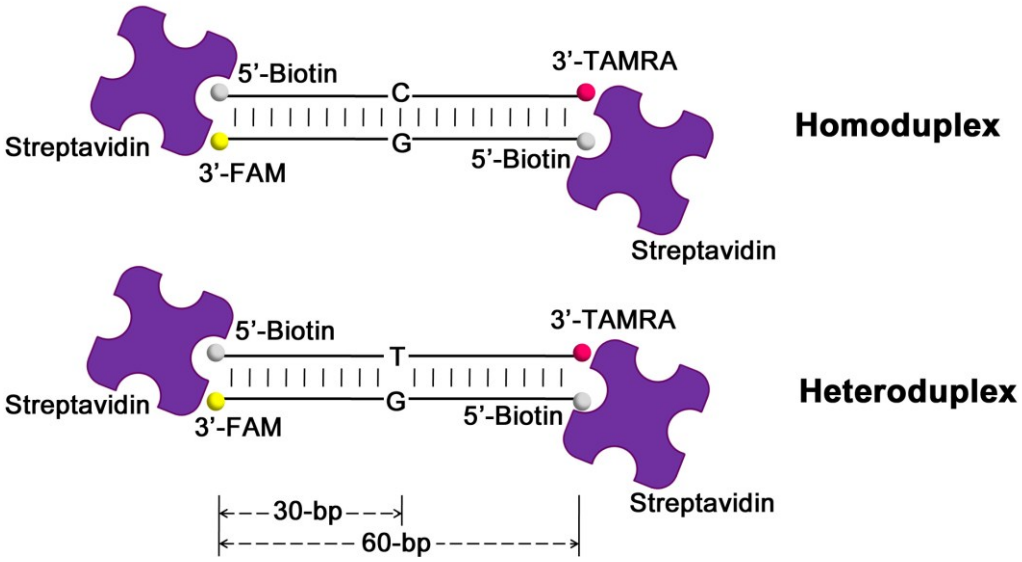


Figure 4-2. Structure of 60-bp blocked-end linear DNAs with fluorescent labels ($BL60^{C/G}$ or $BL60^{T/G}$)

4.2 Results

4.2.1 Nuclease assays of *Nm*MutL on blocked-end linear DNAs

In this section, the assay was carried out with *Nm*MutL independently on DNA with blocked ends. In addition to examining the activity of MutL alone, it was also investigated in the presence of both Mg^{2+} and Mn^{2+} and in the presence of ATP.

To better evaluate the degree of digestion, DNA were quantitated from the denaturing PAGE gel. In the denaturing PAGE gel, smeared Streptavidin complexes with the high molecular weight remained above the 60-bp linear DNA. These complexes were caused by the high-affinity multivalent interaction of Streptavidin and Biotin which was hard to remove completely in denaturing PAGE. Additionally, a highest molecule weight DNA band above the Streptavindin complex always occur in the TAMRA channel in the denaturing gel. Due to this band is not observed during dsDNA preparation, it is very difficult to define what the band it is and why it only occurs on the TAMRA labelled strand. To facilitate the quantitation of data, the 60-nt DNA bands were quantified to determine the percentage of digestion by *Nm*MutL and were then analysed by the charts of straight lines with markers (see Materials and Methods).

Firstly, nuclease assays were performed on the homoduplex DNA. In the absence of metal ions, *Nm*MutL did not show any cleavage of homoduplex DNA ($BL60^{C/G}$) (Fig. 4-3A, B, C, D). In the presence of Mg^{2+}, *Nm*MutL also did not digest $BL60^{C/G}$ DNA (Fig. 4-4 A, B, C, D). On the basis of band quantitation data, in the presence of Mg^{2+} or in the absence of metal ions, the homoduplex DNA strands was not digested beyond 30% with increasing concentrations of *Nm*MutL (Fig. 4-3E, F; 4-4E, F). As far as could be determined from the gel resolution, *Nm*MutL was considered not to exhibit nuclease activity with $BL60^{C/G}$

DNA in the presence of Mg^{2+} or in the absent of metal ions.

In the presence of Mn^{2+}, however, the nuclease activity of *Nm*MutL was detected on both strands of $BL60^{C/G}$ DNA (Fig. 4-5A, B, C, D). Moreover, the digestion of two DNA strand was enhanced with the increasing concentration of *Nm*MutL with Mn^{2+} (Fig. 4-5 A, B, C, D). In addition, there was some weak evidence that addition of ATP inhibited the nuclease activity on the homoduplex DNA (Fig. 4-5 A, B, C, D).

On the basis of band quantitation data, in the presence of Mn^{2+}, the digestion of $BL60^{C/G}$ DNA strands was promoted with increasing concentrations of *Nm*MutL (Fig. 4-4E, F). Meanwhile, *Nm*MutL nuclease activity on the FAM-labelled strand was slightly weaker than it on the TAMRA-labelled strand of $BL60^{C/G}$ DNA with Mn^{2+}. With the highest concentration (2μM) of *Nm*MutL, the TAMRA-labelled strand of $BL60^{C/G}$ is digested over 80%, higher than 58% degradation on the FAM-labelled in the presence of Mn^{2+}. Furthermore, in the presence of Mn^{2+}, the addition of ATP weakly suppressed *Nm*MutL activity on the TAMRA-labelled strand of $BL60^{C/G}$ DNA whereas there was no clear inhibition on the FAM-labelled strand.

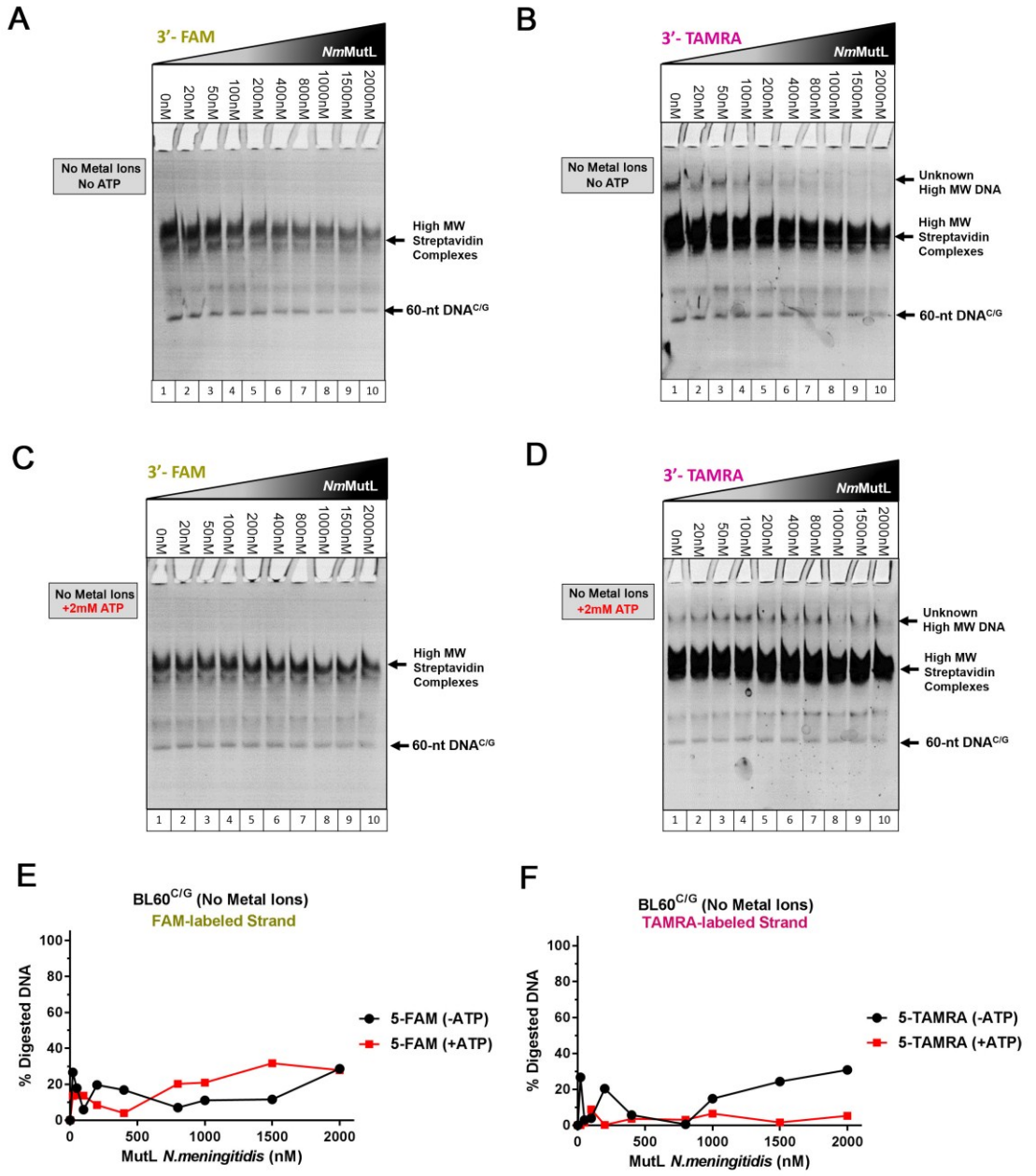


Figure 4-3. The nuclease assay of *Nm*MutL with BL60$^{C/G}$ DNA without metal ions. **(A)(B)(C)(D)** Increasing concentrations of *Nm*MutL were incubated with 40nM 60-bp blocked-end DNA without mismatch without metal ions in the absence or presence of 2mM ATP in the nuclease buffer at 25°C for 2hrs. The results were resolved by 15% denaturing PAGE (see Materials and Methods). **(E)(F)** The data was quantitated from the 60-bp bands in denaturing PAGE gels in the panels (A)(B)(C)(D) to determine the percentage of digested DNA using Image J software and was analysed via GraphPad 7. Data of reactions in the absence of ATP was shown with black lines and markers whereas data in the presence of ATP was exhibited by red lines and markers. This assay was only conducted once.

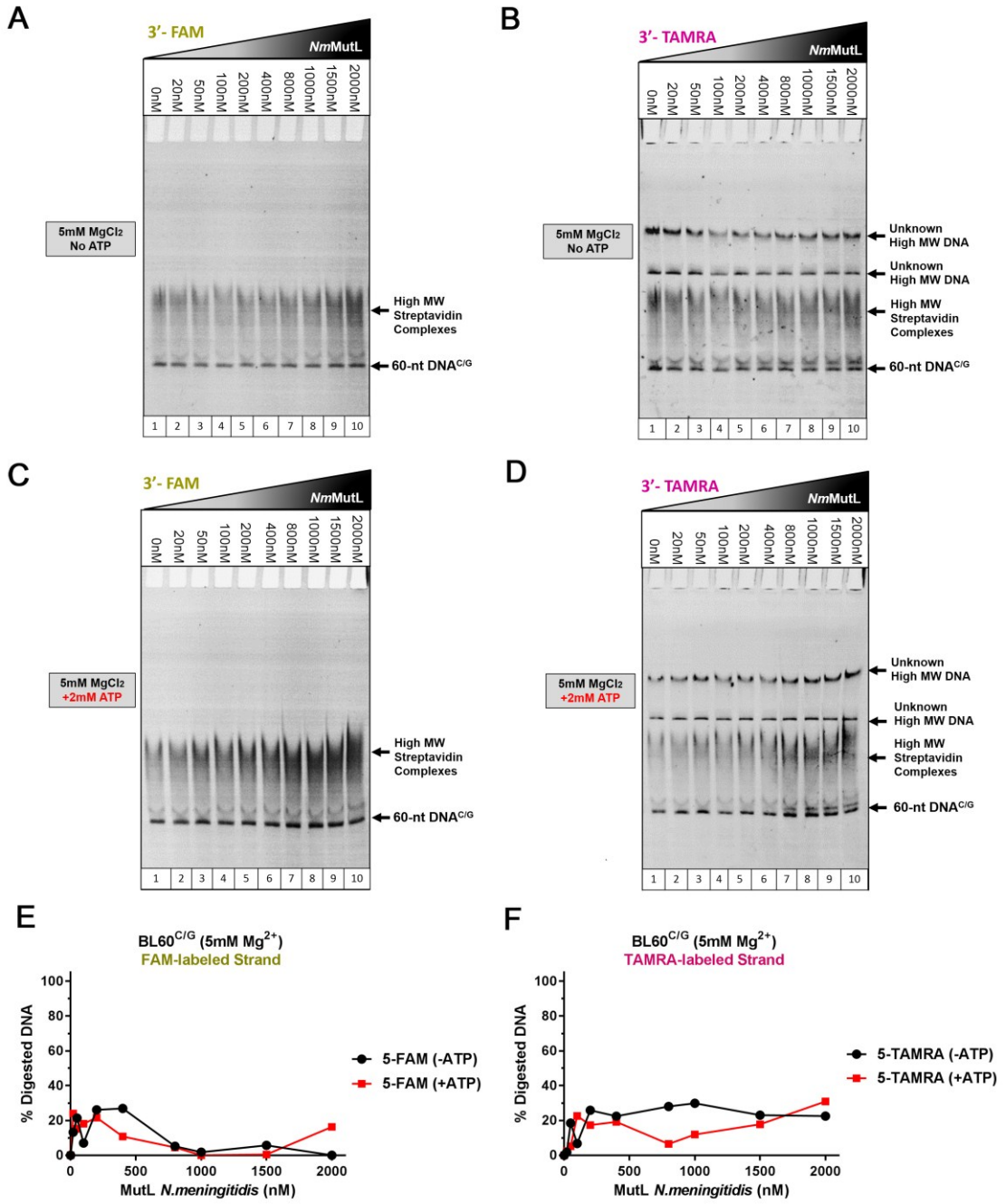


Figure 4-4. The nuclease assay of *Nm*MutL with BL60$^{C/G}$ DNA with 5mM $MgCl_2$. **(A)(B)(C)(D)** Increasing concentrations of *Nm*MutL were incubated with 40nM 60-bp blocked-end DNA without mismatch with 5mM $MgCl_2$ in the absence or presence of 2mM ATP in the nuclease buffer at 25°C for 2hrs. The results were resolved by 15% denaturing PAGE (see Materials and Methods). **(E)(F)** The data was quantitated from the 60-bp bands in denaturing PAGE gels in the panels (A)(B)(C)(D) to determine the percentage of digested DNA using Image J software and was analysed via GraphPad 7. Data of reactions in the absence of ATP was shown with black lines and markers whereas data in the presence of ATP was exhibited by red lines and markers. This assay was only conducted once.

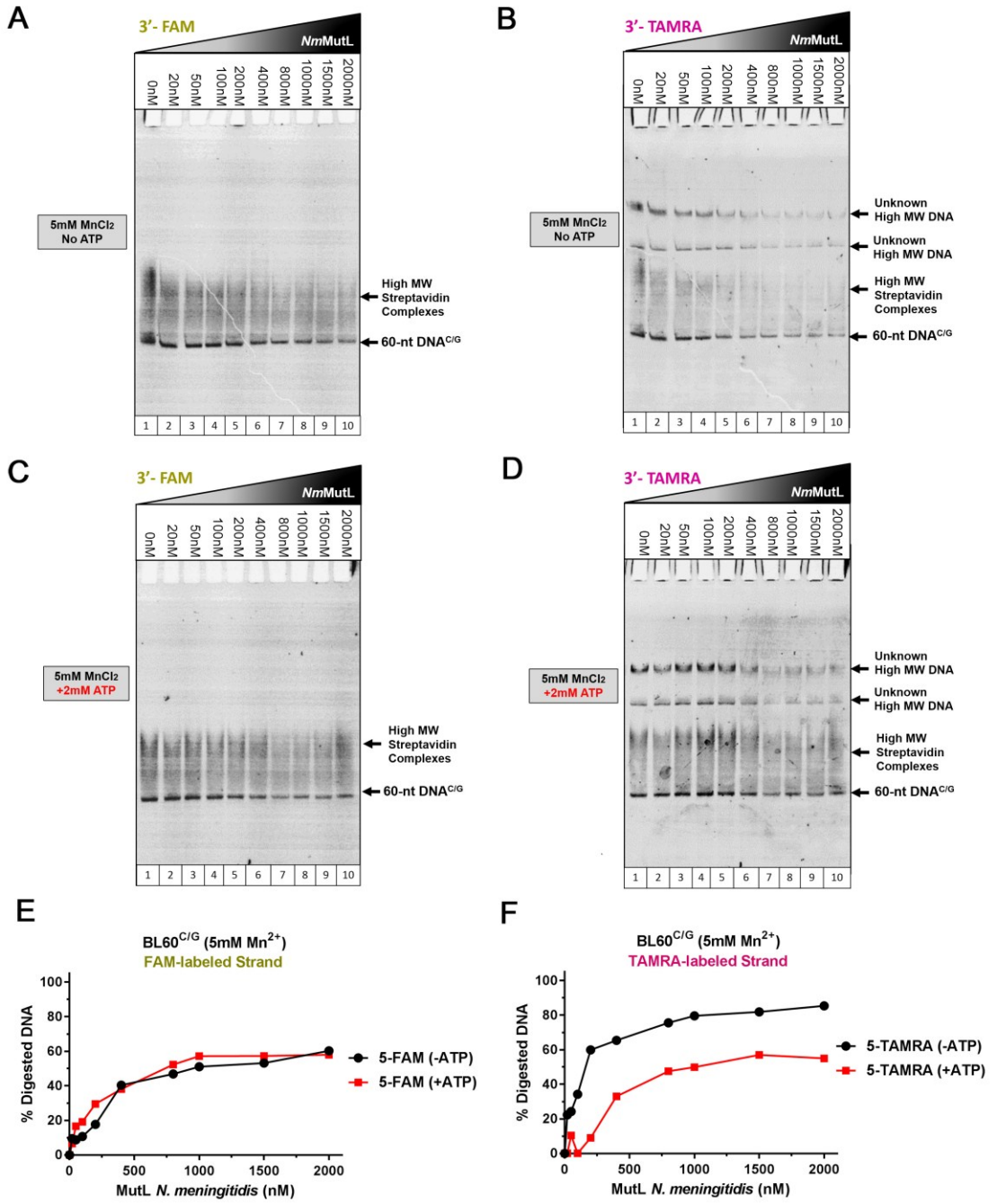


Figure 4-5. The nuclease assay of *Nm*MutL with BL60$^{C/G}$ DNA with 5mM $MnCl_2$. **(A)(B)(C)(D)** Increasing concentrations of *Nm*MutL were incubated with 40nM 60-bp blocked-end DNA without mismatch with 5mM $MnCl_2$ in the absence or presence of 2mM ATP in the nuclease buffer at 25°C for 2hrs. The results were resolved by 15% denaturing PAGE (see Materials and Methods). **(E)(F)** The data was quantitated from the 60-bp bands in denaturing PAGE gels in the panels (A)(B)(C)(D) to determine the percentage of digested DNA using Image J software and was analysed via GraphPad 7. Data of reactions in the absence of ATP was shown with black lines and markers whereas data in the presence of ATP was exhibited by red lines and markers. This assay was only conducted once.

Having examined *Nm*MutL activity with homoduplex DNA, we sought to determine if its activity is at all modulated by DNA with a T/G mismatch. In the absence of metal ions, *Nm*MutL did not cleave T/G mismatched DNA ($BL60^{T/G}$) (Fig. 4-6). In the presence of Mg^{2+}, *Nm*MutL also did not show any cleavage of $BL60^{T/G}$ DNA (Fig. 4-7). In the presence of Mn^{2+}, however, *Nm*MutL clearly digested both strands of $BL60^{T/G}$ DNA (Fig. 4-8). With the addition of ATP, there was no clear effect on *Nm*MutL activity in the absence of metal ions or in the presence of Mg^{2+}. In the presence of Mn^{2+}, the nuclease activity of *Nm*MutL was inhibited by ATP on both strands of $BL60^{T/G}$ DNA (Fig. 4-8).

According to the band quantitation data, *Nm*MutL digestion was not shown in the absence of metal ions or in the presence of Mg^{2+} (Fig. 4-6E, F). In the presence of Mn^{2+}, the rate of *Nm*MutL digestion on $BL60^{T/G}$ DNA strands was raised with the increasing concentration of *Nm*MutL (Fig. 4-7E, F). More than 90% of both strands of $BL60^{T/G}$ DNA was digested with 2μM of *Nm*MutL in the presence of Mn^{2+}. With the addition of ATP, *Nm*MutL nuclease activity was apparently inhibited from lower concentrations of *Nm*MutL. Although *Nm*MutL digestion was still increased at the high concentrations of *Nm*MutL with ATP, *Nm*MutL activity was suppressed by the addition of ATP (Fig. 4-8E, F).

Throughout assays by *Nm*MutL alone on either $BL60^{C/G}$ or $BL60^{T/G}$ DNA, in the presence of Mg^{2+} or without metal ions, *Nm*MutL did not perform any detectable nuclease activity. On the other hand, in the presence of Mn^{2+}, *Nm*MutL apparently digested both strands of either $BL60^{C/G}$ or $BL60^{T/G}$ DNA. Meanwhile, the digestion from *Nm*MutL alone on $BL60^{T/G}$ DNA was slightly stronger than it was on $BL60^{C/G}$ DNA with Mn^{2+}. This implied that the nuclease activity from *Nm*MutL alone has weak mismatch discrimination with Mn^{2+}. Furthermore, with the addition of ATP, the inhibition of *Nm*MutL activity on the homoduplex DNA was weaker than on the dsDNA with a single T/G mismatch.

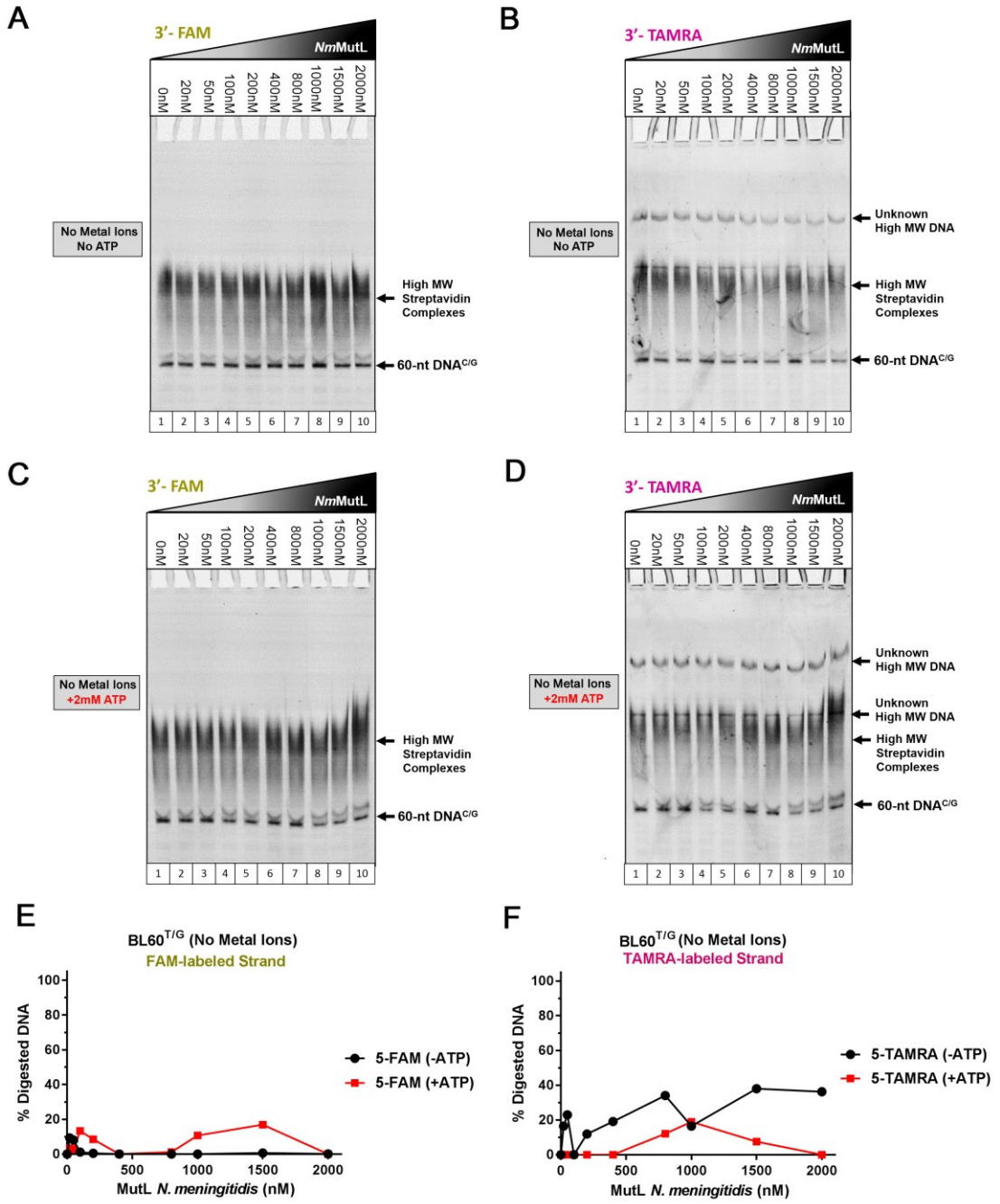


Figure 4-6. The nuclease assay of *Nm*MutL with BL60$^{T/G}$ DNA without metal ions. **(A)(B)(C)(D)** Increasing concentrations of *Nm*MutL were incubated with 40nM 60-bp blocked-end DNA with a T/G mismatch without metal ions in the absence or presence of 2mM ATP in the nuclease buffer at 25°C for 2hrs. The results were resolved by 15% denaturing PAGE (see Materials and Methods). **(E)(F)** The data was quantitated from the 60-bp bands in denaturing PAGE gels in the panels (A)(B)(C)(D) to determine the percentage of digested DNA using Image J software and was analysed via GraphPad 7. Data of reactions in the absence of ATP was shown with black lines and markers whereas data in the presence of ATP was exhibited by red lines and markers. This assay was only conducted once.

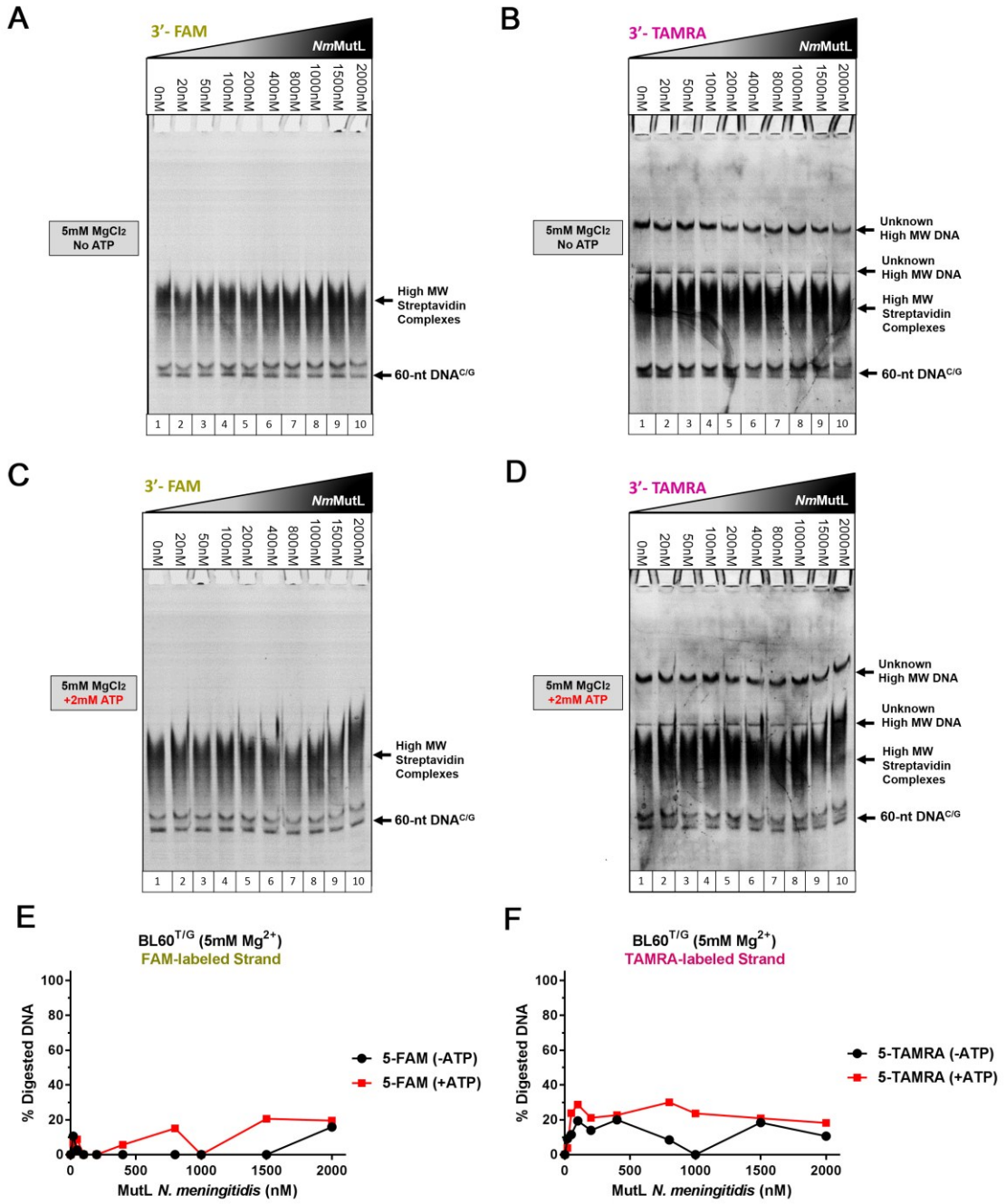


Figure 4-7. The nuclease assay of *Nm*MutL with BL60$^{T/G}$ DNA with 5mM $MgCl_2$. **(A)(B)(C)(D)** Increasing concentrations of *Nm*MutL were incubated with 40nM 60-bp blocked-end DNA with a T/G mismatch with 5mM $MgCl_2$ in the absence or presence of 2mM ATP in the nuclease buffer at 25°C for 2hrs. The results were resolved by 15% denaturing PAGE (see Materials and Methods). **(E)(F)** The data was quantitated from the 60-bp bands in denaturing PAGE gels in the panels (A)(B)(C)(D) to determine the percentage of digested DNA using Image J software and was analysed via GraphPad 7. Data of reactions in the absence of ATP was shown with black lines and markers whereas data in the presence of ATP was exhibited by red lines and markers. This assay was only conducted once.

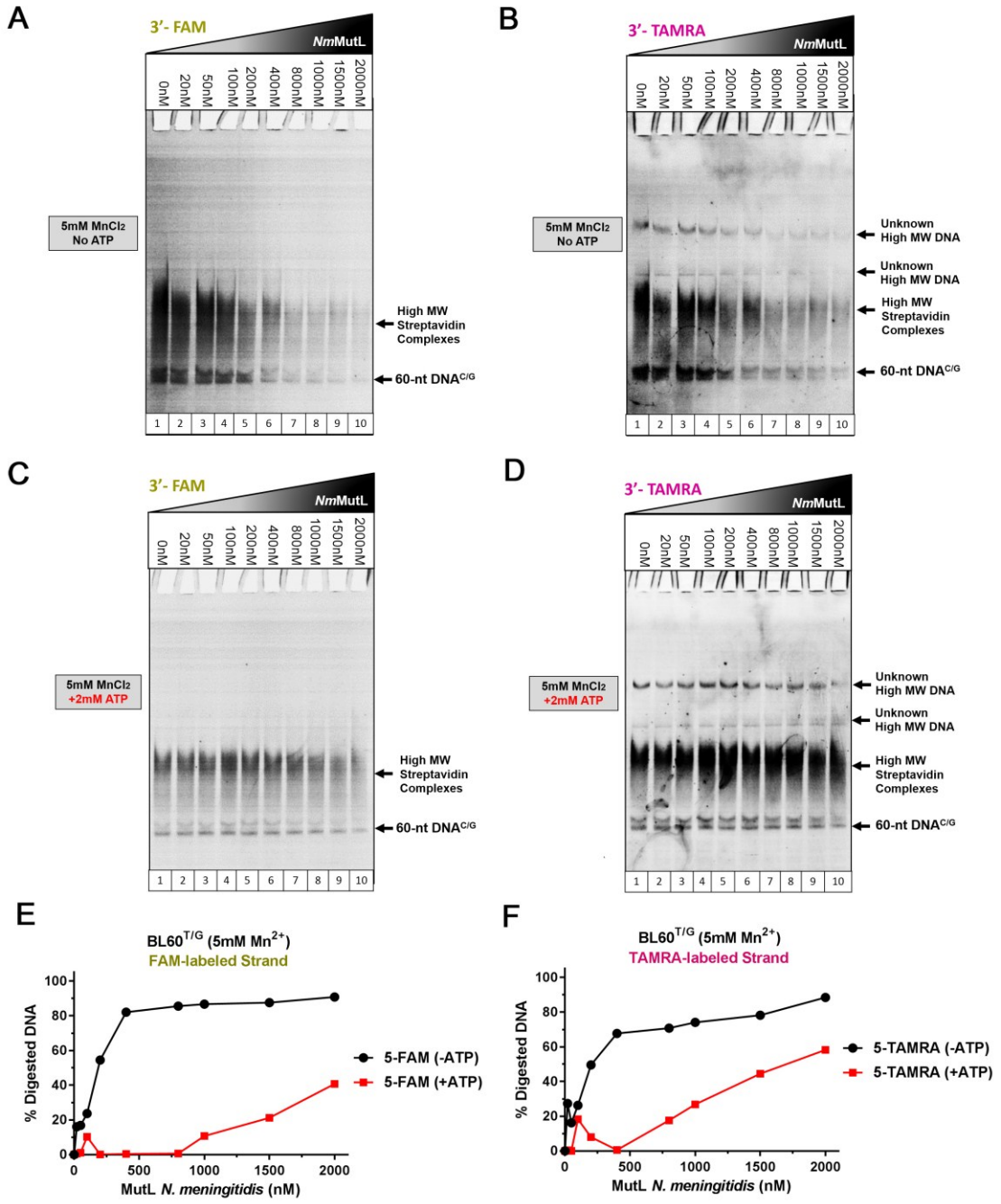


Figure 4-8. The nuclease assay of *Nm*MutL with BL60$^{T/G}$ DNA with 5mM $MnCl_2$. **(A)(B)(C)(D)** Increasing concentrations of *Nm*MutL were incubated with 40nM 60-bp blocked-end DNA with a T/G mismatch with 5mM $MnCl_2$ in the absence or presence of 2mM ATP in the nuclease buffer at 25°C for 2hrs. The results were resolved by 15% denaturing PAGE (see Materials and Methods). **(E)(F)** The data was quantitated from the 60-bp bands in denaturing PAGE gels in the panels (A)(B)(C)(D) to determine the percentage of digested DNA using Image J software and was analysed via GraphPad 7. Data of reactions in the absence of ATP was shown with black lines and markers whereas data in the presence of ATP was exhibited by red lines and markers. This assay was only conducted once.

4.2.2 Nuclease assays of *Nm*MutL with *Nm*MutS on blocked-end linear DNAs

To determine whether *Nm*MutS in any way modulates the nuclease activity of *Nm*MutL, we performed the nuclease assays in the presence of *Nm*MutS with *Nm*MutL on $BL60^{C/G}$ and $BL60^{T/G}$ DNA as well.

For the homoduplex DNA, *Nm*MutL did not digest DNA strands with the addition of *Nm*MutS either in the absence of metal ions or in the presence of Mg^{2+} (Fig. 4-9A, B, C, D; 4-10 A, B, C, D). In the quantitation data of 60-nt DNA bands, the nuclease activity of *Nm*MutL with *Nm*MutS was not observed with Mg^{2+} or without metal ions (Fig. 4-9E, F;4-10E, F).

In the presence of Mn^{2+}, the nuclease activity of *Nm*MutL with *Nm*MutS occurred on both strands of $BL60^{C/G}$ DNA (Fig. 4-11A, B). Furthermore, with the addition of ATP, the Mn^{2+} dependent nuclease activity from *Nm*MutL with *Nm*MutS presented weakly suppression on the homoduplex DNA (Fig. 4-11C, D). In the quantitation data of 60-nt DNA bands, in the presence of Mn^{2+}, the digestion by *Nm*MutL with *Nm*MutS on the FAM-labelled strand of $BL60^{C/G}$ DNA was weaker than on its TAMRA-labelled strand (Fig. 4-11E, F). Moreover, ATP evidently inhibited the nuclease activity on the TAMRA-labelled of $BL60^{C/G}$ DNA, but did not on its FAM-labelled strand (Fig. 4-11E, F). This result was consistent with the nuclease assays on the homoduplex DNA in the absence of *Nm*MutS (Fig. 4-8E, F).

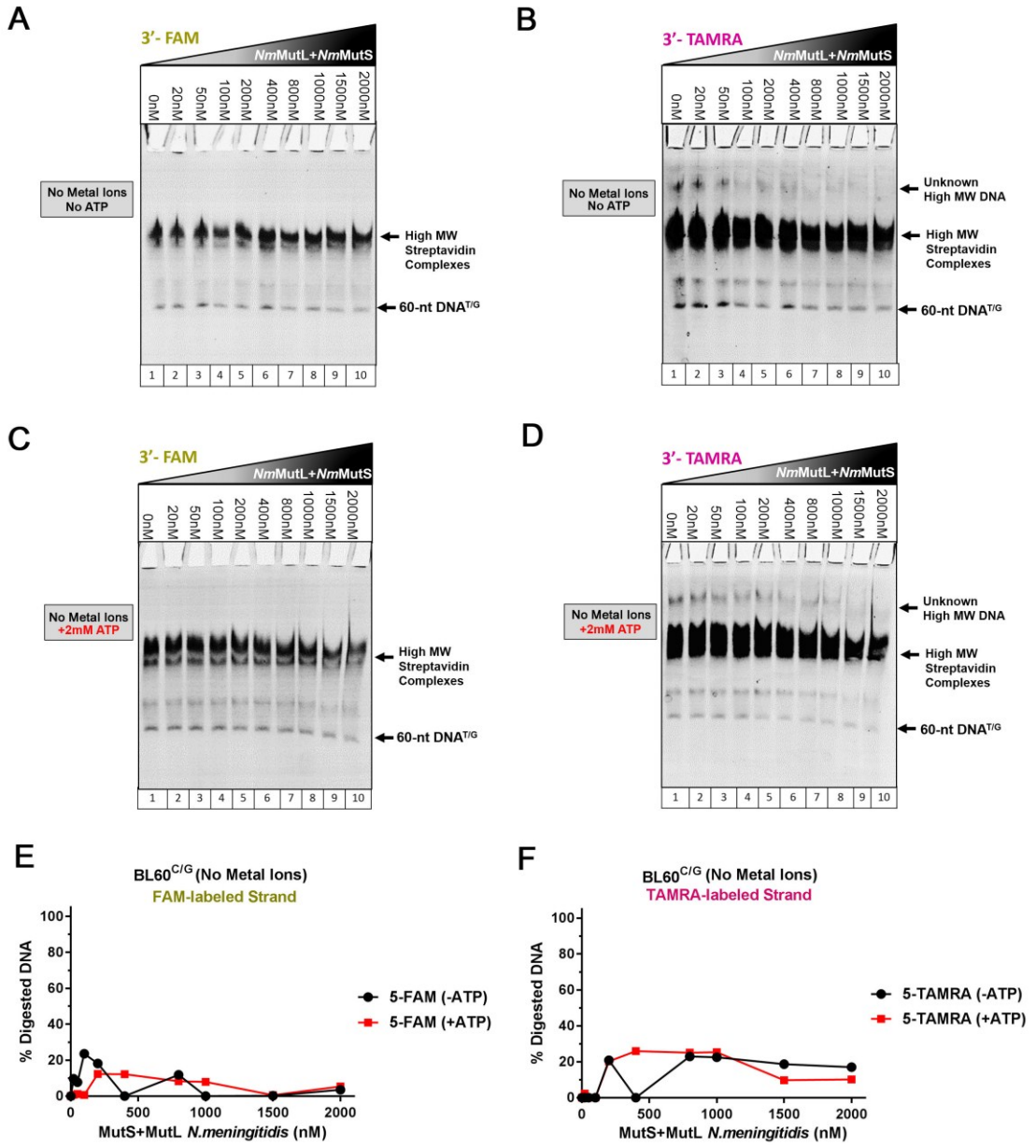


Figure 4-9. The nuclease assay of *Nm*MutL with *Nm*MutS on BL60$^{C/G}$ DNA without metal ions. (A)(B)(C)(D) Increasing concentrations of *Nm*MutL with same concentrations of *Nm*MutS were incubated with 40nM 60-bp blocked-end DNA without mismatch without metal ions in the absence or presence of 2mM ATP in the nuclease buffer at 25°C for 2hrs. The results were resolved by 15% denaturing PAGE (see Materials and Methods). **(E)(F)** The data was quantitated from the 60-bp bands in denaturing PAGE gels in the panels (A)(B)(C)(D) to determine the percentage of digested DNA using Image J software and was analysed via GraphPad 7. Data of reactions in the absence of ATP was shown with black lines and markers whereas data in the presence of ATP was exhibited by red lines and markers. This assay was only conducted once.

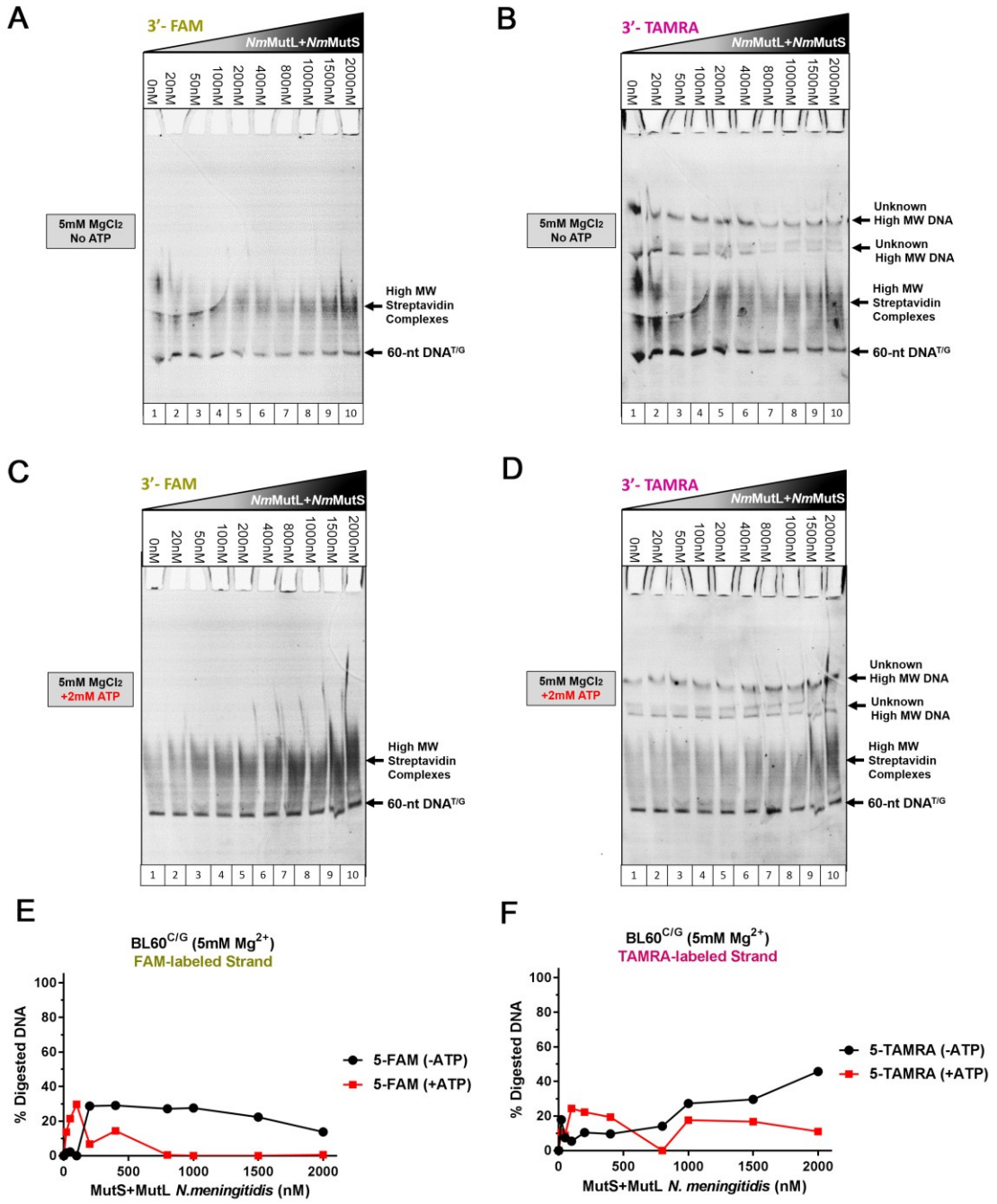


Figure 4-10. The nuclease assay of *Nm*MutL with *Nm*MutS on BL60$^{C/G}$ DNA with 5mM $MgCl_2$. (A)(B)(C)(D) Increasing concentrations of *Nm*MutL with same concentrations of *Nm*MutS were incubated with 40nM 60-bp blocked-end DNA without mismatch with 5mM $MgCl_2$ in the absence or presence of 2mM ATP in the nuclease buffer at 25°C for 2hrs. The results were resolved by 15% denaturing PAGE (see Materials and Methods). **(E)(F)** The data was quantitated from the 60-bp bands in denaturing PAGE gels in the panels (A)(B)(C)(D) to determine the percentage of digested DNA using Image J software and was analysed via GraphPad 7. Data of reactions in the absence of ATP was shown with black lines and markers whereas data in the presence of ATP was exhibited by red lines and markers. This assay was only conducted once.

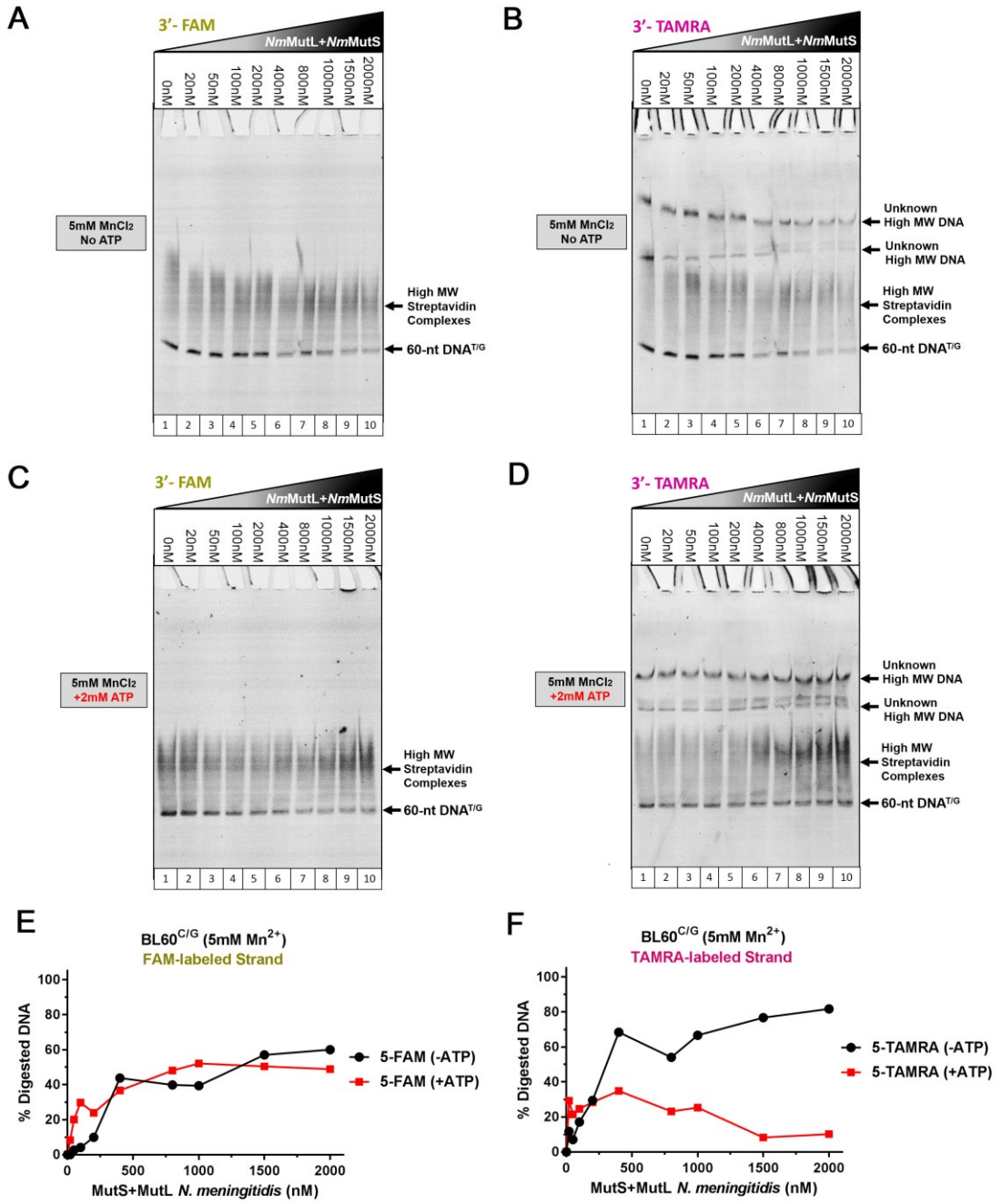


Figure 4-11. The nuclease assay of *Nm*MutL with *Nm*MutS on BL60$^{C/G}$ DNA with 5mM $MnCl_2$. (A)(B)(C)(D) Increasing concentrations of *Nm*MutL with same concentrations of *Nm*MutS were incubated with 40nM 60-bp blocked-end DNA without mismatch with 5mM $MnCl_2$ in the absence or presence of 2mM ATP in the nuclease buffer at 25°C for 2hrs. The results were resolved by 15% denaturing PAGE (see Materials and Methods). **(E)(F)** The data was quantitated from the 60-bp bands in denaturing PAGE gels in the panels (A)(B)(C)(D) to determine the percentage of digested DNA using Image J software and was analysed via GraphPad 7. Data of reactions in the absence of ATP was shown with black lines and markers whereas data in the presence of ATP was exhibited by red lines and markers. This assay was only conducted once.

To establish if *Nm*MutS affects the activity of *Nm*MutL on mismatched DNA, assay was also carried out by *Nm*MutL and NmMutS with $BL60^{T/G}$ DNA. Interestingly, without adding any metal ions, *Nm*MutL with *Nm*MutS digested two strands of $BL60^{T/G}$ DNA which did not happen before (Fig. 4-12A, B, C, D). The data of band quantitation showed that the digestion of mismatched DNA was raised with the increasing concentration of *Nm*MutL and *Nm*MutS in the absence of metal ions (Fig. 4-12E, F). With the highest concentration, 2uM of *Nm*MutL and *Nm*MutS, over 60% of $BL60^{T/G}$ DNA strands was digested by the nuclease activity of *Nm*MutL assisted by *Nm*MutS without metal ions. Moreover, the nuclease activity of *Nm*MutL with *Nm*MutS on $BL60^{T/G}$ DNA strands was obviously inhibited by the addition of ATP, although the digestion of DNA was still increased with high concentrations of *Nm*MutL and *Nm*MutS (Fig. 4-12E, F).

In the presence of Mg^{2+}, *Nm*MutL still did not perform clear cleavage on $BL60^{T/G}$ DNA strands, even *Nm*MutS was added into the reaction (Fig. 4-13A, B, C, D). In the data of band quantitation, there was no clear nuclease activity from *Nm*MutL and *Nm*MutS in the presence of Mg2+ (Fig. 4-13E, F). Although approximately 40% of the last $BL60^{T/G}$ DNA strands seemed to be digested with the addition of ATP in the presence of Mg^{2+}, the data might be interfered by the deformation of bands at the edge of the electrophoresis gel (Fig. 4-13E, F).

In the presence of Mn^{2+}, the nuclease activity of *Nm*MutL was observed effectively on both strands of $BL60^{T/G}$ DNA (Fig. 4-14). With the addition of ATP, *Nm*MutL nuclease activity with *Nm*MutS on $BL60^{T/G}$ DNA was abolished in the absence of metal ions and in the presence of Mn^{2+} (Fig. 4-12; 4-14). Since the stains on the surface of the gel masked a portion of the 60-bp DNA in the presence of Mn^{2+}, the data was quantified by the streptavidin complex (as shown by the red dashed line, Fig. 4-14A, B). In the presence of Mn^{2+}, *Nm*MutL

nuclease activities harbouring *Nm*MutS on both $BL60^{T/G}$ DNA strands were digested to similar degrees and both were improved with the increasing concentration of *Nm*MutL and *Nm*MutS (Fig. 4-14E, F). Furthermore, this nuclease activity of *Nm*MutL and *Nm*MutS was effectively inhibited on both strands of $BL60^{T/G}$ DNA by the addition of ATP (Fig. 4-14E, F).

Overall, in the presence of Mn^{2+}, *Nm*MutL performed nuclease activity on both strands of $BL60^{C/G}$ and $BL60^{T/G}$ DNAs. This Mn^{2+}-dependent nuclease activity was observed some mismatch discrimination that the digestion of the homoduplex DNA was weaker than it on DNA with a T/G mismatch. Moreover, the nuclease activity of *Nm*MutL on DNA with a T/G mismatch was shown the obvious inhibition from the addition of ATP.

The nuclease activity of *Nm*MutL was seemingly improved with the addition of *Nm*MutS in the absence of metal ions. This *Nm*MutS assisted nuclease activity of *Nm*MutL was specific for DNA with a T/G mismatch which is not seem under any other conditions. In the presence of Mg^{2+}, *Nm*MutL nuclease activity was ineffective regardless the addition of *Nm*MutS. In the presence of Mn^{2+}, activity of *Nm*MutL with *Nm*MutS on the homoduplex DNA was similar as the activity of *Nm*MutL alone. Meanwhile, the $BL60^{T/G}$ DNA strands was cleaved with high rates by *Nm*MutL with *Nm*MutS in the presence of Mn^{2+}. Furthermore, in the presence of both *Nm*MutS and Mn^{2+}, *Nm*MutL nuclease activity was performed with the strongest ATP inhibition.

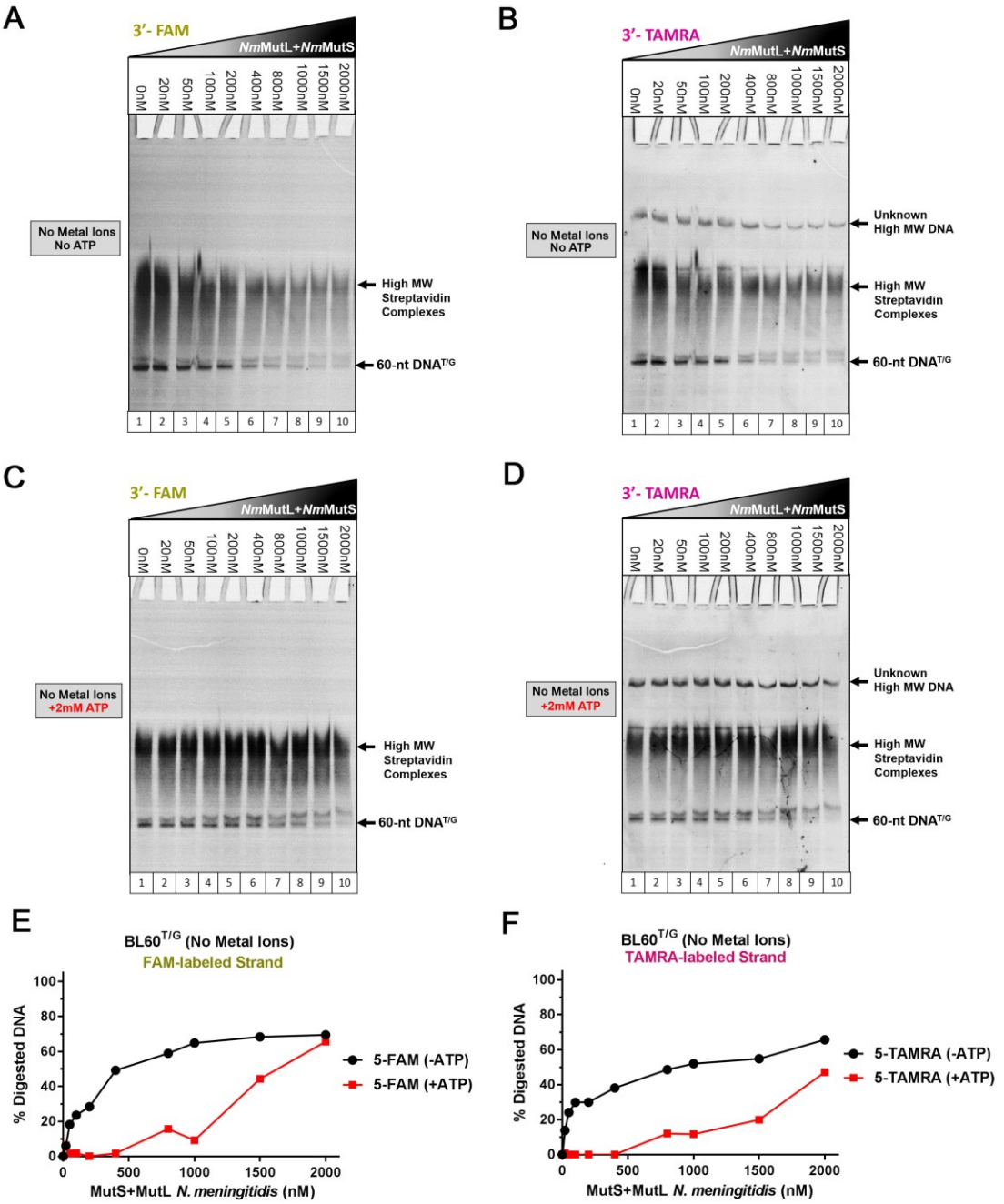


Figure 4-12. The nuclease assay of *Nm*MutL with *Nm*MutS on BL60$^{T/G}$ DNA without metal ions. **(A)(B)(C)(D)** Increasing concentrations of *Nm*MutL with same concentrations of *Nm*MutS were incubated with 40nM 60-bp blocked-end DNA with a T/G mismatch without metal ions in the absence or presence of 2mM ATP in the nuclease buffer at 25°C for 2hrs. The results were resolved by 15% denaturing PAGE (see Materials and Methods). **(E)(F)** The data was quantitated from the 60-bp bands in denaturing PAGE gels in the panels (A)(B)(C)(D) to determine the percentage of digested DNA using Image J software and was analysed via GraphPad 7. Data of reactions in the absence of ATP was shown with black lines and markers whereas data in the presence of ATP was exhibited by red lines and markers. This assay was only conducted once.

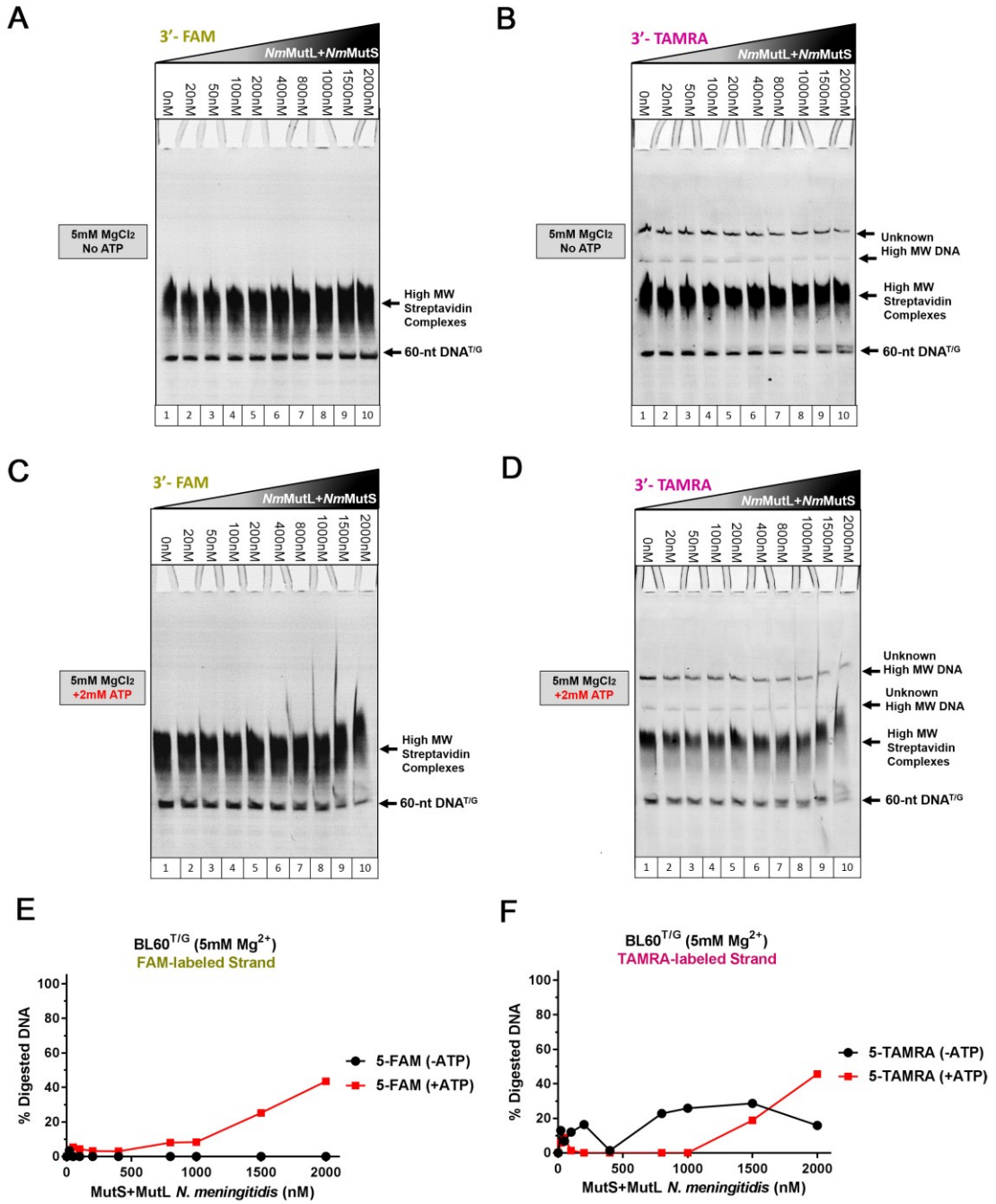


Figure 4-13. The nuclease assay of *Nm*MutL with *Nm*MutS on BL60$^{T/G}$ DNA with 5mM $MgCl_2$. (A)(B)(C)(D) Increasing concentrations of *Nm*MutL with same concentrations of *Nm*MutS were incubated with 40nM 60-bp blocked-end DNA with a T/G mismatch with 5mM $MgCl_2$ in the absence or presence of 2mM ATP in the nuclease buffer at 25°C for 2hrs. The results were resolved by 15% denaturing PAGE (see Materials and Methods). **(E)(F)** The data was quantitated from the 60-bp bands in denaturing PAGE gels in the panels (A)(B)(C)(D) to determine the percentage of digested DNA using Image J software and was analysed via GraphPad 7. Data of reactions in the absence of ATP was shown with black lines and markers whereas data in the presence of ATP was exhibited by red lines and markers. This assay was only conducted once.

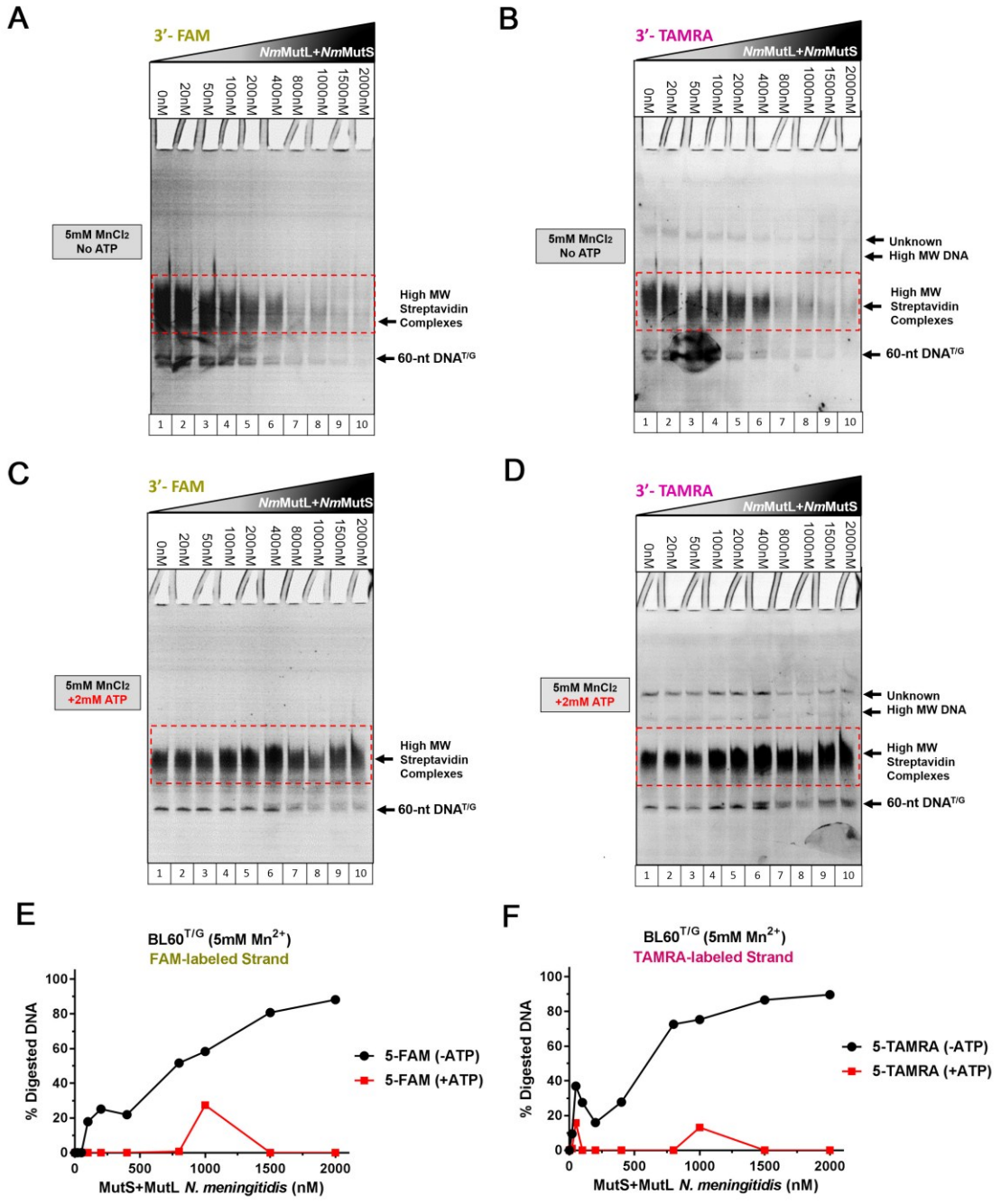


Figure 4-14. The nuclease assay of *Nm*MutL with *Nm*MutS on BL60$^{T/G}$ DNA with 5mM $MnCl_2$. (A)(B)(C)(D) Increasing concentrations of *Nm*MutL with same concentrations of *Nm*MutS were incubated with 40nM 60-bp blocked-end DNA with a T/G mismatch with 5mM $MnCl_2$ in the absence or presence of 2mM ATP in the nuclease buffer at 25°C for 2hrs. The results were resolved by 15% denaturing PAGE (see Materials and Methods). **(E)(F)** The data was quantitated from the high MW streptavidin complexes in denaturing PAGE gels in the panels (A)(B)(C)(D) to determine the percentage of digested DNA using Image J software and was analysed via GraphPad 7. Data of reactions in the absence of ATP was shown with black lines and markers whereas data in the presence of ATP was exhibited by red lines and markers. This assay was only conducted once.

4.2.3 Nuclease assays of *Nm*MutL on open-end linear DNAs with different metal ions

Blocked-end DNA duplex provided a stable complex to perform DNA-protein interactions which was proved in gel shift assays. However, the streptavidin-biotin binding introduced multiple bands in the denaturing gels. Therefore, we also carried out the nuclease assays with the open-end DNA duplex with a single T/G mismatch ($OL60^{T/G}$). Without the multivalent binding of Streptavidin and Biotin on DNA substrates, nuclease assays displayed results with clear single bands of oligonucleotide strands.

We firstly examined the activity of *Nm*MutL alone. In the absence of metal ions, both $OL60^{T/G}$ DNA strands were not affected by the activity of *Nm*MutL (Fig. 4-15A, B ,C, D). In the presence of Mg^{2+}, *Nm*MutL digested $OL60^{T/G}$ DNA with a weak strand discrimination, the cleavage on the FAM-labelled strand was a slightly stronger than on the TAMRA-labelled strand (Fig. 4-16A, B). In the presence of Mn^{2+}, *Nm*MutL nuclease activity was clearly observed on both the TAMRA and FAM labelled DNA strands (Fig. 4-17A, B). Moveover, with the addition of 2mM ATP, the activity of *Nm*MutL was weakly inhibited in the presence of either Mg^{2+} or Mn^{2+} (Fig. 4-16C, D; 4-17C, D).

In the band quantitation data, the digestion of $OL60^{T/G}$ DNA strands was not performed in the absence of metal ions (Fig. 4-15E, F). In the presence of Mg^{2+}, the FAM-labelled strand of $OL60^{T/G}$ DNA was progressively digested with increasing concentrations of *Nm*MutL (Fig. 4-16E). Approximately 60% FAM-labelled strand was digested by 2μM of *Nm*MutL (Fig. 4-16E). On the TAMRA-labelled strand, the *Nm*MutL digestion did not beyond 20.7% in the presence of Mg^{2+} (Fig. 4-16F).

In the presence of Mn^{2+}, the cleavage of both $OL60^{T/G}$ DNA strands was similar and reached approximately 80% when 600nM of *Nm*MutL was added (Fig. 4-17E, F). The results also showed some weak evidence that ATP inhibited the digestion of $OL60^{T/G}$ DNA strands in the presence of Mg^{2+} and Mn^{2+}.

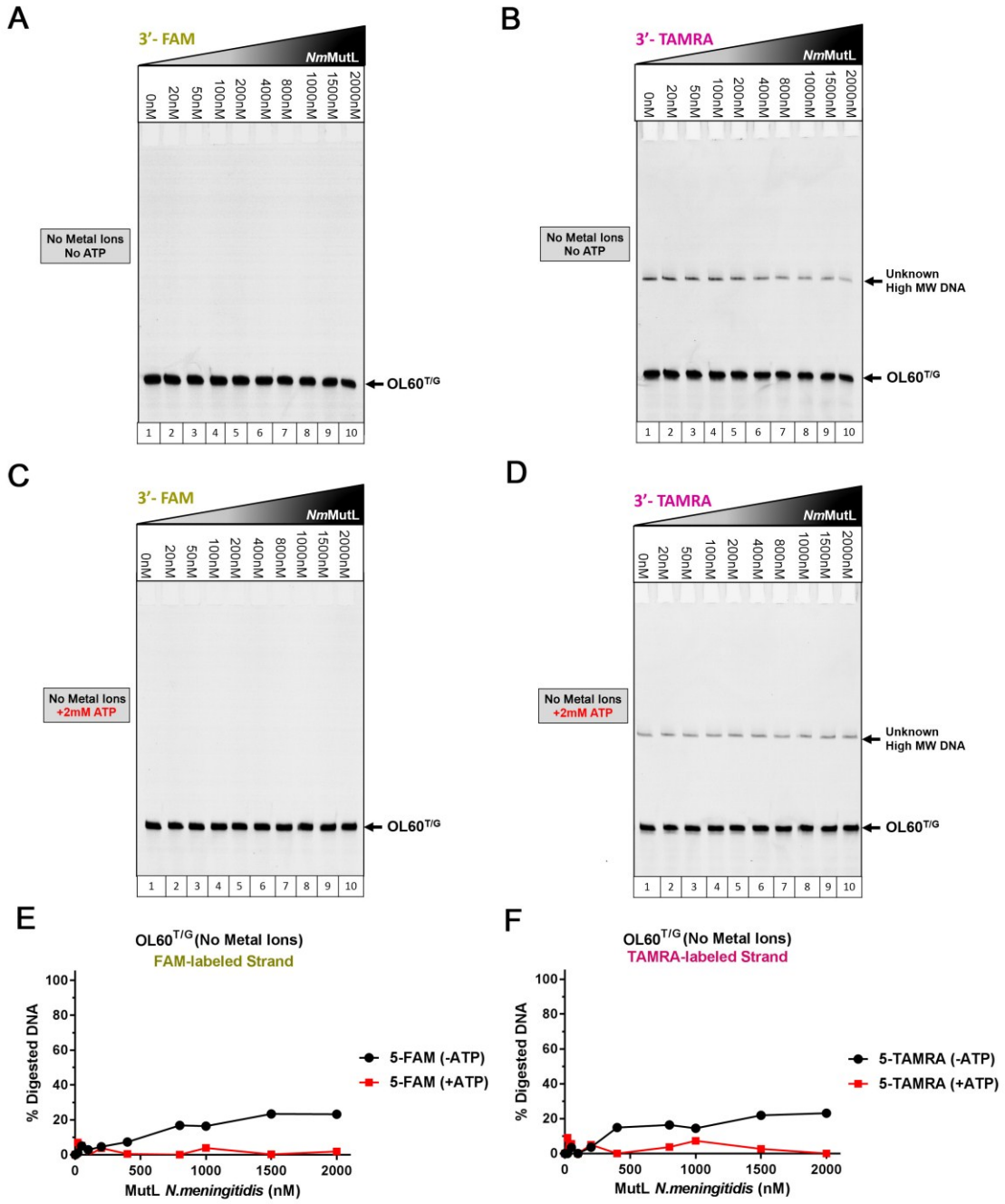


Figure 4-15. The nuclease assay of *Nm*MutL on OL60$^{T/G}$ DNA without metal ions. **(A)(B)(C)(D)** Increasing concentrations of *Nm*MutL were incubated with 40nM 60-bp open-end DNA with a T/G mismatch without metal ions in the absence or presence of 2mM ATP in the nuclease buffer at 25°C for 2hrs. The results were resolved by 15% denaturing PAGE (see Materials and Methods). **(E)(F)** The data was quantitated from the 60-bp bands in denaturing PAGE gels in the panels (A)(B)(C)(D) to determine the percentage of digested DNA using Image J software and was analysed via GraphPad 7. Data of reactions in the absence of ATP was shown with black lines and markers whereas data in the presence of ATP was exhibited by red lines and markers. This assay was only conducted once.

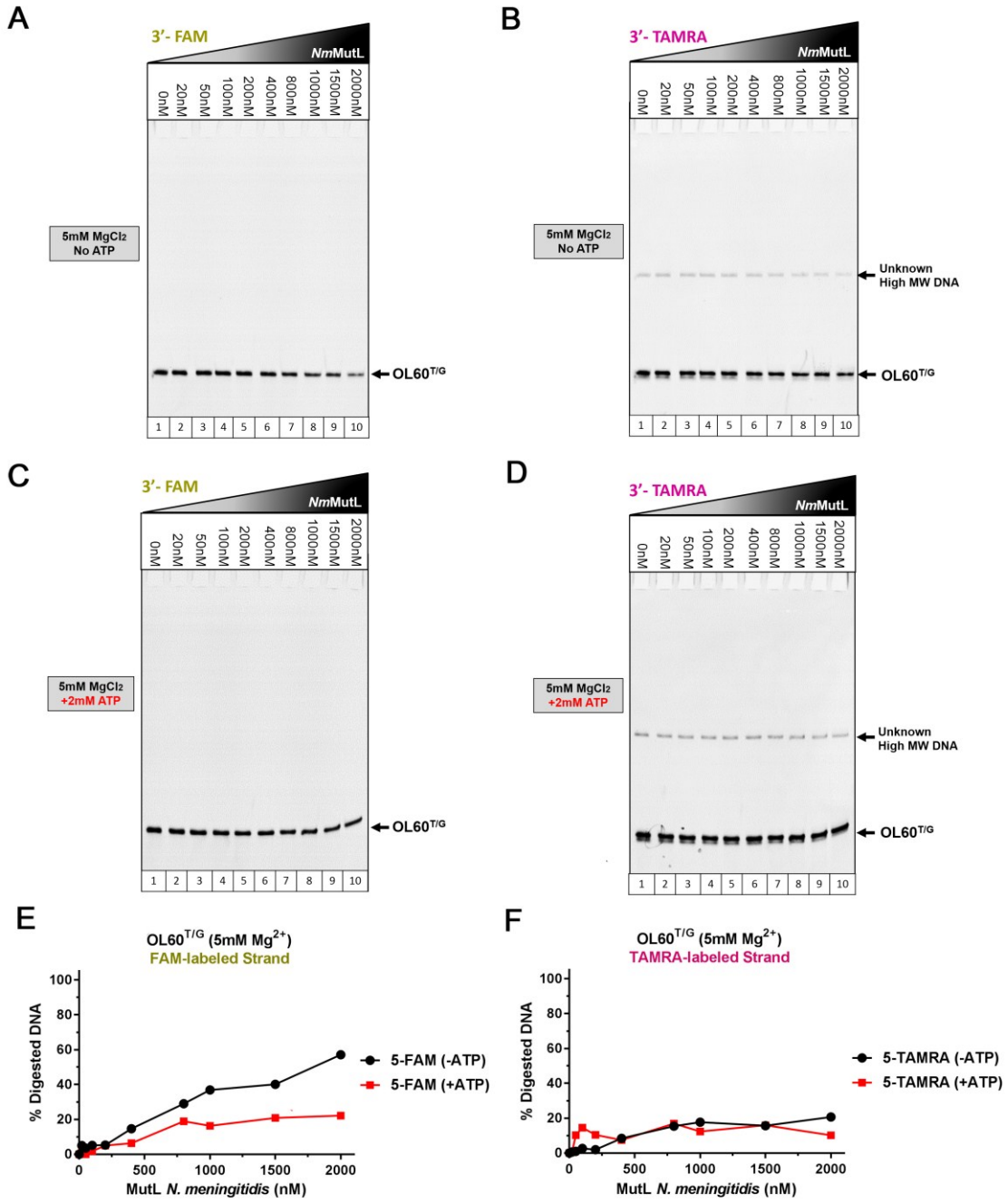


Figure 4-16. The nuclease assay of *Nm*MutL on OL60$^{T/G}$ DNA with 5mM $MgCl_2$. **(A)(B)(C)(D)** Increasing concentrations of *Nm*MutL were incubated with 40nM 60-bp open-end DNA with a T/G mismatch with 5mM $MgCl_2$ in the absence or presence of 2mM ATP in the nuclease buffer at 25°C for 2hrs. The results were resolved by 15% denaturing PAGE (see Materials and Methods). **(E)(F)** The data was quantitated from the 60-bp bands in denaturing PAGE gels in the panels (A)(B)(C)(D) to determine the percentage of digested DNA using Image J software and was analysed via GraphPad 7. Data of reactions in the absence of ATP was shown with black lines and markers whereas data in the presence of ATP was exhibited by red lines and markers. This assay was only conducted once.

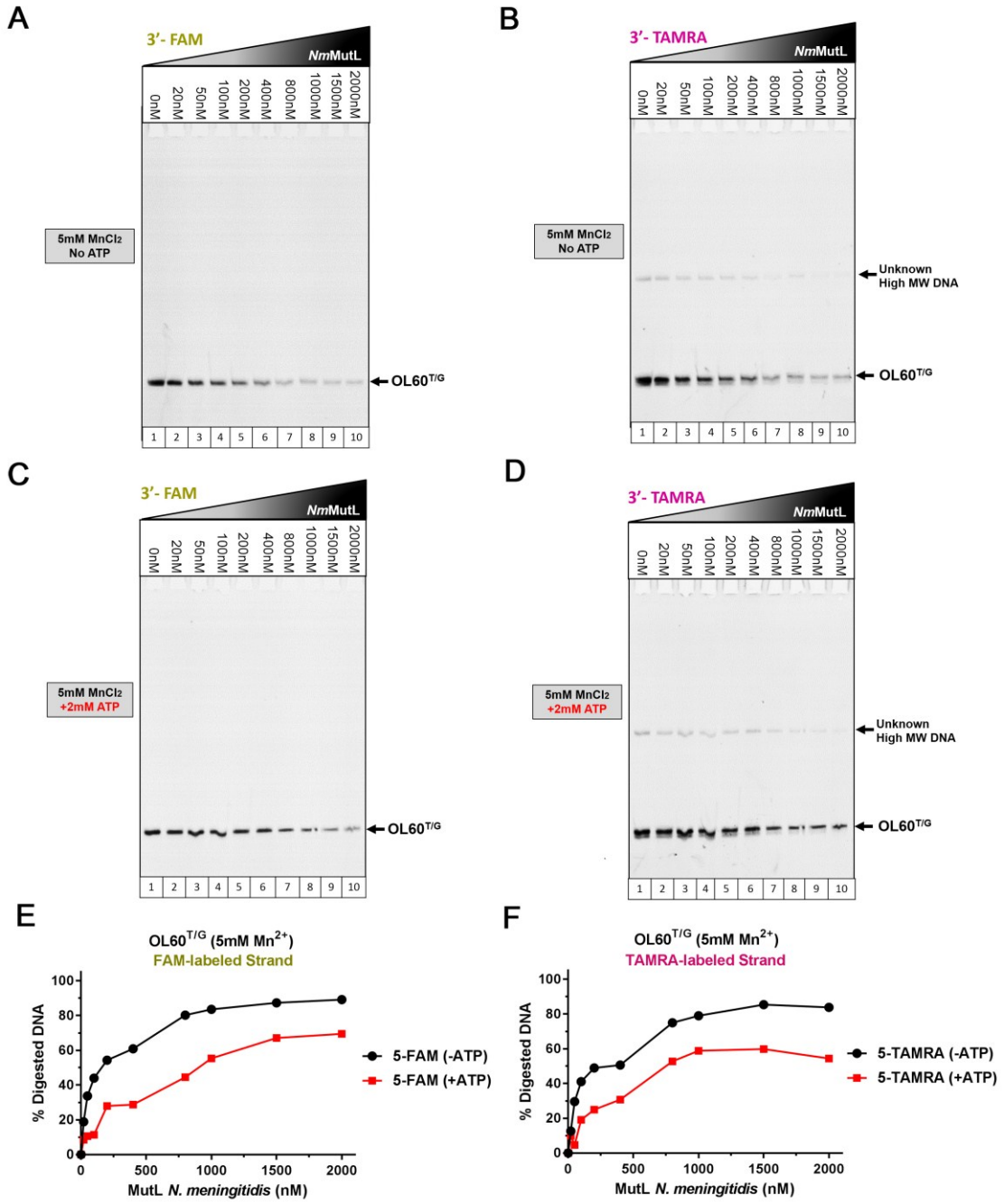


Figure 4-17. The nuclease assay of *Nm*MutL on OL60$^{T/G}$ DNA with 5mM $MnCl_2$. **(A)(B)(C)(D)** Increasing concentrations of *Nm*MutL were incubated with 40nM 60-bp open-end DNA with a T/G mismatch with 5mM $MnCl_2$ in the absence or presence of 2mM ATP in the nuclease buffer at 25°C for 2hrs. The results were resolved by 15% denaturing PAGE (see Materials and Methods). **(E)(F)** The data was quantitated from the 60-bp bands in denaturing PAGE gels in the panels (A)(B)(C)(D) to determine the percentage of digested DNA using Image J software and was analysed via GraphPad 7. Data of reactions in the absence of ATP was shown with black lines and markers whereas data in the presence of ATP was exhibited by red lines and markers. This assay was only conducted once.

We futher also investigated if *Nm*MutS affects the activity of *Nm*MutL on $OL60^{T/G}$ DNA. In the absence of metal ions, *Nm*MutL had no explicit activity on $OL60^{T/G}$ DNA with *Nm*MutS (Fig. 4-18A, B, C, D). In the presence of Mg^{2+}, the digestion of $OL60^{T/G}$ DNA strands presented a strand discrimination by *Nm*MutL and *Nm*MutS (Fig. 4-19A, B). The FAM-labelled strand was digested by *Nm*MutL and *Nm*MutS in the presence of Mg^{2+} (Fig 4-19A) whereas the TAMRA-labelled strand was not (Fig 4-19B). In the presence of Mn^{2+}, both DNA strands of $OL60^{T/G}$ DNA were clearly cleaved by *Nm*MutL nuclease activity with *Nm*MutS (Fig. 4-20A, B). In the presence of Mn^{2+} or Mg^{2+}, *Nm*MutL nuclease activity with *Nm*MutS was inhibited by the addition of ATP (Fig. 4-19C, D; 4-20C, D).

The data of band quantitation showed that, the digestion of $OL60^{T/G}$ DNA strands was still hardly observed the absence of metal ions (Fig. 4-18E, F). In the presence of Mg^{2+}, the FAM-labelled strand of $OL60^{T/G}$ DNA was increasingly digested with the rising concentration of by *Nm*MutL and *Nm*MutS (Fig. 4-19E). Nearly 80% of the FAM-labelled strand had been cleaved by 2μM of *Nm*MutL with *Nm*MutS in the presence of Mg^{2+}. On the contrary, *Nm*MutL and *Nm*MutS did not clearly affect the TAMRA-labelled strand in the presence of Mg^{2+} (Fig. 4-14F). It implies that *Nm*MutL aided by *Nm*MutS seems to play a role in the strand discrimination in the presence of Mg^{2+}. Additionally, in the presence of Mn^{2+}, both strands of $OL60^{T/G}$ DNA were digested by *Nm*MutL and *Nm*MutS with a similar degree (Fig. 4-20E, F). The highest cleavage of both strands reached 80% with 2μM of *Nm*MutL and *Nm*MutS. Furthermore, the addition of ATP performed the strongest inhibition of *Nm*MutL nuclease activity with *Nm*MutS in the presence of Mg^{2+} (Fig. 4-19E).

Through the assays with open-end DNA duplexes, *Nm*MutL did not perform any activity without the addition of metal ions. However, in the presence of Mg^{2+},

the nuclease activity of *Nm*MutL occurred with a strand discrimination which was enhanced with the addition of *Nm*MutS. In the presence of Mn^{2+}, the activity of *Nm*MutL with *Nm*MutS was shown to a similar degree as the activity of *Nm*MutL alone. With the addition of ATP, the suppression of *Nm*MutL activity with *Nm*MutS was stronger than inhibition of *Nm*MutL activity alone in the presence of Mg^{2+} and Mn^{2+}. The strongest ATP inhibition of was observed in the presence of Mg^{2+}.

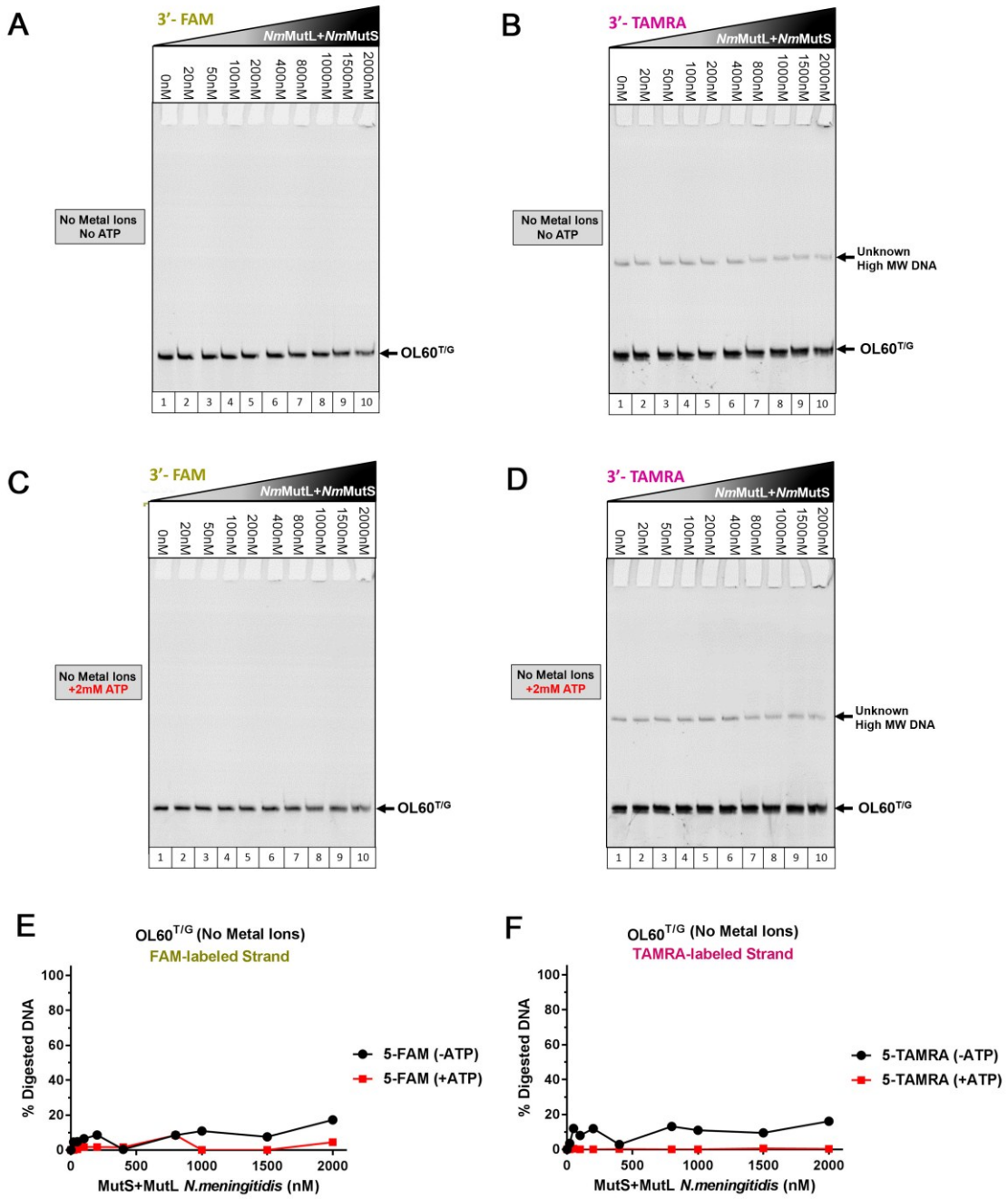


Figure 4-18. The nuclease assay of *Nm*MutL with *Nm*MutS on OL60$^{T/G}$ DNA without metal ions. (A)(B)(C)(D) Increasing concentrations of *Nm*MutL were incubated with 40nM 60-bp open-end DNA with a T/G mismatch without metal ions in the absence or presence of 2mM ATP in the nuclease buffer at 25°C for 2hrs. The results were resolved by 15% denaturing PAGE (see Materials and Methods). **(E)(F)** The data was quantitated from the 60-bp bands in denaturing PAGE gels in the panels (A)(B)(C)(D) to determine the percentage of digested DNA using Image J software and was analysed via GraphPad 7. Data of reactions in the absence of ATP was shown with black lines and markers whereas data in the presence of ATP was exhibited by red lines and markers. This assay was only conducted once.

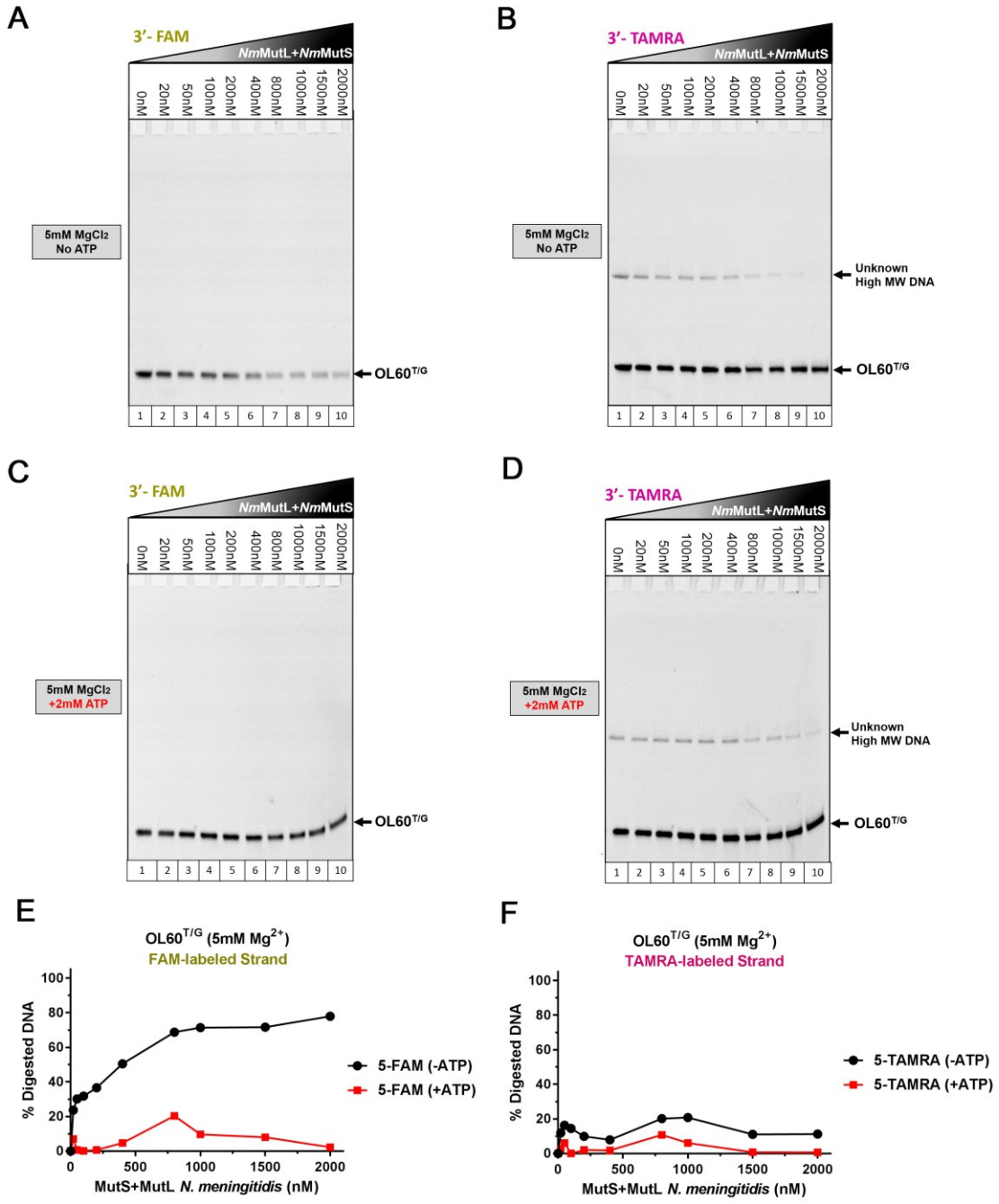


Figure 4-19. The nuclease assay of *Nm*MutL with *Nm*MutS on OL60$^{T/G}$ DNA with 5mM $MgCl_2$. (A)(B)(C)(D) Increasing concentrations of *Nm*MutL were incubated with 40nM 60-bp open-end DNA with a T/G mismatch with 5mM $MgCl_2$ in the absence or presence of 2mM ATP in the nuclease buffer at 25°C for 2hrs. The results were resolved by 15% denaturing PAGE (see Materials and Methods). **(E)(F)** The data was quantitated from the 60-bp bands in denaturing PAGE gels in the panels (A)(B)(C)(D) to determine the percentage of digested DNA using Image J software and was analysed via GraphPad 7. Data of reactions in the absence of ATP was shown with black lines and markers whereas data in the presence of ATP was exhibited by red lines and markers. This assay was only conducted once.

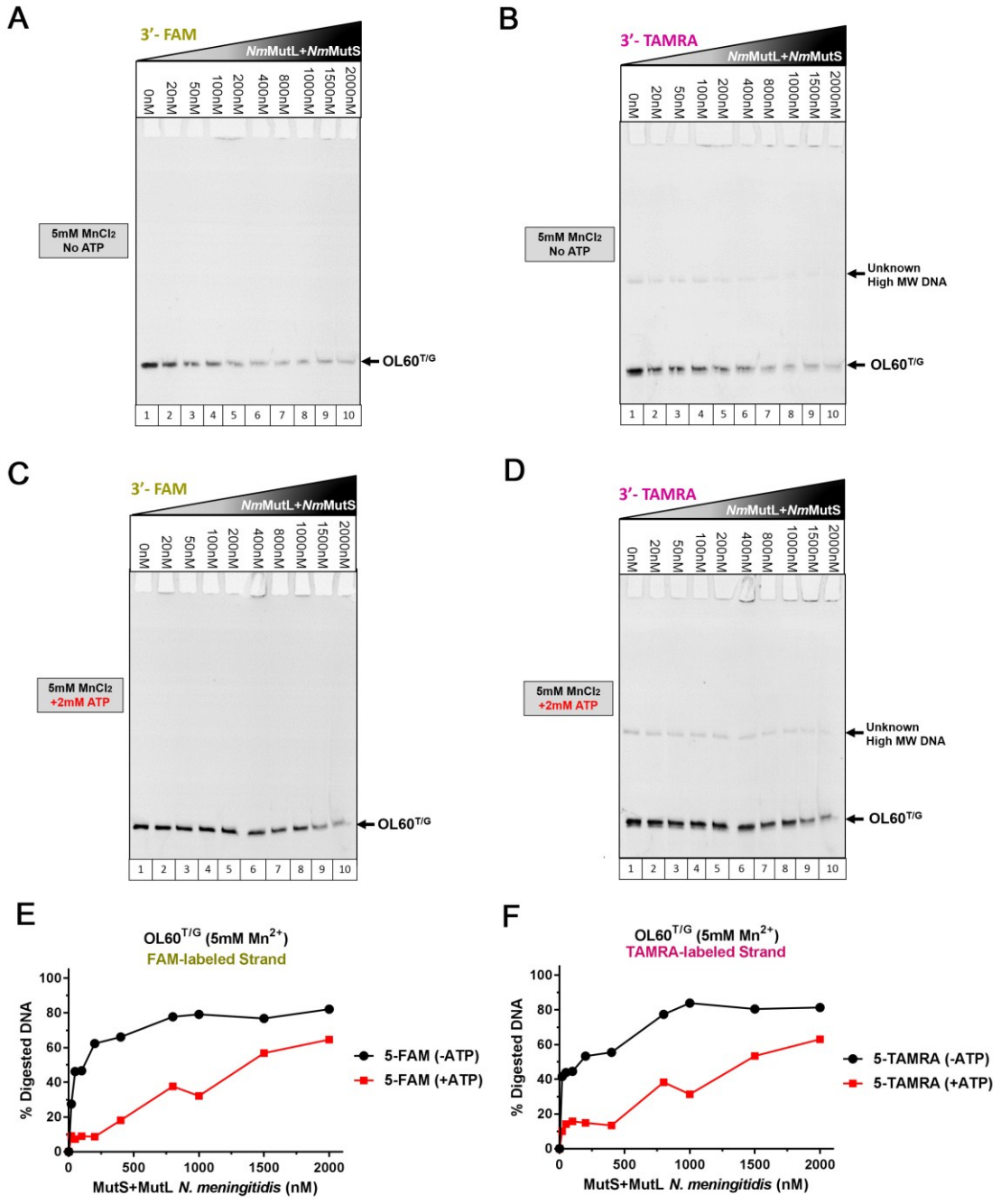


Figure 4-20. The nuclease assay of *Nm*MutL with *Nm*MutS on OL60$^{T/G}$ DNA with 5mM $MnCl_2$. (A)(B)(C)(D) Increasing concentrations of *Nm*MutL were incubated with 40nM 60-bp open-end DNA with a T/G mismatch with 5mM $MnCl_2$ in the absence or presence of 2mM ATP in the nuclease buffer at 25°C for 2hrs. The results were resolved by 15% denaturing PAGE (see Materials and Methods). **(E)(F)** The data was quantitated from the 60-bp bands in denaturing PAGE gels in the panels (A)(B)(C)(D) to determine the percentage of digested DNA using Image J software and was analysed via GraphPad 7. Data of reactions in the absence of ATP was shown with black lines and markers whereas data in the presence of ATP was exhibited by red lines and markers. This assay was only conducted once.

4.3 Discussion

4.3.1 MutL performed a Mn^{2+}-dependent nuclease activity.

In *E. coli*, MutL protein performed an intermediary function that associated with MutS to lead the strand incision by its unusual MutH endonuclease activity (Su & Modrich, 1986). However, *E. coli* MutL lacks the conserved D(M/Q)HAX_2EX_4E metal-binding motif (Fig. 4-1) and does not have intrinsic endonuclease activity (Fukui *et al.*, 2011).

In MutH-lacking organisms, MutL homologues had been reported to possess an endonuclease activity, which was dependent on the integrity of a D(M/Q)HAX_2EX_4E metal-binding motif (Kadyrova & Kadyrov, 2016). Eukaryotic MutLα is a heterodimer as MLH1-PMS2 in human hMutLα and MLH1-PMS1 in yeast yMutLα (Kadyrov *et al.*, 2006； Kadyrov *et al.*, 2007). The endonuclease activity of hMutLa and yMutLa was carried out in the presence of Mn^{2+} on supercoiled plasmid DNA (Kadyrov *et al.*, 2006; Kadyrov *et al.*, 2007). In MutH-lacking bacteria, MutL endonuclease activity is modulated by various metal ions vary from species to species. *Aa*MutL protein nicked supercoiled plasmid (no mismatch) in the presence of Co^{2+}, Ni^{2+}, Mn^{2+} or Zn^{2+} whereas did not with Mg^{2+} or Ca^{2+} (Mauris & Evans, 2009). The endonuclease activity of *Tt*MutL was performed on supercoiled plasmid with Co^{2+}, Ni^{2+} or Mn^{2+} but not in the presence of Ca^{2+}, Mg^{2+} or Zn^{2+} (Fukui *et al.*, 2008). *Bs*MutL showed its endonuclease activity on supercoiled plasmid with Mn^{2+}, but did not with Mg^{2+}, Zn^{2+} or Co^{2+} (Pillon *et al.*, 2010). Also, both *Pa*MutL and *Ng*MutL cleaved supercoiled plasmids in the presence of Mn^{2+} and Mg^{2+} (Duppatla *et al.*, 2009; Correa *et al.*, 2011).

In brief, previous studies of MutL homologues in MutH-lacking organisms were widely found to have Mn^{2+}-dependent endonuclease activity using supercoiled plasmid DNA as the substrate. The closed circular plasmid DNA is extensively

utilized to detect if a protein performs the latent endonuclease activity in *in vitro* assays. The potential endonuclease activity on DNA strands was observed via nicked products, including open-circular DNA and linear DNA. However, assays on supercoiled plasmid DNA only presented the non-specific endonuclease activity with homoduplex DNA that neither the specificity of DNA mismatch nor the mechanism of strand discrimination could be evaluated by MutL activity in the MMR system.

*Nm*MutL contains the DMHAX_2EX_4E metal-binding motif at its C-terminal domain (Fig. 4-1). In this chapter, the activity of *Nm*MutL was examined based on *in vitro* assays with 60-bp linear DNA duplexes to detect two DNA strands via different fluorescent labels. In all examinations, the strand was removed completely form the gel, rather that observing intermediate size bands. It was therefore possible that cleavages were directed from the 3'-ends, thus removing the fluorescent label directly. In the case of *A. aeolicus*, *Aa*MutL was able to fully degrade the supercoiled DNA substrate after incubation (Mauris & Evans, 2009). Therefore, 3' labelled-ends might be entirely removed by the nuclease activity of *Nm*MutL in this study. The mode of *Nm*MutL activity should be further tested using 5' labelled-DNA to evaluate if *Nm*MutL is a 3'-to-5' exonuclease or endonuclease.

In this study, in the presence of 5mM Mn^{2+}, *Nm*MutL performed the apparent digestion on both strands of 60-bp linear DNA regardless of closed or opened ends. Moreover, the results revealed Mn^{2+}-dependent nuclease activity of *Nm*MutL presented a weakly sequence specificity of the T/G mismatch. 2μM of *Nm*MutL carried out about 30% stronger cleavage on the FAM-labelled strand of $BL60^{T/G}$ than the FAM-labelled strand of $BL60^{C/G}$ in the presence of Mn^{2+}(Fig. 4-21). Evidently, the specificity of the T/G mismatch of *Nm*MutL nuclease activity was too weak to challenge the previous conclusion that MutL

endonuclease activity had no sequence-context preferences with Mn^{2+} in MutH-lacking organisms (Fukui *et al.*, 2008; Duppatla *et al.*, 2009; Kadyrov *et al.*, 2007). On the other hand, both strands of mismatched linear DNA were digested with the similar high degree by *Nm*MutL alone in the presence of $MnCl_2$ (Fig. 4-21). Therefore, it is not clear if Mn^{2+}-dependence nuclease activity of *Nm*MutL contributes to strand discrimination so far.

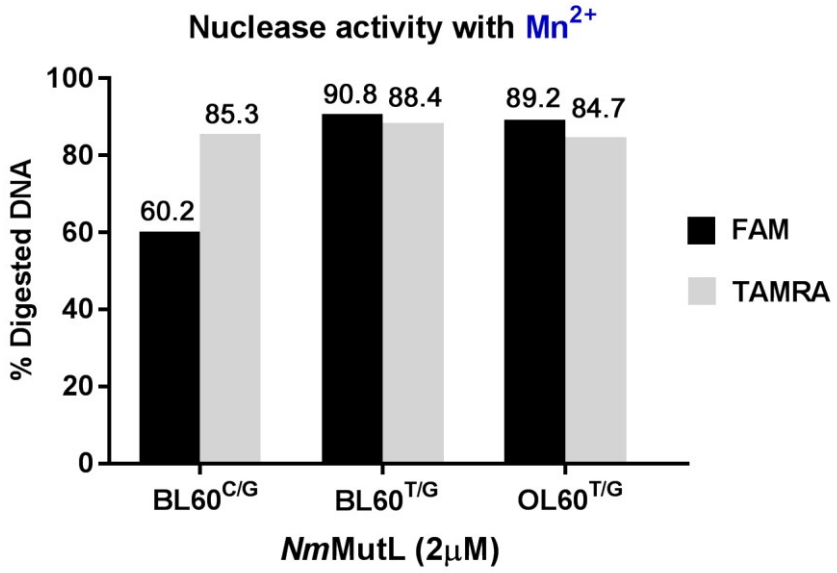


Figure 4-21. MutL nuclease activity on 60-bp linear DNA (- ATP)
The data was quantitated from denaturing PAGE gels in Figure 58C, 60C, and 66C to determine the percentage of digested DNA using Image J software and was analysed via GraphPad Prism 7.

4.3.2 Strand-discriminated nuclease activity of *Nm*MutL in the presence of Mg^{2+}

In previous studies, the nonspecific endonuclease activity of MutL on supercoiled plasmid was also carried out in the presence of Mg^{2+} in *P. aeruginosa* and *N. gonorrhoeae* (Duppatla *et al.*, 2009; Correa *et al.*, 2011). The mismatch repair system from *N. gonorrhoeae* had been identified with the genes which also existed in the genome of *N. meningitidis* MC58. Duppatla *et al.* revealed that *Ng*MutL was able to nick the supercoiled plasmid DNA and to

produce open circular and linear DNA with Mg^{2+}. Therefore, it was necessary to examine the activity of *Neisserial* MutL in the MMR system.

In this study, in the presence of Mg^{2+}, *Nm*MutL did not possess detectable nuclease activity on blocked-end linear DNAs, both without the mismatch or with a T/G mismatch. However, *Nm*MutL performed weak nuclease activities on $OL60^{T/G}$ DNA with Mg^{2+}. It is also worthwhile to notice that this mismatch-dependent nuclease activity of *Nm*MutL only worked on one strand of mismatched DNA, but the other oligonucleotide strand had been kept without cleavage in the presence of Mg^{2+} (Fig. 4-22). 57.1% of the FAM-labelled strand was cleaved, but the digestion of the TAMRA-labelled strand was only carried out about 20.7% after the incubation with 2μM *Nm*MutL in the presence of Mg^{2+}. Once the divalent manganese ions were removed or substituted by Mn^{2+}, the nuclease activity with the strand bias of *Nm*MutL could not be detected. It implies that divalent magnesium cations possibly contribute the process of strand discrimination for MMR. Therefore, the latent mechanism of strand discrimination in *Neisserial* mismatch repair seems to be related to *Nm*MutL activity.

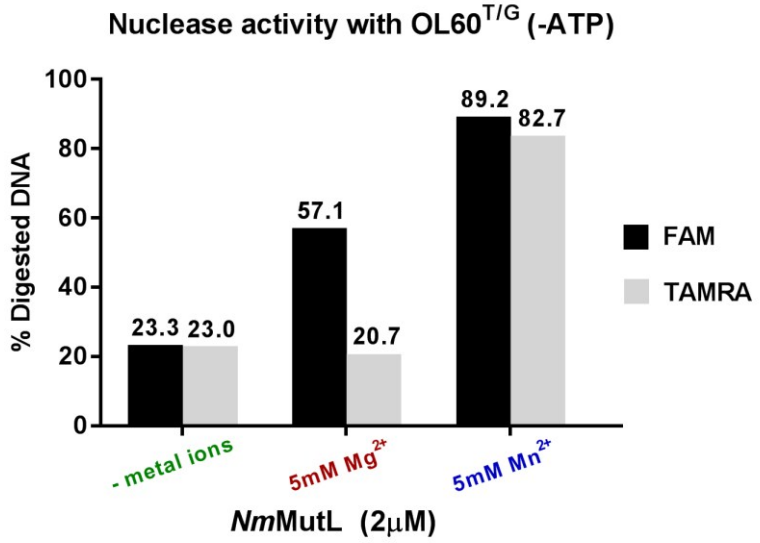


Figure 4-22. *Nm*MutL nuclease activity on $OL60^{T/G}$ DNA (-ATP)

The data was quantitated from denaturing PAGE gels in Figure 66 to determine the percentage of digested DNA using Image J software and was analysed via GraphPad Prism 7.

On the other hand, due to the limitation from the structure of 60-bp linear DNA probe, it only provided a relatively simple structure with a T/G mispairing signal to *Nm*MutL nuclease activity with Mg^{2+}. However, there is no available feature on DNA substrate for *Nm*MutL to discriminate which strand is the parental strand or the daughter strand.

In vitro study of human MMR system, mismatch-dependent hMutLα endonuclease activity performed with the addition of ATP and Mg^{2+} and other MMR proteins on the phage circular DNA containing a 150-bp single strand break nearby the mismatch (Kadyrov *et al.*, 2006). The structure of DNA in this study simulated the discontinuously synthesized lagging strand which had the gap between Okazaki fragments on the daughter strand during DNA replication. Moreover, mismatch-dependent hMutLα endonuclease activity was not found with the closed circular DNA *(*Kadyrov *et al.*, 2006). Although DNA mismatch repair occurred less efficiently on the leading strand than on the lagging strand (Pavlov, Mian & Kunkel, 2003), the latent mechanism of strand discrimination on the leading strand is still unknown in all MutH-lacking organisms.

Therefore, to establish the mechanism of strand discrimination of the template strand and the daughter strand, different DNA substrates with varied mismatch types including insertion-deletion loops should be introduced in a further study. In MutH-lacking bacterial species, mismatch-dependent MutL nuclease activity with Mg^{2+} was only found in *N. meningitidis* so far. More extensive assays of MutL homologues should be carried out in various organisms to demonstrate this hypothesis in future.

4.3.3 *Nm*MutL nuclease activity was inhibited by ATP

*Ec*MutL and other MutL homologues contain a conserved GHKL domain (the abbreviation of Gyrase, Hsp90, Histidine Kinase and MutL) (Dutta & Inouye, 2000), which have been reported that have low rates of ATP hydrolysis (Spampinato & Modrich, 2000). In *E. coli,* MutL ATPase activity occurred to be important for the MMR system. MutH endonuclease activity was stimulated by the hydrolysis of ATP, which was catalysed by *Ec*MutL (Larrea, Lujan & Kunkel, 2010). At the N-terminal domain of *Ec*MutL, DNA fragment encompasses all the conserved residues of MutL family (Ban, Junop & Yang, 1999). The ATP-binding site of *Ec*MutL overlaps with the conserved residues at the N-terminal domain throughout the MutL family (Ban, Junop & Yang, 1999).

In eukaryotes, MutLα subunits are involved in the binding and the hydrolysis of ATP, which introduced the changes of protein conformation (Tran & Liskay, 2000; Sacho *et al.*, 2008). In human, the important amino acid residues of ATP-binding / ATP-hydrolysis were reported in studies of human MMR system. The key residues of ATP-binding are the N45 and D70 in subunit PMS2 of hMutLα, and are the N38 and D63 in subunit MLH1 of hMutLα (Ban & Yang, 1998; Ban, Junop & Yang, 1999; Räschle *et al.*, 2002; Tomer *et al.*, 2002). These residues in two MutLα subunits are functional similar with each other (Tomer *et al.*, 2002). Furthermore, the residues which catalyse ATP-hydrolysis for hMutLα subunits PMS2 and MLH1 are the E42 and E34 (Ban & Yang, 1998; Ban, Junop & Yang, 1999; Räschle *et al.*, 2002; Tomer *et al.*, 2002). Mutational studies found that the replacement of ATP-hydrolysis related residues in both PMS2 and MLH1 caused the inhibition of mismatch-dependent endonuclease activity of hMutLα (Räschle *et al.*, 2002). Importantly, these essential amino acid residues has been found at the N-terminal domain of other MutH-lacking bacteria including *N. meningitidis* (Fig. 4-23).



Figure 4-23. Sequence alignments of part of N-terminal domain of MutL homologues

Alignment of ATP-binding / ATP-hydrolysis residues was performed using ClustalW. The residues of ATP-binding were highlighted with red shadow. The residue of ATP-hydrolysis was highlighted with black shadow. The NCBI GI number are as follows: 4505913 (hMutLα), 46562124 (yMutLα), 499183481 (*Aa*MutL), 730578203 (*Nm*MutL), 998401886 (*Ng*MutL), 970333247 (*Pa*MutL), 16078768 (*Bs*MutL), 55981292 (*Tt*MutL), and 269852789 (*Ec*MutL)

In this study, the DNA binding of *Nm*MutL was slightly enhanced by ATP in the gel shifit assay. However, the nuclease activity of *Nm*MutL was inhibited by the addition of ATP on both homoduplex DNA and DNA with a T/G mismatch in the absence of metal ions or in the presence of Mg^{2+} or Mn^{2+}. Different effects of the addition of ATP on *Nm*MutL DNA-dependent activitys might be caused by the ATP-hydrolysis. It implies that ATP could be involved in the coordination of *Nm*MutL activity. ATP inhibition was also observed in studies of MutL homologues in *P. aeruginosa, N. gonorrhoeae* and *T. thermophiles*. The addition of ATP suppressed the nonspecific endonuclease activity of *PaMutL, Ng*MutL, and *Tt*MutL on supercoiled plasmid (Fukui *et al.*, 2008; Duppatla *et al.*, 2009; Correa *et al.*, 2001).

However, endonuclease activity of *Bs*MutL was stimulated by 0.5mM ATP but was inhibited by 5mM ATP which was considered by excess chelating metal ions away. Moreover, the promoting effect of ATP was reported in *Aa*MutL endonuclease activity at high concentration of *Aa*MutL (Mauris & Evans, 2009). But *Aa*MutL endonuclease activity was inhibited at low concentrations of *Aa*MutL (Mauris & Evans, 2009). Furthermore, the mismatch-dependent activity of human MutL*α* required the activation from 2mM ATP. Meanwhile, the Mn^{2+}-

dependent endonuclease activity of hMutL*α* and yMutL*α* were activated with the addition of 0.5mM ATP (Kadyrov *et al.*, 2006, Kadyrov *et al.*, 2007; Shimada *et al.*, 2013). In brief, the addition of ATP played a diametrically opposite role in MutL activity in different organisms.

As describe above, the ATPase motif is at the N-teriminal domain of MutL family whereas the metal binding motif is at the C-terminal domain (Fukui *et al.*, 2011). In *N. gonorrhoeae,* the protein only containing the C-terminal domain of *Ng*MutL performed similar endonuclease activity with the full-length *Ng*MutL, but its activity was not affected by adding ATP (Duppatla *et al.*, 2009). In *A. aeolicus,* one notion of the interdomain interaction between two domains was predicted and verified using the recombinant two terminal domains of *Aa*MutL (Iion *et al.*, 2011). *Aa*MutL C-terminal domain performed the endonuclease activity and was activated by it N-terminal domain with zinc ions (Iion *et al.*, 2011). Consequently, it would be necessary to understand whether interdomain interaction happens in *Nm*MutL and what the basic role of each domain of *Nm*MutL during its nuclease activity.

Meanwhile, in previous studies, it was reported that AMPPNP, which is a non-hydrolysable ATP analogue, provoked *Aa*MutL endonuclease activity with high concentrations of *Aa*MutL (Mauris & Evans, 2009). However, in *B. subtilis,* the endonuclease activity of *Bs*MutL was not activated with the addition of AMPPNP under the identical conditions which used in the study of *Aa*MutL (Pillon, *et al.*, 2010). Therefore, it is also necessary to verify if ATP-binding or ATP-hydrolysis is essential for modulating MutL endonuclease activity. Further experiments could be designed to precisely determine the role of the cofactor in the *Neisserial* system, for instance preferring assays with ADP or ADPPNP.

4.3.4 The effect of *Nm*MutS on *Nm*MutL activity

In this study, *Nm*MutS protein was incubated with *Nm*MutL in nuclease assays, to investigate the effect of *Nm*MutS on *Nm*MutL activity. Without *Nm*MutL, *Nm*MutS showed no detectable activity on either blocked- and open-end 60-bp linear DNA in denaturing PAGE (data not shown). In assays on the homoduplex DNA, *Nm*MutS performed no detectable effect on the activity of *Nm*MutL in the absence of metal ions or in the presence of Mg^{2+} or Mn^{2+}. However, *Nm*MutS seemed to stimulate *Nm*MutL nuclease activity with a T/G mismatch on both strands of $BL60^{T/G}$ DNA (Fig. 4-24). This presumptive aiding function from *Nm*MutS to *Nm*MutL nuclease activity was not shown in the presence of metal ions on blocked-end DNA. There is no evidence to reveal that the presence of Mn^{2+} or Mg^{2+} enhances the roles of *Nm*MutS.

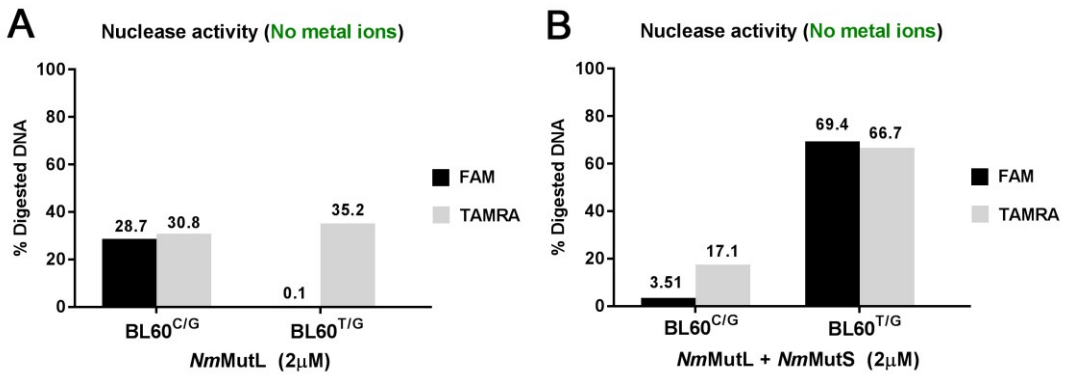


Figure 4-24. Nuclease activity of *Nm*MutL and *Nm*MutS on $BL60^{C/G}$ and $BL60^{T/G}$
The data was quantitated from denaturing PAGE gels in Figure 58A, 60A, 62A and 64A to determine the percentage of digested DNA using Image J software and was analysed via GraphPad Prism 7.

We also examined whether the addition of ATP affects the nuclease activity of various concentrations of *Nm*MutL in the presence *Nm*MutS. While ATP was found to be inhibitory, the nuclease activity of *Nm*MutL with *Nm*MutS showed weakly stronger ATP inhibition than the activity of *Nm*MutL only. It is hardly to

conclude if the requirement of ATP hydrolysis from *Nm*MutS could activate the nuclease activity of *Nm*MutL. These results are inconsistent with studies of other MutL homologues activity in other organisms (Kadyrov *et al.*, 2006; Shimada *et al.*, 2013). In human, the mismatch-dependent endonuclease activity of hMutLα was stimulated by MutS homologue MutSα and other MMR proteins in the presence of Mg^{2+} and ATP. In *T. thermophilus*, *Tt*MutL mismatch-dependent endonuclease activity was required the activation form *Tt*MutS and the addition of Mn^{2+} and ATP (Shimada *et al.*, 2013). Nevertheless, it is still too far to conclude the difference between *Neisserial* MMR system and that in other organisms.

Furthermore, in this study, the Mg^{2+}-dependent nuclease activities of *Nm*MutL was weakened in the absence of *Nm*MutS on open-end mismatched DNA substrates. The result showed that *Nm*MutS enhanced the strand-discriminated nuclease activity of *Nm*MutL on the open-end mismatched DNA with Mg^{2+} (Fig. 4-25). It implies that the interaction between *Nm*MutS and *Nm*MutL may promote the strand discrimination on mismatched DNA. It raised a hypothesis that *Nm*MutS and *Nm*MutL may correlate with a mechanism of stand discrimination.

In *E. coli* mismatch repair system, strand discrimination was performed by MutH endonuclease to recognize the hemimethylated GATC site (Modrich, 1989). Therefore, MutS from *E. coli* was not required to determine strand discrimination. However, in many MutH-lacking organisms, MutS might transmit the signal of strand discrimination to MutL. Evidently, as discussed above, in human MMR system, the presence of magnesium ions is crucial for strand discrimination on circular DNA containing a 150-bp single strand break nearby the mismatch. In this study, during the nuclease assay of the combination of *Nm*MutS and *Nm*MutL, the open ends of DNA might be recognised as the pre-

existing excisions, thereby stimulating the nuclease activity. To the contrary, on the blocked-end DNA, the relative closed structure of DNA might prevent the signal of strand discrimination. These results implie that strand discrimination of *Neisserial* MMR might occur in the presence of Mg^{2+}.

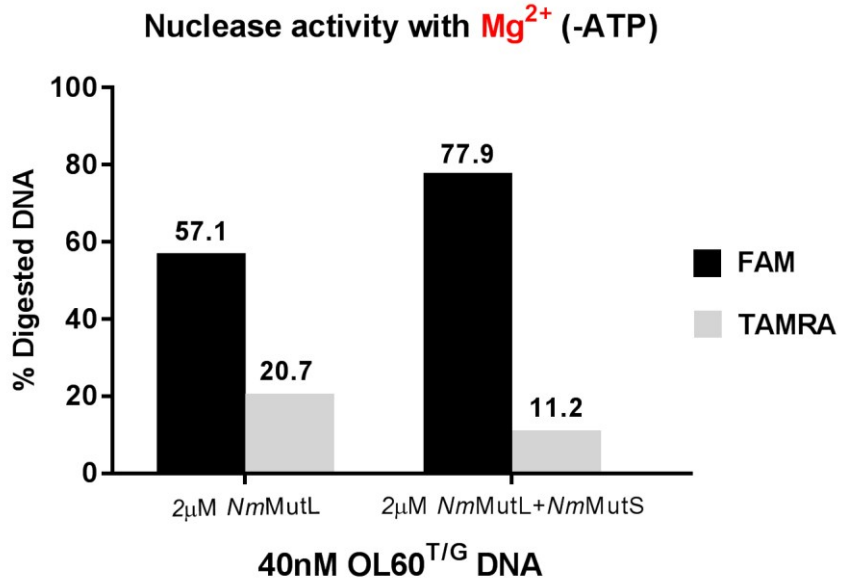


Figure 4-25. Nuclease activity of *Nm*MutL and *Nm*MutS on $OL60^{T/G}$
The data was quantitated from denaturing PAGE gels in Figure 66B and 68B to determine the percentage of digested DNA using Image J software and was analysed via GraphPad Prism 7.

Beyond the interaction with MutS, MutL has also been shown to be able to interact with the β-clamp in *B. Subtilis* (Pillon, *et al.*, 2011) and in *E. coli* (de Saro *et al.*, 2006) and the clamp loader in *E. coli* (Li *et al.*, 2008). Kadyrov *et al.* reported that, in human, hMutLα performed endonuclease activity to nick DNA with a pre-existing mismatch and MMR proteins including MutSα, PCNA as the β-clamp, the clamp loader homologue RFC, and in the presence of ATP and Mg^{2+} (Kadyrov *et al.*, 2006). Furthermore, the endonuclease activity of yeast homologs of MutL has been shown to be enhanced by the presence of PCNA (Kadyrov *et al.*, 2007). These results suggested that other MMR proteins could also participate the activity of MutL and even the mechanism of the strand discrimination. Consequently, further study of the strand discrimination should

be carried out in coordination with DNA replication machinery from *N. meningitidis* which had been successfully prepared in this study. Meanwhile, more repetitive experiments would be performed to reduce errors of results from experimental operation as far as possible.

Chapter 5

Conclusion & Future work

5.1 Conclusion

In this study, the expression and purification of active components of DNA Pol III HE, TEV protease, MutS and MutL proteins from *N. meningitidis (Nm*MutS and *Nm*MutL*)* and MutS from *E. coli* (*Ec*MutS) were achieved in good yield. *Neisserial* DNA Pol III complex was reconstituted from individual subunits *in vitro* which was compatible with the assembly protocol of *E. coli* DNA Pol III HE with a similar functional stoichiometry. The function of *Neisserial* DNA Pol III HE was examined by the extension of primed ssDNA substrates.

The mismatch recognition activity of *Nm*MutS was proved via specifically binding the T/G mismatch in the gel shift assay. However, it presented a very weak binding with low affinity compared to the gel shift assay carried out with *EcMutS* under the same conditions. This implied that *Nm*MutS might require other MMR proteins to assist its mismatch recognition activity. *Nm*MutL nonspecifically bound to DNA with or without mismatch. It partially verified similar results from other studies with MutL protein from other bacterial species where non-specific DNA binding was observed (Fukui *et al.*, 2008; Duppatla *et al.*, 2009). The combination of *Nm*MutS and *Nm*MutL also non-specifically bound to DNA. There was no evidence to prove that *Nm*MutL could help the mismatch binding of *Nm*MutS.

Through *in vitro* assays on fluorescent labelled linear DNA, nuclease activity of *Nm*MutL was detect with several cofactors including ATP, metal ions (Negative, Mg^{2+} and Mn^{2+}), DNA specificity (T/G mismatched or non-mismatched; blocked-ends or open-ends), *Nm*MutS and strand discrimination. The results revealed that *Nm*MutL had inherent nuclease activity in the presence of Mn^{2+}, although this cofactor appeared to reduce mismatch specificity. *Nm*MutL could specifically digest mismatched DNA aided by *Nm*MutS in the absence of metal ions. In addition, *Nm*MutL seems to present a random strand preference for

digesting one of mismatched DNA strands in the presence of Mg^{2+}. It suggests that the nuclease activity of *Nm*MutL could be related to strand discrimination in MMR. Nevertheless, the results of nuclease activities can be used to deduce whether *Nm*MutL is an endonuclease or exonuclease due to the limitation of the DNA substrate. All in all, to precisely establish the mechanism of mismatch recognition and strand discrimination of MMR in *N. meningitidis,* further functional studies are required to be carried out *in vitro* and even *in vivo.*

5.2 Future work

There are a number of questions to be clarified in the future work. Firstly, how is the mismatch dependency of MMR system in *N. meningitidis*? This work has carried out mismatch recognition with a typical "T/G" mismatch by *Nm*MutS and *Nm*MutL via gel shift assays. However, there are 8 possible base mis-pairings in all. In *E. coli*, MMR system is reported that is poor at correcting "C/C" base pair mismatches (Minnick & Kunkel, 1996). Gel shift assays should be used to further examine the dependency on different mismatched DNA templates. Using differing templates will allow the exploration of whether the identity of the mismatch has a significant effect on the efficiency of MMR. Furthermore, homopolymeric repeats are implicated in the phase variation capability of *N. meningitidis*. The assay with homopolymers will allow exploration of their correction with quantitative output. In the same way, design of the *in vitro* DNA template gives free reign to explore frameshifts and bubbles and their correction by MMR system.

Secondly, as discussed earlier, MMR proteins MutS and MutL from either prokaryotes or eukaryotes have been found to interact with the β–clamp of the DNA replication machinery (PCNA in eukaryotes) and with several subunits of the clamp loader complex. Interactions between the β-clamp and MutS and MutL have been shown to be crucial for competent MMR. Therefore, a series

of questions are raised. What is the minimum system requirement for *Neisserial* MMR up to the point of mismatch excision? Is DNA Pol III required to direct strand discrimination? Is the β-clamp required? The specific activity of MutS and MutL should be assayed in the presence of specific components of the system. By further studying this MMR system *in vitro*, the roles of individual component parts of the system will be assayed for their requirement. As well as examining the role of individual elements of the MMR mechanism, the further assays will allow exploration of the molecular mechanism of phase variation in *N. meningitidis* by choosing DNA templates with have a foundation in phase variation biology.

Furthermore, although the gel shift assay is extensively used to detect the interaction between proteins and DNA substrates, the equilibrium between free DNA and protein-DNA complexes can be compromised by various factors during PAGE, such as local pH, temperature and salt concentration of the gel electrophoresis buffer. Fluorescence anisotropy is used to probe the fluorophore's rotational mobility under highly mimic *in vivo* conditions, hence not only providing accurate information of molecular shape and weight, but also offering its viscosity with the fluorescent background. Therefore, fluorescence anisotropy could be used to detect the changes of polymers and other molecules in molecular weights when the interaction happens. This method is also highly desirable for examining protein-DNA interactions as a supplement for the gel shift assay.

Moreover, several key motifs in MutL and MutS have been identified as important for MMR *in vivo*. Mutation of these residues will allow their effect to be studied *in vitro*. These motifs include the MutL C-terminus and MutS β-clamp interacting motifs. Additionally, mutation of the metal binding domains in MutL would allow the nuclease activity of MutL to be further explored. A combination

of the functional assay, *Nm*MutL activity assay and gel shift assays would be used to explore how mutation of key residues affects the function of *Nm*MutS and *Nm*MutL. Relative time courses can be performed to compare fitness of mutants and fitness of the system when lacking components. Hydrolysable, slowly hydrolysable and non-hydrolysable analogues of ATP and ADP are also necessary to examine the dependency of the system on the nucleotide hydrolysis state of *Nm*MutS and *Nm*MutL. These experiments may rely on the presence of or absence of nucleotide hydrolysis in DNA Pol III HE in *N. meningitidis.*

Chapter 6

Materials & methods

6.1 General materials

This section describes general materials used for molecular and cellular biology applications.

6.1.1 Chemicals and enzymes

Chemicals were supplied from Sigma-Aldrich (Dorset, UK). Plasmid-Safe™ ATP-Dependent DNase was from Epicentre (Madison, USA). All remaining commercial enzymes were supplied from New England Biolabs (NEB) (Hitchin, UK).

6.1.2 Media

Medium	Composition
LB (Luria Bertani Broth)	10 g/L Bacto-Typtone, 5 g/L Bacto-Yeast Extract, 10 g/L NaCl
LB agar	10 g/L Bacto-Typtone, 5 g/L Bacto-Yeast Extract, 10 g/L NaCl, 15 g/L Agar
2X YT Media	16 g/L Bacto-Typtone, 5 g/L Bacto-Yeast Extract, 5 g/L NaCl

Table 6-1. Compositions of media

Media and plates were prepared as described in Table 6-1 and were sterilized by autoclave.

6.1.3 Antibiotics

Antibiotic solutions were added into sterilized LB media for plasmid based selection at appropriate concentrations above. Antibiotics were filter-sterilized and stored at -20°C before use.

Antibiotics	Stock Concentration	Working Concentration
Ampicillin	100 mg/mL	100 μg/mL
Kanamycin	50 mg/mL	50 μg/mL

Table 6-2. Antibiotics' stock and working concentrations

6.1.4 Kits

Kit	Supplier	Use
E.Z.N.A.® Plasmid Mini Kit I, V(capped) Spin	Omega bio-tek	Isolation of plasmid DNA.
E.Z.N.A.® Gel Extraction Kit , Q-Spin	Omega bio-tek	Purification of PCR products.
Qubit®Protein Assay Kit	Thermo Scientific	Quantification of protein
Qubit®ssDNA Assay Kit	Thermo Scientific	Quantification of ssDNA
Qubit®dsDNA BR Assay Kit	Thermo Scientific	Quantification of dsDNA

Table 6-3. Summary of commercial kits

6.1.5 Bacterial strains

E. coli K12 strain DH5a, which genotype is [*fhuA2 Δ(argF-lacZ)U169 phoA glnV44 Φ80 Δ(lacZ)M15 gyrA96 recA1 relA1 endA1 thi-1 hsdR17*], was the cloning strain and was supplied from New England BioLabs. *E. coli* BL21

Rosetta (DE3) pRARE strain, which genotype is (F- *ompT- lon- dcm λ(DE3)[lacI, lacUV5-T7gene 1, ind1, sam7, nin5] pRARE [camr proL leuW argW glyT argU ilex])* was used for protein expression and was purchased from Novagen (Nottingham, UK).

6.1.5.1 Preparation of $CaCl_2$ chemically competent cells

The bacterial single colony was inoculated and incubated in 10ml of LB media containing 100 μg ml^{-1}. The start cell culture was incubated at 37˚C for overnight. The saturated culture was then added into 100ml of antibiotic free LB media in a 250ml flask. The flask containing cells was shaked in the incubator at 37˚C till OD_{600}= 0.2. Subsequently, aftering transfering into a sterile 50ml Falcon tube, the culture was chilled on ice for 20 minutes, and was then centrifuged (10 minutes, 4,000 rpm, 4˚C). After discarding the supernatant, the resuspension of the cell pellet was carried out in 10ml of pre-chilled sterile 50mM $CaCl_2$ (15% glycerol). Further incubation on ice was last about 30 minutes. Centrifuging of the cell culture and discarding of the supernatant were repeated once as before. Competent cells were split to 50μL aliquots in sterile eppendolfs and stored at -80˚C for use.

6.1.6 Plasmids

Plasmid	Resistance	Encode
pPROEX-HTb	Ampicillin	Multiple cloning site (MCS) under control of *trc* promoter
pETM43	Kanamycin	MCS under control of *T7* promoter

Table 6-4. Summary of DNA plasmids used in this study

pPROEX-HTb plasmid was supplied by Dr. Jan Silhan. pETM43 plasmid was supplied by Dr. Marko Storch.

6.2 Molecular and cellular methods

6.2.1 Plasmid DNA isolation

In this study, plasmid DNA was purified using the Plasmid Mini Kit I (Omega Bio-tek). 5ml of cell culture with relavant antibiotics was grown at 37°C for overnight. Cells were pelleted via centrifuging at 1,000 rpm at room temperature (RT). Then, the cell pellet was lysed and neutralized by a series of alkaline lysis solutions. After centrifuging (10min, 13k rpm, RT), plasmid DNA was extracted from the supernatant and transferred into the anion exchange column (Omega Bio-tek). Plasmid DNA was spinned on the membrane of the column (1min, 13k rpm, RT). The salt solution was then added into the column to wash out other impurities. Finally, plasmid DNA was eluted with the sufficient yield with 30~50 μL of sterile water and further (2min, 13k rpm, RT). The concentration of plasmid DNA was monitored by NanoDrop 1000 Spectrophotometer (Thermo Scientific).

6.2.2 Polymerase chain reaction (PCR)

General PCRs were carried out with 1 μl of 10-fold dilution of plasmid DNA (approximately 100ng) and specific primers with Phusion® DNA Polymerase system (NEB, UK) containing Phusion DNA polymerase, 10 x HF Buffer, DMSO and dNTPs in 0.2 ml PCR tubes (STARLAB international GmbH, Hamburg, Germany). A gradient PCR were run as described in Table 6-5 following the PCR conditions given in Table 6-6 to screen the optimum annealing temperatures. PCR products were examed using agarose gel electrophoresis (Section 6.2.4).

Full-scale PCRs were conducted as described in Table 6-5 following the PCR conditions in Table 6-6 to yield a large volume of product. The selection of the annealing temperature for full-scale PCR depended on the result of gradient

PCR which had the clear band with a strong signal at the correct size. The correct band of full scale PCR products were purified using agarose gel electrophoresis (Section 6.2.3) and gel extraction (Section 6.2.4).

Reagent	Gradient PCR	Full-scale PCR
Milli-Q H_2O	60 µl	60 µl
5 x HF buffer	20 µl	20 µl
10mM dNTPs	2 µl	2 µl
Forward Primer (10µM)	5 µl	5 µl
Reverse Primer (10µM)	5 µl	5 µl
DMSO (100%)	3 µl	3 µl
Template DNA (100 ng/µl)	4 µl	4 µl
Phusion polymerase (2U/µl)	1 µl	1 µl
Final	10 x 10 µl	2 x 50 µl

Table 6-5. PCR Reaction system

Step	Temperature	Time	Cycle
Initial Denaturing	98°C	3 minutes	1x
Denaturing	98°C	10 seconds	25x
Annealing	Gradient 65°C ± 8°C	30 seconds	
Elongation	72°C	30 seconds	
Final elongation	72°C	10 minutes	1x
Storage	4°C	Forever	

Table 6-6. PCR conditions

6.2.3 Agarose gel electrophoresis

In this study, agarose gels were prepared in the concentration of 0.8~2.0% (w/v) dependent on the molecular weight of DNA fragments. Agarose were dissolved in 1 X TBE solution (Invitrogen^{TM}, UK) by heating in the microwave. After pouring the thoroughly dissolved gel solution into the gel caster, a gel comb was plugged into the unsolid solution. The agarose gel was solidified at RT for 30 minutes. Gel electrophoresis was run in 1 X TBE solution for 60-100 minutes at 90 volts. DNA samples were mixed with 1 X SYBER Green I (Bio-Rad, USA) and 1 x DNA Loading Dye [5% (v/v) glycerol, 0.05% (w/v) bromophenol blue, 0.05% (w/v) xylene cyanol FF] prior to loading in agarose gel wells. Agarose gels were imaged by a Fuji LAS-4000 Cooled CCD Camera Gel Documentation System (FujiFilm, Japan). Molecular weights of DNA fragments were compared to 1kb DNA ladder or Low Molecular Weight DNA Ladder (NEB, UK).

6.2.4 Gel extraction of PCR products

Gel extraction of PCR products was carried out by E.Z.N.A.® Gel Extraction Kit, Q-Spin (Omega bio-tek, USA). DNA bands were excised from the agarose gel. The gel slices containing the target fragments were incubated and melted in the binding buffer at 60°C for 10 minutes. The lysate was transfered and bound to the ion exchange column using centrifugation at 13,000 rpm for 1 minute at the RT. Salt solution was added into the column and then centrifuged 13,000 rpm for 1 minute at the RT to clean off impurities. Finally, 30-50 µl of Milli-Q H_2O was loading onto the central of th column membrane and then centrifuged 13,000 rpm for 2 minutes at the RT to elute purified DNA. The concentration of plasmid DNA was monitored by NanoDrop 1000 Spectrophotometer (Thermo Scientific).

6.2.5. Restriction enzyme digestion of DNA

The insertion DNA and the backbone DNA from the vector were prepared as Section 6.2.4 were subjected to 10 μl of double digest reactions by specific restriction enzymes (NEB) (Table 6-7). Digestions were performed at appropriate temperature for 2 hours. Restriction enzymes were inactivated by heating at the specific temperature. The digestion product of backbone DNA was assessed and purified using agarose gel electrophoresis (Section 6.2.3) and gel extraction (Section 6.2.4).

Reagent	Volumes	Reagent	Volumes
Insertion DNA	100 ng	**Backbone DNA**	1 μg
Restriction Enzyme 1	1 μl	**Restriction Enzyme 1**	1 μl
Restriction Enzyme 2	1 μl	**Restriction Enzyme 2**	1 μl
1 mg/ml BSA	1 μl	**1 mg/ml BSA**	1 μl
Milli-Q H_2O	To 10μl	**Milli-Q H_2O**	To 10μl

Table 6-7. Double digestion of DNA by restriction enzymes

6.2.6 Ligation of DNA

Reagent	Volumes
T4 DNA Ligase	100 ng
10 x T4 Ligation Buffer	1 μl
Backbone DNA	X μl
Insertion DNA	Y μl
Milli-Q H_2O	To 10μl

Table 6-8. Ligation system

Digested dsDNA had 3' or 5' overhanging ends by restriction enzymes as described above. Overhanging ends of the insertion DNA were engaged with the corresponding overhangings of the backbone DNA by nucleic acid base pairing using T4 DNA ligation system (NEB, USA) (Table 6-8). The 10μl ligation reaction was performed at 4 °C overnight. The molar ratio of insert to backbone was 9:1. Finally the ligation product was transformed into *E. coli* DH5α cells (see Section 6.2.7).

6.2.7 Transformation of competent cells

Approximately 100 ng of ligation product was added to 50μl of deforested competent DH5α cells and incubated on ice for 20 minutes. The cells containing plasmid DNA were then heated at 42°C for 45 seconds and further incubated on ice for 20 minutes. The cells were recovered in 1ml of sterile antibiotic-free LB medium and further incubated with shaking at 37°C for 1 hour and then centrifuged at 4,000 rpm for 1 minute at RT. After discarding the supernatant, the cell pellet was resuspended in 100μl sterile LB media, spread on an LB agar-plate containing appropriate antibiotics and grown at 37°C overnight. Three single colonies were restreaked onto antibiotic containing agar plates.

6.2.8 Storage of cell strains

A single colony of the cell strain containing the plasmid DNA was inoculated in 3 ml of LB media containing the appropriate antibiotic and incubated at 37°C overnight. 500 μl of overnight grown cell culture was added with 500 μl of 80% autoclaved glycerol solution and mixed thoroughly in a sterile 1.5 ml tube (Starlab, Germany) to make a 40% (v/v) cell glycerol stock. The glycerol stock was stored at -80°C for further use.

6.2.9 Detection of target genes

The cell strain containing the plasmid DNA was inoculated in 5 ml of LB media containing the appropriate antibiotic and incubated at 37°C overnight. Plasmid DNA was prepared using E.Z.N.A.® Plasmid Mini Kit I (Omega Bio-tek) as described in Section 6.2.1. Purified plasmid DNA was used for insertion DNA using small-scale PCR (Section 6.2.2) and visualised by agarose gel electrophoresis (Section 6.2.3). One of plasmid DNAs which obtained the correct size bands were sent for sequencing services (Supplied by Beckman Coulter Genomics, UK).

6.2.10 Specific gene cloning strategies

6.2.10.1 Cloning for MBP-δ' fusion protein

Approximately ~1.0kbp fragment containing the DNA Pol III subunit δ' gene *holB* was prepared from *N. meningitidis* MC58 genmic DNA by PCR amplification (see Section 6.2.2). Two primers were created the underlined unique *NcoI* and *XhoI* flanking restriction sites for the directional cloning and inserted *Tobacco Etch Virus* (TEV) protease cleavage sites (Table 6-9). The specific annealing temperature was at 62°C. Subsequently, the digestion of amplified fragments was carried out by the restriction enzymes NcoI and XhoI (see Section 6.2.5) gel purified (see Section 6.2.6). The gene *holB* was cloned into the expression vector petM43 (see Section 6.1.6) which had the gene of maltose binding protein tag (MBP-tag) at the N-terminus (Kindly supplied by Dr. Marko Storch, lab data). The ligate was then transformed into *E. coli* DH5α strain (see Section 6.1.5) using heat shock method (see Section 6.2.7). The gene *holB* was detected by DNA sequencing (served by Source Bioscience, UK).

Primer ID	Oligo Sequence 5'⟶ 3'	Restriction site	Tm
1Delp_F	CTACCATGGCTGAAAACCTGTATT TTCAGGGCG	NcoI	63.5°C
1Delp_R	CACTCGAGACCTTGAAAGTAAAG ATTCTCCCCGTTCTC	XhoI	63.9°C

Table 6-9. PCR primers for the cloning of MBP-δ' (*N. meningitidis*)

6.2.10.2 Cloning for MBP-δ·δ' fusion protein

N. meningitidis DNA Polymerase III subunit δ gene *holA* and subunit δ' gene *holB* of approximately ~1.0kbp were amplified from *N. meningitidis* MC58 genomic DNA by PCR (see Section 6.2.2). Two sets of primers were appended unique restriction sites respectively at the upstream and the downstream of *holA* and *holB* fragments (Table 6-10). The forward primer "2Del_F" created KpnI site in the upstream of *holA* and contained TEV protease cleavage site sets. A SpeI site and 3 stop codes were inserted in the downstream of *holA* by the reverse primer "2Del_F". The forward primer of *holB* (2Delp_F) created a HindIII site and a ribosome bind site (RBS) with spacer before the start code of *holB* alignment. A XhoI site was created in the downstream of stop code of gel *holB*. All these inserted restriction enzyme sites were not located in the backbone vector pETM43.

PCR-amplified DNA fragment containing gene *holB* and the vector pETM43 were digested with KpnI and SpeI (see Section 6.2.5) and gel purified (see Section 6.2.4). The DNA fragment containing gene *holB* was ligated with the backbone DNA from vector pETM43 (see Section 6.2.6). The ligation product was then transformed into *E. coli* DH5α strain (see Section 6.1.5) using heat shock method (see Section 6.2.7). Gene *holB* was detected by sequencing (Source Bioscience).

Subsequently, purified plasmid DNA containing gene *holB* was prepared as described in Section 6.2.1. Restriction enzyme HindIII and XhoI digested PCR-amplified DNA fragment containing gene *holA* and plasmid DNA containing gene *holB* (see Section 6.2.5). DNA fragments were gel purified (see Section 6.2.4). The insertion fragment of gene *holA* was ligated with the backbone DNA containing gene *holB* (see Section 6.2.6). The ligation product was then transformed into *E. coli* DH5α strain (see Section 6.1.5) using heat shock method (see Section 6.2.7). Gene *holA* was detected by DNA sequencing (served by Source Bioscience, UK). The cloning of the co-expression vector was completed collaboratively with Sarah Woodly.

Primer ID	Oligo Sequence 5'⟶ 3'	Restriction site	Tm
2Del_F	TTTCCATGGGAAAACCTGTATTTTCAGG	KpnI	57.7°C
2Del_R	TTTACTAGTTCATCATTATTCCGCCAGCG	SpeI	58.7°C
2Delp_F	TTTAAGCTTAAGGAGATATACCAAGATGATTTATCCG	HindIII	57.8°C
2Delp_R	TTTCTCGAGTCACCCGTTCTC	XhoI	56.5°C

Table 6-10. PCR primers for the cloning of MBP-δ•δ' (*N. meningitidis*)

6.2.10.3 Cloning of MutS from *E. coli*

DNA fragment containing *E. coli* MutS gene *mutS* was amplified from the genome DNA from *E. coli* K12 strain by PCR (see Section 6.2.2) using two primers which created the underlined unique BamHI and HindIII flanking restriction sites (Table 6-11). The PCR-amplified fragments and the vector pPROEX-HTb were digested with BamHI and HindIII (see Section 6.2.5) and

gel purified (see Section 6.2.4). DNA fragment containing gene *mutS* was ligated with the backbone DNA from the vector at BamHI and HindIII sites (see Section 6.2.6). The ligation product was then transformed into *E. coli* DH5α strain (see Section 6.1.5) using heat shock method (see Section 6.2.7). Gene *mutS* was detected by DNA sequencing (served by Source Bioscience, UK).

Primer ID	Oligo Sequence 5'→ 3'	Restriction site	Tm
EMutS_F	CTGCGGCGGATCCATGAGTGCAA TAG	BamHI	63.4°C
EMutS_R	CTACCCAAGCTTACACCAGGCTC TTC	HindIII	60.7°C

Table 6-11. PCR primers for the cloning of MutS (*E. coli*)

6.3 Biochemical methods of protein preparation

6.3.1 Expression and purification of DNA Pol III subunit δ and δ' with the MBP-tag.

DNA Pol III subunit δ and δ' from *N. meningitidis* was cloned into the vector pETM43 which had a N-terminus MBP-tag (see Section 6.8.3). Two DNA constructs with the correct sequence (served by Source Bioscience) were transformed in *E. coli* strain BL21 (DE3) (see Section 6.2.7). The well-grown colony of each construct was restreaked on an LB agar plate containing 50μg/ml kanamycin and single colonies were used to inoculate 10ml LB media containing 50μg/ml kanamycin at 37°C overnight. The overnight cultures were inoculated into 1L of LB media which was add 50μg/ml kanamycin. The start culture was grown at 37°C for ~2 hour when the OD_{600} of cell reached about 0.4. Subsequently, the expression of the target protein was induced by adding 1mM of IPTG and then incubated and shaked at 18°C for overnight. 2% (w/v)

glucose was added into the media to reduce the cost of substrate before 1mM IPTG induction. 1ml of cell samples were collected and normalised before and after the IPTG induction to detect the expression state. The analysis was resolved on a 12% SDS-PAGE gel (see Section 6.3.3).

The expressed cultures were harvested by centrifuging for 20 minutes at 4k rpm at 4°C. The cell pellets were resuspended by MBP Buffer (20mM Tris-HCl, pH 7.5, 0.2 M NaCl, 1mM EDTA, 1mM DTT) and stored in a Falcon tube at -20°C. MBP-tag purification was set up in the column with 4ml of Amylose Resin High Flow (NEB) and equilibrated with 2 column volumes of MilliQ H_2O, 2 column volumes of 0.1%SDS, 2 column volumes of MilliQ H_2O, 5 column volumes of MBP Buffer. The column was stored at 4°C and washed by 2 column volumes of MBP Buffer before use. An EDTA free protease inhibitor tablet (NEB) was added into the defrosted cell pellet. The cells were lysed by sonication (40% amplification, 2s for pulse and 2s for rest, 10 min for full process, 2-3 times, on ice). After sonication, cells were centrifuged for 40minutes at 12,000 rpm at 4°C, and the soluble fraction decanted. The washed amylose resin was mixed with the soluble protein. The mixture of resin and protein was then incubated on ice for 1 hour with intermittently mixing. After centrifuging the mixture (2min, 2k rpm, 4°C), the supernatant was collected and labelled as “flow through”. The mixture of bead and protein was washed three times by 50ml MBP Buffer and the washed supernatant was collected for backup. The mixture of resin and protein was added 400μl TEV protease (Homemade) which has an N-terminus His-tag and incubated at 4°C overnight. After loading back to the column, the tag-free fractions were collected by 0.5ml aliquots till no protein outflow. They were detected by Bradford assay reagent (Bio-Rad Laboratories, Inc., USA). Positive fractions were blue. Poured aliquots was loaded into a fresh Ni^{2+} chelating column (GE Healthcare, USA) to remove remained TEV protease. The aliquots flew through the Ni^{2+} chelating column were collected. “Whole cells”, “Soluble

fraction", "Flow through" and tag-free fractions were loaded on 12% SDS-PAGE gels. The positive fractions were combined and dialysed in 14 kDa dialysis tubing (Visking, Medicell Membranes Ltd, UK) against 1L of fresh MonoQ Buffer (20mM Tris-HCl pH 7.5, 50mM NaCl, 0.1 EDTA, 1mM DTT, 10% glycerol) at 4°C overnight. Protein samples were quantified by Folin Lowry assay kit (Bio-Rad Laboratories, Inc., USA) and stored at -20°C with 20% sterile glycerol.

6.3.2 Expression and purification of MMR enzymes with the His-tag

Genes of MMR enzymes from *N. meningitides* were cloned in the vector pPROEX-HTb (amp_R) respectively which includes a His-tag at the N-terminus (Dr. Jan Silhan, lab data). Cloning of MutS from *E. coli* was also performed in the same vector (see Section 6.2.8.3.3). The optimal condition of expression was detected by 50ml small scale expression assays which induced by 1mM IPTG.

The well-grown colony of each construct was restreaked on an LB agar plate containing 100µg/ml ampicillin and single colonies were used to inoculate 10ml LB media containing 100µg/ml ampicillin at 37°C for overnight. The overnight cultures were inoculated into 1L of LB media which was add 100µg/ml ampicillin. The start culture was grown at 37°C for ~2 hour when the OD_{600} of cell reached about 0.4. 1mM of IPTG was added to the cell cultures to induce protein expression with 4hr incubation and shaking at 25°C. 1ml of cell samples were collected and normalised to an OD600 of 0.4 before and after the IPTG induction to detect the expression state via a 12% SDS-PAGE gel (see Section 6.3.3).

His-tag purification of MMR enzymes was performed in the Ni^{2+} chelating beads column using Chelating Sepharose Fast Flow (GE Healthcare Life Sciences

Ltd., USA) which was equilibrated by with HT Buffer (20mM Tris-HCl, pH8.0, 500mM NaCl, 50mM Imidazole, 2mM β-mercaptoethanol) before use. The protein-resin binding method is identical with the MBP-tag purification as described above (see Section 6.3.2). After washing by three times of 50ml HT buffer, target protein was eluted with 500mM Imidazole in HT Buffer in 1ml fractions which were detected in the Bradford assay (Bio-Rad). The positive fractions were pooled in 14kDa dialysis tubing (Visking) and dialysed against 1L of Imidazole-free buffer (20mM Tris-HCl, pH8.0, 500mM NaCl, 2mM β-mercaptoethanol) with 400μl TEV protease (Homemade) at 4°C on the stirrer. His-tag free protein was flown through the fresh Ni^{2+} chelating beads column to remove residual un-cleaved His-tag fusion proteins and TEV protease. Subsequently, His-tag free proteins were dialysed against the storage buffer (20mM Tris-HCl, pH7.5, 50mM NaCl, 2mM β-mercaptoethanol) and quantified by Qubit® protein assay kit using the Qubit® 2.0 Fluorometer (Thermo Fisher Scientific, USA). Protein samples were imaged on 12% SDS-PAGE gels and stored at -20°C with 20% sterile glycerol.

6.3.3 Size-exclusion chromatography

In the study, tag-free proteins were further purified via size-exclusion chromatography. Purications of DNA Pol III subunits were carried out via gel filtration SuperDex 75 column (320ml) (GE Healthcare, USA) using a ÄKTA FPLC system (GE Healthcare, USA). Purification of *Ec*MutS, *Nm*MutS and *Nm*MutL were performed via BioSuite HR SEC column (250Å) (Waters, UK) using a Finnigan Surveyor HPLC System (Thermo Scientific, USA).

6.3.4 SDS-polyacrylamide eletrophoresis

Gel	Composition
12% SDS Resolving Gel	2 ml 30%(29:1) Acrylamide 1.27 ml 1.5M Tris-HCl pH 8.8 50 μl 10% SDS 1.6 ml Milli-Q H_2O 66.7 μl 10% (w/v) APS 7.1 μl TEMED
5% SDS Stacking Gel	0.83 ml 30%(29:1) Acrylamide 0.63 ml 1 M Tris-HCl pH 6.8 50 μl 10% SDS 3.4 ml Milli-Q H_2O 50 μl 10% (w/v) APS 10 μl TEMED

Table 6-12. Components of SDS-PAGE electrophoresis gels

Buffer / Dye	Composition
4 x SDS loading Dye	50 mM Tris-HCl, pH6.8 50 mM dithiothreitol, 2% w/v SDS 0.1% bromophenol blue 10% glycerol
10 x SDS running buffer (1 L)	1L Milli-Q H_2O 30 g Tris 144 g Glycine 10 g SDS
Coomassie staining solution (1 L)	1 g Coomassie blue R-250 dye 450 ml 100% methanol 100ml glacial acetic acid 450ml distilled H_2O
De-staining solution (1 L)	200 ml 100% methanol 100 ml glacial acetic acid 700 ml distilled H_2O

Table 6-13. Components of SDS-PAGE electrophoresis buffers and dyes

The electrophoresis was performed at the RT under 200 volts for 30 minutes. The SDS-PAGE gel was stained by Coomassie staining solution for 20 minutes and subsequentlly de-stained by de-staining solution for 30 minutes. The gel was visualised by the photo scanner (Hewlett-Packard Company, USA)

6.3.5 Bradford protein assay

Arginine and aromatic residues within proteins can be bound by Coomassie Blue, resulting in an absorbance shift that serves as a colorimetric test. In its unbound cationic form, Coomassie Blue has a maximum absorbance of 470 nm and appears brown. In its bound anionic form, the maximum absorbance is 595 nm and the complex appears blue colour. The Bradford protein assay is thus based on the number of arginine and aromatic residues. The Bradford protein assay is linear within a range of 0-1 mg ml-1 protein and therefore is suitable for determination of lower protein concentrations. Higher concentrations can be determined by diluting the sample with specific buffers prior to mixing it with the Bradford reagent. Routinely, 10 µl (or 5 µl for highly concentrated samples) protein sample was mixed 190 µl of Bradford reagent in a 96-microwell plate (Thermo Scientific).

6.3.6 Quantificiation of protein

6.3.6.1 Folin Lowry protein assay

To reduce the effect of protein quantification from reagents in the buffer, purified protein was quantified via Modified Lowry Protein Assay Kit (Thermo Scientifics, USA). In this assay, the purified protein was reacted in an alkaline solution which containing tartate and cupric and forms the complex of protein-tetradentate copper. With the addition of Folin-Ciocalteu reagent, the chelated complexes were reduced and the mixture presented in the blue colour, which could be monitered at 750nM. The strandard curve of protein concentrations

was defined by the dilutions of bovine serum albumin (BSA) with known concentrations. The concention of the purified protein was calculated and compared which the standard curve of BSA.

6.3.6.2 Qubit protein assay

During this study, the reagent of Folin Lowry protein assay kit was contaminated in the lab. Therefore, some proteins were quantified using the Qubit® Protein Assay Kit (Thermo Scientifics, USA). Qubit protein assay was used with the Qubit® fluorometer 2.0 (Thermo Scientifics, USA). The assay quantified proteins with the specific fluorescent dye compared to pre-diluted BSA standards. 1 µl of concentrated assay reagent was diluted in 199 µl of assay buffer to gain the assay solution. 1 µl of concentrated protein sample was mixed with 199 µl of the assay solution thoroughly. After 15 minutes' incubation at the RT, the concentration was read from the fluorometer.

6.3.7 Reconstitution of DNA Pol III complex.

DNA Pol III subunits α, ε, $\gamma.\tau$ and potentially δ have been purified from the plasmid pPROEX-HTb (amp_R) with an N-terminal His tag in the previous research (Dr. Jan Silhan, lab data). In this study, the His-tag of each subunit was cleaved by TEV protease (Homemade) and dialyzed in 14kDa dialysis tubing (Visking) against 1L of fresh MonoQ Buffer (20mM Tris-HCl pH 7.5, 50mM NaCl, 0.1 EDTA, 1mM DTT, 10% glycerol) at 4°C overnight. Proteins were quantified by Folin Lowry assay kit (Bio-Rad) and imaged on 12% SDS-PAGE gels stored at -20°C.

DNA Pol III complex is constituted by two parts, DNA Pol III Core complex (subunits α and ε) and the clamp loader complex (subunits γ, τ, δ and δ'). To form DNA Pol III core complex, 72 nmol of subunit α and 108 nmol of subunit ε was mixed and incubated at 4 ºC for overnight. The α–ε complex was purified

and chromatographed on the MonoQ 5/50 GL column (GE) in FPLC ÄKTA system and eluted by 0-0.4M NaCl with linear gradient in MonoQ buffer. Fractions of 0.4ml were gathered and further analysed using 12% SDS-PAGE gel electrophoresis. Positive fractions were then quantified by Folin Lowry method (Bio-rad), assuming a 1:1 ratio of α:ε. The standard curve of the Folin Lowry method was BSA in MonoQ Buffer. The used column was used with MonoQ Buffer contained 1M NaCl until the UV baseline returns to 0. Subsequently, the column was washed by five column volumes of MilliQ H_2O and further equilibrated with five column volumes of MonoQ buffer for later use.

In order to constitute the clamp loader complex, 102nmol of subunit γ.τ and 53nmol of subunit δ. δ' were mixed and incubated on ice for 2hrs. 55nmol of DNA Pol III core complex was added into the clamp loader complex mixture and dialysed against MonoQ buffer overnight at 4 ºC. The mixture of DNA Pol III complex was purified and chromatographed on the MonoQ 5/50 GL column (GE) and eluted by NaCl with the 0-0.4M linear gradient in MonoQ buffer. Fractions of 0.4ml were gathered and futher analysed via 12% SDS-PAGE gel electrophoresis. Positive fractions were then quantified by Folin Lowry method (Bio-rad), assuming a 1:1 ratio of core complex: clamp loader complex.

6.4 Enzyme assays *in vitro*

6.4.1 Polymerase extension assay

6.4.1.1 Preparation of M13KE ssDNA

M13KE Bacteriophage (NEB) ssDNA was used as a template for polymerase extension assays, was propagated in *E. coli* K12 strain ER2738 (NEB, UK).

E. coli K12 strain was isolated and incubated in 2.5ml of LB at 37°C for overnight. 0.5ml of 10^3-fold dilution of M13KE Phage stock ($1x10^{13}$ pfu/ml) (NEB) was added in the cell culture to infect at room templature for 5min.The infected cell culture was diluted into 250ml of 2YT media in a 2L flack and was then shaked in the incubator at 37°C for 5 hours. The infected cells were harvested via centrifugation (15mins, 4k rpm, 4°C). The supernatant was added with 10g of PEG and 7.5 of NaCl and mixture at 4°C for overnight via a magnetic stirrer. The precipitate was centrifugated (20mins, 10K rpm, 4°C). After centrifiugation, the centrifuge tube was inverted for 2-3mins to remove any remaining supernatant. The precipitate was dissolved by 10ml of 10mM Tris-Cl (pH8.0) and added with equal volume of equilibriated phenol. Subsequently, the solution was mixed via the vortex for 2 minutes and then centrifuged at 3K rpm from 5 minutes at RT. The aqueous layer was then transferred into a flash falcon tuber. The extraction of DNA could be repeated with 10ml of equilibriated phenol. About 10ml of the aqueous layer liquid was added 0.5ml of 3M sodium acetate (pH 5.2) and 11ml of ethanol to each tube, and was then mixed well and left for 15 mins at RT. The precipitated ssDNA was recoverd using centrifugation (4°C, 12K rpm, 10mins). After discarding the supernatant, 30ml of 70% ethonal was added to the precipitate and centrifuged (4°C, 12K rpm, 10mins). The supernatant was carefully removed as much as possible, thereby allowing the residual ethanol to be evaporated. The purified ssDNA pellet was dissolved in 1ml of Milli-Q H_20. ssDNA was purified via agarose gel and electro-eluted

against 0.1 X TBE and then concentrated. The quantification of ssDNA was carried out by Qubit® ssDNA assay using the Qubit® 2.0 Fluorometer (Thermo Scientific). The sequence of ssDNA was detected via sequencing service (Source Bioscience, UK). The stock of ssDNA was stored at -20 °C.

6.4.1.2 Preparation of M13KE RF dsDNA

M13KE RF dsDNA were prepared from the infected E. coli K12 cell. After infection and incubation in 250ml of 2YT media at 37°C for 5 hours, cell harvet was obtained via centrifugation (15mins, 4k rpm, 4°C). The cell pellet was resuspended by 100ml ice-cold STE buffer (10 mM Tris-Cl pH 8.0, 0.1M NaCl, 1mM EDTA) and then recovered by centrifugation (15 mins, 4K rpm, 4°C). The recoverd cell pellet was further resuspended within 9ml of Alkaline lysis solution I (50 mM glucose, 25 mM Tris-Cl pH 8.0, 10 mM EDTA) and added with 1ml of 10mg/ml lysozyme. Subsequantly, 20ml of Alkaline lysis solution II (0.2 M NaOH, 1% w/v SDS) was added and mixed with repeated inversion. After further 10mins Incubation for at RT, 10ml of pre-chilled Alkaline lysis solution III (6ml of 5M potassium acetate, 1.15ml of glacial acetic acid, 2.85ml of H_20 of Milli-Q water). The mixture was gently swirled and incubated on ice for 10 mins. After centrifugation (30mins, 12K rpm, 4°C), clear supernatant was decanted and mixed 0.6 volumen of isopropanol in a fresh bottle and incubated at RT for 10 mins. The precipitated DNA was recoverd by further centrifugation (15mins, 12K rpm, RT) and was washed by 70% ethanol using spinning centrifugers. Ethanol was discarded and allowed to evaporate at RT. The purified dsDNA pellet was dissolved in 1ml of Milli-Q H_2O. ssDNA was purified via agarose gel and electro-eluted against 0.1 X TBE and then concentrated. The quantification of dsDNA was carried out by Qubit® dsDNA BR assay using the Qubit® 2.0 Fluorometer (Thermo Scientific). The sequence of dsDNA was detected via sequencing service (Source Bioscience, UK). The stock of M13KE dsDNA was stored at -20 °C.

6.4.1.3 Preparation of primed ssDNA templates

M13KE phage circle ssDNA and dsDNA were detected by DNA sequencing using primer “PE_1” and “PE_R” (served by Source Bioscience). It was then primed with three primers in the same direction to assemble three templates of polymerase extension assay. “PE_1” was annealed with M13 ssDNA for “Template 1”. “Template 2” was primed with two primers, “PE_1” and “PE_2”. “Template 3” was primed by “PE_1” and “PE_3”. 2μM of M13ssDNA was annealed with 3μM oligonucleotides in the annealing buffer (10mM Tris-HCl pH7.5, 10mM EDTA, 500mM NaCl) at 95°C and cooled *in situ* to RT over 8 hrs. Primed ssDNAs were purified using a S300 microspin column (GE healthcare Scientifics, USA).

Oligo ID	Oligo Sequence 5’⟶ 3’	Length	Tm
PE-1	ACAGCCCTCATAGTTAGCGTAACG	26	58.5°C
PE-2	TTGTATCGGTTTATCAGCTTGC	22	53.3°C
PE-3	TGTCCATCACGCAAATTAACCG	22	56.0°C
PE-R	TTATTCGCAATTCCTTTAGTGGTACC	26	55.3°C

Table 6-14. Summary of primers used in extension assays
Primed M13KE ssDNA templates were quantified by both the Qubit® ssDNA assay using the Qubit® 2.0 Fluorometer.

6.4.1.4 DNA pol III holoenzyme extension assay

In the polymerase extension assay, 1.5nM of three types of primed M13KE circle ssDNA were treated with 200nM DNA Pol III and 400nM beta clamp in 25mM Tris-HCl pH 7.5, 8mM $MgCl_2$, 5mM DTT, 0.5mM ATP, 40ug/ml BSA, 4% glycerol, 100nM of each dNTP, in a volume of 20 ul. The assay mixtures were incubated at 25°C for 20 min before being inactivated by heating at 80°C for 10min. DNA products from extension assays were analysed in the 0.8% agarose gel electrophoresis. Agarose gels were stained in 0.5mg/ml EtBr for 30min and destained in Milli-Q H_20 for 5min.

6.4.2 Gel shift assay

6.4.2.1 Preparation of DNA substrates for gel shift assay

6.4.2.1.1 Preparation of 30-bp linear DNA

All oligonucleotides used in the gel shift assay were supplied by Integrated DNA Technologies (Table 6-15). The oligonucleotide "30L-G" is labelled with 6-Carboxyfluorescein (FAM) whose excitation maximum is at 495nm and emission maximum is at 521nm. "30L-C" is complementary to "30L-G". "30L-T" only changes the 15th nucleotide in "30L-C" from Cytidine to Thymidine. Specific extinction coefficients of oligonucleotides were examined at OD260 by Ultrospec 2100 Pro UV-Vis Spectrophotometer (GE Amersham Pharmacia, USA). The concentration of purified oligonucleotides was calculated from the sum of the individual extinction coefficient (ε260) (Equation 1) following the Beer–Lambert law (Equation 2). Oligonucleotides were stored at -20^{o}C.

$$\varepsilon 260 = [7.05\,(C) + 12.01(G) + 15.02(A) + 8.40(T)] \times 10^3\ M^{-1}cm^{-1} + 20960\ (FAM)\ M^{-1}cm^{-1}$$

Eq.1

$$\text{Concentration of oligonuleotide} = OD260 * \text{Dilution factor} / \varepsilon 260 * 1$$

Eq.2

The oligonucleotide "30L-G" was annealed with oligonucleotides "30L-C" to assemble a complementary dsDNA. "30L-T" was annealed with "30L-G" to gain dsDNA with a T/G mismatch mismatch. The annealing was performed by the identical molar of oligonucleotides in the annealing buffer (10mM Tris-HCl pH7.5, 10mM EDTA, 500mM NaCl) at 95°C and cooled *in situ* to RT over 8 hours. Annealed dsDNA was purified using 10% non-denaturing PAGE (see Section 6.4.2.2).

Oligo ID	Oligo Sequence 5'⟶ 3'	Length	Tm
30L-T	AACTGCGACGGACTTGTGGTCACAGT CTTT	30	70.8°C
30L-C	AACTGCGACGGACTCGTGGTCACAGT CTTT	30	71.7°C
30L-G	**FAM/**AAAGACTGTGACCACGAGTCCGT CGCAGTT	30	71.7°C

Table 6-15. Oligonucleotides for 30-bp linear DNA used in gel shift assays
The mismatched base was highlighted in blue; the mismatch-corresponding complementary bases of the homoduplex DNA are highlighted in red.

6.4.2.1.2 Preparation of mini-circular DNA

A strategy of 120-bp mini-circle DNA was carried out to provide a closed dsDNA structure to tightly integrate with MMR proteins. The circular DNA was composed of two dsDNAs (dsDNA_1 and dsDNA_2) containing complemented overhangs at both ends via Taq ligase (NEB, USA). Each dsDNA was formed by two complemented oligonucleotides via annealing (Table 6-16). "dsDNA_1" was annealed by "MC1" and "MC2". "dsDNA_2" was annealed by "MC3-C" or "MC3-T" with "MC4". "MC3-C" is complementary to "MC4". "MC3-T" was changed the 32th nucleotide in "30L-C" from Cytidine to Thymidine. The annealing was performed by the identical molar of oligonucleotides in the annealing buffer (10mM Tris-HCl pH7.5, 10mM EDTA, 500mM NaCl) at 95°C and cooled *in situ* to RT over 8 hours. "dsDNA_1" and "dsDNA_2" were annealed at the longest overhang by the identical molar at 45°C for 2 hours. Subsequently, the short overhang was ligated by T4 ligase (NEB, USA). The circular DNA was detected by Epicentre® Plasmid-Safe™ ATP-Dependent DNase (Biozym Scientific GmbH, Germany).

Oligo ID	Oligo Sequence 5'⟶3'	Length	Tm
MC1	**Phos/TG**GTTGAATTCTCTGTCTTGTTG GACGGATCTGTCTGCGGAGTCTAAGC TTCTCAGGTGCTAGTTCTG	68	70.3°C
MC2	**Phos/GTCCATCGTGTCAG**CAGAAGTA GCACCTGAGAAGCTTAGACTCCGCAG ACAGATCCGTCCAACAAGACAGAGAA TTCAAC	80	71.0°C
MC3-C	**Phos/CTGACACGATGGAC**TCTGGATC CGATGCTG**C**AGGACAATCTCTCGCCT CAAG	52	70.8°C
MC3-T	**Phos/CTGACACGATGGAC**TCTGGATC CGATGCTG**T**AGGACAATCTCTCGCCT CAAG	52	69.7°C
MC4-G	**Phos/CA**CTTGAGGCGAGAGATTGTCC T**G**CAGCATCGGATCCAGA	40	69°C

Table 6-16. Oligonucleotides for mini-circular DNA used in gel shift assays
Overhangs were highlighted in green; the mismatched base was highlighted in blue; the mismatch-corresponding complementary bases are highlighted in red.

The mini-circular DNA was purified by 2% agarose gel electrophoresis and concentrated using the vacuum concentrator Savant SpeedVac Kit (Thermo Scientific) and quantified by Qubit dsDNA BR assay (Thermo Scientific)

6.4.2.1.3 Preparation of 60-bp blocked-ended DNA

Oligo ID	Oligo Sequence 5’ ⟶ 3’	Length	Tm
60L-T	**Biotin**/TGACACGATGGACTCTGGATCC GATGCTGTAGGACAATCTCTCGCCTCA AGTGGTTGAAT	60	70.8°C
60L-C	**Biotin**/TGACACGATGGACTCTGGATCC GATGCTGCAGGACAATCTCTCGCCTC AAGTGGTTGAAT	60	71.7°C
60L-G	**Biotin**/ATTCAACCACTTGAGGCGAGAG ATTGTCCTGCAGCATCGGATCCAGAGT CCATCGTGTCA	60	71.7°C

Table 6-17. Oligonucleotides for 60-bp blocked-ended DNA in gel shift assays
The mismatched base was highlighted in blue; the mismatch-corresponding complementary bases of the homoduplex DNA are highlighted in red.

As summarized in Table 6-17, oligonucleotides for 60-bp blocked-ended DNA used in gel shift assays were supplied and purified via HPLC purification from Integrated DNA Technologies, Inc. (Coralville, USA). All target oligonucleotide strands were labelled with biotinylation (Biotin) at the 5’ terminus. Purified oligonucleotides were quantified by calculating specific ε260 (Equation 1) following the Beer–Lambert law (Equation 2) as described in Section 6.4.2.1.1.

Oligonucleotide “60L-G” was annealed with “60L-C” and “60L-T” respectively by the identical molar of oligonucleotides in the annealing buffer (10mM Tris-HCl pH7.5, 10mM EDTA, 500mM NaCl) at 95°C and cooled *in situ* to RT over 8 hours. Annealed dsDNA was purified using 10% non-denaturing PAGE (see Section 6.4.2.2). Target DNA bands were cut and electro-eluted in the dialysis tubing against 0.1 x TBE. DNA duplexes were concentrated by and quatitated by Qubit dsDNA BR assay.

The purified DNA duplex bound to the Streptavidin first. 80 nM of DNA was incubated with 800 nM of Streptavidin (Thermo Scientifics) in the gel shift buffer (20mM Tris-HCl pH 7.5, 10mM NaCl, 1mM $MgCl_2$, 1mM DTT, 0.1mg/ml BSA) containing 5% sterile glycerol at 25°C for 1 hour. The Streptavidin bound DNA was then used in the gel shift assay.

6.4.2.2 Non-denaturing PAGE

Gel	Composition
6% non-denaturing PAGE gel (12 ml, 2 x gels)	2.4 ml 30%(75:1) Acrylamide solution 0.6 ml 10 x TBE pH 7.5 8.89 ml Milli-Q H_2O 100 μl 10% (w/v) APS 10 μl TEMED
10% non-denaturing PAGE gel (12 ml, 2 x gels)	3 ml 40%(19:1) Acrylamide solution 0.6 ml 10 x TBE pH 7.5 8.29 ml Milli-Q H_2O 100 μl 10% (w/v) APS 10 μl TEMED

Table 6-18. Components of non-denaturing PAGE gels

7.5 g of acrylamide and 0.1 g of N,N'-methylenebisacylamide were dissolved by Milli-Q H20 in a final volume of 25.3 ml to make the 30% (75:1) Acrylamide solution. All the weighting process was performed in the fume cupboard due to the high toxicity of acrylamide and N,N'-methylenebisacylamide powers. This solution was filtered by 0.22 μm Millex-GV Syringe Filter Unit (Millipore, Fisher). The non-denaturing PAGE gel was solid at the RT for 20 minutes.

6.4.2.3 Gel shift assay of mismatch repair proteins

In the first assay with 30-bp open-ended linear dsDNA, 20nM of DNA with or without the T-G mismatch was incubated with three concentrations, 2μM, 1μM and 500nM of MutS and MutL in the gel shift buffer (20mM Tris-HCl pH 7.5, 10mM NaCl, 1mM $MgCl_2$, 1mM DTT, 0.1mg/ml BSA) at 25°C for 30 minutes.

1mM ATP was added to initially detect the ATPase activity dependency of MutS and MutL. All samples were fully mixed with the loading dye (0.042% bromophenol blue, 0.042% xylene cyanol, 40% sucrose) and were then loaded onto a 5% polyacrylamide gel. PAGE was performed at constant 40 volts in 1 x TBE buffer for 2 hours at 4°C. All gels were visualised via Fuji FLA-5000 fluorescent imager (Fuji Film, Japan).

The second assay with mini-circular DNA was performed that 2μM of MutS was incubated with 100nM of DNA with and without mismatch in the gel shift buffer (20mM Tris-HCl pH 7.5, 10mM NaCl, 1mM $MgCl_2$, 1mM DTT, 0.1mg/ml BSA) at 25°C for 30 minutes. Betaine glycine was added to 1mM, and the samples were incubated at 25°C for 5 minutes. All samples were fully mixed with the loading dye (0.042% bromophenol blue, 0.042% xylene cyanol, 40% sucrose) and were then loaded onto a 5% polyacrylamide gel. PAGE was performed at constant 60 volts in 1 x TBE buffer for 120 minutes at 4°C. The gels were stained against 0.5ug/ml of EtBr (Thermo Scientifics) for 30 minutes and destained in Mill-Q H_20 for 20 minutes. All the gels were visualised via Fuji FLA-5000 fluorescent imager (Fuji Film, Japan).

The third assay with the blocked-ended linear DNA was carried out with 40 nM of Streptavidin bound DNA (see Section 6.4.2.1.3) and the gradient concentration (from 20 nM to 2μM) of *Ec*MutS, *Nm*MutS and *Nm*MutL in the gel shift buffer (20mM Tris-HCl pH 7.5, 10mM NaCl, 1mM $MgCl_2$, 1mM DTT, 0.1mg/ml BSA) at 25°C for 30 minutes. All samples were then mixed with the loading dye (0.042% bromophenol blue, 0.042% xylene cyanol, 40% sucrose) and were loaded onto a 6% polyacrylamide gel. The running buffer of non-denaturing PAGE was 0.5 x TBE (pH 7.5). The electrophoresis was performed in a cold room at 4°C under 40 volts. For gel shift assays on blocked-ended DNA, the electrophoresis ran for 12 hours. The non-denaturing PAGE gel was

stained by 0.5 μg/ml EtBr for 30 minutes and de-stained by Milli-Q H_20 for 20 minutes. All the gels were visualised via Fuji FLA-5000 fluorescent imager (Fuji Film, Japan).

In this assay, the data was analysed via GraphPad Prism 7 fitting the Hill equation (Equation 3). Hill equation provides an equilibrium dissociation constant (K_d) and a cooperative coefficient (n). X is the concentration of proteins. Y is the percentage of bound DNA. Bmax is the capacity of binding with the same unit as Y:

$$Y = \frac{Bmax * [X]^n}{K_d{}^n + [X]^n}$$

Eq. 3

6.4.3 Nuclease assay

6.4.3.1 Preparation of DNA substrates for nuclease assay

Oligo ID	Oligo Sequence 5'⟶ 3'	Length	Tm
60TAMRA-T	**Biotin**/TGACACGATGGACTCTGGATCC GATGCTGTAGGACAATCTCTCGCCTCA AGTGGTTGAAT/**TAMRA**	60	70.7°C
60TAMRA-C	**Biotin**/TGACACGATGGACTCTGGATCC GATGCTGCAGGACAATCTCTCGCCTCA AGTGGTTGAAT/**TAMRA**	60	71.0°C
60FAM-G	**Biotin**/ATTCAACCACTTGAGGCGAGAG ATTGTCCTGCAGCATCGGATCCAGAGT CCATCGTGTCA/**FAM**	60	71.7°C

Table 6-19. Oligonucleotides used in all nuclease assays
The mismatched base was highlighted in blue; the mismatch-corresponding complementary bases of the homoduplex DNA are highlighted in red.

As summarized in Table 6-1, oligonucleotides in all nuclease assays were synthesized and purified via HPLC purification by Integrated DNA Technologies, Inc. (Coralville, USA). All oligonucleotide strands had the identical sequences

as in gel shift assays in Chapter 3 (Described in Section). Target oligonucleotide strands remarked as “TAMRA” were labelled with biotinylation (Biotin) at the 5’ terminus, and were labelled with 5-(and-6)-carboxytetramethylrhodamine (TAMRA) at the 3’ terminus. Oligonucleotide strands remarked as “FAM” were labelled with Biotin at the 5’ terminus, and were labelled with 6-carboxyfluorescein (FAM) at the 3’ terminus.

Specific extinction coefficients of oligonucleotides were examined at OD260 (ε260) by Ultrospec 2100 Pro UV-Vis Spectrophotometer (GE Amersham Pharmacia, USA). The concentration of purified oligonucleotides was calculated from the sum of the individual extinction coefficient (Equation 1) following the Beer–Lambert law (Equation 2).

Homoduplex and heteroduplex substrates were annealed by TAMRA-labelled strands and the FAM-labelled strand with the equal molar respectively. Oligonucleotide “60L-G” was annealed with “60L-C” and “60L-T” respectively by the identical molar of oligonucleotides in the annealing buffer (10mM Tris-HCl pH7.5, 10mM EDTA, 500mM NaCl) at 95°C and cooled *in situ* to RT over 8 hours. Annealed dsDNA was purified using 10% non-denaturing PAGE (see Section 6.4.2.2). Target DNA bands were cut and electro-eluted in the dialysis tubing against 0.1 x TBE. DNA duplexes were concentrated by and quatitated by Qubit dsDNA BR assay.

6.4.3.2 Urea denaturing PAGE

Gel	Composition
15% Denaturing PAGE gel solution	3.75 ml 40%(19:1) Acrylamide 10 ml 10 x TBE 18.5 ml Milli-Q H_2O 42 g Urea

Table 6-20. Components of urea denaturing PAGE gels

The solution was incubated at 55°C for 30 minutes to dissolve urea particles. The final volume of the gel solution was 100 ml. Subsequently, the solution was filtered and cooled to the RT. 300 ml of 10% (w/v) APS and 100 ml of TEMED were mixed with the solution just before pool it into the gel caster. The gel was solid at the RT for 1 hour.

The running buffer of the electrophoresis was 1 x TBE solution. The denaturing PAGE pre-ran at 1500 volts for 1 hour to at 55~60°C. Gel wells were washed by syringed prior to loading samples. The electrophoresis performed at 1000 volts for 2.5 hours and kept the gel temperature at 55~60°C.

6.4.3.3 Nuclease activity assay

Fluorophore-labelled DNA substrates (40nM) were incubated with HPLC purified proteins for 2 hours at 25°C in the nuclease assay buffer [20mM Tris-HCl (pH 7.5), 10mM NaCl, 1mM DTT] containing 5mM $MgCl_2$ or $MnCl_2$ as different physiological ionic strengths, in a volume of 20μl. All of reactions were subsequently inactivated by heating at 80°C for 20 minutes. 20μl of 2 x formamide loading dye [95% deionized formamidem, 0.05% bromophenol blue, 0.5M EDTA (pH 8.0)] was added to reactions prior to 15% urea denaturing PAGE (see Section 6.4.3.2). Gels were visualised by fluorescent labels using Fuji FLA-5000 fluorescent image analyser. DNA was quantified using ImageJ software and was analyzed using GraphPad Prim 7.0 software.

Chapter 7

References

Acharya, S., Foster, P. L., Brooks, P. & Fishel, R. (2003) The coordinated functions of the *E. coli* MutS and MutL proteins in mismatch repair. *Molecular Cell*. 12 (1), 233-246.

Acharya, S. (2008) Mutations in the signature motif in MutS affect ATP-induced clamp formation and mismatch repair. *Molecular Microbiology*. 69 (6), 1544-1559.

Alani, E., Lee, J. Y., Schofield, M. J., Kijas, A. W., Hsieh, P. & Yang, W. (2003) Crystal structure and biochemical analysis of the MutS· ADP· beryllium fluoride complex suggests a conserved mechanism for ATP interactions in mismatch repair. *Journal of Biological Chemistry*. 278 (18), 16088-16094.

Alexander, H. L., Rasmussen, A. W. & Stojiljkovic, I. (2004) Identification of *Neisseria meningitidis* genetic loci involved in the modulation of phase variation frequencies. *Infection and Immunity*. 72 (11), 6743-6747.

Alexander, H. L., Richardson, A. R. & Stojiljkovic, I. (2004) Natural transformation and phase variation modulation in *Neisseria meningitidis*. *Molecular Microbiology*. 52 (3), 771-783.

Allen, D. J., Makhov, A., Grilley, M., Taylor, J., Thresher, R., Modrich, P. & Griffith, J. D. (1997) MutS mediates heteroduplex loop formation by a translocation mechanism. *The EMBO Journal*. 16 (14), 4467-4476.

Ariyoshi, M., Vassylyev, D. G., Iwasaki, H., Nakamura, H., Shinagawa, H. & Morikawa, K. (1994) Atomic structure of the RuvC resolvase: a Holliday junction-specific endonuclease from E. coli. *Cell*. 78 (6), 1063-1072.

Au, K. G., Welsh, K. & Modrich, P. (1992) Initiation of methyl-directed mismatch repair. *Journal of Biological Chemistry*. 267, 12142-12148.

Avery, O. T., Macleod, C. M. & McCarty M. (1944) Studies on the Chemical Nature of the Substance Inducing Transformation of Pneumococcal Types. *The Journal of Experimental Medicine*. 79 (2), 137-158.

Baitinger, C., Burdett, V. & Modrich, P. (2003) Hydrolytically Deficient MutS E694A Is Defective in the MutL-dependent Activation of MutH and in the Mismatch-dependent Assembly of the MutS· MutL· Heteroduplex Complex. *The Journal of Biological Chemistry*. 278, 49505-49511.

Baker, T. A., & Wickner, S. H. (1992) Genetics and Enzymology of DNA Replication in Escherichia Coli 1. *Annual review of genetics*, *26*(1), 447-477.

Ban, C., Junop, M. & Yang, W. (1999) Transformation of MutL by ATP binding and hydrolysis: a switch in DNA mismatch repair. *Cell*. 97 (1), 85-97.

Ban, C. & Yang, W. (1998) Crystal structure and ATPase activity of MutL: implications for DNA repair and mutagenesis. *Cell*. 95 (4), 541-552.

Banach-Orlowska, M., Fijalkowska, I. J., Schaaper, R. M. & Jonczyk, P. (2005) DNA polymerase II as a fidelity factor in chromosomal DNA synthesis in *Escherichia coli*. *Molecular Microbiology*. 58 (1), 61-70.

Bayliss, C. D., van de Ven, T. & Moxon, E. R. (2002) Mutations in *poll* but not *mutSLH* destabilize *Haemophilus influenzae* tetranucleotide repeats. *The EMBO Journal*. 21, 1465-1476.

Belland, R. J. (1991) H-DNA formation by the coding repeat elements of neisserial *opa* genes. *Molecular Microbiology*. 5 (10), 2351-2360.

Bende, S. M. & Grafström, R. H. (1991) The DNA binding properties of the MutL protein isolated from *Escherichia coli*. *Nucleic Acids Research*. 19 (7), 1549-1555.

Berg, J. M., Tymoczko, J. L., Stryer, L. & Clarke, N. D. (2002) DNA Replication of Both Strands Proceeds Rapidly from Specific Start Sites. In: Berg, J. M., Tymoczko, J. L. & Stryer, L. (eds.) *Biochemistry*. New York, W.H. Freeman and Company.

Biswas, I. & Vijayvargia, R. (2000) Heteroduplex DNA and ATP induced conformational changes of a MutS mismatch repair protein from Thermus aquaticus. *Biochemical Journal*. 347 (3), 881-886.

Bjelland, S. & Seeberg, E. (2003) Mutagenicity, toxicity and repair of DNA base damage induced by oxidation. *Mutation Research/Fundamental and Molecular Mechanisms of Mutagenesis*. 531 (1), 37-80.

Bjornson, K. P., Blackwell, L. J., Sage, H., Baitinger, C., Allen, D. & Modrich, P. (2003) Assembly and Molecular Activities of the MutS Tetramer. *The Journal of Biological Chemistry*. 278, 34667-34673.

Blackwell, L. J., Bjornson, K. P., Allen, D. J. & Modrich, P. (2001) Distinct MutS DNA-binding modes that are differentially modulated by ATP binding and hydrolysis. *Journal of Biological Chemistry*. 276 (36), 34339-34347.

Blackwell, L. J., Martik, D., Bjornson, K. P., Bjornson, E. S. & Modrich, P. (1998) Nucleotide-promoted release of hMutSα from heteroduplex DNA is consistent with an ATP-dependent translocation mechanism. *Journal of Biological Chemistry*. 273 (48), 32055-32062.

Blattner, F. R., Plunkett, G., Bloch, C. A., Perna, N. T., Burland, V., Riley, M., Collado-Vides, J., Glasner, J. D., Rode, C. K., Mayhew, G. F., Gregor, J., Davis, N. W., Kirkpatrick, H. A., Goeden, M. A., Rose, D. J., Mau, B. & Shao, Y. (1997) The complete genome sequence of Escherichia coli K-12. *Science*. 277 (5331), 1453-1462.

Blinkowa, A. L. & Walker, J. R. (1990) Programmed ribosomal frameshifting generates the *Escherichia coli* DNA polymerase III γ subunit from within the τ subunit reading frame. *Nucleic Acids Research*. 18 (7), 1725-1729.

Boulton, S. J. & Jackson, S. P. (1996) Saccharomyces cerevisiae Ku70 potentiates illegitimate DNA double-strand break repair and serves as a barrier to error-prone DNA repair pathways. *The EMBO Journal*. 15 (18), 5093.

Brautigam, C. A. & Steitz, T. A. (1998) Structural and functional insights provided by crystal structures of DNA polymerases and their substrate complexes. *Current Opinion in Structural Biology*. 8 (1), 54-63.

Burdett, V., Baitinger, C., Viswanathan, M., Lovett, S. T. & Modrich, P. (2001) *In vivo* requirement for RecJ, ExoVII, ExoI, and ExoX in methyl-directed mismatch repair. *Proceedings of the National Academy of Sciences of the United States of America*. 98 (12), 6765-6770.

Burnouf, D. Y., Olieric, V., Wagner, J., Fujii, S., Reinbolt, J., Fuchs, R. P. P. & Dumas, P. (2004) Structural and Biochemical Analysis of Sliding Clamp/Ligand Interactions Suggest a Competition Between Replicative and Translesion DNA Polymerases. *Journal of Molecular Biology*. 335 (5), 1187-1197.

Camps, M. & Loeb, L. A. (2004) When Pol I Goes into High Gear: Processive DNA Synthesis by Pol I in the Cell. *Cell Cycle*. 3 (2), 114-116.

Carpenter, E. P., Corbett, A., Thomson, H., Adacha, J., Jensen, K., Bergeron, J., Kasampalidis, I., Exley, R., Winterbotham, M., Tang Christoph, Baldwin, G. S. & Freemont, P. (2007) AP endonuclease paralogues with distinct activities in DNA repair and bacterial pathogenesis. *The EMBO Journal*. 26 (5), 1363-1372.

Champoux, J. J. (2001) DNA Topoisomerases: Structure, Function, and Mechanism. *Annual Review of Biochemistry*. 70, 369-413.

Chargaff, E. (1951) Structure and function of nucleic acids as cell constituents. In *Federation proceedings*. Vol. 10, No. 3, p. 654.

Conte, E., Vincelli, G., Schaaper, R. M., Bressanin, D., Stefan, A., Dal Piaz, F. & Hochkoeppler, A. (2012) Stabilization of the *Escherichia coli* DNA polymerase III ε subunit by the θ subunit favors *in vivo* assembly of the Pol III catalytic core. *Archives of Biochemistry and Biophysics*. 523 (2), 135-143.

Cooper, D. L., Lahue, R. S. & Modrich, P. (1993) Methyl-directed mismatch repair is bidirectional. *The Journal of Biological Chemistry*. 268, 11823-11829.

Correa, E. M., Martina, M. A., De Tullio, L., Argaraña, C. E. & Barra, J. L. (2011) Some amino acids of the Pseudomonas aeruginosa MutL D (Q/M) HA (X) 2 E (X) 4 E conserved motif are essential for the in vivo function of the protein but not for the in vitro endonuclease activity. *DNA Repair*. 10 (11), 1106-1113.

Dallmann, H. G., Kim, S., Pritchard, A. E., Marians, K. J. & McHenry, C. S. (2000) Characterization of the Unique C Terminus of the *Escherichia coli* τ DnaX Protein MONOMERIC C-τ BINDS α AND DnaB AND CAN PARTIALLY REPLACE τ IN RECONSTITUTED REPLICATION FORKS. *The Journal of Biological Chemistry*. 275, 15512-15519.

Dallmann, H. G., Thimmig, R. L. & McHenry, C. S. (1995) DnaX Complex of *Escherichia coli* DNA Polymerase III Holoenzyme CENTRAL ROLE OF τ IN INITIATION COMPLEX ASSEMBLY AND IN DETERMINING THE FUNCTIONAL ASYMMETRY OF HOLOENZYME. *The Journal of Biological Chemistry*. 270, 29555-29562.

Davidsen, T. & Tønjum, T. (2006) Meningococcal genome dynamics. *Nature Reviews Microbiology*. 4, 11-22.

Deitsch, K. W., Lukehart, S. A. & Stringer, J. R. (2009) Common strategies for antigenic variation by bacterial, fungal and protozoan pathogens. *Nature Reviews Microbiology*. 7, 493-503.

de Saro, F. J. L., Georgescu, R. E. & O'Donnell, M. (2003) A peptide switch regulates DNA polymerase processivity. *Proceedings of the National Academy of Sciences*. 100 (25), 14689-14694.

de Saro, F. J. L., Marinus, M. G., Modrich, P. & O'Donnell, M. (2006) The β sliding clamp binds to multiple sites within MutL and MutS. *Journal of Biological Chemistry*. 281 (20), 14340-14349.

De Vlaminck, I., van Loenhout, M. T., Zweifel, L., den Blanken, J., Hooning, K., Hage, S., Kerssemakers, J. & Dekker, C. (2012) Mechanism of homology recognition in DNA recombination from dual-molecule experiments. *Molecular Cell*. 46 (5), 616-624.

Dillingham, M. S. & Kowalczykowski, S. C. (2008) RecBCD enzyme and the repair of double-stranded DNA breaks. *Microbiology and Molecular Biology Reviews*. 72 (4), 642-671.

Doublié, S. & Ellenberger, T. (1998) The mechanism of action of T7 DNA polymerase. *Current Opinion in Structural Biology*. 8 (6), 704-712.

Doublié, S., Tabor, S., Long, A. M., Richardson, C. C. & Ellenberger, T. (1998) Crystal structure of a bacteriophage T7 DNA replication complex at 2.2 Å resolution. *Nature*. 391, 251-258.

Dupes, N. M., Walsh, B. W., Klocko, A. D., Lenhart, J. S., Peterson, H. L., Gessert, D. A., Pavlick, C. E. & Simmons, L. A. (2010) Mutations in the Bacillus subtilis β Clamp That Separate Its Roles in DNA Replication from Mismatch Repair. *Journal of Bacteriology*. 192 (13), 3452-3463.

Duppatla, V., Bodda, C., Urbanke, C., Friedhoff, P. & Rao, D. N. (2009) The C-terminal domain is sufficient for endonuclease activity of Neisseria gonorrhoeae MutL. *Biochemical Journal*. 423 (2), 265-277.

Dutta, R. & Inouye, M. (2000) GHKL, an emergent ATPase/kinase superfamily. *Trends in biochemical sciences*, *25*(1), 24-28.

Elez, M., Murray, A. W., Bi, L. J., Zhang, X. E., Matic, I. & Radman, M. (2010) Seeing mutations in living cells. *Current Biology*. 20 (16), 1432-1437.

Elez, M., Radman, M. & Matic, I. (2012) Stoichiometry of MutS and MutL at unrepaired mismatches in vivo suggests a mechanism of repair. *Nucleic Acids Research*, gkr1298.

Engler, M. J. & Richardson, C. C. (1982) 1 DNA Ligases. *The enzymes*, *15*, 3-29.

Fay, P. J., Johanson, K. O., McHenry, C. S. & Bambara, R. A. (1982) Size classes of products synthesized processively by two subassemblies of Escherichia coli DNA polymerase III holoenzyme. *The Journal of Biological Chemistry*. 257, 5692-5699.

Feng, G., Tsui, H. C. & Winkler, M. E. (1996) Depletion of the cellular amounts of the MutS and MutH methyl-directed mismatch repair proteins in stationary-phase Escherichia coli K-12 cells. *Journal of Bacteriology*. 178 (8), 2388-2396.

Fishel, R., Lescoe, M. K., Rao, M. R. S., Copeland, N. G., Jenkins, N. A., Garber, J., Kane, M. & Kolodner, R. (1993) The human mutator gene homolog MSH2 and its association with hereditary nonpolyposis colon cancer. *Cell*. 75 (5), 1027-1038.

Fishel, R. & Wilson, T. (1997) MutS homologs in mammalian cells. *Current Opinion in Genetics & Development*. 7 (1), 105-113.

Fradkin, L. G. & Kornberg, A. (1992) Prereplicative complexes of components of DNA polymerase III holoenzyme of Escherichia coli. *Journal of Biological Chemistry*. 267 (15), 10318-10322.

Frangioni, J. V. & Neel, B. G. (1993) Solubilization and purification of enzymatically active glutathione S-transferase (pGEX) fusion proteins. *Analytical Biochemistry*. 210 (1), 179-187.

Franklin, R. E. & Gosling, R. G. (1953) Evidence for 2-chain helix in crystalline structure of sodium deoxyribonucleate. *Nature*. 172, 156-157.

Fried, M. & Crothers, D. M. (1981) Equilibria and kinetics of lac repressor-operator interactions by polyacrylamide gel electrophoresis. *Nucleic acids research*, *9*(23), 6505-6525.

Friedberg, E. C., Walker, G. C., Siede, W., Wood, R. D., Schultz, R. A. & Ellenburger, T. (2005) *DNA repair and mutagenesis*. American Society for Microbiology Press.

Friedhoff, P., Thomas, E. & Pingoud, A. (2003) Tyr212: a key residue involved in strand discrimination by the DNA mismatch repair endonuclease MutH. *Journal of molecular biology*, *325*(2), 285-297.

Fukui, K. (2010) DNA mismatch repair in eukaryotes and bacteria. *Journal of Nucleic Acids*. 2010.

Fukui, K., Nishida, M., Nakagawa, N., Masui, R. & Kuramitsu, S. (2008) Bound nucleotide controls the endonuclease activity of mismatch repair enzyme MutL. *Journal of Biological Chemistry*. 283 (18), 12136-12145.

Fukui, K., Shimada, A., Iino, H., Masui, R. & Kuramitsu, S. (2011) Biochemical properties of MutL, a DNA mismatch repair endonuclease. *DNA repair—on the pathway to fixing DNA damage and errors. Intech, Rijeka*. 123-142.

Fuss, J. O. & Cooper, P. K. (2006) DNA repair: dynamic defenders against cancer and aging. *PLoS Biology*. 4 (6), e203.

Galio, L., Bouquet, C. & Brooks, P. (1999) ATP hydrolysis-dependent formation of a dynamic ternary nucleoprotein complex with MutS and MutL. *Nucleic Acids Research*. 27 (11), 2325-2331.

Gao, D. & McHenry, C. S. (2001a) τ Binds and Organizes *Escherichia coli* Replication Proteins through Distinct Domains DOMAIN IV, LOCATED WITHIN THE UNIQUE C TERMINUS OF τ, BINDS THE REPLICATION FORK HELICASE, DnaB. *The Journal of Biological Chemistry*. 276, 4441-4446.

Gao, D. & McHenry, C. S. (2001b) τ Binds and Organizes *Escherichia coli* Replication Proteins through Distinct Domains PARTIAL PROTEOLYSIS OF TERMINALLY TAGGED τ TO DETERMINE CANDIDATE DOMAINS AND TO ASSIGN DOMAIN V AS THE α BINDING DOMAIN. *The Journal of Biological Chemistry*. 276, 4433-4440.

Garavito, R. M., & Ferguson-Miller, S. (2001) Detergents as tools in membrane biochemistry. *Journal of Biological Chemistry*, *276*(35), 32403-32406.

Glover, B. P. & McHenry, C. S. (1998) The χψ Subunits of DNA Polymerase III Holoenzyme Bind to Single-stranded DNA-binding Protein (SSB) and Facilitate Replication of an SSB-coated Template. *The Journal of Biological Chemistry*. 273, 23476-23484.

Glover, B. P., Pritchard, A. E. & McHenry, C. S. (2001) τ Binds and Organizes *Escherichia coli* Replication Proteins through Distinct Domains DOMAIN III, SHARED BY γ AND τ, OLIGOMERIZES DnaX. *The Journal of Biological Chemistry*. 276, 35842-35846.

Gradia, S., Acharya, S. & Fishel, R. (1997) The human mismatch recognition complex hMSH2-hMSH6 functions as a novel molecular switch. *Cell*. 91 (7), 995-1005.

Gradia, S., Subramanian, D., Wilson, T., Acharya, S., Makhov, A., Griffith, J. & Fishel, R. (1999) hMSH2–hMSH6 Forms a Hydrolysis-Independent Sliding Clamp on Mismatched DNA. *Molecular Cell*. 3 (2), 255-261.

Grilley, M., Welsh, K. M., Su, S. S. & Modrich, P. (1989) Isolation and characterization of the Escherichia coli mutL gene product. *Journal of Biological Chemistry*, *264*(2), 1000-1004.

Guarné, A., Junop, M. S. & Yang, W. (2001) Structure and function of the N-terminal 40 kDa fragment of human PMS2: a monomeric GHL ATPase. *The EMBO Journal*. 20 (19), 5521-5531.

Gueneau, E., Dherin, C., Legrand, P., Tellier-Lebegue, C., Gilquin, B., Bonnesoeur, P., Londino, F., Quemener, C., Du, M. L., Márquez, J. A., Moutiez, M., Gondry, M., Boiteux, S. & Charbonnier, J. (2013) Structure of the MutLα C-terminal domain reveals how Mlh1 contributes to Pms1 endonuclease site. *Nature structural & molecular biology*, *20*(4), 461-468.

Haber, L. T. & Walker, G. C. (1991) Altering the conserved nucleotide binding motif in the Salmonella typhimurium MutS mismatch repair protein affects both its ATPase and mismatch binding activities. *The EMBO Journal*. 10 (9), 2707-2715.

Hallet, B. (2001) Playing Dr Jekyll and Mr Hyde: combined mechanisms of phase variation in bacteria. *Current Opinion in Microbiology*. 4 (5), 570-581.

Harfe, B. D. & Jinks-Robertson, S. (2000) DNA mismatch repair and genetic instability. *Annual Review of Genetics.* 34, 359–399.

Hellman, L. M. & Fried, M. G. (2007) Electrophoretic mobility shift assay (EMSA) for detecting protein–nucleic acid interactions. *Nature Protocols*. 2 (8), 1849-1861.

Hendrickson, W. G. (1985) Protein-DNA interactions studied by the gel electrophoresis-DNA binding assay. *BioTechniques*, *3*(3), 198-207.

Iino, H., Kim, K., Shimada, A., Masui, R., Kuramitsu, S. & Fukui, K. (2011) Characterization of C-and N-terminal domains of *Aquifex aeolicus* MutL endonuclease: N-terminal domain stimulates the endonuclease activity of C-terminal domain in a zinc-dependent manner. *Bioscience Reports*. 31 (5), 309-322.

Isaacs, R. J., Rayens, W. S. & Spielmann, H. P. (2002) Structural Differences in the NOE-derived Structure of G–T Mismatched DNA Relative to Normal DNA are Correlated with Differences in 13 C Relaxation-based Internal Dynamics. *Journal of Molecular Biology*. 319 (1), 191-207.

Iyer, R. R., Pluciennik, A., Burdett, V. & Modrich, P. L. (2006) DNA Mismatch Repair: Functions and Mechanisms. *Chemical Reviews*. 106 (2), 302-323.

Jäger, J. & Pata, J. D. (1999) Getting a grip: polymerases and their substrate complexes. *Current Opinion in Structural Biology*. 9 (1), 21-28.

Jiricny, J., Su, S. S., Wood, S. G., & Modrich, P. (1988) Mismatch-containing oligonucleotide duplexes bound by the E. coli mutS-encoded protein. *Nucleic acids research*, *16*(16), 7843-7853.

Jiricny, J. (1998) Eukaryotic mismatch repair: an update. *Mutation Research/DNA Repair*. 409 (3), 107-121.

Jiricny, J. (2006) The multifaceted mismatch-repair system. *Nature reviews Molecular cell biology*, *7*(5), 335-346.

Joshi, A., Sen, S. & Rao, B. J. (2000) ATP-hydrolysis-dependent conformational switch modulates the stability of MutS–mismatch complexes. *Nucleic Acids Research*. 28 (4), 853-861.

Jun, S. H., Kim, T. G. & Ban, C. (2006) DNA mismatch repair system. *FEBS Journal*. 273 (8), 1609-1619.

Junop, M. S., Obmolova, G., Rausch, K., Hsieh, P. & Yang, W. (2001) Composite active site of an ABC ATPase: MutS uses ATP to verify mismatch recognition and authorize DNA repair. *Molecular Cell*. 7 (1), 1-12.

Kadyrov, F. A., Dzantiev, L., Constantin, N. & Modrich, P. (2006) Endonucleolytic function of MutLα in human mismatch repair. *Cell*. 126 (2), 297-308.

Kadyrov, F. A., Holmes, S. F., Arana, M. E., Lukianova, O. A., O'Donnell, M., Kunkel, T. A. & Modrich, P. (2007) Saccharomyces cerevisiae MutLα is a mismatch repair endonuclease. *Journal of Biological Chemistry*. 282 (51), 37181-37190.

Kadyrova, L. Y. & Kadyrov, F. A. (2016) Endonuclease activities of MutLα and its homologs in DNA mismatch repair. *DNA Repair*. 38, 42-49.

Kapust, R. B. & Waugh, D. S. (1999) *Escherichia coli* maltose-binding protein is uncommonly effective at promoting the solubility of polypeptides to which it is fused. *Protein Science*. 8 (08), 1668-1674.

Kelman, L. M. & Kelman, Z. (2004) Multiple origins of replication in archaea. *Trends in Microbiology*. 12 (9), 399-401.

Kelman, Z. & O'Donnell, M. (1995) DNA Polymerase III Holoenzyme: Structure and Function of a Chromosomal Replicating Machine. *Annual Review of Biochemistry*. 64, 171-200.

Kelman, Z., Yuzhakov, A., Andjelkovic, J. & O'Donnell, M. (1998) Devoted to the lagging strand—the χ subunit of DNA polymerase III holoenzyme contacts SSB to promote processive elongation and sliding clamp assembly. *The EMBO Journal*. 17, 2436-2449.

Kim, S., Dallmann, H. G., McHenry, C. S. & Marians, K. J. (1996a) Coupling of a Replicative Polymerase and Helicase: a τ–DnaB Interaction Mediates Rapid Replication Fork Movement. *Cell*. 84 (4), 643-650.

Kim, S., Dallmann, H. G., McHenry, C. S. & Marians, K. J. (1996b) τ Protects β in the Leading-strand Polymerase Complex at the Replication Fork. *The Journal of Biological Chemistry*. 271, 4315-4318.

Kolodner, R. D. & Marsischky, G. T. (1999) Eukaryotic DNA mismatch repair. Current Opinion in Genetics & Development. 9 (1), 89-96.

Kunkel, T. A. & Erie, D. A. (2005) DNA mismatch repair. *Annual Reviews of Biochemistry*. 74, 681-710.

LaDuca, R. J., Crute, J. J., McHenry, C. S. & Bambara, R. A. (1986) The beta subunit of the *Escherichia coli* DNA polymerase III holoenzyme interacts functionally with the catalytic core in the absence of other subunits. *The Journal of Biological Chemistry*. 261, 7550-7557.

Lahue, R. S., Au, K. G. & Modrich, P. (1989) DNA Mismatch Correction in a Defined System. *Science*. 245 (4914), 160-164.

Lamers, M. H., Georgijevic, D., Lebbink, J. H., Winterwerp, H. H., Agianian, B., De Wind, N. & Sixma, T. K. (2004) ATP increases the affinity between MutS ATPase domains Implications for ATP hydrolysis and conformational changes. *Journal of Biological Chemistry*. 279 (42), 43879-43885.

Lamers, M. H., Perrakis, A., Enzlin, J. H., Winterwerp, H. H., de Wind, N. & Sixma, T. K. (2000) The crystal structure of DNA mismatch repair protein MutS binding to a G· T mismatch. *Nature*. 407 (6805), 711-717.

Larrea, A. A., Lujan, S. A. & Kunkel, T. A. (2010) SnapShot: DNA mismatch repair. *Cell*. 141 (4), 730-730.

Lee, S. D. & Alani, E. (2006) Analysis of interactions between mismatch repair initiation factors and the replication processivity factor PCNA. *Journal of Molecular Biology*. 355 (2), 175-184.

Lee, J. Y., Chang, J., Joseph, N., Ghirlando, R., Rao, D. N. & Yang, W. (2005) MutH Complexed with Hemi-and Unmethylated DNAs: Coupling Base Recognition and DNA Cleavage. *Molecular Cell*. 20 (1), 155-166.

Leu, F. P., Hingorani, M. M., Turner, J. & O'Donnell, M. (2000) The δ Subunit of DNA Polymerase III Holoenzyme Serves as a Sliding Clamp Unloader in *Escherichia coli*. *The Journal of Biological Chemistry*. 275, 34609-34618.

Levene, P. A. T. & Bass, L. W. (1931) *Nucleic acids*. New York, The Chemical Catalog Company, Inc.

Lever, M. (1977) Peroxides in detergents as interfering factors in biochemical analysis. *Analytical Biochemistry*. 83 (1), 274-284.

Li, F., Liu, Q., Chen, Y. Y., Yu, Z. N., Zhang, Z. P., Zhou, Y. F., Deng, J. Y., Bi, L. J. & Zhang, X. E. (2008) Escherichia coli mismatch repair protein MutL interacts with the clamp loader subunits of DNA polymerase III. *Mutation Research/Fundamental and Molecular Mechanisms of Mutagenesis*. 637 (1), 101-110.

Lieber, M. R. (2010) The mechanism of double-strand DNA break repair by the nonhomologous DNA end joining pathway. *Annual Review of Biochemistry*. 79, 181.

Liu, Y., Prasad, R., Beard, W. A., Kedar, P. S., Hou, E. W., Shock, D. D. & Wilson, S. H. (2007) Coordination of steps in single-nucleotide base excision repair mediated by apurinic/apyrimidinic endonuclease 1 and DNA polymerase β. *Journal of Biological Chemistry*. 282 (18), 13532-13541.

Livak, K. J., Flood, S. J., Marmaro, J., Giusti, W., & Deetz, K. (1995) Oligonucleotides with fluorescent dyes at opposite ends provide a quenched probe system useful for detecting PCR product and nucleic acid hybridization. *Genome Research*, *4*(6), 357-362.

Löbrich, M. & Jeggo, P. A. (2007) The impact of a negligent G2/M checkpoint on genomic instability and cancer induction. *Nature Reviews Cancer*, *7*(11), 861-869.

Lodish, H., Berk, A., Zipursky, L. S., Matsudaira, P., Baltimore, D. & Darnell, J. (2000) *Molecular Cell Biology*. 4th ed. New York, W. H. Freeman and Company.
Lodish, H., Baltimore, D., Berk, A., Zipursky, S. L., Matsudaira, P. & Darnell, J. (2004) *Molecular Cell Biology*. 6th ed. New York, W.H. Freeman and Company.

Luche, S., Santoni, V. & Rabilloud, T. (2003) Evaluation of nonionic and zwitterionic detergents as membrane protein solubilizers in two-dimensional electrophoresis. *Proteomics*. 3 (3), 249-253.

Maki, H., Maki, S. & Kornberg, A. (1988) DNA Polymerase III holoenzyme of Escherichia coli. IV. The holoenzyme is an asymmetric dimer with twin active sites. *The Journal of Biological Chemistry*. 263, 6570-6578.

Mapelli, M., Panjikar, S. & Tucker, P. A. (2005) The crystal structure of the HSV-1 ssDNA binding protein suggests the structural basis for flexible, cooperative single-stranded DNA binding. *The Journal of Biological Chemistry*. 280, 2990-2997.

Martin, P., Sun, L., Hood, D. W. & Moxon, E. R. (2004) Involvement of genes of genome maintenance in the regulation of phase variation frequencies in *Neisseria meningitidis*. *Microbiology*. 150, 3001-3012.

Matson, S. W. (1986) *Escherichia coli* helicase II (urvD gene product) translocates unidirectionally in a 3'to 5'direction. *Journal of Biological Chemistry*, *261*(22), 10169-10175.

Mauris, J. & Evans Jr, T. C. (2009) Adenosine triphosphate stimulates Aquifex aeolicus MutL endonuclease activity. *PLoS One*. 4 (9), e7175.

McInerney, P. & O'Donnell, M. (2004) Functional Uncoupling of Twin Polymerases MECHANISM OF POLYMERASE DISSOCIATION FROM A LAGGING-STRAND BLOCK. *The Journal of Biological Chemistry*. 279, 21543-21551.

McVey, M. & Lee, S. E. (2008) MMEJ repair of double-strand breaks (director's cut): deleted sequences and alternative endings. *Trends in Genetics*. 24 (11), 529-538.

Mendillo, M. L., Putnam, C. D. & Kolodner, R. D. (2007) *Escherichia coli* MutS tetramerization domain structure reveals that stable dimers but not tetramers are essential for DNA mismatch repair in vivo. *Journal of Biological Chemistry*. 282 (22), 16345-16354.

Miguel, V., Correa, E. M., De Tullio, L., Barra, J. L., Argarana, C. E. & Villarreal, M. A. (2013) Analysis of the Interaction Interfaces of the N-Terminal Domain from Pseudomonas aeruginosa MutL. *PloS One*. 8 (7), e69907.

Minnick, D. T., & Kunkel, T. A. (1995) DNA synthesis errors, mutators and cancer. *Cancer surveys*, *28*, 3-20.

Modrich, P. (1989) Methyl-directed DNA mismatch correction. *Journal of Biological Chemistry*, *264*(12), 6597-6600.

Modrich, P. & Lahue, R. (1996) Mismatch Repair in Replication Fidelity, Genetic Recombination, and Cancer Biology. *Annual Review of Biochemistry*. 65, 101-133.

Monti, M. R., Miguel, V., Borgogno, M. V. & Argaraña, C. E. (2012) Functional analysis of the interaction between the mismatch repair protein MutS and the replication processivity factor β clamp in Pseudomonas aeruginosa. *DNA Repair*. 11 (5), 463-469.

Moore, C. L. & Sharp, P. A. (1985) Accurate cleavage and polyadenylation of exogenous RNA substrate. *Cell*. 41 (3), 845-855.

Moxon, E. R., Rainey, P. B., Nowak, M. A. & Lenski, R. E. (1994) Adaptive evolution of highly mutable loci in pathogenic bacteria. *Current Biology*. 4 (1), 24-33.

Nakano, T., Morishita, S., Katafuchi, A., Matsubara, M., Horikawa, Y., Terato, H., Salem, A. M. H., Izumi, S., Pack, S. P., Makino, K. & Ide, H. (2007) Nucleotide excision repair and homologous recombination systems commit differentially to the repair of DNA-protein crosslinks. *Molecular Cell*. 28 (1), 147-158.

Nasheuer, H. P., Smith, R., Bauerschmidt, C., Grosse, F. & Weisshart, K. (2002) Initiation of eukaryotic DNA replication: Regulation and mechanisms. *Progress in Nucleic Acid Research and Molecular Biology*. 72, 41-94.

Natrajan, G., Lamers, M. H., Enzlin, J. H., Winterwerp, H. H., Perrakis, A. & Sixma, T. K. (2003) Structures of Escherichia coli DNA mismatch repair enzyme MutS in complex with different mismatches: a common recognition mode for diverse substrates. *Nucleic Acids Research*. 31 (16), 4814-4821.

Negishi, K., Loakes, D. & Schaaper, R. M. (2002) Saturation of DNA mismatch repair and error catastrophe by a base analogue in Escherichia coli. *Genetics*. 161 (4), 1363-1371.

Neidhardt, F. C. & Curtiss, R. (1996) *Escherichia coli and Salmonella typhimurium: Cellular and Molecular Biology*. 2nd ed. Washington, DC, American Society for Microbiology Press.

Oakley, A. J., Prosselkov, P., Wijffels, G., Beck, J. L., Wilce, M. C. J. & Dixon, N. E. (2003) Flexibility revealed by the 1.85 Å crystal structure of the β sliding-clamp subunit of *Escherichia coli* DNA polymerase III. *Acta Crystallographica Section D: Biological Crystallography*. 59, 1192-1199.

Obmolova, G., Ban, C., Hsieh, P. & Yang, W. (2000) Crystal structures of mismatch repair protein MutS and its complex with a substrate DNA. *Nature*. 407, 703-710.

O'Donnell, M. E. (1987) Accessory proteins bind a primed template and mediate rapid cycling of DNA polymerase III holoenzyme from Escherichia coli. *The Journal of Biological Chemistry*. 262, 16558-16565.

O'Donnell, M., Jeruzalmi, D. & Kuriyan, J. (2001) Clamp loader structure predicts the architecture of DNA polymerase III holoenzyme and RFC. *Current Biology*. 11 (22), R935-R946.

O'Donnell, M., Onrust, R., Dean, F. B., Chen, M. & Hurwitz, J. (1993) Homology in accessory proteins of replicative polymerases--E. coli to humans. *Nucleic Acids Research*. 21 (1), 1-3.

O'Donnell, M. & Studwell, P. S. (1990) Total reconstitution of DNA polymerase III holoenzyme reveals dual accessory protein clamps. *The Journal of Biological Chemistry*. 265, 1179-1187.

Oyama, T., Ishino, Y., Cann, I. K. O., Ishino, S. & Morikawa, K. (2001) Atomic Structure of the Clamp Loader Small Subunit from *Pyrococcus furiosus*. *Molecular Cell*. 8 (2), 455-463.

Pardo, B., Gómez-González, B. & Aguilera, A. (2009) DNA repair in mammalian cells. *Cellular and Molecular Life Sciences*. 66 (6), 1039-1056.

Parker, B. O. & Marinus, M. G. (1992) Repair of DNA heteroduplexes containing small heterologous sequences in Escherichia coli. *Proceedings of the National Academy of Sciences of the United States of America*. 89 (5), 1730-1734.

Parkhill, J., Achtman, M., James, K. D., Bentley, S. D., Churcher, C., Klee, S. R., Morelli, G., Basham, D., Brown, D., Chillingworth, T., Davies, R. M., Davis, P., Devlin, K., Feltwell, T., Hamlin, N., Holroyd, S., Jagels, K., Leather, S., Moule, S., Mungall, K., Quail, M. A., Rajandream, M. A., Rutherford, K. M., Simmonds, M., Skelton, J., Whitehead, S., Spratt, B. G. & Barrell, B. G. (2000) Complete DNA sequence of a serogroup A strain of *Neisseria meningitidis* Z2491. *Nature*. 404, 502-506.

Patel, M., Jiang, Q., Woodgate, R., Cox, M. M. & Goodman, M. F. (2010) A new model for SOS-induced mutagenesis: how RecA protein activates DNA polymerase V. *Critical Reviews in Biochemistry and Molecular Biology*. 45 (3), 171-184.

Pavlov, Y. I., Mian, I. M. & Kunkel, T. A. (2003) Evidence for preferential mismatch repair of lagging strand DNA replication errors in yeast. *Current Biology*. 13 (9), 744-748.

Phan, J., Zdanov, A., Evdokimov, A. G., Tropea, J. E., Peters, H. K., Kapust, R. B., Li, M., Wlodawer, A. & Waugh, D. S. (2002) Structural basis for the substrate specificity of tobacco etch virus protease. *Journal of Biological Chemistry*. 277 (52), 50564-50572.

Pillon, M. C., Lorenowicz, J. J., Uckelmann, M., Klocko, A. D., Mitchell, R. R., Chung, Y. S., Modrich, P., Walker, G. C., Simmons, L. A., Friedhoff, P. & Guarné, A. (2010) Structure of the endonuclease domain of MutL: unlicensed to cut. *Molecular Cell.* 39 (1), 145-151.

Pillon, M. C., Miller, J. H. & Guarné, A. (2011) The endonuclease domain of MutL interacts with the β sliding clamp. *DNA Repair.* 10 (1), 87-93.

Podobnik, M., Weitze, T. F., O'Donnell, M. & Kuriyan, J. (2003) Nucleotide-Induced Conformational Changes in an Isolated *Escherichia coli* DNA Polymerase III Clamp Loader Subunit. *Structure*. 11 (3), 253-263.

Pomerantz, R. T. & O'Donnell, M. (2007) Replisome mechanics: insights into a twin DNA polymerase machine. *Trends in Microbiology*. 15 (4), 156-164.

Ranjha, L., Anand, R. & Cejka, P. (2014) The Saccharomyces cerevisiae Mlh1-Mlh3 heterodimer is an endonuclease that preferentially binds to Holliday junctions. *Journal of Biological Chemistry*. 289 (9), 5674-5686.

Räschle, M., Dufner, P., Marra, G. & Jiricny, J. (2002) Mutations within the hMLH1 and hPMS2 subunits of the human MutLα mismatch repair factor affect its ATPase activity, but not its ability to interact with hMutSα. *Journal of Biological Chemistry*. 277 (24), 21810-21820.

Ren, S. & Nassal, M. (2001) Hepatitis B virus (HBV) virion and covalently closed circular DNA formation in primary tupaia hepatocytes and human hepatoma cell lines upon HBV genome transduction with replication-defective adenovirus vectors. *Journal of virology*, *75*(3), 1104-1116.

Revzin, A. (1989) Gel electrophoresis assays for DNA-protein interactions. *BioTechniques*, *7*(4), 346-355.

Reyes-Lamothe, R., Sherratt, D. J. & Leake, M. C. (2010) Stoichiometry and Architecture of Active DNA Replication Machinery in *Escherichia coli*. *Science*. 328 (5977), 498-501.

Richardson, A. R. & Stojiljkovic, I. (2001) Mismatch repair and the regulation of phase variation in *Neisseria meningitidis*. *Molecular Microbiology*. 40 (3), 645-655.

Richardson, A. R., Yu, Z., Popovic, T. & Stojiljkovic, I. (2002) Mutator clones of *Neisseria meningitidis* in epidemic serogroup A disease. *Proceedings of the National Academy of Sciences of the United States of America*. 99 (9), 6103-6107.

Ruiz, M. (2007) *DNA replication*. Available from: https://commons.wikimedia.org/wiki/File:DNA_replication_en.svg [Accessed: 7th November 2016].

Sachdev, D. & Chirgwin, J. M. (1998) Solubility of proteins isolated from inclusion bodies is enhanced by fusion to maltose-binding protein or thioredoxin. *Protein Expression and Purification*. 12 (1), 122-132.

Sacho, E. J., Kadyrov, F. A., Modrich, P., Kunkel, T. A. & Erie, D. A. (2008) Direct visualization of asymmetric adenine nucleotide-induced conformational changes in MutLα. *Molecular Cell.* 29 (1), 112-121.

Schofield, M. J. & Hsieh, P. (2003) DNA Mismatch Repair: Molecular Mechanisms and Biological Function. *Annual Review of Microbiology*. 57, 579-608.

Schofield, M. J., Nayak, S., Scott, T. H., Du, C. & Hsieh, P. (2001) Interaction of *Escherichia coli* MutS and MutL at a DNA mismatch. *Journal of Biological Chemistry*, *276*(30), 28291-28299.

Shell, S. S., Putnam, C. D. & Kolodner, R. D. (2007) The N terminus of Saccharomyces cerevisiae Msh6 is an unstructured tether to PCNA. *Molecular Cell*. 26 (4), 565-578.

Shimada, A., Kawasoe, Y., Hata, Y., Takahashi, T. S., Masui, R., Kuramitsu, S. & Fukui, K. (2013) MutS stimulates the endonuclease activity of MutL in an ATP-hydrolysis-dependent manner. *FEBS Journal*. 280 (14), 3467-3479.

Simmons, L. A., Davies, B. W., Grossman, A. D. & Walker, G. C. (2008) β clamp directs localization of mismatch repair in Bacillus subtilis. *Molecular Cell*. 29 (3), 291-301.

Spampinato, C. P., Gomez, R. L., Galles, C. & Lario, L. D. (2009) From bacteria to plants: A compendium of mismatch repair assays. *Mutation Research/Reviews in Mutation Research*. 682 (2-3), 110-128.

Spampinato, C. & Modrich, P. (2000) The MutL ATPase is required for mismatch repair. *Journal of Biological Chemistry*. 275 (13), 9863-9869.

Steitz, T. A. (1998) Structural biology: A mechanism for all polymerases. *Nature*. 391, 231-232.

Stephens, D. S., Greenwood, B. & Brandtzaeg, P. (2007) Epidemic meningitis, meningococcaemia, and *Neisseria meningitidis*. *The Lancet*. 369 (9580), 2196-2210.

Stewart, J., Hingorani, M. M., Kelman, Z. & O'Donnell, M. (2001) Mechanism of β Clamp Opening by the δ Subunit of *Escherichia coli* DNA Polymerase III Holoenzyme. *The Journal of Biological Chemistry*. 276, 19182-19189.

Studwell, P. S. & O'Donnell, M. (1990) Processive replication is contingent on the exonuclease subunit of DNA polymerase III holoenzyme. *The Journal of Biological Chemistry*. 265, 1171-1178.

Studwell-Vaughan, P. S. & O'Donnell, M. (1991) Constitution of the twin polymerase of DNA polymerase III holoenzyme. *The Journal of Biological Chemistry*. 266, 19833-19841.

Studwell-Vaughan, P. S. & O'Donnell, M. (1993) DNA polymerase III accessory proteins. V. Theta encoded by holE. *The Journal of Biological Chemistry*. 268, 11785-11791.

Stukenberg, P. T., Studwell-Vaughan, P. S. & O'Donnell, M. (1991) Mechanism of the sliding beta-clamp of DNA polymerase III holoenzyme. *The Journal of Biological Chemistry*. 266, 11328-11334.

Su, S. S., Lahue, R. S., Au, K. G. & Modrich, P. (1988) Mispair specificity of methyl-directed DNA mismatch correction in vitro. *The Journal of Biological Chemistry*. 263, 6829-6835.

Su, S. S. & Modrich, P. (1986) Escherichia coli mutS-encoded protein binds to mismatched DNA base pairs. *Proceedings of the National Academy of Sciences*. 83 (14), 5057-5061.

Sutton, M. D. & Walker, G. C. (2001) Managing DNA polymerases: Coordinating DNA replication, DNA repair, and DNA recombination. *Proceedings of the National Academy of Sciences of the United States of America*. 98 (15), 8342-8349.

Taft-Benz, S. A. & Schaaper, R. M. (2004) The θ Subunit of *Escherichia coli* DNA Polymerase III: a Role in Stabilizing the ε Proofreading Subunit. *Journal of Bacteriology*. 186 (9), 2774-2780.

Temin, H. M. & Mizutani, S. (1970) RNA-dependent DNA polymerase in virions of Rous sarcoma virus. *Nature*. 226, pp. 1211–1213.

Tettelin, H., Saunders, N. J., Heidelberg, J., Jeffries, A. C., Nelson, K. E., Eisen, J. A., Ketchum, K. A., Hood, D. W., Peden, J. F., Dodson, R. J., Nelson, W. C., Gwinn, M. L., DeBoy, R., Peterson, J. D., Hickey, E. K., Haft, D. H., Salzberg, S. L., White, O., Fleischmann, R. D., Dougherty, B. A., Mason, T., Ciecko, A., Parksey, D. S., Blair, E., Cittone, H., Clark, E. B., Cotton, M. D., Utterback, T. R., Khouri, H., Qin, H., Vamathevan, J., Gill, J., Scarlato, V., Masignani, V., Pizza, M., Grandi, G., Sun, L., Smith, H. O., Fraser, C. M., Moxon, E. R., Rappuoli, R. & Venter, J. C. (2000) Complete Genome Sequence of *Neisseria meningitidis* Serogroup B Strain MC58. *Science*. 287 (5459), 1809-1815.

Tomer, G., Buermeyer, A. B., Nguyen, M. M. & Liskay, R. M. (2002) Contribution of human mlh1 and pms2 ATPase activities to DNA mismatch repair. *Journal of Biological Chemistry*. 277 (24), 21801-21809.

Tondnevis, F., Gillilan, R. E., Bloom, L. B. & McKenna, R. (2015) Solution study of the *Escherichia coli* DNA polymerase III clamp loader reveals the location of the dynamic ψχ heterodimer. *Structural Dynamics*. 2, 054701.

Tran, P. T. & Liskay, R. M. (2000) Functional studies on the candidate ATPase domains of Saccharomyces cerevisiae MutLα. *Molecular and Cellular Biology*. 20 (17), 6390-6398.

Tsuchihashi, Z. & Kornberg, A. (1989) ATP interactions of the tau and gamma subunits of DNA polymerase III holoenzyme of Escherichia coli. *The Journal of Biological Chemistry*. 264, 17790-17795.

Tsuchihashi, Z. & Kornberg, A. (1990) Translational frameshifting generates the gamma subunit of DNA polymerase III holoenzyme. *Proceedings of the National Academy of Sciences of the United States of America*. 87 (7), 2516-2520.

Turner, J., Hingorani, M. M., Kelman, Z. & O'Donnell, M. (1999) The internal workings of a DNA polymerase clamp□loading machine. *The EMBO Journal*. 18, 771-783.

Viswanathan, M. & Lovett, S. T. (1998) Single-strand DNA-specific exonucleases in Escherichia coli: roles in repair and mutation avoidance. *Genetics*, *149*(1), 7-16.

Walker, J. E., Saraste, M., Runswick, M. J. & Gay, N. J. (1982) Distantly related sequences in the alpha-and beta-subunits of ATP synthase, myosin, kinases and other ATP-requiring enzymes and a common nucleotide binding fold. *The EMBO Journal*. 1 (8), 945.

Wang, J. C. (2002) Cellular roles of DNA topoisomerases: a molecular perspective. *Nature Reviews Molecular Cell Biology*. 3, 430-440.

Waters, L. S., Minesinger, B. K., Wiltrout, M. E., D'Souza, S., Woodruff, R. V. & Walker, G. C. (2009) Eukaryotic translesion polymerases and their roles and regulation in DNA damage tolerance. *Microbiology and Molecular Biology Reviews*, *73*(1), 134-154.

Watson, J. D., Baker, T. A., Gann, A., Levine, M. & Losick, R. (2004) *Molecular Biology of the Gene*. 5th ed. New York, Cold Spring Harbor Laboratory Press.
Watson, J. D., Baker, T. A., Gann, A., Levine, M. & Losick, R. (2013) *Molecular Biology of the Gene*. 7th ed. New York, Cold Spring Harbor Laboratory Press.

Watson, J. D. & Crick, F. H. (1953) Letters to nature: molecular structure of nucleic acid. *Nature*. 171 (737), 738.

Weber, P. C., Ohlendorf, D. H., Wendoloski, J. J. & Salemme, F. R. (1989) Structural origins of high-affinity biotin binding to streptavidin. *Science*, *243*(4887), 85.

Weigel, C., Schmidt, A., Rückert, B., Lurz, R. & Messer, W. (1997) DnaA protein binding to individual DnaA boxes in the *Escherichia coli* replication origin, *oriC*. *The EMBO Journal*. 16 (21), 6574–6583.

Welsh, K. M., Lu, A. L., Clark, S. & Modrich, P. (1987) Isolation and characterization of the *Escherichia coli mutH* gene product. *Journal of Biological Chemistry*. 262 (32), 15624-15629.

West, S. C. (2003) Molecular views of recombination proteins and their control. *Nature reviews Molecular Cell Biology*. 4 (6), 435-445.

Witte, G., Urbanke, C. & Curth, U. (2003) DNA polymerase III χ subunit ties single-stranded DNA binding protein to the bacterial replication machinery. *Nucleic Acids Research*. 31 (15), 4434-4440.

Wyman, C., Ristic, D. & Kanaar, R. (2004) Homologous recombination-mediated double-strand break repair. *DNA Repair*. 3 (8), 827-833.

Xiao, H., Dong, Z. & O'Donnell, M. (1993) DNA polymerase III accessory proteins. IV. Characterization of chi and psi. *The Journal of Biological Chemistry*. 268, 11779-11784.

Yakovchuk, P., Protozanova, E. & Frank-Kamenetskii, M. D. (2006) Base-stacking and base-pairing contributions into thermal stability of the DNA double helix. *Nucleic Acids Research*. 34 (2), 564-574.

Yamamoto, A., Schofield, M. J., Biswas, I. & Hsieh, P. (2000) Requirement for Phe36 for DNA binding and mismatch repair by Escherichia coli MutS protein. *Nucleic Acids Research*. 28 (18), 3564-3569.

Yang, W. (2006) Poor base stacking at DNA lesions may initiate recognition by many repair proteins. *DNA Repair*. 5 (6), 654-666.

Yao, N., Leu, F. P., Anjelkovic, J., Turner, J. & O'Donnell, M. (2000) DNA Structure Requirements for the *Escherichia coli*γ Complex Clamp Loader and DNA Polymerase III Holoenzyme. *The Journal of Biological Chemistry*. 275, 11440-11450.

Yuzhakov, A., Turner, J. & O'Donnell, M. (1996) Replisome Assembly Reveals the Basis for Asymmetric Function in Leading and Lagging Strand Replication. *Cell*. 86 (6), 877-886.

Zhang, Y., Yuan, F., Presnell, S. R., Tian, K., Gao, Y., Tomkinson, A. E., Gu L. Y. & Li, G. M. (2005) Reconstitution of 5′-directed human mismatch repair in a purified system. *Cell*. 122 (5), 693-705.

Chapter 8

Appendices

NATURE PUBLISHING GROUP LICENSE TERMS AND CONDITIONS

Nov 21, 2016

This Agreement between Liang Xue ("You") and Nature Publishing Group ("Nature Publishing Group") consists of your license details and the terms and conditions provided by Nature Publishing Group and Copyright Clearance Center.

License Number

3993681291365

License date

Nov 21, 2016

Licensed Content Publisher

Nature Publishing Group

Licensed Content Publication

Nature Reviews Molecular Cell Biology

Licensed Content Title

The multifaceted mismatch-repair system

Licensed Content Author

Josef Jiricny

Licensed Content Date

May 1, 2006

Licensed Content Volume Number

7

Licensed Content Issue Number

5

Type of Use

reuse in a dissertation / thesis

Requestor type

academic/educational

Format

print and electronic

Portion

figures/tables/illustrations

Number of figures/tables/illustrations

1

High-res required

no

Figures

I seek your permission to reuse the Figure 2 "The MutS sliding clamp and its activation" from the article "The multifaceted mismatch-repair system" in my thesis.

Author of this NPG article

no

Your reference number

Title of your thesis / dissertation

Analysis of DNA mismatch repair system from Neisseria Meningitidis

Expected completion date

Nov 2016

Estimated size (number of pages)

225

Requestor Location

Liang Xue

Flat A, 25 Warkworth Street

Cambridge, CB1 1EG

United Kingdom

Attn: Liang Xue

Billing Type

Invoice

Billing Address

Liang Xue

Flat A, 25 Warkworth Street

Cambridge, United Kingdom CB1 1EG

Attn: Liang Xue

Total

0.00 GBP

Terms and Conditions

Terms and Conditions for Permissions

Nature Publishing Group hereby grants you a non-exclusive license to reproduce this material for this purpose, and for no other use,subject to the conditions below:

1. NPG warrants that it has, to the best of its knowledge, the rights to license reuse of this material. However, you should ensure that the material you are requesting is original to Nature Publishing Group and does not carry the copyright of another entity (as credited in the published version). If the credit line on any part of the material you have requested indicates that it was reprinted or adapted by NPG with permission from another source, then you should also seek permission from that source to reuse the material.

2. Permission granted free of charge for material in print is also usually granted for any electronic version of that work, provided that the material is incidental to the work as a whole and that the electronic version is essentially equivalent to, or substitutes for, the print version.Where print permission has been granted for a fee, separate permission must be obtained for any additional, electronic re-use

(unless, as in the case of a full paper, this has already been accounted for during your initial request in the calculation of a print run).NB: In all cases, web-based use of full-text articles must be authorized separately through the 'Use on a Web Site' option when requesting permission.

3. Permission granted for a first edition does not apply to second and subsequent editions and for editions in other languages (except for signatories to the STM Permissions Guidelines, or where the first edition permission was granted for free).

4. Nature Publishing Group's permission must be acknowledged next to the figure, table or abstract in print. In electronic form, this acknowledgement must be visible at the same time as the figure/table/abstract, and must be hyperlinked to the journal's homepage.

5. The credit line should read:
   Reprinted by permission from Macmillan Publishers Ltd: [JOURNAL NAME] (reference citation), copyright (year of publication)
   For AOP papers, the credit line should read:
   Reprinted by permission from Macmillan Publishers Ltd: [JOURNAL NAME], advance online publication, day month year (doi: 10.1038/sj.[JOURNAL ACRONYM].XXXXX)

   Note: For republication from the *British Journal of Cancer,* the following credit lines apply.
   Reprinted by permission from Macmillan Publishers Ltd on behalf of Cancer Research UK: [JOURNAL NAME] (reference citation), copyright (year of publication)For AOP papers, the credit line should read:
   Reprinted by permission from Macmillan Publishers Ltd on behalf of Cancer Research UK: [JOURNAL NAME], advance online publication, day month year (doi: 10.1038/sj.[JOURNAL ACRONYM].XXXXX)

6. Adaptations of single figures do not require NPG approval. However, the adaptation should be credited as follows:

   Adapted by permission from Macmillan Publishers Ltd: [JOURNAL NAME] (reference citation), copyright (year of publication)

   Note: For adaptation from the *British Journal of Cancer,* the following credit line applies.
   Adapted by permission from Macmillan Publishers Ltd on behalf of Cancer Research

UK: [JOURNAL NAME] (reference citation), copyright (year of publication)

7. Translations of 401 words up to a whole article require NPG approval. Please visit http://www.macmillanmedicalcommunications.com for more information.Translations of up to a 400 words do not require NPG approval. The translation should be credited as follows:

   Translated by permission from Macmillan Publishers Ltd: [JOURNAL NAME] (reference citation), copyright (year of publication).

   Note: For translation from the *British Journal of Cancer,* the following credit line applies.
   Translated by permission from Macmillan Publishers Ltd on behalf of Cancer Research UK: [JOURNAL NAME] (reference citation), copyright (year of publication)

We are certain that all parties will benefit from this agreement and wish you the best in the use of this material. Thank you.
Special Terms:
v1.1
Questions? customercare@copyright.com or +1-855-239-3415 (toll free in the US) or +1-978-646-2777.